DEVELOPMENT OF A VOLUMETRIC STRAIN INFLUENCE GROUND IMPROVEMENT PREDICTION MODEL WITH SPECIAL REFERENCE TO IMPACT COMPACTION

ALAN DAVID BERRY

Dissertation submitted in partial fulfilment of the requirements of the degree of

MASTER OF ENGINEERING

in the

FACULTY OF ENGINEERING, BUILT ENVIRONMENT AND INFORMATION TECHNOLOGY

UNIVERSITY OF PRETORIA
PRETORIA

July 2001

ACKNOWLEDGEMENTS

I would like to thank the following people who made this project report possible:

- The directors of Landpac, particularly Charles Davis, who have given me the permission to publish this work, which is largely based on the research I did for the company. The use of the material and time spent is gratefully acknowledged. It has been a privilege to be afforded the opportunity to undertake this research.
- Professor A T Visser and Professor E Rust, my supervisors for their guidance and enthusiasm.
- Mr D Mulville of Mulville & Associates for the loan of the FLAC software.
- Mr H Greyling and Mr E Nkosi for their assistance with much of the field work.
- Permission from the CSIR to publish the references compiled by themselves is also acknowledged.
- Mr G Byrne of Franki Africa for permission to publish some of the dynamic compaction test data from the Mozal Smelter site in Mozambique.
- My mother and late father, for their encouragement to study further.
- Karen, my wife, for her love and support while buried in the books or staring into the computer screen.
- To my Maker, the Giver of all good gifts, for a greater degree of understanding than I had before.

DISSERTATION SUMMARY

DEVELOPMENT OF A VOLUMETRIC STRAIN INFLUENCE GROUND IMPROVEMENT PREDICTION MODEL WITH SPECIAL REFERENCE TO IMPACT COMPACTION

ALAN DAVID BERRY

Supervisor: Professor A T Visser
Co-supervisor: Professor E Rust
Department: Civil Engineering
University: University of Pretoria
Degree: Master of Engineering (Geotechnical Engineering)

Aubrey Berrangé, a South African roads engineer, invented the impact compactor in 1949 with the intention of achieving improved compaction to greater depths than possible with conventional equipment available at the time. The aim of this dissertation is to present a simple prediction model for the profile of improvement in the ground, using surface settlement as the main input parameter. The model is based on the information reviewed, observation of field data and a static numerical analysis. For simplicity sake, no attempt is made to predict the energy requirement to achieve the input value of settlement. The model is then verified on fifteen impact compaction profiles at six different sites. A 2 ton-meter dropping mass compactor was also used in the verification process with reasonable success. In addition, the model was tested against comprehensive testing performed at a dynamic compaction site with very promising results. The method is also shown to give acceptable results for prediction of density increase during a vibratory compaction trial. It is concluded that the improvement in the ground can be estimated with reasonable success if the surface settlement is monitored, providing lateral strains are taken into account.

Keywords: Compaction, Compaction modelling, compaction prediction, impact compaction, dynamic compaction, ground improvement, volumetric strain, plastic deformations

SAMEVATTING VAN VERHANDELING

DIE ONTWIKKELING VAN 'N VERVORMINGSINVLOED GRONDVERBETERING VOORSPELLINGSMODEL MET SPESIALE VERWYSING NA SLAGROLLERS

ALAN DAVID BERRY

Promotor:	Professor A T Visser
Medepromotor	Professor E Rust
Departement:	Siviele Ingeneurswese
Universiteit:	Universiteit van Pretoria
Graad:	Magister in Ingenieurswese (Geotegniese Ingenieurswese)

Aubrey Berrangé, 'n Suid Afrikaanse padingenieur, het die eerste slagroller in 1949 ontwerp. Die bedoeling was om beter kompaksie tot groter dieptes te behaal invergelyking met wat die kompaksie toerusting van daardie tyd moontlik was. Die doel van hierdie verhandeling is om 'n vervormingsinvloed grondverbetering voorspellingsmodel voor te stel, met die oppervlak-versakking as hoof invoer parameter. Die metode is gebaseer op veldmetings asook analitiese berekenige. Geen voorspelling van energie behoeftes word gemaak nie. Die model is op vyftien veskillende grondprofiele op ses verskillende slagroltereine getoets. 'n 2 ton vallenende massa kompakteerder was ook gebruik in die verifierings proses met bevrediginde resultate. Die model is ook op 'n dinamiese kompaksie terein getoets. Daar is gevind dat digtheid vebetering voorspellings verkry uit die model, beveredigend is op onversadigde materiale. Die navorsing wys dat die grondverbetering 'n funksie is van die grondoppervlakte versakking met dien verstande dat laterale vervorming in ag geneem word.

Sleutelwoorde: Kompaksie, kompaksie modelering, kompaksie voorspelling, slagrollers, dinamiese kompaksie, grondverbetering, volumetriese vervorming, plastiese verformings

TABLE OF CONTENTS

LIST OF FIGURES

LIST OF TABLES

LIST OF PHOTOGRAPHS

CHAPTER 1

INTRODUCTION

1.1 BACKGROUND

Impact compaction was invented by Aubrey Berrangé in 1949 in order to address the deep compaction problems experienced by the Cape Roads Department at the time (Paige-Green, 1998). The use of impact compaction has since grown and recently it was used for the construction of the runways at Chep Lap Kok airport in Hong Kong, one of the largest construction projects of the 20th century.

Initial development was undertaken by the CSIR in Pretoria where a 4 sided impact compactor was successfully developed. Berrangé later left the CSIR to continue the commercial development of his ideas, designing both three sided machines and five sided machines shown below.

Plate 1.1: ***A 3 sided impact compactor***

Plate 1.2: ***A 5 sided impact compactor***

On his retirement he sold the patents to the manufacturers of the machines based in Nigel, along with the South African contracting wing he owned. The new company, Landpac, has continued the development and has been largely responsible for funding the research presented here.

1.2 PROBLEM STATEMENT AND STUDY OBJECTIVES

Most methods currently available to predict the improvement in the ground after compaction are either entirely empirical or semi-empirical in nature, or based on laboratory testing. Recently, sophisticated computer based models have been combined with laboratory testing to predict the improvement in the ground with some success.

However, there is currently no simple method of predicting the reduction in the void ratio of the soil after compaction using impact compactors.

Although it is intuitively obvious that the ground improvement is proportional to the surface settlement, none of the literature surveyed made use of this easily measurable parameter to predict the improvement that can be achieved. In addition, little clarity was found in the literature regarding the fundamental mechanisms at work, which result in compaction of the ground.

The purpose of this dissertation is to show that the profile of improvement in the ground after impact compaction is predictable and proportional to the surface settlement of the compacted ground, provided lateral deformation is taken into account. The objective is therefore to measure, model and predict the typical volumetric response of the soil during the impact compaction process.

A need therefore exists for a simple model that can be used with some degree of confidence. The aim of this dissertation is to provide such a model.

1.3 SCOPE OF DISSERTATION

This report firstly reviews the literature for predictive models that can be used or modified for use the address the problem stated. In order to support the hypothesised ground improvement model, a static numerical analysis is undertaken to examine the induced strain profile. To allow a reasonable estimate of the maximum dynamic force for input into the software, the decelerations of the impact compaction masses were measured. The influence of the cohesion and friction angle of the soil in, on the strain profile is also investigated.

Based on the numerical analysis and patterns observed in the field, a prediction model is presented for unsaturated conditions and verified on various sites. This is done for both impact compaction and dynamic compaction. The possible use of the model for conventional compaction is also demonstrated. The effect of layered soils is also briefly discussed.

Based on the findings made during the investigation, areas of further research are also suggested.

1.4 METHODOLOGY

The stated objective was addressed in the following sequence:

- Collect, compile and review the relevant papers and publications
- Determine the range of dynamic forces imparted to firstly, a initially soft soil, and secondly a hard soil [establish the upper and lower bound decelerations]
- Perform numerical analyses
- Develop a volumetric strain influence ground improvement prediction model
- Verify model and discuss shortcomings
- Summarise in report form

1.5 LAYOUT OF THE REPORT

The report is arranged in the following order:

- Chapter 1 introduces the problem and how it will be solved
- Chapter 2 summarised the finding of the literature review.
- Chapter 3 describes how the decelerations were measured and reviews the results
- Chapter 4 details the numerical analysis and the influence of the Mohr Coulomb soil parameters on the strain profile
- Chapter 5 presents the proposed prediction model
- Chapter 6 summarised the verification of the model on various sites and discusses the main issues and difficulties in modelling this complex subject
- Chapter 7 draws conclusions
- References
- Appendices

CHAPTER 2

LITERATURE STUDY

2 INTRODUCTION

The aim of this section of the report is summarise and synergise the most promising ground improvement prediction models found in the literature. Impact compaction literature is first reviewed, followed by those models found in the dynamic compaction and conventional (cylindrical vibrating drum) literature. Lastly, compaction models based on the soil characteristics are covered.

Some useful prediction models were found. Although much work has been done in the field of dynamic compaction (DC), most models found are still semi-empirical in nature. This is probably due to the influence of the water table, compactor geometry, soil parameters and surface settlement being largely ignored. From the DC literature it is concluded that the primary *impact compactor* parameters required for a prediction model are the compactor mass, drop height, contact area and total energy.

The more general compaction literature is mostly concerned with predicting compactor performance over a standard depth, through the use of empirical methods. Some useful models were found.

2.1 PREVIOUS WORK DONE ON IMPACT COMPACTION (IC)

A detailed review of the impact compaction literature was undertaken by the CSIR (Paige-Green, 1998). The author makes the observation that "Impact compaction…results in compaction at depth, with disturbance of the upper portion of the layer". This is the simplest form of prediction, and well known to most users of impact compaction. He also notes that "larger loads and larger contact areas are better for deep compaction". This is one of the main limiting factors of conventional cylindrical compactors in deep compaction: the contact width of the applied line load is difficult to enlarge. In considering the large force imparted by impact compactors Clifford (1978) noted that "principles that hold true for impact

devices hold true for impact rollers, except that, in addition, an impact roller delivers generated momentum due to the rotational effect of the roller mass". In a report investigating this hypothesis, it was found that this was not the case (Heyns, 1998), and that the potential energy of the machines formed the bulk of the imparted energy. In this report typical decelerations were found to be in the order of 100m/s^2 to 200m/s^2 (10 to 20 g's). Clifford rightfully notes in his conclusion that "the paucity of mathematical studies on various aspects on compaction, from generated energy to the soil response limits, show how difficult evaluation is".

In a recent paper, Berry et al (1998) noted that the impact compaction trials undertaken at Kriel revealed a peak in density in the post compaction test pits that were dug, and that this appeared similar to the shape of the Schmertman strain influence diagram (Schmertman, 1970). A trial pit excavation revealed the strain profile shown in Figure 2.1.

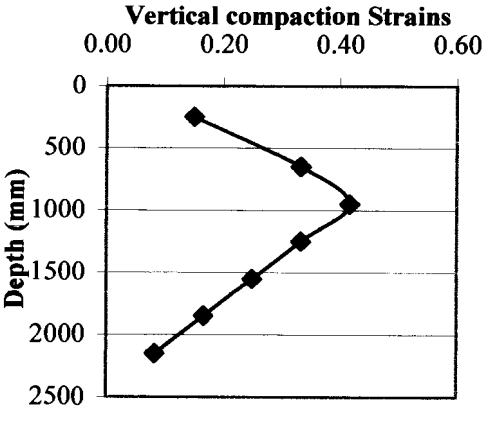

Figure 2.1: Trial indicating variation of strain with depth (Berry et al, 1998)

The above results were obtained by excavating a trial pit to a depth of 2.5m and replacing the soil carefully in 300mm layers. The interface between layers was marked with a chalk layer. After compaction by the 25kJ impact compactor, the pit was carefully excavated and the compression of the layers measured throughout the profile. Details of the measurements are given in Appendix A. Apart from this observation, no mention was found of any prediction model in the IC literature, only descriptive trends.

2.2 AN OVERVIEW OF PREDICTION MODELS USED IN DYNAMIC COMPACTION

In the 1960's a French engineer Louis Menard devised a method of compacting the ground by using a crane to lift a mass weighing a couple of tons to the full lift height of the crane and then releasing it. The nett effect was that the imparted force on impact was effectively 10 to 20 times larger than the static mass due to the inertia force imparted. This compaction technique has since become used world-wide, and much study has been undertaken in order to better understand the technology. The following parameters are typically predicted: patterns of improvement, depth of influence, surface settlement, settlement profile, surface stress, stress profile, residual horizontal stress profile and more recently, the void ratio reduction profile.

2.2.1 Descriptive/observational pattern of improvement

Initially, before the development of any mathematical prediction tools typical patterns of behaviour based on in-situ test results are all that is available to the engineer. Usually these offer little explanation. The most useful of these is given by Lukas (1986) and shown in Figure 2.2.

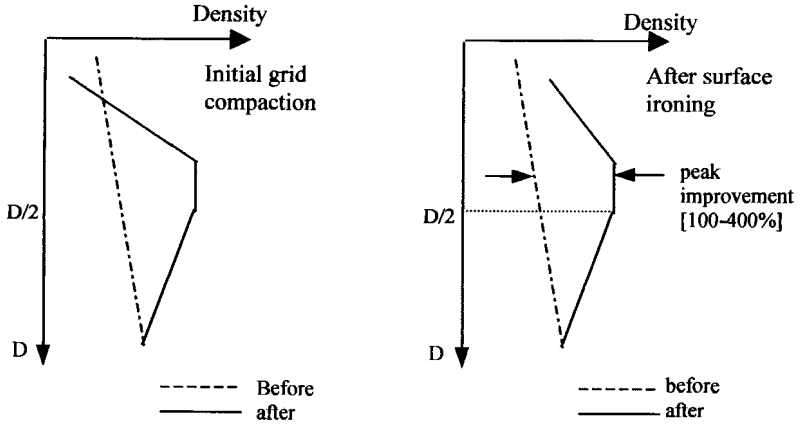

Figure 2.2: Descriptive pattern of DC soil improvement (Lukas, 1986)

This improvement pattern seems to tie in with the observation by Paige-Green, that the surface is loosened, and compaction takes place deeper down.

2.2.2 Predictions of depth of influence

One of the most important questions that needs answering is the depth to which improvement is achieved. To this end Menard et al (1976) suggested the well-known relation

$$d_{max} = \sqrt{W.H} \qquad \text{(Eq. 2.1)}$$

where W=pounder mass (t), H=drop height (m)

and d_{max}=maximum depth of influence

This was revised with experience and Lukas (1976) suggested

$$d_{max} = n\sqrt{W.H} \qquad \text{(Eq. 2.2)}$$

where *n=an empirical coefficient (0.3-0.8 typically)*

The modified Menard equation (Eq. 2.2) is still widely used in the industry, with the factor n=C.δ, where C=the velocity efficiency and δ= the stratagraphic coefficient (Varaksin, 1991). In the same publication Varaksin notes "In any type of unsaturated soil the shock causes a Proctor type compaction." and that "the phenomenon becomes highly complex in saturated or impervious soil". He then gives a formula to predict the increase in pore water pressure under saturated conditions. According to Varaksin, C=0.9 for cable drop and 1.2 for free fall. He also noted that 67% of the energy is dissipated in the Rayleigh surface wave, that this is represented by the δ coefficient. Once the point of liquifaction is reached, a rest period is required for the pore water pressures to dissipate. This rest period is of predictable duration. As impact rollers are generally used in non-saturated conditions, this is not pursued any further, other than to note that the presence of the water table is of great consequence and needs to be considered if present.

A typical energy-depth of influence chart from the use of the above equations is given in Figure 2.3.

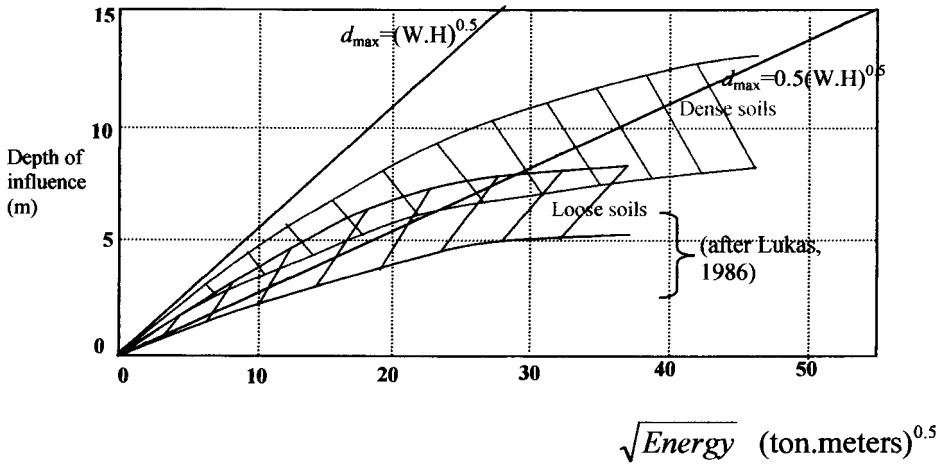

Figure 2.3: Typical energy-depth of influence chart for DC (Slocombe, 1989)

It is interesting to note that the depth of influence is thought to increase for denser materials. Note: "Energy" is defined in DC as ton.meters (t.m), which is not strictly correct as the gravitational constant is omitted.

Scott and Pearce (1976) presented an idealized model of the depth of the compacted zone in an energy dissipation analysis using a elasto-plastic soil model. The paper high-lights the many difficulties in analysing the problem and adopts a one-dimensional approach to obtain an equation for the depth of the compacted zone:

$$h = \frac{m}{\rho_c}\left\{\sqrt{1+\frac{k\rho(V-\mathrm{v})^2}{\sigma_L}}-1\right\} \qquad \text{(Eq. 2.3)}$$

where h=depth of compacted zone, m=mass/unit area

ρ_c=compacted soil density, ρ=initial soil density, V=impact velocity

v=velocity of radiated stress wave, σ_L=elastic stress limit and

$$k = \frac{\rho}{\rho_c - \rho} \qquad \text{(Eq. 2.3a)}$$

From the equation for h it is clear that the compacted density is required to determine the depth of compaction, which is almost self-defeating. The paper does not clearly indicate if the density is constant over the depth h, but the use of and average compacted density (ρ_c) seems to indicate that this is the case. To complicate matters, the velocity of impact and of the radiating stress wave is required, making the model dependent on extensive in-situ measurements.

2.2.3 Predictions of impact displacements/settlement

In a massless soil of constant stiffness k (kPa/mm) the displacement is given by (Sears et al, 1982):

$$y = \frac{1}{2}\left[\frac{2mg}{k} + \sqrt{\left(\frac{2mg}{k}\right)^2 + \frac{8mgh}{k}}\right] \text{, where } \frac{mg}{k} = \text{static displacement} \qquad \text{(Eq. 2.4)}$$

This is an elastic model, however, and would therefore rebound entirely if the theory was correct.

Kwang et al (1990) suggested that the ground improvement is related to the enforced (plastic) settlement curve and that this is uniquely related to the energy input and the pressuremeter limit pressure. The proposed curve is shown in Figure 2.4. The energy intensity characteristic I_s, is a function of only the energy imparted per unit area (E_B) and the pressuremeter limit pressure (P_L). The method indicates a "saturation energy intensity" after which there are limited returns. It fails to clearly describe the influence of moisture however, and gives no guidance as to the distribution of the improvement with depth. The enforced strain, η_{SE}, is defined below as

$$\eta_{SE} = \frac{S_E}{H_t} \text{ , } S_E = \text{enforced settlement , } H_t = \text{thickness requiring treatment} \qquad \text{(Eq. 2.4a)}$$

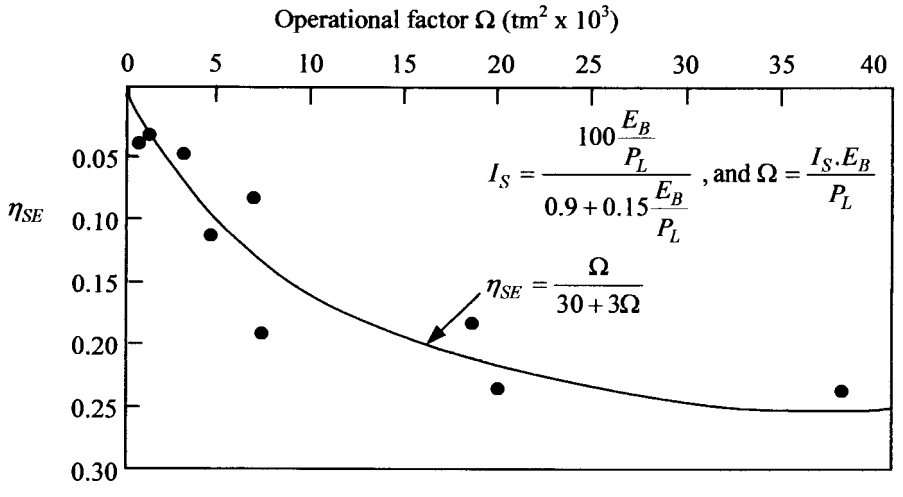

Figure 2.4: Unique enforced strain diagram (Kwang et al, 1990)

The selection of the depth requiring treatment, H_T, is left to the engineer, and leaves the method open to overestimation of this parameter.

It is nevertheless a step forward as it demonstrates that there is a predictable level of energy input after which there is little gain in the ground improvement. It confirms that the ground improvement is a function of the enforced surface settlement. The critical parameters required by the method are the input energy (Σmgh) and the limit pressure of the soil.

Davies et al (1995) proposed a useful elastodynamic prediction of the surface displacement, velocity and acceleration on and after a load impacts the ground. Good agreement was obtained between predicted and measured data over the first wavelength of displacement. The displacement equation used is as follows:

$$z = V_o.e^{\left(-\varpi_n.D.t\right)}.\sin\left(\varpi_d.t\right)/\varpi_d \qquad \text{Eq. 2.5}$$

not given in the paper are the velocity and acceleration equations :

$$v = V_o.e^{-\varpi_n.D.t}.\left[Cos(\varpi_d.t) - D.\frac{\varpi_n}{\varpi_d}.Sin(\varpi_d.t)\right] \qquad \text{Eq. 2.5a}$$

$$a = V_o.e^{-\varpi_n.D.t}.\left[Sin(\varpi_d.t)\left(\frac{\varpi_n^2.D^2}{\varpi_d}\right) - 2\varpi_n.D.Cos(\varpi_d.t)\right] \qquad \text{Eq. 2.5b}$$

where z = displacement, v = velocity, a = acceleration, t = time
D = damping ratio, ϖ_n = undamped natural frequency
ϖ_d = damped natural frequency, V_o = impact velocity

The above equations were used to estimate the displacement, velocity and accelerations of the Landpac 10kJ, 15kJ and 25kJ impact compactors. The results of the calculations are given in Appendix B, and are of a sensible order of magnitude for the parameters used. The method is best suited to prediction of Falling Weight Deflectometer (FWD) deflections where the materials behave fairly elastically.

2.2.4 Prediction of settlement profile

Wallays (1983) suggested a method to predict the settlement at various depths below the compacted surface, i.e a settlement profile. The potential energy from the drop of the mass is equated to the work done by the vertical stress induced in

the soil, plus the work done in moving the soil mass by the residual settlement. The derivation results in equations for a layered soil, predicting the surface stress, the surface settlement and the settlement profile:

$$\therefore \sigma_{max} = \frac{1}{B^2}\sqrt{\frac{\eta.G.H}{A}}\left[\sqrt{1+\left(\frac{F}{2\sqrt{\eta.G.H.A}}\right)^2}-\frac{F}{2\sqrt{\eta.G.H.A}}\right] \quad \text{(Eq 2.6}$$

$$s_{max} = \sigma_{max}.B^2.A \quad \text{(Eq 2.6a)}$$

$$s_z = \sigma_{max}.B^2.\left[\sum_{i=j+1}^{n}\frac{1}{E_i}\left(\frac{1}{B+z_{i-1}}-\frac{1}{B+z_i}\right)+\frac{1}{E_j}\left(\frac{1}{B+z}-\frac{1}{B+z_j}\right)\right] \quad \text{(Eq. 2.6b)}$$

where σ_{max} = maximum contact stress, B=load diameter, E_i=stiffness of layer i, z_i=top of layer i, s_{max}=maximum settlement, A & F are influence factors, s_z=settlement at depth z, the efficiency factor $\eta=\eta_w.\eta_i.h_d$, where η_w = mass efficiency (typically=2/3), η_i= impact efficiency (typically=1/3) and η_d= heave loss factor (typically = 2/3)

The method does not specifically predict improvement, but may well be used or extended to obtain more measurable parameters such as density or void ratio. It does not clearly indicate the effect of the water table or the effect of Poisson's ratio (lateral strains). Material properties are dealt with indirectly through the stiffness used in the equations. Results are given in charts showing the measured settlement compared to the predicted settlement. The efficiency factors are presumably obtained empirically.

2.2.5 Predictions of impact stresses

Intuitively, the contact stress has a large influence on the ground improvement. Estimates of this were of the first to be made, as this could then readily be input into a stress distribution formula. Jessberger and Beine (1981) proposed laboratory testing with an accelerometer attached to a falling mass to determine the relationship between the decelerations and the impact velocity. The constant of proportionality, α, was then used in the equation:

$$\sigma_{0,dyn} = \alpha \frac{m}{A}\sqrt{2gh} \qquad \text{(Eq. 2.7)}$$

where $\sigma_{0,dyn}$ =dynamic contact stress, *m=mass, A=base area of rammer, h=drop ht, g=9.81m/s²*

This shows that the contact stress is proportional to the impact momentum, since the impact velocity, $v = \sqrt{2.g.h}$, for a constant base area. Mayne (1983) proposed a slightly different form of equation, based on the integral of the area under measurements of the impact deceleration-time graph:

$$\sigma_z = \frac{V_s\sqrt{WHB}}{4(B)^2} \qquad \text{(Eq. 2.8)}$$

where *Vs=shear wave velocity, H=drop ht, B=contact dia., W=mass (t)*

The formula Mayne gives for the deceleration ratio (a/g), gives values close to what has been measured by Heyns (1998) on the tube axles of impact compaction plant (this is demonstrated in chapter 3):

$$\frac{a_{\max}}{g} = V_s\sqrt{\frac{HB}{W}} \qquad \text{(Eq. 2.9)}$$

where a_{max}=maximum acceleration of pounder, g=9.81m/s²

Lewis (1957) proposed an equation that related the contact stress to the impact energy:

$$p = \sqrt{\frac{1}{2}.mv^2.\frac{k_s}{A}} \qquad \text{(Eq. 2.10)}$$

where *m=mass,* v=*impact velocity, g=9.81m/s², A=base area, k_s= spring constant*

Therefore, to maintain a constant impact pressure the energy (½mv²) must be proportional to the square root of the base area (for a square base, proportional to the side dimension B). i.e it is difficult to keep the contact stresses down as the energy levels are raised as the compactor dimensions are generally fixed.

The critical parameters for determining contact stress are therefore the mass, the pounder base area, the drop height and the soil stiffness. The deceleration, impact velocity, energy and momentum are related to these parameters.

2.2.6 Predictions of dynamic stress profile

The proponents of the above contact stress predictions usually assumed some form of distribution of stress with depth to give a dynamic stress profile estimate. Jessberger and Beine (1981) proposed the following stress distribution based on Frolich's 1934 equation:

$$\frac{\sigma_{z,dyn}}{\sigma_{0,dyn}} = 1 - \left(\frac{z}{\sqrt{z^2 + r^2}} \right)^{v} \qquad \text{with } 7 < v < 15 \qquad \text{(Eq. 2.11)}$$

$\sigma_{o,dyn}$=contact stress (from equation 2.6), $\sigma_{z,dyn}$=stress at depth z, r=contact radius

Similarly, Mayne (1983) proposed the dynamic stress distribution:

$$\sigma_z = \frac{V_s \sqrt{WHB}}{4(B+z)^2}, \textit{variables defined in equation Eq 2.7 above} \qquad \text{(Eq. 2.12)}$$

The authors assume that having this information allows the likely compaction to then be evaluated. No guidance was found on how to convert the applied dynamic stress into effective compaction. It seems that it is assumed that the higher the stress and the deeper the stress profile, the better the compaction.

2.2.7 Prediction of residual stress profile

A method commonly used to predict the increase in horizontal stresses against retaining structures by compaction plant (Norvais Ferriera, 1983) shows the residual horizontal stresses after compaction (Figure 2.5). This method is usually used for the prediction of the increase in lateral stresses against retaining structures, but may also be used in compaction away from structures (Duncan et al, 1986).

The peak in the residual lateral stress diagram is a function of the assumed active and passive pressure lines and the applied dynamic stress profile.

This means that the larger the applied stress and plate/pounder size, the deeper the peak residual horizontal strain. As the method was aimed mainly at the prediction of residual stresses, no attempt was made to use the method for prediction of the compaction profile.

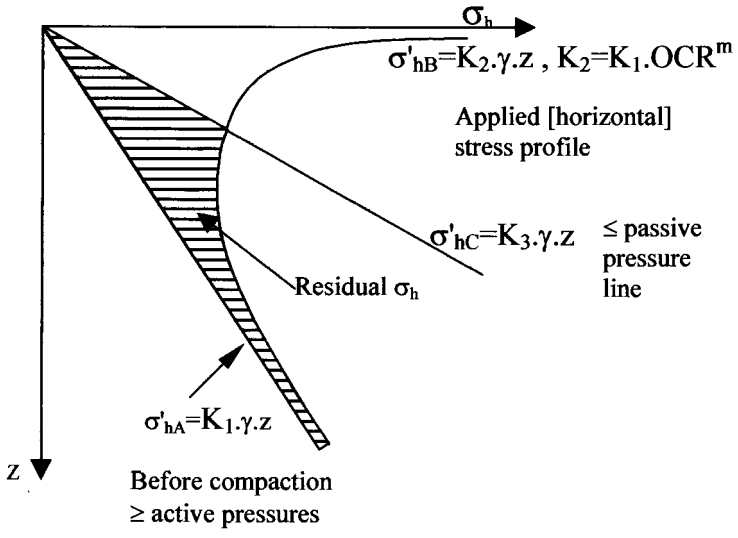

Figure 2.5: Predicted residual horizontal stresses after compaction (Novais Ferriera, 1983)

It is notable that the predicted profile appears to correspond to that found by Berry et al (Figure 2.2).

2.2.8 Prediction of void ratio reduction

Oshima et al (1997) proposed a model that predicts the degree of compaction achieved in terms of the relative density, D_r, based on model testing in sand. They showed that the improvement could be predicted in terms of the total momentum of the pounder:

$$Z = a_z + b_z \log(mvN)$$
$$R = a_R + b_R \log(mvN) \qquad \text{(Eq. 2.13)}$$

where Z=the vertical depth of improvement, R=radial improvement ,mvN=ram momentum, and a & b are empirical constants from laboratory testing.

The method was specifically aimed at dynamic compaction, and if used for the much lower energy/momentum levels of impact compactors, results in negative answers from below 15 passes of a 25kJ machine. With a different format of equation, the model may give better results. A notable omission from the model is the pounder base area. Empirical constants are available for changes in D_r of 40%, 20% and 10% respectively. This enables the bottom half of the profile of improvement to be drawn, including the depth of influence. The model does not predict the entire improvement profile, as the improvement immediately below the pounder is not evaluated.

A similar model was postulated by Poran et al (1992), based on total energy rather than momentum. The model equations are:

$$\frac{b}{D} = j + k\log\left(\frac{N.W.H}{A.b}\right) \qquad \text{(Eq.2.14)}$$

$$\frac{a}{D} = l + m\log\left(\frac{N.W.H}{A.b}\right) \qquad \text{(Eq.2.14a)}$$

where W=mass of pounder, A=base area,
j,k,l &m are empirical constants, H=drop height

The equations must be solved iteratively. The model does not incorporate the effect of the water table (testing was on dry sand), and specific correlation coefficients must be obtained relevant to the conditions under consideration.

Charles' solution (1978) for cohesive materials gives the lowest depth of influence predictions (see Figure 2.6), consistent with the known difficulty of compacting clayey materials. The behaviour is contrary to the other methods, as the depth of influence decreases with increasing pounder dimension (A_p=B^2):

$$D = 0.4\sqrt{\frac{E_d B}{A_p.c_u}} \qquad \text{(Eq.2.15)}$$

where E_d=energy, A_p=compactor base area, B=pounder width, and
c_u=undrained shear strength

2.2.9 Computer simulation based on the wave equation-profile of improvement prediction (Black box solution)

In a paper presented to the American Society of Civil Engineers, Chow et al (1992), gave the most comprehensive (and complicated) predictive model found in the literature surveyed. This method predicts the reduction in the void ratio as measured by the relative density D_r as well as the surface settlement (Figure 2.6).

Central to the method is a software program that solves partial differential equations of a non-linear (spring and dashpot) soil model that takes plastic behaviour of the soil into account.

Good correlation was found between predicted and measured parameters. It is again noteworthy that a peak appears in the improvement profile is also predicted by this model.

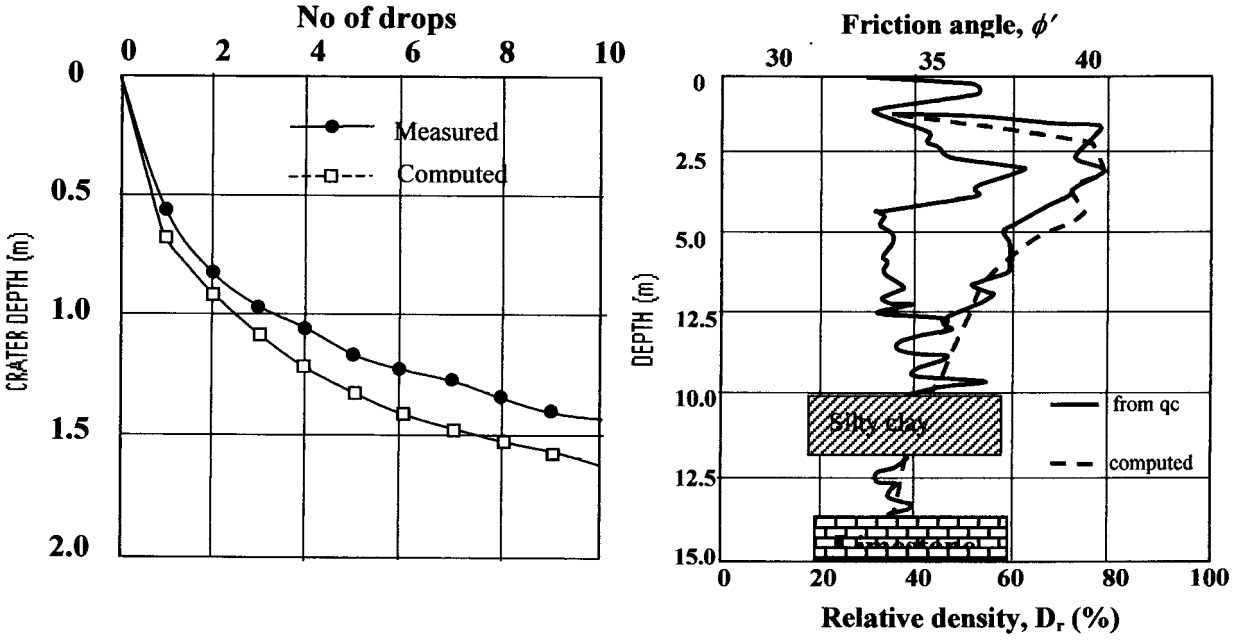

Figure 2.6 : Wave equation modelling of soil improvement (Chow et al, 1992)

The model could well be used to predict the behaviour of impact compactors, but has the following drawbacks:

- The modelling is complex: it requires a computer program to solve the wave equation model. This means that no understanding of the patterns of behaviour can be obtained without the use of the software. [i.e a black box solution].
- Laboratory testing is required to determine the "phenomenological" soil model.
- The spring and damping constants (k_s & c_s) have to be measured in the laboratory
- The soil springs behave in an elastic-perfectly plastic manner
- ϕ' is estimated from empirical equations [$\phi'=28+15.D_r$ (Meyerhof, 1976)]
- The ratio of vertical to horizontal stresses is estimated from empirical equations (the analysis is sensitive to this)-i.e the model is sensitive to the value of Poisson's ratio used.
- Clarity on the effect of the water table was not given
- The "measured" value of the relative density, Dr, was based on Dutch Cone point resistance values, q_c,and not block samples-i.e entirely empirical answers were obtained

The method is able to predict both the settlement and the reduction in void ratio as measured by the relative density [D_r], and then, using Meyerhof's empirical equation, an estimate of the increase in friction angle is made.

The same authors (Chow et al, 2000) performed a parametric study using the model developed and suggested the following equation to predict the crater depth for dynamic compactors:

$$d_c = \frac{E_B}{31.2 + 0.39E_B} - 0.125 \qquad \text{(Eq. 2.16)}$$

where d_c=crater depth (m) and E_B=input energy (ton.meters)

The authors then go on to give an estimate of the depth of improvement based on the energy input (E_B in ton.meters):

$$d_{max} = \frac{E_B}{5 + 0.075E_B} \qquad \text{(Eq. 2.17)}$$

These equations are valid for pounder base areas of between $3m^2$ and $4m^2$, and initial SPT penetration resistance of 1-15 blows/300mm.

This is the most comprehensive compaction modelling reviewed thus far.

Using the above equations for a 25kJ impact compactor yields a depth of influence of 3.7m and a crater depth of 0.62m, at 20 passes/blows (at one point). This is clearly an overestimation and the model is thus only applicable to the dynamic compactors for which it was developed.

Figure 2.7 shows a comparison of the various depths of improvement predicted by the models reviewed. The sensitivity of the Menard type equations to the empirical coefficient (n in Eq.2.2) is clearly shown.

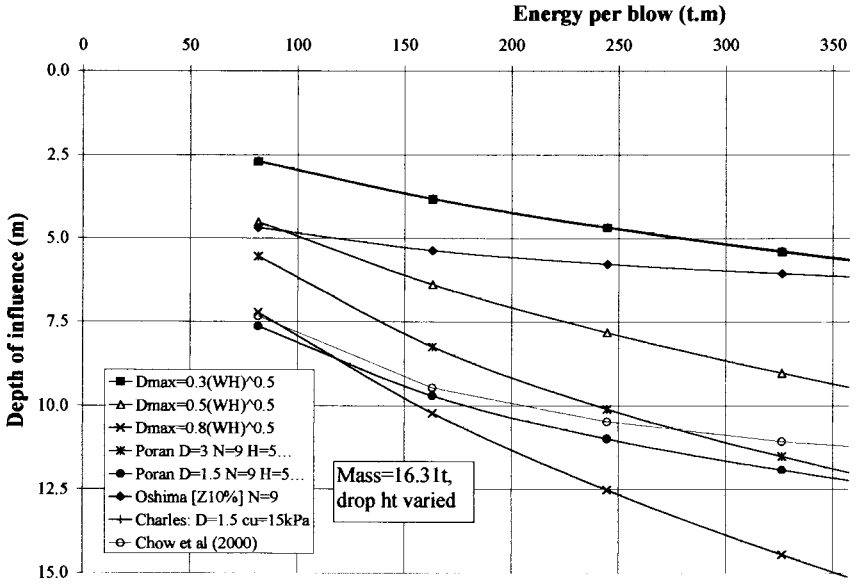

Figure 2.7 : Comparison of various prediction models – DC depth of influence

The figure shows a wide scatter in the predictions using the various models. This may be a result of the water table depth and the compactor contact area often not being considered. Also few of the models differentiate between soil types in their formulation. Only the model by Chow (2000) takes the soil consistency prior to compaction into account.

2.3 AN OVERVIEW OF PREDICTION MODELS USED IN CONVENTIONAL COMPACTION

2.3.1 INTRODUCTION

This section has been sub-divided into three parts. Firstly, the most common type of prediction model (that which assists the engineer to evaluate the likely success of the compaction equipment on a soil layer of standard/known thickness) is discussed. Then, models that take elasto-plasticity into account are looked at. Thirdly, some models that allow the achievable compaction, based on the soils characteristics, are reviewed. Lastly, appropriate, pertinent comments by experts in the field of compaction are given.

2.3.2 PREDICTIONS OF COMPACTOR PERFORMANCE

Biarez (1980) noted that an increase in density of the soil requires permanent deformation, which implies the yield stress is exceeded. Assuming an elastic perfectly plastic soil model (ϕ=0), this means that a pressure p=π.c (i.e 3 x cohesion) is required to compact the soil. He suggested that the bearing capacity formula be used as the permanent deformation reference stress:

$$q = \frac{1}{2}\gamma.B.N\gamma + c.N_c \qquad \text{Eq. 2.18}$$

with B= load contact width, γ=unit mass of soil, c=effective cohesion and N_c and N_γ are the bearing capacity factors.

The contact pressure and imprint width can be evaluated from Hertz's elastic formula:

$$p = \sqrt{\frac{Mg}{L.d}}.\frac{1}{2\sqrt{2}}.\sqrt{\frac{E}{1-v^2}} \qquad \text{Eq. 2.18a}$$

$$B = 2\sqrt{2}.\sqrt{\frac{Mg.d}{L}}.\sqrt{\frac{1-v^2}{E}} \qquad \text{Eq. 2.18b}$$

where B=compactor width (cm), Mg=mass (kg), L=contact length (cm), E =elastic stiffness (units not given), v=Poisson's ratio, d=diameter (cm)

Biarez further suggested that the layer thickness be restricted by the vertical stress at the bottom of the layer and that this thickness be calculated from:

$$z = 0.3\sqrt{Mg} \quad \text{with } Mg \text{ in kg, z in cm} \qquad \text{Eq. 2.18c}$$

Inherent in this thinking is the assumption that the compaction is proportional to the contact stress (assumed to be 8 bar in Eq. 2.18), it's magnitude, and the contact area. The above equation yields a 31cm layer thickness for an 11000kg roller.

Yoo and Selig (1979) proposed the use of a coefficient of compaction (fc) for the evaluation of vibratory roller performance and amount of compaction.

The performance prediction model is based on a dynamic analytical model as shown in Figure 2.8, the output of which is the transmitted dynamic force Ft.

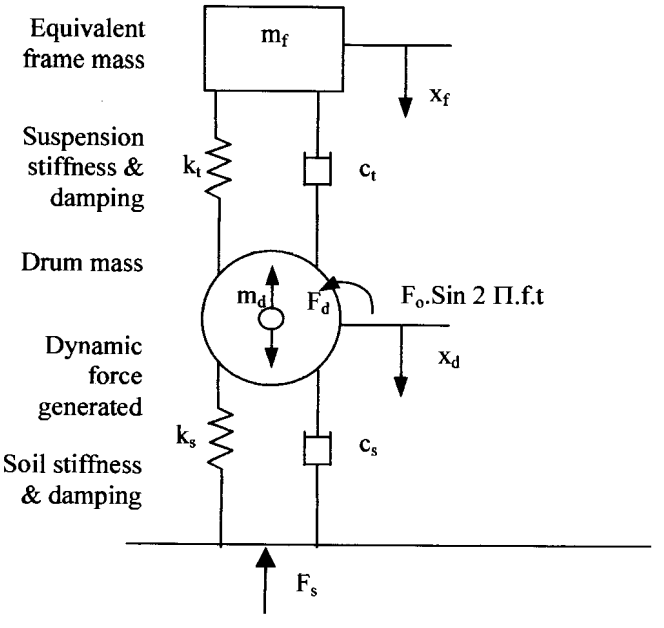

Figure 2.8: Dynamic analytical vibratory compaction model (Yoo & Selig, 1979)

An important finding of this work was that although the generated force can theoretically be increased with increasing vibration frequency (within the limits of the mechanical strength of the machine), the transmitted force reaches a maximum value and then decreases (Figure 2.9).

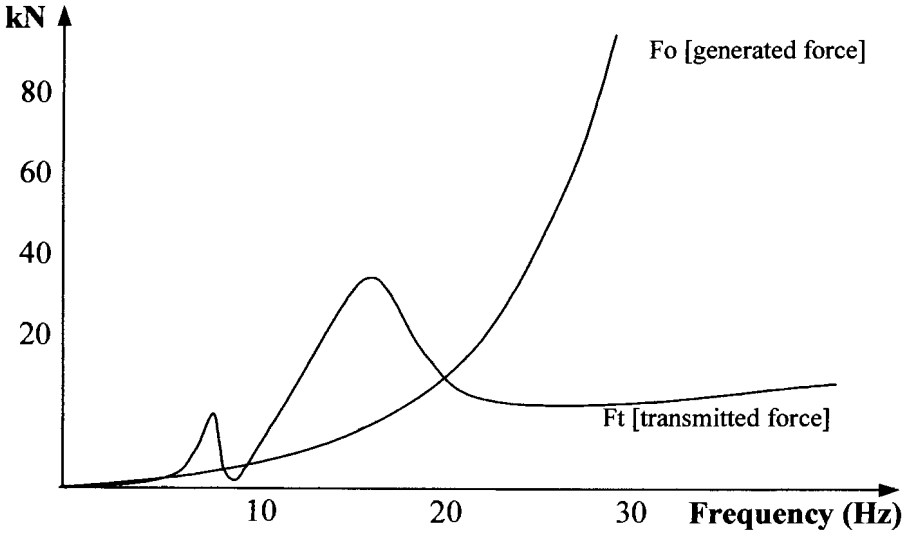

Figure 2.9: Dynamic forces in vibratory compaction (Yoo & Selig, 1979)

The authors conclude that the "possibility of developing relationships between roller motions and the amount of compaction" exists. They note that the main roller characteristic appears to be the drum displacement during vibration.

At the International Conference on Compaction the following year in Paris Yoo (1980) noted that the dimensionless coefficient of compaction f_c is given by the expression:

$$f_c\left(\frac{W}{B}\right) = f_s\left(\frac{W}{B}\right) + f_d\left(\frac{f.A}{s}\right) \qquad \text{(Eq.2.19)}$$

where W=mass (kN), B=contact length (m), A=occilation magnitude (m), s=travel speed (m/s) and f= vibration frequency (Hz), f_s=static coefficient, f_d=group dynamic coefficient

This coefficient of compaction "relates roller mass, roller width, number of roller passes, and compacted layer thickness to the roller compactive effort per unit volume". Values of f_d are obtained from field tests and f_s from compaction tests without vibration. The value of A is calculated from the model given in Figure 2.8. The paper concludes that the amount of compaction is a function the two components on the right hand side of equation 2.19: the first representing the static linear load (SSL) and the second a group dynamic parameter (f.A/s). From these parameters a conventional compactor's performance can be evaluated.

The French (LCPC, 1986) now classify compactors according to the product of the static linear load and the theoretical amplitude:

$$\frac{M1}{L}.\sqrt{AO} \qquad (2.20)$$

"where *M1*=total mass fitting over the generator of a cylinder (kg), *L*=cylinder length in cm [*M1/L=SSL*] and *AO*=theoretical amplitude = 1000 *m.e / MO*, where *m.e*=moment of the eccentric stage of the shaft of unbalance, *MO* is the mass of the vibrating part attached to the shaft of unbalance".

Compactors are then grouped from V1 to V5 types, according to this product. A V1 compactor is for shallow compaction and a V5 compactor for deep compaction (Dunn, 2000). The grouping takes into account the average achievable density throughout a layer as well as the average density of the bottom 8cm of the layer, as shown in Figure 2.10.

pdm = average dry volume mass on the whole thickness of the compacted layer

pdfc = average dry volume mass over the bottom 8cm of the compacted layer

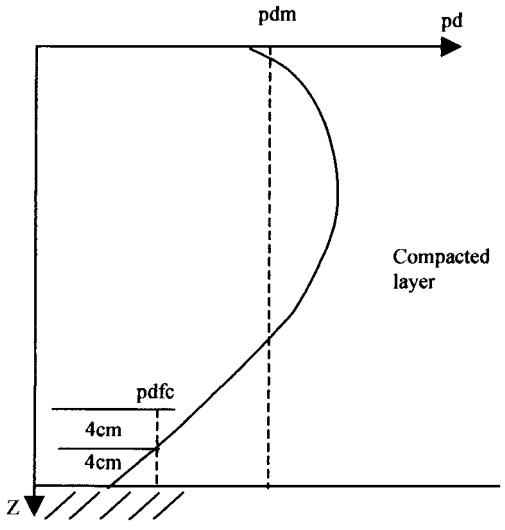

Figure 2.10 : Definitions used in French compaction literature (LCPC, 1986)

The prediction is therefore one of the ability of the compactor to achieve minimum values of pdm and pdfc. It is also clear that a peak in the density profile occurs below the surface, after which the density drops off quite rapidly.

It is interesting to note that the shape of the density profile depicted in Figure 2.10 is one that appears in many of the results given in the literature. None of the literature reviewed discusses the mechanisms that cause this typical profile.

With the advent of continuous compaction control (CCC), some sophisticated models are becoming available. Recent work by Adam and Kopf (2000), incorporates complex predictions that allow both conventional oscillatory and horizontally adjusted *VARIO* rollers to be evaluated. The authors use the substructure method to evaluate the dynamic soil-structure interaction, whereby the various components are evaluated separately while ensuring compatibility is satisfied. The soil substructure is modelled as a translational cone as shown in Figure 2.11.

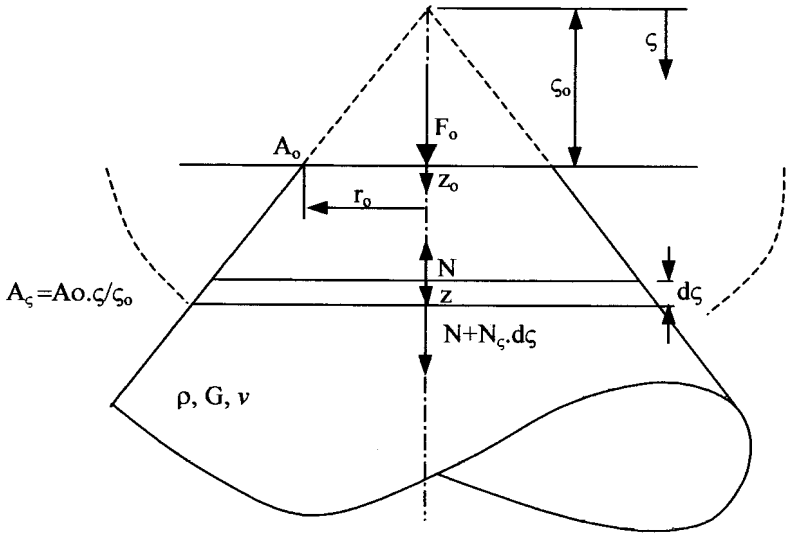

Figure 2.11 : Soil substructure as a translational cone (Adam and Kopf, 2000)

Horizontal motions can be accounted for in a similar fashion. Dynamic equilibrium is achieved using the wave equation. The model gives equations for the spring and dashpot coefficients, *K* and *C*. Non-cohesive soils are modelled separately from cohesive soils. In doing so, the authors note that the Poisson;s ratio for non cohesive soils is typically between 0.25 and 0.35, while for cohesive soils, it increases from 0.33 to 0.5. In the contact zone "elastic behaviour is no longer sufficient to describe the behaviour of soil correctly". Compaction is said to take place in a "plastic zone" that is "embedded within the contact area". Total displacement consists of both elastic and plastic parts, z_o and z_p.

A new parameter is introduced called the plasticity parameter, ε, defined by:

$$\varepsilon = \frac{k^p}{K + k^p} \qquad \text{Eq. 2.21}$$

The plasticity parameter ε, varies from 0 to 1 as the soil varies from entirely plastic to perfectly elastic in behaviour (Figure 2.12). The parameter ε, is a new plasticity parameter derived from the ratio of elastic to total strains:

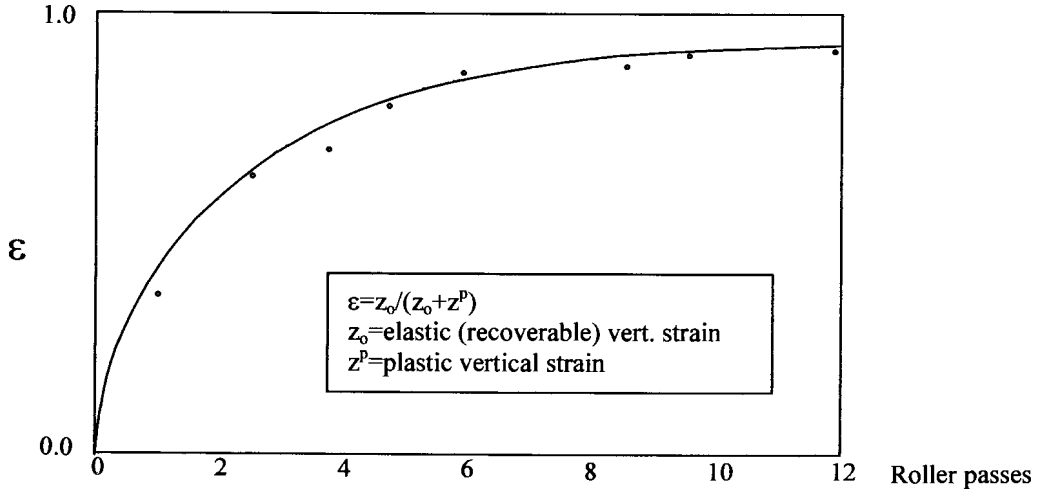

Figure 2.12 : Variation of plasticity parameter ε with roller passes

The result of the model is the ability to predict continuous compaction control parameters (OMEGA, CMV and RMV). Although these parameters are indicators of compaction, the soil improvement profile is not predicted.

Hussein & Selig (1980) predict the performance of a compactor and give equations for the towed force, the compactive effort, the compactive effort per unit volume, the rate of compaction and finally, the power required. The prediction uses the coefficient of compaction, f_c, described above:

$$H = d.f_c.W.S \qquad \text{Eq. 2.20}$$

where d=units conversion factor (HP/(N.km/hr)=3.8×10^{-4}, W=mass (N), S=speed (km/hr), H=power required (horsepower)

Again, due to the nature of conventional compaction, thin layers are invariably used, which results in the assumption that the density is approximately constant throughout the layer. The above model therefore predicts the power required to achieve a constant average density through the layer being considered.

2.3.3 COMPACTION MODELS

2.3.3.1 *Stress based models*

Spangler and Handy (1982) noted that compaction must avoid dilation of the soil and thus the mean normal effective stress (p) must increase without allowing the maximum effective shearing stress (q) to exceed the line indicated by the K_f line (Figure 2.13). i.e if the apex of the Mohr circle is below the K_f line, behaviour is perfectly elastic.

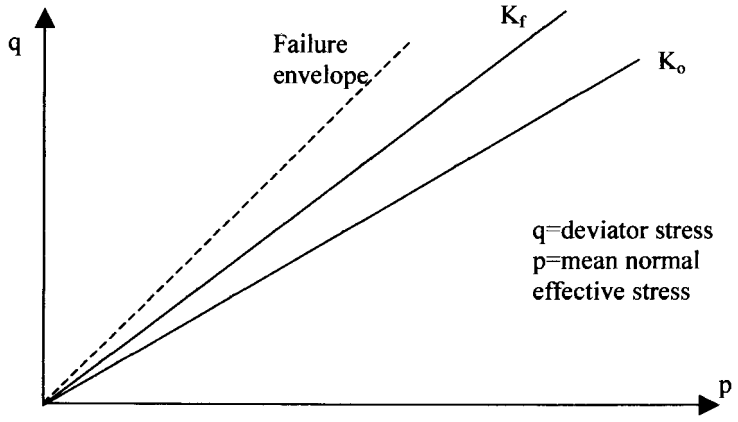

Figure 2.13 : Mohr Coulomb lines indicating elastic or plastic behaviour (Spangler & Handy, 1982)

They note that "during the initial stages of compaction, soil will start at or above the critical void ratio, so the Kf and Ko lines will coincide, and the maximum allowable q will be low. … but on successive passes, the Kf line will be higher and shearing stresses tolerated without dilatancy." They continue to state that one of the main problems with compaction is that the lateral stresses dissipate more rapidly with depth than the vertical stresses do.

A stiff base assists in ensuring that the vertical and horizontal stress difference is reduced. This allows compaction zones to form at the top and bottom of the layer, as shown in Figure 2.14.

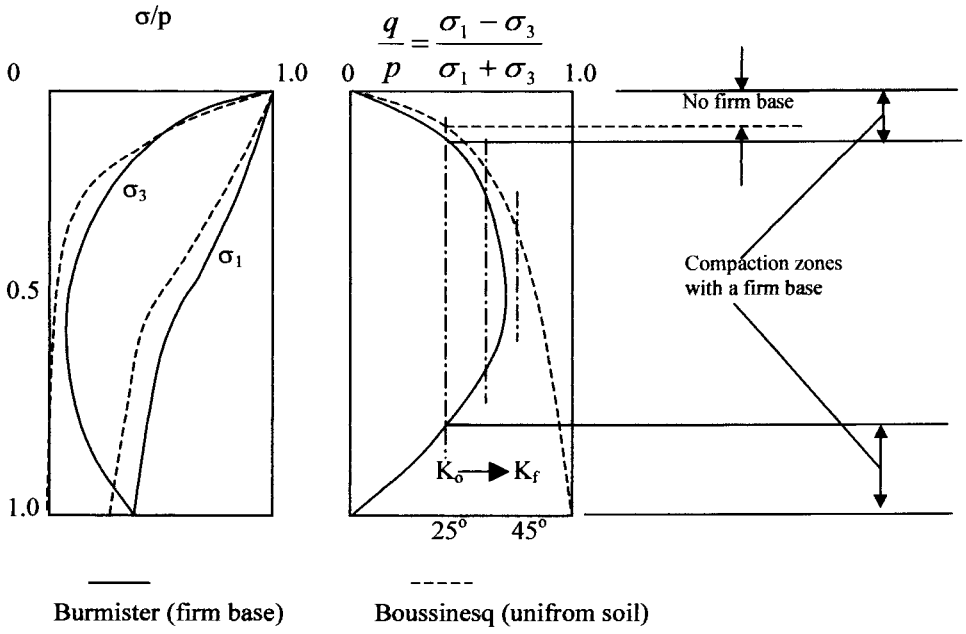

Figure 2.14: Compaction mechanism according to Spangler & Handy (1982)

With successive passes, this theory suggests that the compaction works it's way to the center, with the bottom compacted zone effectively becoming part of the "firm base" after each pass. It is noteworthy that if there is no firm base then compaction only takes place from the top down, according to this model. The material is thus assumed to behave plasticly only if the Mohr Coulomb failure criteria is satisfied (i.e perfectly elastic behaviour inside the yield surface).

2.3.3.2 *Strain based models*

Ullah and Selig (1980) assumed that the volumetric strain equals the vertical strain (zero horizontal strains) and suggested the following equation for predicting the density increase under a vibratory plate compactor on a 152mm layer:

$$\gamma = (1+\varepsilon)\left[\frac{\gamma_f}{1+\varepsilon_f}\right] \qquad \text{Eq. 2.21}$$

where γ = density of soil after any pass (kg/m^3), ε = soil strain after any pass, γ_f = soil density after 16 passes (kg/m^3), ε_f = soil strain after 16 passes

This confirms the intuitive observation that the degree of densification is proportional to the surface settlement. The predicted density is the average measured over the layer thickness. Hence the authors assume that the strain is evenly distributed throughout the layer.

The relationship between settlement and density was confirmed by Forssblad (1980b) when investigating the compaction meter for improved compaction control. The data from his paper is re-plotted with the x axis on a natural scale instead of a log scale, in Figure 2.15.

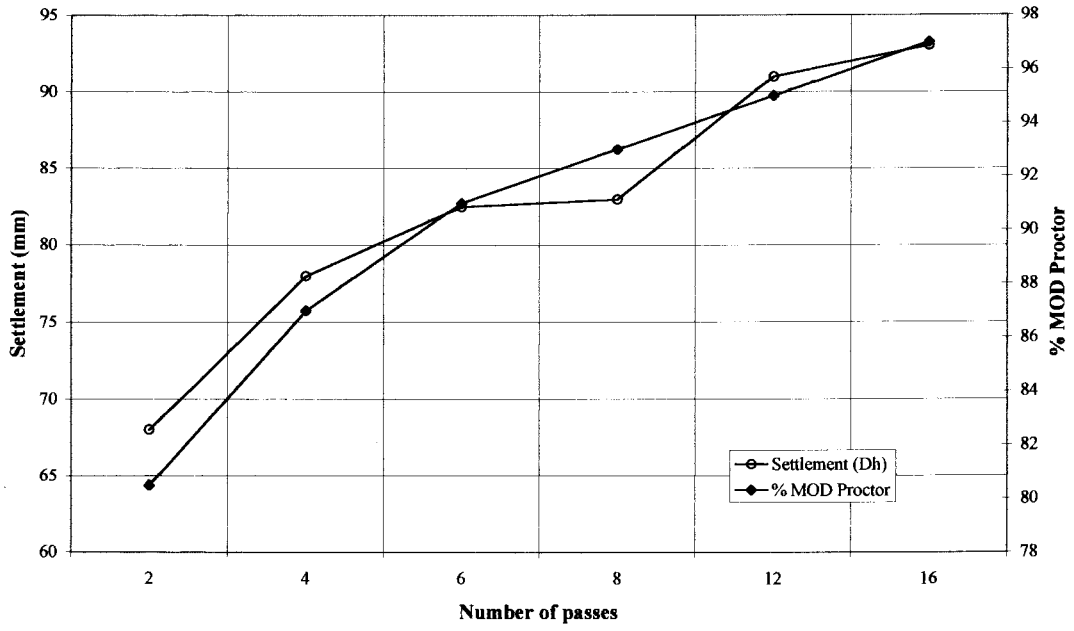

Figure 2.15: Relationship between surface settlement and density (Forssblad, 1980b)

A clear correlation between settlement and the compaction meter value is also seen in Figure 2.16:

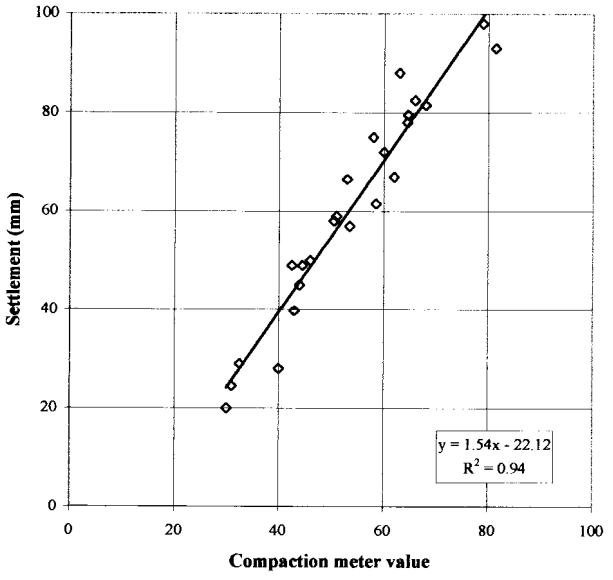

Figure 2.16: Relationship between surface settlement and compaction meter values (Forssblad, 1980b)

The implication of Figure 2.15 is that reliable and accurate measurement of the surface settlement (permanent/plastic strain) is just as good as fitting compaction meters to the compaction equipment. It is interesting to note that both impact compaction contractors and dynamic compaction contractors use settlement as an indicator of when compaction should cease.

2.3.3.3 *Work done based models*

Lytton (1999) has proposed a model that relates the dry density of a soil to the volumetric water content, θ, and the soil suction pressure. The equation is of the well known form:

$$\gamma_d = \frac{G_s.\gamma_w}{1+\theta\left(1+a.|h|^m\right)} \qquad \text{Eq. 2.22}$$

where γ_d=dry density (kg/m^3), h=soil suction head (m), a & m are constants

G_s=soil unit mass (kg/m^3), γ_w=unit mass of water (kg/m^3)

An equation relating the cumulative plastic strain to the cumulative dissipated strain energy is also given:

$$\varepsilon^p = \theta_a.e^{-\left[\frac{\rho}{N.\Delta E}\right]^\beta} \qquad \text{Eq. 2.23}$$

where θa=volumetric air content, ρ = a scale factor, β= logarithmic rate of work hardening

The shape of the curve given by equation 2.23 is similar to that given by Adam and Kopf in Figure 2.12 above. There appears to be consensus, therefore that the magnitude of plastic strain decreases with increasing compactive effort.

2.3.3.4 *Hysteresis and cyclic loading models*

Yandel (1971) proposed a mechano-lattice analogy to predict the permanent deformation and the development of residual stresses in road materials. The prediction was aimed mainly at the post construction evaluation of roads. The model takes the hysteresis into account by using different loading and unloading moduli, as shown in Figure 2.17:

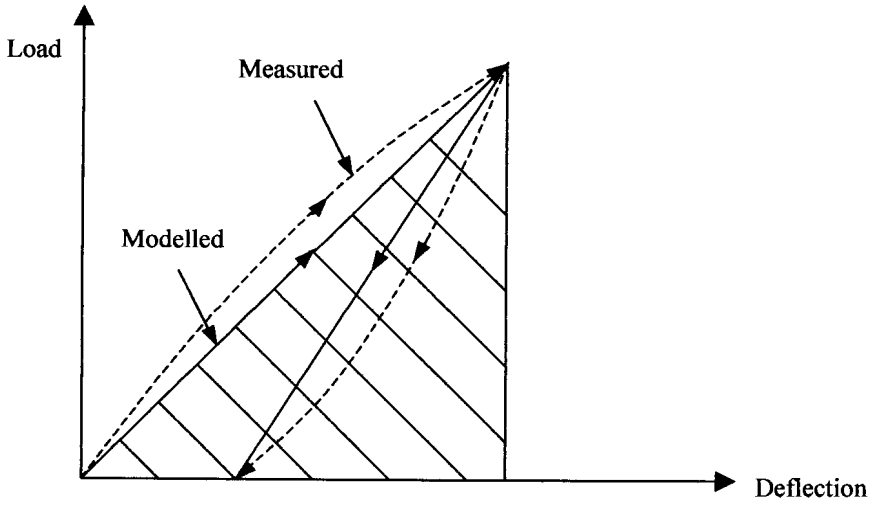

Figure 2.17 : Modeling of hysteresis (Yandell, 1971)

This is then incorporated into either a plane strain or three dimensional mechano-lattice grid to perform the calculations. In addition to permanent deformations, the model allows prediction of residual horizontal stresses, as shown for a thin asphalt layer rolled with a pneumatic tyre in Figure 2-18.

The presence of these residual horizontal stresses cannot occur without the presence of residual horizontal strains. The vertical residual stresses are almost zero.

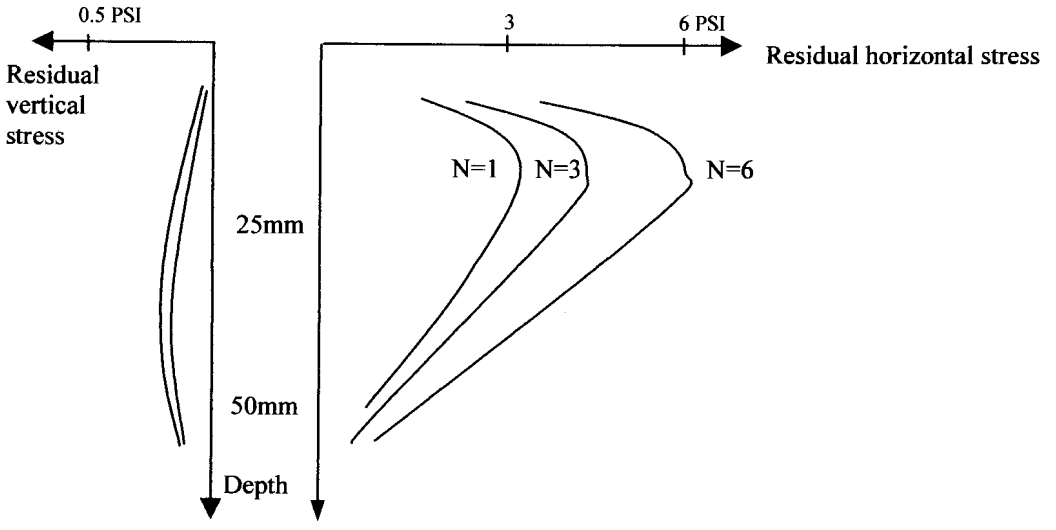

Figure 2-18 : Residual horisontal stresses from mechano-lattice model (Yandell, 1971)

Sawicki and Swidzinski (1990) developed a finite element method that predicts compaction beneath repeated wheel loads. The model is solved numerically by calculating the maximum strains in the subsoil, from which the second invariant of strain amplitude deviator is calculated:

$$J = \frac{1}{3}\left[\left(E_x - E_y\right)^2 + E_x.E_y\right] + E_{xy}^2 \qquad \text{Eq. 2.23}$$

where E_x, E_y and E_{xy} are components of the maximum strain tensor in MPa, corresponding to the maximum load, P.

The compaction , Φ, is given by the constitutive equation:

$$\frac{d\Phi}{dN} = D_1.J.e^{-D_2.\Phi} \qquad \text{Eq. 2.24}$$

where D_1 and D_2 are obtained in the lab, N=number of load repetitions

The settlement is then calculated from:

$$S = \frac{n_0}{1-n_0}\int \Phi.dy \qquad \text{Eq. 2.25}$$

where n_0=initial porosity

Sawicki and Swidzinski (1989) describe a common compaction curve (Figure 2.19) which in their opinion play "a fundamental role in the mechanics of granular materials subject to cyclic loadings, as one of the basic characteristics of granular soils".

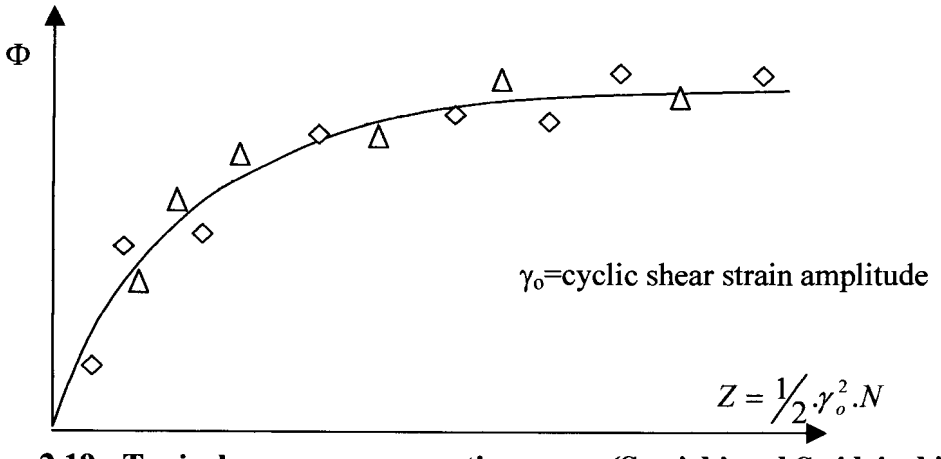

Figure 2.19 : Typical common compaction curve (Sawicki and Swidzinski (1989)

The compaction Φ, is a measure of the irreversible porosity decrease. There is some similarity between Figure 2.19 and the enforced strain diagram proposed by Kwang et al (1990) (Figure 2.4).

Intergration of the distribution of J with depth then leads to the formula,

$$\Phi = C_1.\ln(1 + C_2 J.N) \qquad \text{Eq. 2.26}$$

(where C_1 & C_2 are laboratory determined constants, N=No. of loading cycles) from which "the irreversible volume changes can be computed".

The paper does not show a distribution of the compaction Φ with depth, for vertical cyclic loading, so no indication of the predicted distribution of compaction with depth could be extracted.

A cyclic loading model based on Cam Clay theory, has been presented by Muir Wood (1991). The author notes that simple models do not allow for energy dissipation for states that fall within the yield surface. A "Bubble" model is suggested as one of the solutions to the problem, whereby sub-yield surfaces

within the ultimate failure surface are used. The modelling is complex and no global patterns of improvement in the ground can be easily gleaned from the theory.

2.3.3.5 *Semi-empirical models*

Marr and Christian (1981) give a semi empirical prediction of the settlement of structures based on the accumulated volumetric strains 'on a system" using the following equation:

$$\varepsilon_{vc} = 3.6\left(\frac{\tau_{cy}}{\sigma_{no}}\right)^{3} 2.5^{\log N} \qquad \text{Eq.2.27}$$

where τ_{cy}=cyclic shear stress (kPa), σ_{no}=mean consolidation normal stress (kPa) and N = number of cycles

The predicted versus measured settlements show good agreement. No distribution of the cumulative volumetric strains with depth is given.

O'Riordan (1991) also noted that the surface behaviour (settlement) of silos and circular storage tanks can typically be estimated from:

$$\delta_t = \delta_i 1.5^{\log N}$$

Eq 2.28

where δ_i = initial settlement (mm), N=number of filling/emptying cycles

Some reasonable estimates of cyclic surface settlement therefore appear possible, but none of the predictions discuss the distribution of the strains below the surface.

The models discussed below are not compaction models in the sense that the predictions are of post-construction deformations in road pavements. They are never-the-less reviewed as they show methods that could be adopted for use in compaction modelling.

Wolff and Visser (1994) noted that "permanent deformation takes place with every load repetition, although traffic loading normally induces stresses far below the failure stress of the material defined by the Mohr-Coulomb failure envelope".

In view of this fact, a model was proposed based on extensive measured data from Heavy Vehicle Simulator (HVS) testing that more realistically predicted the pavement deformation at a large number of load repetitions. The model relates the bulk stress θ, at the centre of the layer being considered, to the expected deformation of the layer. The deformation of a specific layer was found to be represented well by an equation of the following form:

$$y = (m.x + a)(1 - e^{-bx}) \qquad \text{Eq. 2.29}$$

where x is the number of load repetitions, y=permanent strain in the layer and a,m, and b are regression constants

The model allows the average strain in a particular layer to be estimated based on the average bulk stress level at the centre of the layer. A summation of the plastic vertical strains predicted for each of the pavement layers then gives the surface deformation.

Lotfi et al (1988) proposed a model whereby the permanent strain at the top of the subgrade of a road could be calculated at any stage of the cyclic loading cycle. The loading modulus E_{lo} is assumed to stiffen continuously according to the equation:

$$E_{lo} = \frac{Mr}{1 + \mu.N^{\alpha}}$$

where $\mu = \frac{ab}{\varepsilon_r}$ and $\alpha = 1 - b$, ε_r = resilient vertical strain (a and b are two new material parameters) Eq. 2.30

The resilient (rebound) modulus, M_r, is assumed to remain constant throughout.

The stiffening model is shown in Figure 2.20:

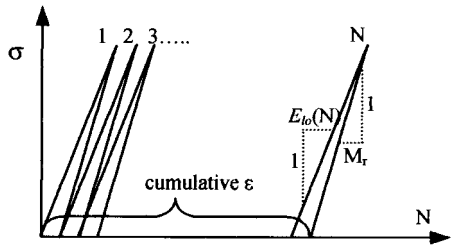

Figure 2.20 : Calculation of cumulative plastic strains at top of subgrade (Lotfi et al, 1988)

The model was found to provide good estimations of subgrade rutting. Charts are given that show the influence of compaction on the anticipated deformation of the pavement. The model is semi-empirical as the constants are obtained from test data. No distribution of the vertical strains with depth is given.

2.3.4 PREDICTION OF ACHIEVABLE COMPACTION BASED ON SOIL CHARACTERISTICS

The models found in this category generally make the assumption that density is achieved by using sufficiently thin layers and adequate energy per unit volume. The models are based on the standard soil classification tests.

Wang and Huang (1984) presented a model that predicts the maximum dry density and optimum moisture content of a soil based on the grading (D_{10}), fineness modulus (FM), plastic limit and uniformity coefficient (U) of the material. The equations are as follows:

Maximim dry density model: [R^2=0.954]

$$\frac{\gamma_{d\max}}{\gamma_{bulk}}.100 = 45.6 - 1.28\overline{FM}.\log(D_{10}) - 4.4.10^{-2}\overline{FM}.\overline{PL} + 1.43.\overline{FM} \qquad \text{Eq. 2.31}$$

Optimum moisture content model: [R^2=0.886]

$$w_{opt}.100 = 2.614 + 12.7\overline{PL} - 95\overline{FM}^2 - 88.1\log^2 U \qquad \text{Eq. 2.32}$$

The authors also give equations for estimating the 90% relative bulk density.

Semmelink and Visser (1995) proposed the use of a similar model that uses the standard classification test information such as the grading and plasticity data, as well as two new tests, the Shakedown Bulk Density (SBD) and Weighted Fractional Density test (WFD). Their model allows the prediction of the optimum compaction moisture content as well as the maximum dry density achievable over a spectrum of moisture contents, as shown in Figure 2.21.

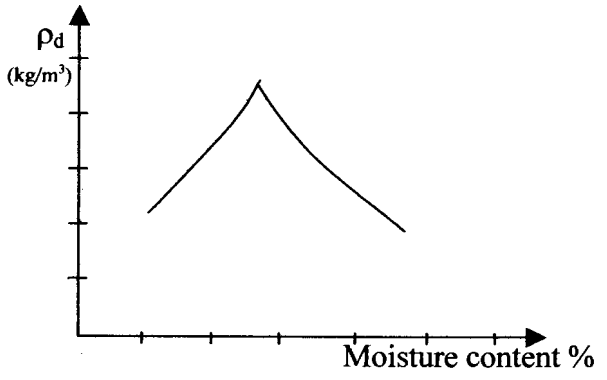

Figure 2.21 : Typical output from Semmelink and Visser (1994) model

The authors conclude that "nearly all design parameters required for road building materials could be obtained from the grading after compaction, LL, LS, SBD, SF (or WFD)". The model is designed to indicate what is achievable with a particular material and therefore does not predict any distribution of compaction through a layer compacted. The SBD and WFD tests may prove useful in a predictive model for compaction, though, as the tests can be used to give the minimum and maximum void ratios of compacted materials. The regression models could also prove useful.

2.3.5 OBSERVATIONS BY EXPERTS

Forssblad (1980a) noted: "When the degree of compaction is successively increased the soil is getting more and more solid and elastic, and, as already said, the theories of Boussinesq can be used with good results, to calculate for example the compaction effect of a pneumatic-tyred roller. Also at vibratory compaction the stress distribution, at least approximately, can be calculated according to the theories of Boussinesq. The reason that the dynamic stresses can be calculated according to the same rules as the static is that the impulse times at vibratory

compaction, around 0.01 to 0.02 seconds, are of such a comparatively low magnitude that the distribution of the dynamic loads is rather similar to the distribution of the corresponding static loads".

Selig (1980) made the following remarks at the same conference: "compaction is the process of producing strains. More specifically, it's the process of producing volumetric compression. Therefore measurement of strain will indicate the amount of compaction. The percent change in density from compaction is equal to the percent volumetric strain which is the sum of the three principal strains". Prof. Selig also noted that the compaction strain measured using induction coil strain measurements showed most of the strains in vibratory compaction were vertical.

2.4 CONCLUSIONS

Little information was found in the impact compaction literature that could assist in a prediction model for ground improvement using impact compaction plant. This is probably due, apart from the complexity of the problem, to impact compaction only being used in a few countries throughout the world to date. This is changing however, and research is currently underway locally, in Australia, and in China.

The dynamic compaction literature survey produced some useful models, although the bulk of the work has ignored the contact area of the rammer, which is a critically important parameter. The work of Chow (1992) indicates that the use of the wave equation and a phenomological model give good results for computer based solutions using finite element analysis. A parametric study of the variables by the same authors (Chow et al 2000) resulted in settlement and depth of improvement prediction equations based on the energy input. Unfortunately the paper does not assist in the understanding of the mechanisms at work, other than to note that the wave-equation is suitable for the modelling of the compactor-soil interaction. The work of Wallays (1983) and Poran and Rodriguez (1992) appear to be the most promising in terms of assisting in the understanding of the mechanisms at work.

Most of the modelling surveyed did not clearly differentiate between saturated and unsaturated conditions.

The literature covering conventional compaction only predicted compactor performance over a limited depth layer, assuming a constant density throughout the layer thickness.

This is probably due to much of the research being undertaken by manufacturers, who are mostly concerned with productivity. This is no doubt also the driving force behind the amount of work that has gone into the development of compaction meters that is installed in many of these compactors today.

The recent theoretical approach proposed by Lytton et al (1999), relating the dissipated strain energy is promising, but full details are not currently available.

The work done by Sawicki and Swidzinski (1990) and Yandell (1971) on cyclic loading and hysteresis effects, although being computer based and thus tend to be black box solutions, could be used to evaluate general patterns that could simplify the understanding of the compaction process.

The model given by Spangler and Handy in Figure 2.12 is believed by the author to be the opposite of what actually happens in practice. The high stresses in the top layer do not generally lead to compaction, but dilation and decompaction. This has been observed in much the test data surveyed in this study. It is therefore of utmost importance to correlate the theory with observation of field behaviour.

Consensus was found in the proposed models, that the incremental increase in compaction decreases with increasing compactive effort. A negative exponential form of equation was commonly used to model this effect. The strong correlation between surface settlement and compaction achieved was confirmed in the review.

None of the literature surveyed was found to contain a prediction model based on surface settlement. The patterns observed in the field test data for both impact and dynamic compaction were similar to that noted by Lukas (Figure 2.2).

The model proposed in this dissertation attempts to offer some explanation for these patterns and a simple means of estimating the void ratio reduction possible.

CHAPTER 3

COMPACTOR FORCE MEASUREMENTS

3.1 INTRODUCTION

In order to estimate the applied pressure in the numerical analysis (undertaken in Chapter 4) the typical range of decelerations of the masses of the impact compactor drums during the compaction process is required. From the deceleration measurements maximum and minimum strains and the depth of influence of the compactors can be estimated (Chapter 4). Knowledge of the input force is also useful for comparison with other compaction plant.

3.2 PREVIOUS WORK

As mentioned in section 2.1, Heyns (1998) undertook a detailed analysis of the three sided and five sided impact compactors using a MATLAB model to estimated the energy imparted to the soil. This was backed up by accelerometer testing on one site. Good agreement was achieved between the estimated and measured accelerations in this study. The results showed a deceleration of the three-sided compactor of 186 m/s^2 (19 g's) on hard ground.

Heyns showed that the imparted force increases with the speed at which the compactors are towed (Figure 3.1).

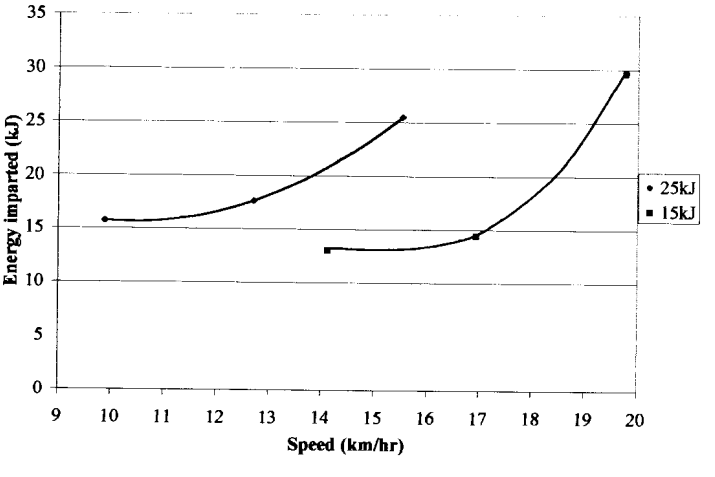

Figure 3.1 : Variation of imparted energy with towing speed (Heyns, 1998)

In his overview in the report Heyns noted that "this work is based on a multi-body dynamics approach, (which) entails that the system be modelled in terms of rigid bodies, connected to one another by means of arbitary non-linear springs and dampers, as well as constraints such as common points, or light rigid rods." He goes on to say that "the system response is found by Runge-Kutta time domain integration of system equations of motion under the influence of time-varying state dependant external variables." He verified the model by comparing simulated responses with measured accelerometer readings. For the parameters assumed in the MATLAB model, it was found that the machines must be towed at about 12 to 17km/hr to achieve the rated energy levels. The 14km/h recommended by the manufacturers is in the middle of this theoretical range.

3.3 AIM OF THE CURRENT TESTING

The objective of this additional testing was to ascertain the *range* of decelerations that are likely over the range of soil stiffnesses encountered. This is necessary as the decelerations are higher in a stiffer soil and lower in a soft soil. From this information, a typical average impact force can be estimated for use in a numerical analysis.

3.4 EQUIPMENT USED

The three standard Landpac impact compactors were used, namely the 10kJ, 15kJ and 25kJ machines. A PCB 353B14 shear accelerometer capable of measuring up to 1000g's was used. The data was collected via a Quatech 16 bit DAQP-16 A/D card with 16 channels capable of measuring up to 100kHz.

Measurement was typically done at 5kHz-10kHz to ensure sufficient definition in the result as the peaks were expected to be quite steep. The data and calibration sheet of the accelerometer and A/D card are given in Appendix C.

3.5 SITE SELECTION

Two sites were selected in the Nigel (South Africa) area close to NCS Engineering, were the machines are manufactured. The first site was chosen due to the presence of a shallow ferricrete layer (at about 600mm below ground level), which represents a very hard subgrade. The site was already well compacted by testing of the impact compactors. The second site was located about two kilometres from the first on very soft, loose hillwash material, with the ferricrete nodules only appearing at 1.6m and becoming hardpan at a depth of about 2.4m. Figure 3.2 shows the site positions.

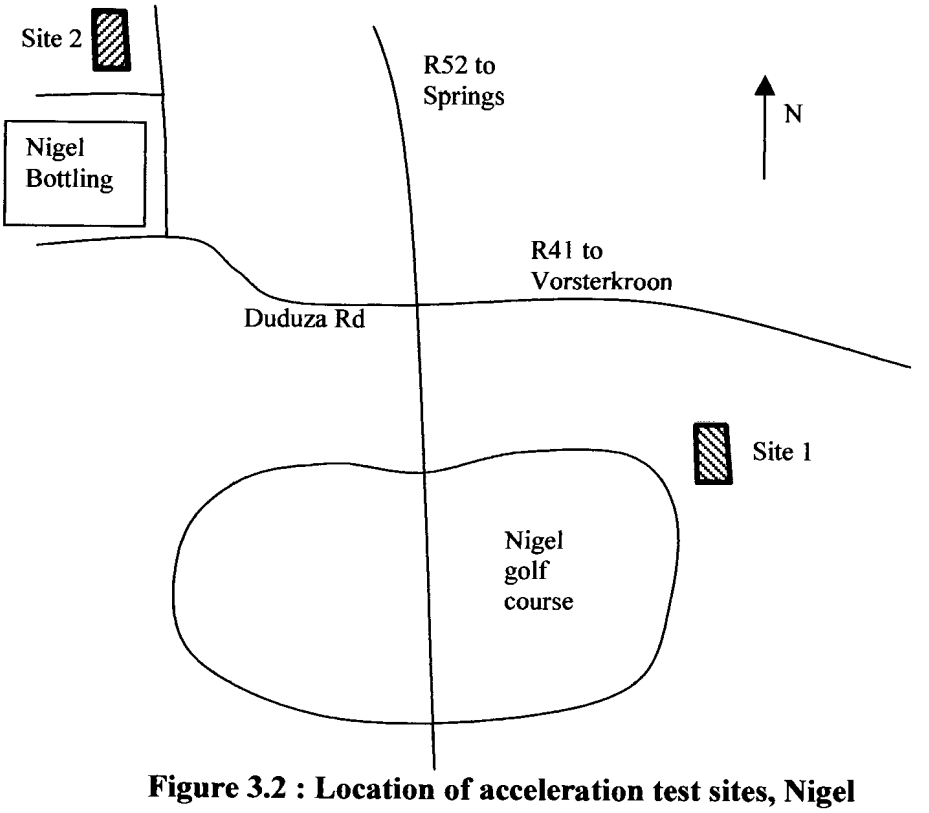

Figure 3.2 : Location of acceleration test sites, Nigel

3.6 ESTIMATION OF ACCELERATIONS USING MAYNE (1983)

In order to estimate the magnitudes of the decelerations of the machines, the method proposed by Mayne (1983) for dynamic compaction was used. The results, shown in Figure 3.3, seem quite reasonable and appeared to confirm the values predicted and measured by Heyns (1998).

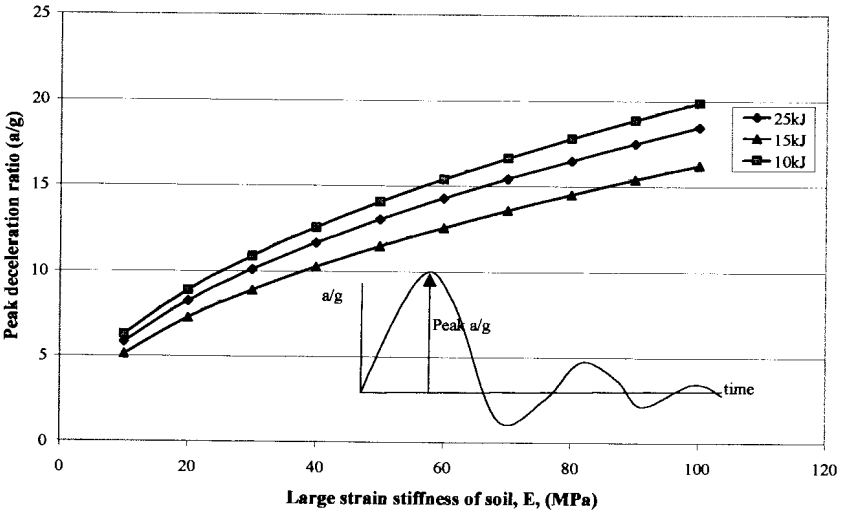

Figure 3.3 : Estimation of decelerations of impact compactors (Mayne, 1983)

The PCB accelerometer available was capable of measuring up to 1000g's to an accuracy of 0.1g. Although the instrument was being used at the bottom of the scale, the results were deemed sufficiently accurate for the purposes of the study.

3.7 PRESENTATION OF TEST RESULTS

Table 3.1 shows typical deceleration ratios measured.

Table 3.1 : Measured deceleration ratios (a/g)

	Soft ground (10-15MPa)	Hard ground (±75MPa)
10kJ	6.9	10.2
15kJ	5.2	14.2
25kJ	5.4	17.4

The pattern of decelerations measured on soft ground conforms to that predicted in Figure 3.3. The 10kJ impact compactor values appear low and do not conform to the predictions using Mayne's method. This may be due a slower speed than required.

The deceleration of the 10kJ is higher that the 15kJ machine due to it's lighter mass. Examination of Maynes formula will clarify this behaviour.

Measurements taken when the machines moved at low speed, or when slowing down for corners, showed a decrease in the impact force, as expected.

Typical deceleration plots are given in Appendix E.

3.8 CONCLUSIONS

The testing confirmed the magnitude of the decelerations predicted by Heyns (1998), as well as the occurrence of higher decelerations on stiffer ground. The range of accelerations found varied from just above 5g's to 19g's. An average value of 10g's is therefore reasonable for use in a numerical model.

CHAPTER 4

VOLUMETRIC STRAINS UNDER A IMPACT COMPACTOR

4.1 INTRODUCTION

This chapter investigates the profile of volumetric strain produced by a single blow of an impact compactor. The volumetric strain profile is reviewed rather than the orthogonal components, as it seems logical that to produce permanent volume changes in the soil, a relationship must exist between the volumetric strain profile and the void ratio reduction profile.

From this perspective, some logical conclusions are hoped to be found regarding the patterns of improvement that can be expected under a compactive load.

4.2 AIMS OF THE ANALYSIS

The aim of the modelling was to determine the approximate distribution of volumetric strain under an impact compactors' imprint. The influence of using various soil models is also briefly investigated in order to answer the basic geotechnical questions:

- How does the profile of volumetric strains vary under a loaded area using various soil models?
- How variable is the volumetric strain profile?
- Do all these variations need to be built into a model?
- Can the patterns be represented in a simple manner?

The effect of dynamics was approximated by using a load approximately equal to the peak dynamic load as measured in the previous chapter (i.e using a deceleration ratio of about 10. It is hoped that this simplification will shed some light on the approximate nature of the volumetric strains that can be expected, thus providing a point of departure for the development of a prediction model for compaction using impact compactors.

4.3 MODELLING METHODOLOGY AND LIMITATIONS

The effects of layering and that of the water table are not included in order to keep the analysis simple. These effects must be taken into account in a more detailed study. Not including the water table in the analysis is a reasonable simplification, as impact compaction is not generally undertaken under saturated conditions.

The soil was analysed using a perfectly elastic constitutive model (i.e no failure possible) as well as an elastic-plastic model with a Mohr-Coulomb failure criteria, for comparative purposes.

Figure 4.1 shows the essential differences in the stress – strain curves of various soil models:

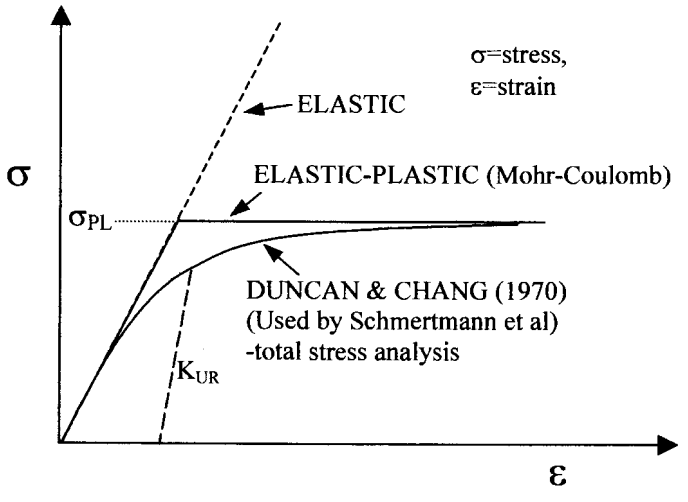

Figure 4.1 : Comparison of soil models

Both non-linear models allow the cumulative plastic strain to be evaluated with the aid of an unload-reload modulus within the failure surface. The total strain can therefore be partitioned into both elastic and plastic components. An important difference between the Duncan and Chang model and the Mohr Coulomb model is that plastic strains only occur after the plastic limit (σ_{PL}) is reached in the latter model. This will tend to mean that plastic strains tend to occur only in the vacinity of the compactive load. The hyperbolic form of the Duncan and Chang model, (more realistically) allows plastic strains to occur at

loads below the plastic limit. None of the above models take the effects of hysteresis into account and are therefore not entirely appropriate for modelling compaction directly. Although the software used in the analysis did not have the Duncan and Chang model, an initial indication of the approximate distributions of strain can be evaluated from both the elastic and Mohr-Coulomb models.

Furthermore, all of the above analyses were static analyses, and it must be noted that the dynamic stress profile is probably slightly deeper. This was highlighted by Hansbo (1979), who noted that the dynamic strain profile is more hyperbolic in nature than the static strain profile, as shown in Figure 4.2.

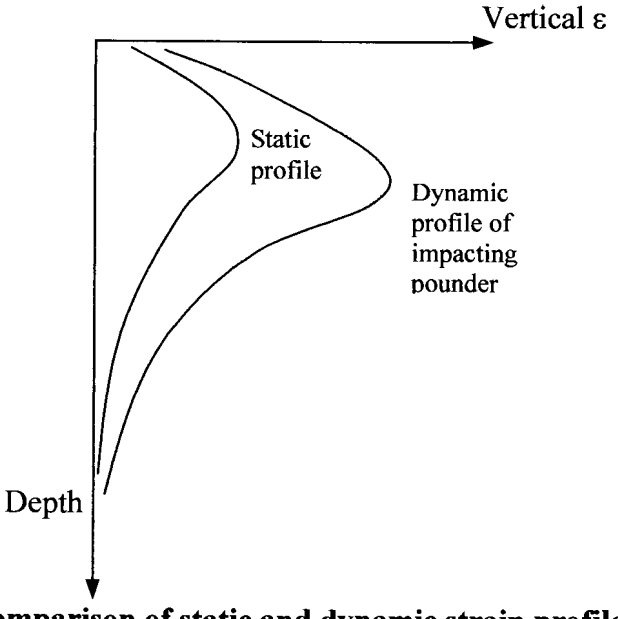

Figure 4.2 : Comparison of static and dynamic strain profiles (Hansbo, 1979)

The magnitudes of the stiffness used in the analysis are typical of those found in un-compacted ground, but due to the comparative nature of the analysis the exact value is not of primary importance. A subgrade stiffness of 25 MPa was used in most of the analyses.

Measurement of average plan area of the three sided impact compactor's indent based on a 40mm penetration of the curved surface yields an approximately square area of 900mm x 900mm. Using this area, the load imprint was modelled with an equivalent circular area of radius 0.5m.

4.4 ELASTIC ANALYSIS OF THE VOLUMETRIC STRAIN PROFILE

According to the generalized Hooke's law the unit volumetric strain ε_{vol} is given (Gear and Timoshenko, 1984): (for axi-symmetric loading):

$$\varepsilon_{vol} = \frac{\Delta V}{V} = (1+\varepsilon_z)(1+\varepsilon_\theta)(1+\varepsilon_r) - 1 \qquad \text{Eq. 4.1}$$

which for small strain becomes :

$$\varepsilon_{vol} \approx \varepsilon_z + \varepsilon_\theta + \varepsilon_r = \varepsilon_z + 2\varepsilon_r \qquad \text{Eq. 4.2}$$

The volumetric strain can also be written in terms of stress as follows for the three dimensional case:

$$\varepsilon_{vol} = \frac{1-2v}{E}(\sigma_1 + \sigma_2 + \sigma_3) = \frac{1-2v}{E}\theta \qquad \text{Eq. 4.3}$$

The volumetric strain and bulk stress, θ are invariants (independent of axis orientation). The above equations show that they are a measure of the change in a fundamental soil property, the volumetric strain and hence also related to void ratio changes. Equation 4.2 shows that the volumetric strain is independent of shearing strains. This may be an indication that the normal strains are more important in the compaction process than shear strains. Similarly, equation 4.3 shows the volumetric strain is proportional only to the normal stresses (no shear stresses in the equation) for small strains.

Equation 4.3 also highlights the significant effect of Poisson's ratio on the elastic volume change in a soil. The use of v=0.5 for saturated materials yields no volume change. Table 4.1 demonstrates the *relative* volume change in an elastic material for a constant bulk stress and stiffness, with Poisson's ratio varied. The volumetric strain for a Poisson's ratio of 0.25 is used as the reference point - using equation 4.3 above:

Table 4.1 : Effect of Poisson's ratio on volume change (elastic material)

v	(1-2v)	Relative volume change
0.25	0.5	100%
0.30	0.4	80%
0.35	0.3	60%
0.40	0.2	40%
0.45	0.1	20%

The conclusion drawn from the above table is that Poisson's ratio is very significant in soil volume changes.

Figure 4.4 shows a summary of the various strains using elastic equations (Huang, 1993) under the centre of a flexible plate, loaded to 10g's (by a 25kJ impact compactor).

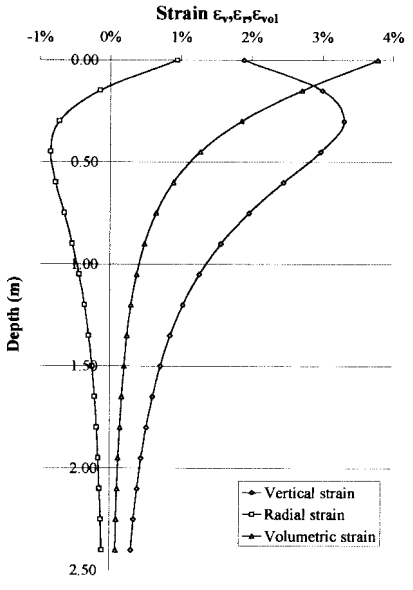

Figure 4.3 : Elastic volumetric strains under a flexible plate (ν=0.3)

Figure 4.3 shows that the volumetric strain profile is similar in shape to the profile of vertical stress according to elastic theory, and does *not* have a peak like the vertical strain profile.

An elastic *FLAC* analysis was also undertaken to check the distribution of volumetric strains beneath the contact area, using a rigid rather than flexible plate. This is shown in Figure 4.4, where it can be seen that the distribution is fairly similar throughout, except near the edge of the loaded area, where higher volumetric strains occur close to the contact surface. Something that should be investigated further is that the ratio of the vertical to horizontal strains according to the above equations is not constant (and equal to Poisson's ratio).

The reduction in volumetric strain is also less rapid that given by the flexible equation above.

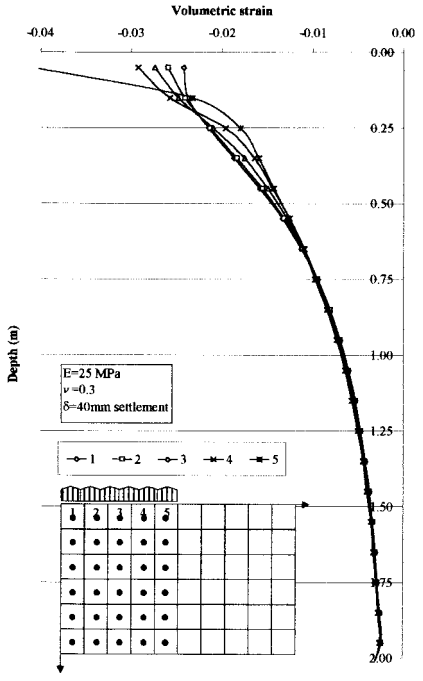

Figure 4.4 : Elastic volumetric strains under a rigid circular plate (a/g=10)

According to elastic theory, all of the volumetric strain shown above returns to zero on removal of the load. This is clearly not what happens in reality, as a proportion of the strains are permanent, resulting in compaction of the soil.

The effect of elasto-plastic soil models on the strain profile is investigated below.

4.5 ELASTIC-PLASTIC STRAINS

The *FLAC* [Fast Lagrangian Analysis of Continua] finite difference software (Version 2.7) (Starfield and Cundel, 1988) was used in the further analysis. The software allows the Mohr-Coulomb constitutive model to be used in addition to standard elastic analysis.

The software also uses the equations of motion in conjunction with local damping to ensure equilibrium is achieved. The pseudo-static analysis should therefore be reasonably realistic.

The analysis therefore has a dynamic basis, although the dynamic module was not utilised (or available) in the analyses performed.

The aim of this analysis was to assess the profile of volumetric strain and compare this with that found in the elastic analysis.

The FLAC finite difference grid is shown in Figure 4.5. For ease of calculation of strains, a uniform grid of 100mm x 100mm was used. The load was applied by applying slowly applying a fixed surface settlement to the grid over the plate of radius (0.5m.) and ensuring that the force was of the correct order of magnitude.

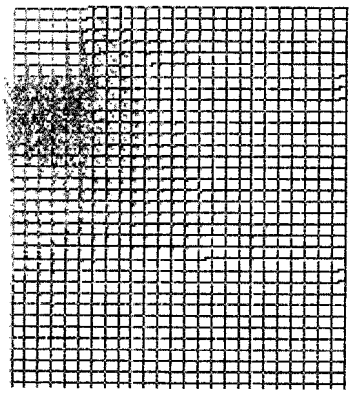

Figure 4.5 : FLAC grid and velocity vectors

To assess the effect of changes in the Mohr Coulomb parameters on the strain profile, the values given in Table 4.2 were used. The parameters that were varied are shown in bold letters. Details not presented below are attached in Appendix G.

Table 4.2 : Mohr-Coulomb model parameters (ν=0.3)

Analysis	E (MPa)	G (MPa)	K (MPa)	c' (kPa)	ϕ'	δ (mm)
MC1	25	9.62	20.83	1	***25***	40
MC2	25	9.62	20.83	1	***30***	40
MC3	25	9.62	20.83	1	***35***	40
MC4	25	9.62	20.83	***5***	25	40
MC5	25	9.62	20.83	***10***	25	40

The vertical, horizontal and volumetric strains were calculated over a depth of 2m below the contact area, for each of the five grid zones [numbered 1 to 5] adjacent the axis of symmetry beneath the loaded area.

The manner in which the total volumetric strains (sum of elastic and plastic strains) varies underneath the rigid loaded area is shown in Figure 4.6.

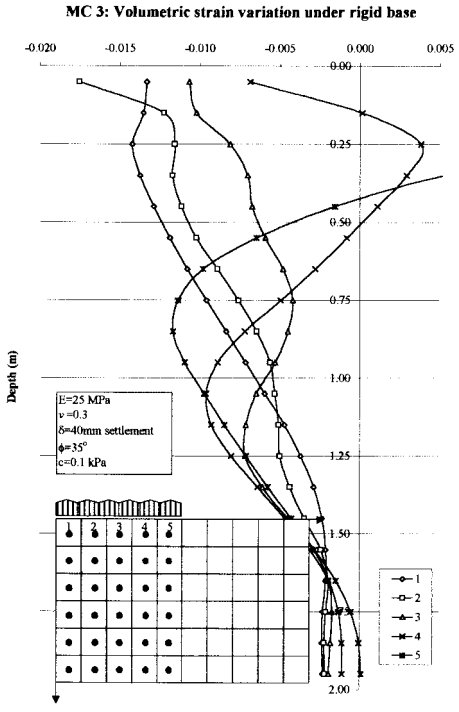

Figure 4.6 : Elastic-plastic volumetric strains under a rigid plate

It is immediately apparent that volumetric strains vary from the centre of the load to the edge quite significantly. Near the axis of symmetry the volumetric profile is similar to the elastic volumetric strain profile, but nearer the edges a reduction occurs due to dilation and a reduction in lateral frictional restraint. The behaviour is complex. It seems reasonable however, to use an average value of volumetric strain to evaluate patterns of behaviour, as the impact imprints vary in position, resulting in an averaged nett volumetric change after a number of passes. Soil testing will also tend to evaluate averages.

Figure 4.7 shows the average volumetric strain for all of the analyses listed in Table 4.1.

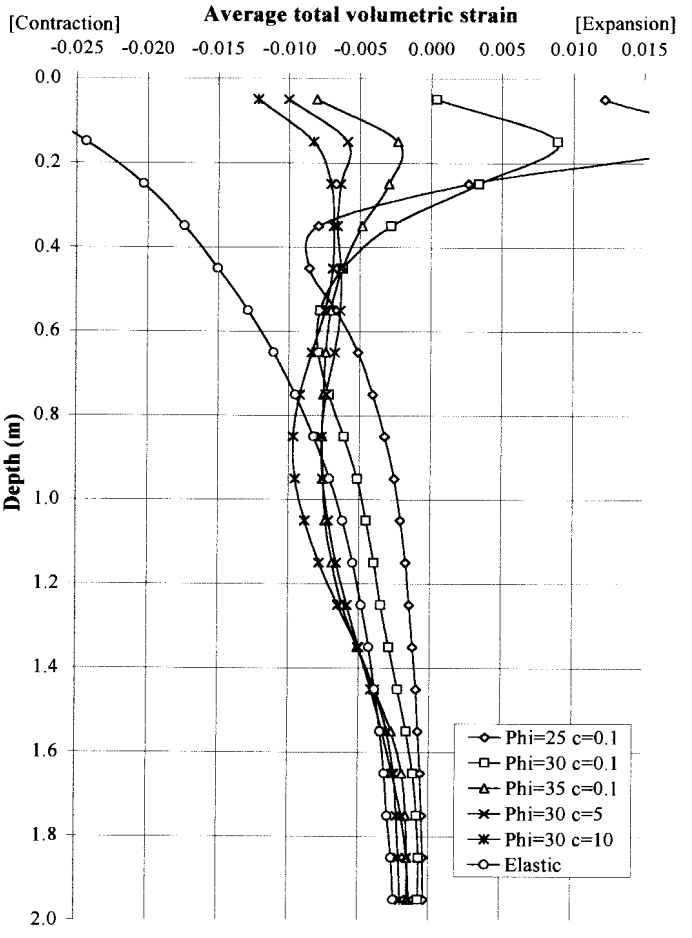

Figure 4.7 : Elastic-plastic volumetric strain variation with soil parameters

For comparison, the elastic volumetric strain is also shown. From the above analyses, the following patterns are evident:

- The "elastic" analysis over-estimates the surface volume changes
- The Mohr-Coulomb analyses show reduced strains just below the load due to plastic behaviour and dilation. This results in a peak in the volumetric strain profile below the surface and very often an "S" shaped profile. [This looks remarkably similar to the diagram on the left of Figure 2.2 in Chapter 2].
- The weaker materials exhibited a greater tendency to dilate just below the loaded area
- The stronger materials (high cohesion and friction angles) showed a deeper peak in the total strain profile.

The use of an appropriate model is therefore essential.

Notwithstanding the limitations in the modelling undertaken, an estimate of the approximate volumetric strain distribution under the application of a single load has been obtained. It would appear reasonable that under the application of repeated loading the shape of the above profiles would be accentuated, with peaks becoming more pronounced.

In summary, the volumetric strain profile has been evaluated using both elastic and elasto-plastic soil models and some patterns of behaviour highlighted, although the behaviour is complex. The soil strength parameters were found to significantly effect the volumetric strain profile, but in what appears to be a predictable manner. In order to simplify the currently proposed model, a single profile of improvement is currently proposed that is believed to simulate average behaviour, but refinements are certainly possible.

4.6 CONCLUSIONS

Significant differences are found when comparing the vertical, horizontal and volumetric strains when using different soil models. An elastic analysis shows little variation in the volumetric strains from the centre to the edge of the loaded area, while a Mohr-Coulomb model indicates a tendency for the soil to dilate towards the edge of the loaded area near the surface.

As the behaviour under the loaded area is complex it is therefore proposed that the average behaviour under a rigid plate can be represented in a manner similar to that of Figures 4.7 and 4.9, where an "S" shape is apparent. The depth of influence is in the order of 2 to 3 times the compactor diameter in the above analyses. A simplified model simulating this behaviour is constructed in the next chapter.

CHAPTER 5

DEVELOPMENT OF A A VOLUMETRIC STRAIN INFLUENCE GROUND IMPROVEMENT PREDICTION MODEL

5.1 INTRODUCTION

This chapter proposes a volumetric strain influence ground improvement prediction model based on the results of numerical analysis, observation of field data and the literature surveyed. The basic hypothesis on which the model is based is given first. Then the model development is overviewed, showing the initial improvement profile hypothesis and the revision that followed. Simplifying assumptions and limitations are high-lighted. Verification of the proposed model is done in Chapter 6.

The main input into the model is the compactor contact dimensions and the surface settlement achieved after compaction. No attempt is made to predict the compaction energy requirements.

5.2 BASIC HYPOTHESIS

From field observations of the typical improvements during the substantial trials undertaken by Africon Engineering for Landpac (Africon, 1998), some patterns of behaviour became apparent (Berry et al, 1998) as discussed in Chapter 2 (Figure 2.1). Subsequent observation of much of the field data seemed to confirm that there is often a peak in the improvement obtained and that this peak appeared to be similar to the Schmertman (1970) vertical strain influence diagram used in the calculation of foundation settlement.

The initial model development therefore focused on using the profile of vertical strain, rather than volumetric strain, as the vertical strain profile has a pronounced peak, which Schmertman simulated with a triangular distribution.

The use of the volumetric strain in the proposed model was a subsequent development, outlined later in the Chapter. None of the compaction models reviewed in chapter 2 specifically discussed a peak in the improvement profile, or the use of surface settlement as an input parameter into the modelling. However, the patterns observed by Lukas (1986) and summarised in Figure 2.2 were confirmed in this study and support the hypothesis of the model proposed here.

The basic hypothesis is as follows:
It is proposed that the plastic volumetric strain profile produced during the compaction process is proportional to the total volumetric strain profile produced by the compactive load. For simplicity sake, it is proposed that this proportion (β) is constant with depth as shown in Figure 5.1.

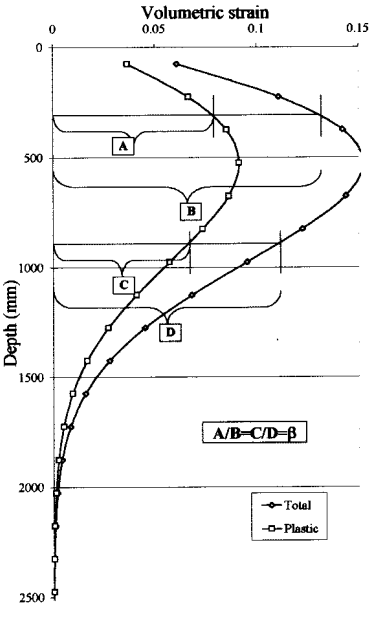

Figure 5.1 : Hypothesised relationship between total and plastic strains

As the surface settlement is the integral of the plastic vertical strain over the depth of influence of the load, it is proposed that this cumulative strain can be re-distributed over the depth of influence of the load, in proportion to the magnitude of the volumetric strain at the depth in question. Provided an estimate of the plastic lateral strains is made, the plastic volumetric strain can be calculated.

Rigid adherence to a single volumetric strain profile pattern is not intended, as the profile is affected by many factors. However, for the initial model development a single profile of volumetric strain is proposed for simplicity sake.

The central hypothesis is therefore that the surface settlement can be re-distributed with depth according to the likely distribution of volumetric strain, which will vary depending on soil parameters. Making allowance for lateral strains allows the volumetric changes in the soil to be estimated.

Layered soils are therefore not excluded from the above hypothesis, as it is proposed that only shape the volumetric strain profile would change, and the back-analysis adjusted accordingly. This further hypothesis is not tested in this study for brevity and simplicity sake, but warrants further investigation.

The above hypothesis has the limitation that the water table is not within the depth of influence of the compactive load. As most impact compaction takes place under unsaturated conditions, the omission of the water table from the model is justified.

To develop and verify the proposed model, however, further simplifying assumptions and limitations have been made as detailed below.

5.3 INITIAL MODEL DEVELOPMENT

Initially the void ratio reduction profile after impact compaction was thought to be proportional to the *vertical* strain distribution below the compactive load.

In the initial development of the prediction model the following simplifying assumptions were made:

- The void ratio reduction profile is proportional to the vertical strain profile, which has a similar shape to the Schmertman strain influence diagram.

- A homogeneous soil is considered, with no layering (i.e a semi-infinite uniform half space)
- The effect of variations in the permanent volumetric strain profile due to changes in friction angle and cohesion are ignored and an average profile assumed representative.
- The magnitude of the surface settlement is either measured in a field trial or estimated (i.e surface settlement is not predicted but used as input into the model).
- The settlement measured at the end of a field trial on granular material is all plastic. (i.e there is no creep recovery).
- Swelling due to wetting up of the soil is ignored.

For ease of calculation, the Rayleigh distribution (Broch, 1980) was used instead of the vertical strain influence factor distribution as proposed by Schmertman (1970). The difference between the two distributions is shown in Figure 5.2. The use of a continuous distribution has obvious benefits in terms of calculations to be made, but is also more realistic. [It can certainly be used as a revision to the triangular strain influence diagram in Schmertman settlement calculations].

The Rayleigh distribution has two useful properties: Firstly, the depth of the peak is at $z=\sigma$ in meters. Secondly, the depth of influence is at $z=3.5\sigma$. The shape of the distribution can therefore be adjusted in a simple manner. According to Schmertman (1970), the maximum vertical strains occur at a depth of between B/2 and B below the foundation/load, depending on the length/width (L/B) ratio of the loaded area (B is the smaller load dimension). As an impact compactor makes a series of impacts in the longitudinal direction and successive passes reinforce this effect, a peak somewhere between B/2 (square load) and B (long load) seems reasonable as a first start to the modelling. The proposed improvement profile was therefore modelled with the depth of the peak vertical strain between 0.67B and 0.8B [B=0.9m in the case of an impact compactor].

Using the Rayleigh distribution results in the depth of influence ranging from about 2m to 2.5m, which ties in with both numerical analyses and field observations. The use of the Rayleigh distribution therefore seems justified.

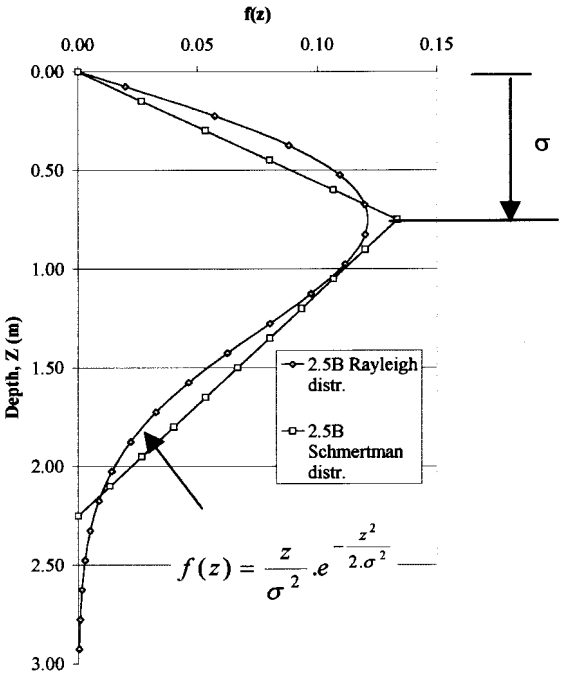

Figure 5.2: Comparison of Rayleigh and Schmertmann distributions of vertical strains

Surface settlement can be conveniently represented by a negative exponential curve as shown in Figure 5.3.

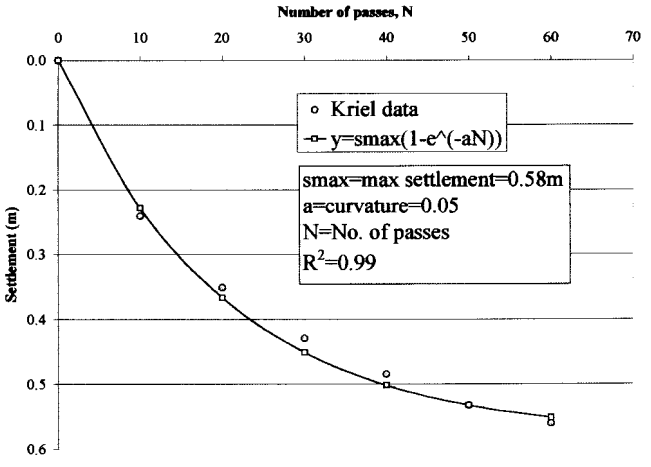

Figure 5.3 : Settlement approximation using a negative exponential curve

The rate of volume change with depth it is argued, is directly proportional to the rate of surface settlement. It is further proposed, that the variation of plastic volumetric strain with depth be simulated by a Rayleigh distribution. The resulting hypothesised three-dimensional surface is given in Figure 5.4.

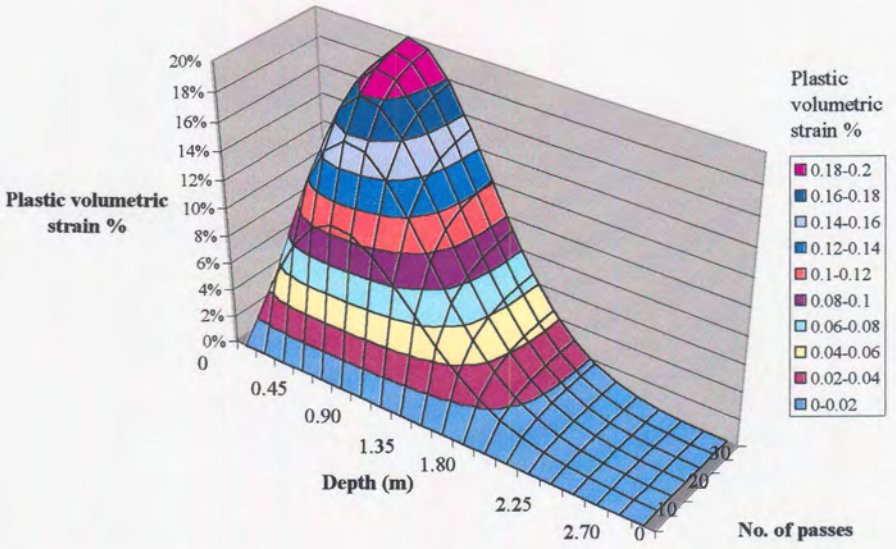

Figure 5.4 : Initial model proposed : Variation of permanent volumetric strain with number of compactor passes

5.4 REVISED MODEL

Calculations based on the above model consistently overestimated the void ratio reduction profile (discussed further in Chapter 6) and this lead to the conclusion that the volumetric strain rather than the vertical strain should be considered as the indicator of the improvement profile. Both vertical, horizontal and tangential strains occur below the compactive load, the sum of which gives the net volumetric strain. In the same manner than permanent vertical strains are produced, permanent lateral and tangential strains result during compaction, and hence permanent volumetric strains are produced. In order to take this into account the method proposed by Gere and Timoshenko (1984) is proposed: Consider a unit volume of soil under uniaxial loading (Figure 5.5).

The initial volume $V_o = a.b.c$

The final volume after compressive strain ε is $Vf = a.b.c\ (1+\varepsilon)(1-v\varepsilon)(1-v\varepsilon)$, So the change in volume is given by $\Delta V = Vf - V_o = a.b.c\ (1+\varepsilon)(1-v\varepsilon)(1-v\varepsilon) - a.b.c$

Which becomes $\Delta V = a.b.c\ (1-2v).\varepsilon$, ignoring higher order terms

So, $\Delta V/V_o = \varepsilon\ (1-2v)$ = unit elastic volumetric strain

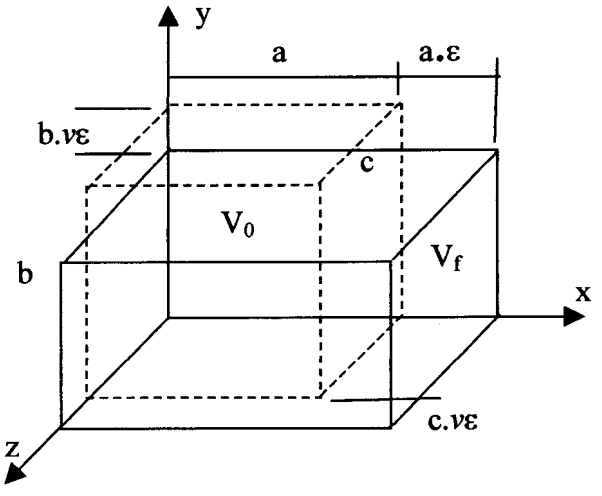

Figure 5.5: Volumetric strain under uniaxial loading

In compaction a proportion of this unit volumetric strain is non-recoverable, and to take this into account, it is proposed that the above formula is modified as follows: $\Delta V/V_o = \varepsilon\ (1-2v_{pl})$, where $v_{pl} = \alpha.v$ and $0 < \alpha < 1.0$ (v=Poisson's ratio, v_{pl} is the operative Poisson's ratio, and α = plastic proportion). It is proposed that initially, during the compaction process, α=1 and as compaction proceeds, approaches a value of about 0.4 for impact compaction, where full surface coverage is standard, and 0.7 for dynamic compaction where compaction is usually done on in grid.

The value of v_{pl} is obtained from back-calculation of field densities from the surface settlements. If the elastic Poisson's ratio, v, is known, α can then be estimated. The back-calculation process is discussed in Chapter 6. The above simplified analysis provides a method of estimating volume change from the vertical strain, if the operative Poisson's ratio is known.

The numerical analysis confirmed that this behaviour is complex and to simplify an average volumetric strain profile is proposed for use in the prediction model. Examples of these patterns of behaviour will be given in chapter 6. A modification to the Rayleigh distribution is proposed to take into account the average volumetric behaviour under an impacting load.

This modified distribution is shown in Figure 5.6 after it has been normalised (i.e the area under the curve made a unit magnitude).

The modification is achieved in a spreadsheet by assuming the peak at the surface is some proportion of the lower peak, say 1.1 times larger.

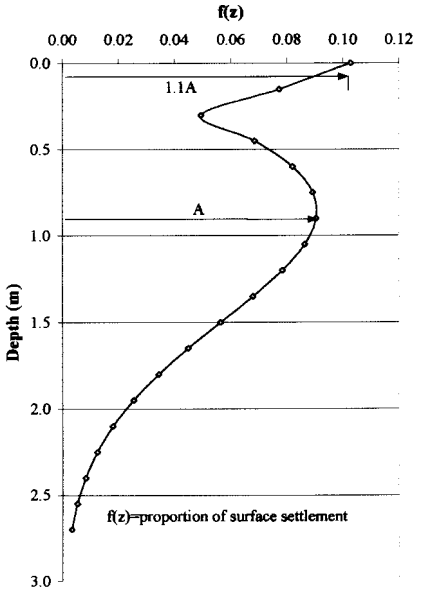

Figure 5.6 : Modified volumetric strain influence distribution

Due to the many simplifications, the exact magnitude of the surface strains is not of primary importance provided the average shape of the volumetric profile is approximated. The hypothesised variation of the permanent volumetric strain profile with increasing number of passes is shown in Figure 5.7.

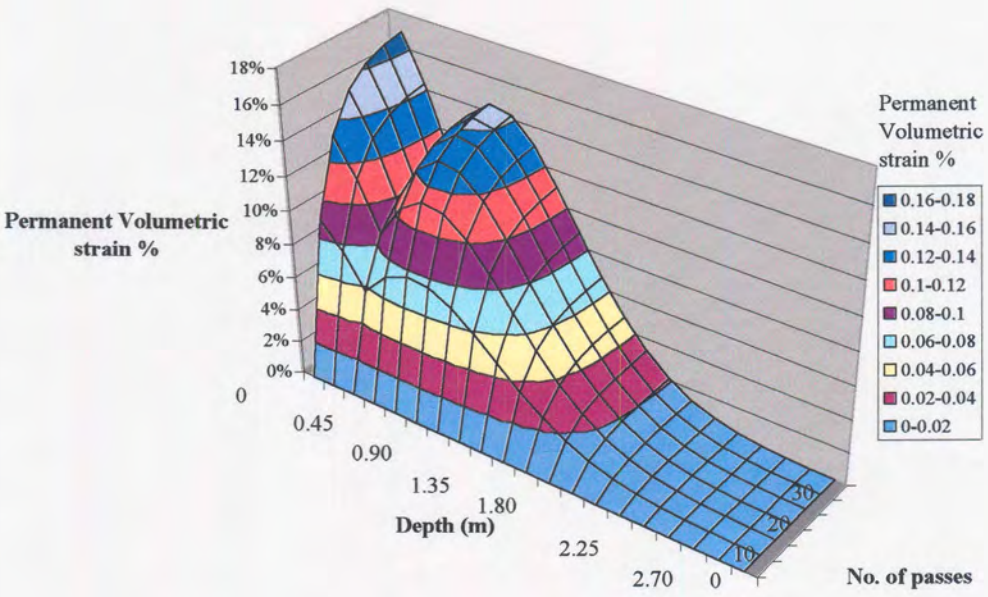

Figure 5.6 : Modified volumetric strain prediction model to take large surface strains into account

The noteworthy aspects of the proposed model are:

- The depth of influence of the compaction load is approximately three times the contact diameter of the loaded area. [Schmertmann (1970) proposed 2B for a square load and 4B for a long load for his settlement model]. Hansbo (1979) also noted that the dynamic strain profile is deeper than the static profile. (Hence a depth of influence profile >2B is justifiable)
- Two peaks appear in the model to simulate the average volumetric behaviour under the compactive load, which is assumed to best represent the profile most likely to be measured in verification testing
- The use of energy as the input parameter is avoided, by using surface settlement. This is both a strength and a weakness. The use of surface settlement bypasses the complication of addressing the different compactive efforts required by differing materials of differing moisture content, structure and grading. This is also a drawback, as most contractors are most interested in the effort required to achieve a specific level of improvement.
- Lateral strains must be taken into account, as will be shown in Chapter 6.

- The principles of volume change are the most important aspect of the proposed model-the exact volumetric distribution needs further detailed dynamic analysis. However, the simplified profile suggested has been found to yield satisfactory results.

An accurate knowledge of the volumetric behaviour near the surface is perhaps not necessary for structural foundations, as the footings are usually placed some depth below the surface. A more detailed knowledge may, however, be warranted for road pavements.

5.5 CONCLUSIONS

A simplified volumetric strain influence ground improvement prediction model is proposed. The main input into the model is the surface settlement, the compactor geometry and the operative Poisson's ratio. A distribution of the permanent volumetric strains with depth is suggested, from which void ratio reduction profile for unsaturated conditions can be estimated.

CHAPTER 6

MODEL VERIFICATION AND DISCUSSION

6.1 INTRODUCTION

In the previous chapter a simplified model for predicting the improvement in the ground based on the profile of volumetric strain, was put forward. The aim of this chapter is to verify the proposed model, discuss some of the shortfalls and suggest some areas for further research.

The calculation procedure is first explained, before verification of the model on fifteen impact compaction soil profiles on six different sites. Reasonable agreement with measured values was found once permanent lateral strains had been taken into account. The model was then checked against the results on a dynamic compaction site, and good correlation found. The effect of lateral strains was found to be more significant on dynamic compaction sites. It is thought that this is due to the relatively large compaction grid spacing.

The use of surface settlement to predict the improvement in a layer compacted with a conventional vibratory compactor is also demonstrated. This confirms that surface settlement can be used to estimate the ground improvement, if the distribution of the permanent strains is known even when simplifying assumptions about the distribution are made.

Confirmation of the patterns of behaviour noted by Lukas (Figure 2.2) and modelled here is also offered via the presentation of various other results. (cone penetrometer results, stiffness measurements etc).

After some discussion, conclusions are drawn and recommendations made regarding the various areas that warrant further investigation. The effect of compaction with the water table present within the depth of influence of the compactor is also hypothesised.

6.2 CALCULATION PROCEDURE

The calculation procedure is outlined below:

Step 1: The surface settlement is either estimated from past experience or obtained from a field trial at the site in question (the latter is preferable)

Step 2: The soil profile is divided into about 20 layers over the depth of influence (DI) of the compactor, assumed to be approximately 3B for an impact compactor, where B is the lessor compactor contact dimension. This is dependant on the energy and drop height of the compactor, as well as the type of materials being compacted. A depth of between 3B and 4B is provisionally recommended for dynamic compactors in the unsaturated conditions commonly found in South Africa.

Step 3: An appropriate volumetric strain influence distribution is selected for the back-calculation process. The modified Rayleigh distribution is suggested as the default, but this need not rigidly be adhered to. The depth of influence can be adjusted by changing the depth of the peak (σ) in the Rayleigh distribution as $DI=3.5\sigma$. From field measurements with impact compactors this depth appears to be between 0.6m and 0.9m (i.e 0.67-1.0B). A provisional value of 0.75B is recommended. This gives a depth of influence of $DI=3.5(0.75B)=3.5(0.75x0.9)=2.363m$ for current model impact compactors. For dynamic compactors the diameter typically varies from 1.4m to 2.4m. Repeating the above exercise and assuming the peak is at 1.0B due to the larger dynamic forces, the calculated depth of influence is between 4.9m and 8.4m. This corresponds well with field measurements in the Gauteng region using this equipment.

Step 4: The settlement that originated in each layer is then back-calculated from $\Delta H=f(z).\delta$, where ΔH is the settlement of the layer, z is the depth to the centre of the layer, and δ is the total measured (or estimated) surface settlement, f(z) is the normalised ordinate of the modified Rayleigh distribution at depth z

Step 5: The vertical strain in the layer is given by $\varepsilon_v=\Delta H/H$, where H is the layer thickness

Step 6: Using an appropriate value of v_{pl}, calculate the permanent volumetric strain from the vertical strain, $\varepsilon_{vol}=(1-2v_{pl}).\varepsilon_v = \Delta V/V_o$, where ΔV is the change in volume and V_o is the initial volume ($V_o=1+e_o$, where e_o is the initial void ratio obtained from pre-compaction testing). Typical values of v_{pl} for impact compaction range from 0.1 to 0.3, with the higher value yielding a conservative estimate of the improvement possible. A value of 0.2 at the end of the compaction process is provisionally recommended. As this is obtained from back-calculation from field data, the model is semi-empirical in nature.

Step 7: The change in volume is obtained from $\Delta V=(1+e_o).(1-2v_{pl}).\varepsilon_v$

Step 8: The final density is given by $\rho=Gs/(V_o-\Delta V)$, where Gs is the relative density of the soil=2650kg/m^3 (typically).

Step 9: Lastly, the void ratio reduction is calculated using the measured initial and predicted final densities. This is done to highlight the changes in the improvement profile before and after compaction, with a view to identifying patterns. This last step is not necessary for routine calculation.

6.3 VERIFICATION ON IMPACT COMPACTION SITES

A list of the impact compacted sites where the model was verified is given in Table 6.1. On all of these sites the primary means of verification was by the measurement of void ratios before and after compaction. The method of void ratio determination is indicated in the table.

Table 6.1 : Impact compaction sites used in model verification

Site No.	Name	Reference	No. of profiles	Void ratio from:
1	Thubelethle, Kriel	Landpac, 1991	4	Sand replacement
2	Thubelethle, Kriel	Africon, 1998	2	Sand replacement
3	Highveld Steel	Clegg, 1969	1	Block samples
4	Middleburg	Barrett & Wrench, 1984	2	Block samples
5	Villa Lisa	Solesbury & Walker (1991)	2	Oedometer
6	Serowe-Orapa	Pinard, 1988	4	
		Total	15	

All calculations for the figures presented are attached in Appendix H.

6.3.1 Site No. 1 – Thubelethle Township, Kriel (1991)

Extensive trials were undertaken at the Thubelethle township in 1991, prior to the construction of the township road network. Testing was supervised by Messrs Schwartz and Tromp consulting engineers. Sand replacement density testing both before and after impact compaction enabled the construction of the void ratio reduction profiles given in Figures 6.1 to 6.4. The back-calculated void ratio reduction assuming one-dimensional strains generally over-estimates the reduction in the void ratio. The model was therefore revised as discussed in chapter 5, assuming that permanent lateral strains are the cause of the overestimation of improvements possible.

The effect of lateral strains is demonstrated by showing two values the operative Poisson's ratio (ν_{pl}). In most cases ν_{pl} ranged from 0.075 to 0.175 at the end of the compaction process (60 passes of the 25kJ impact compactor used). The importance of the permanent lateral strains is highlighted, as a one-dimensional assumption tends to overestimate the volume changes by 15%-35%.

In the 1991 Kriel results, the sampling showed a single peak in the profile. It may be that in fine-grained uniformly graded sands such as those at Kriel, the volumetric strain profile may be better modelled using the initial volumetric strain influence diagram proposed in Figure 5.2 (i.e with a pure Rayleigh distribution). Figure 6.4 indicates that surface dilation may even have occurred.

As the back-calculated void ratio reduction profile yields a consistent value of the operative Poisson's ratio, indicates that prediction using the proposed model appears feasible.

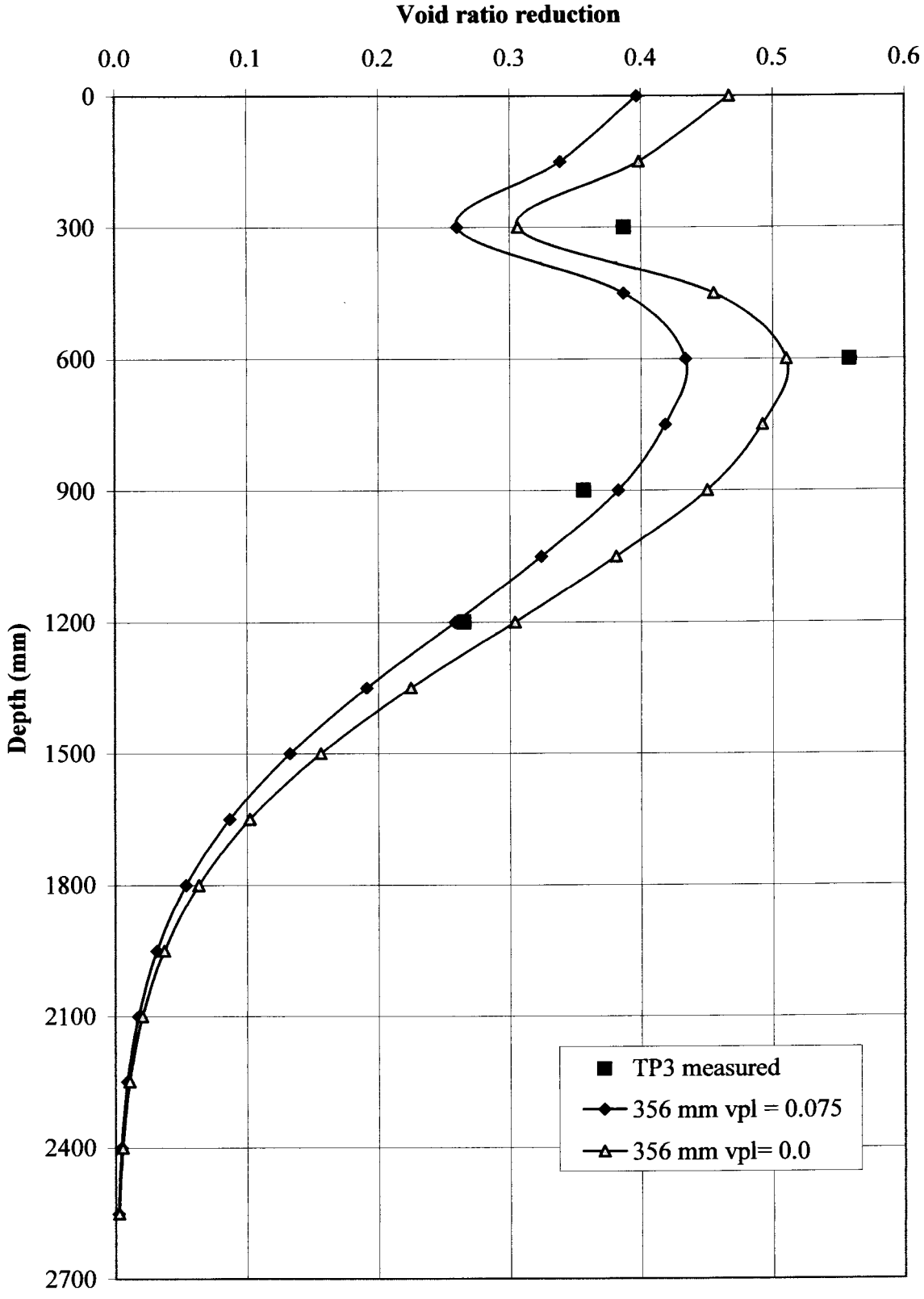

Figure 6.1 : Model verification - TP3 - Kriel, 1991

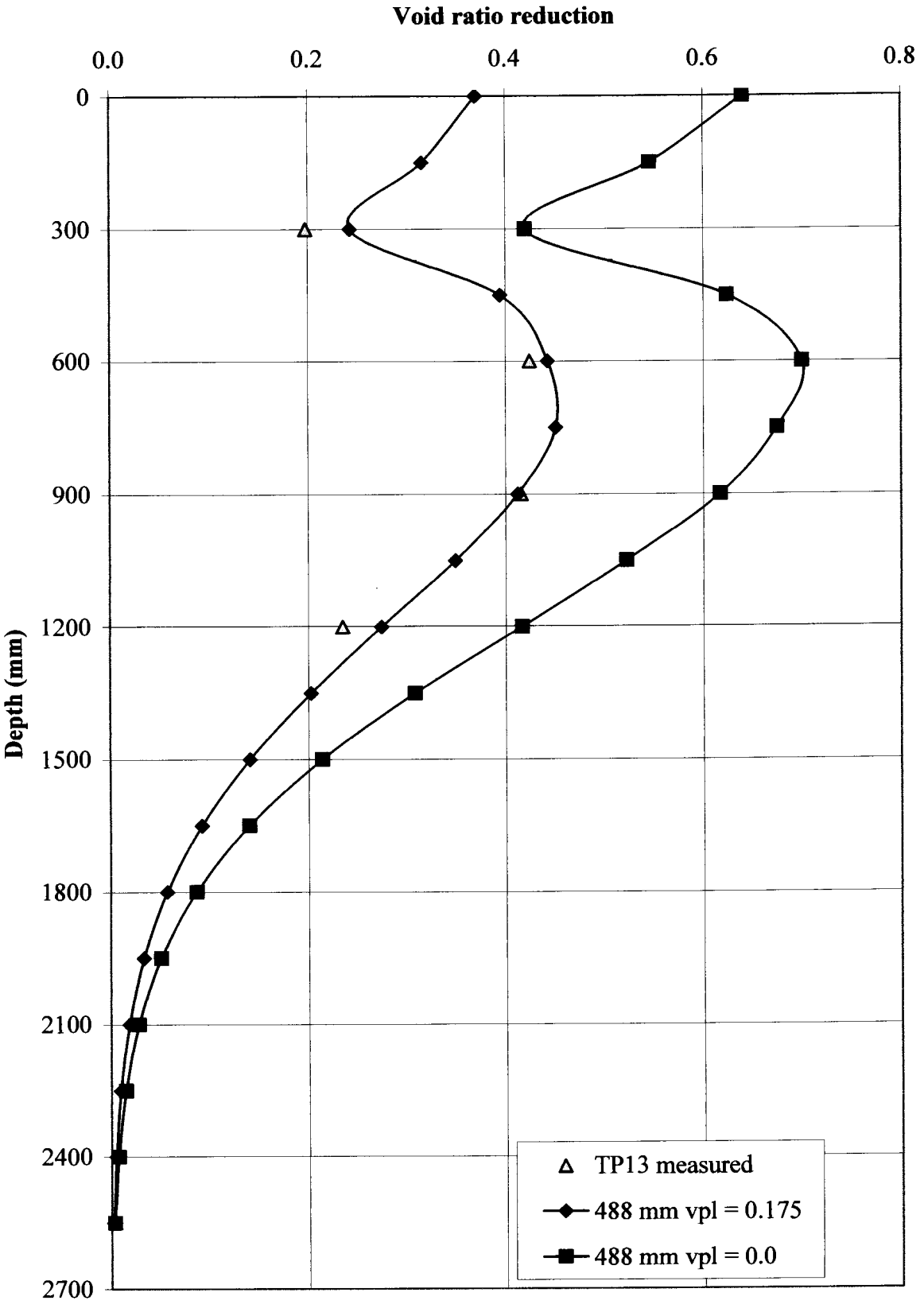

Figure 6.2 : Model verification -TP13 - Kriel, 1991

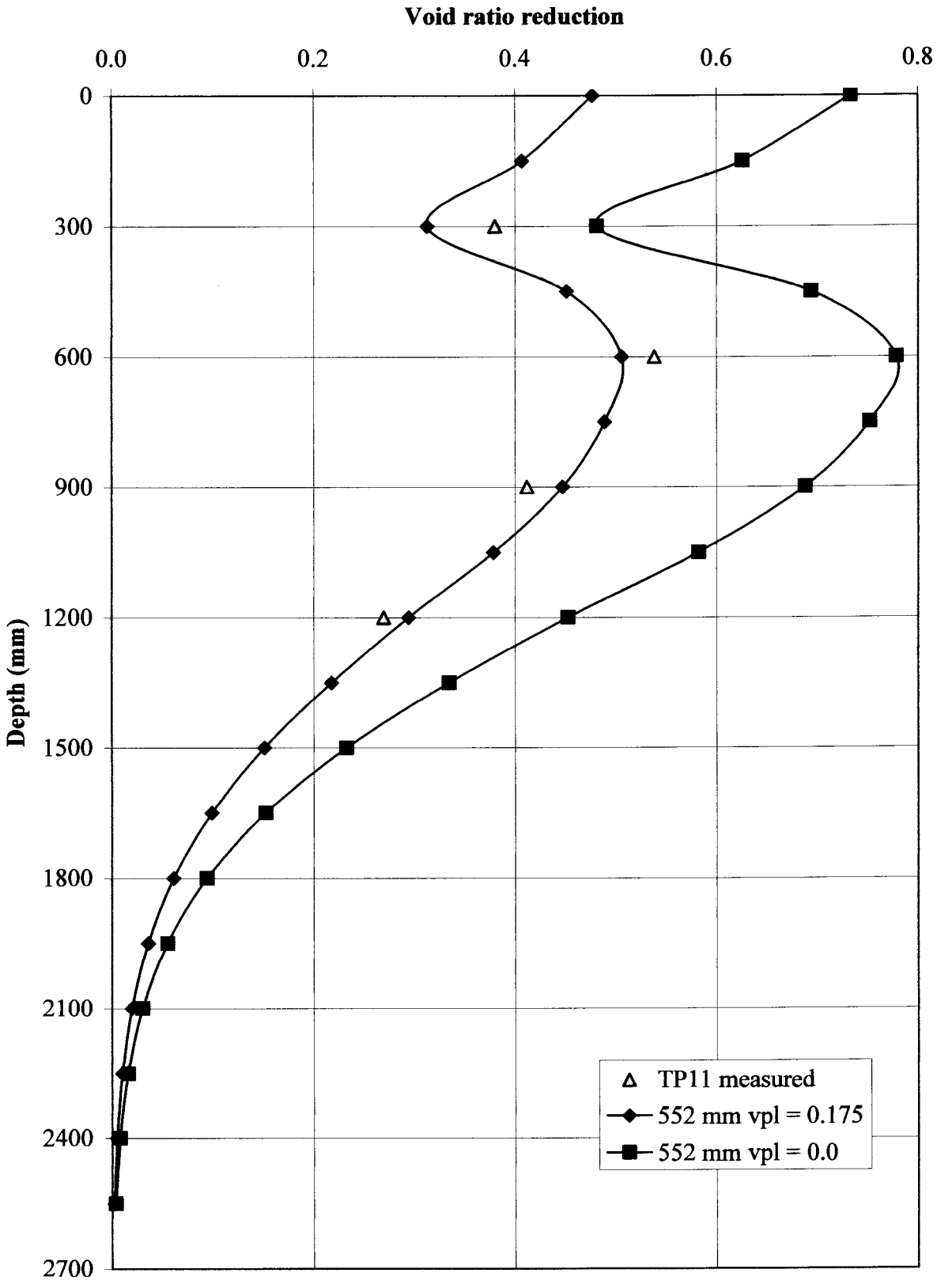

Figure 6.3 : Model verification - TP11 - Kriel, 1991

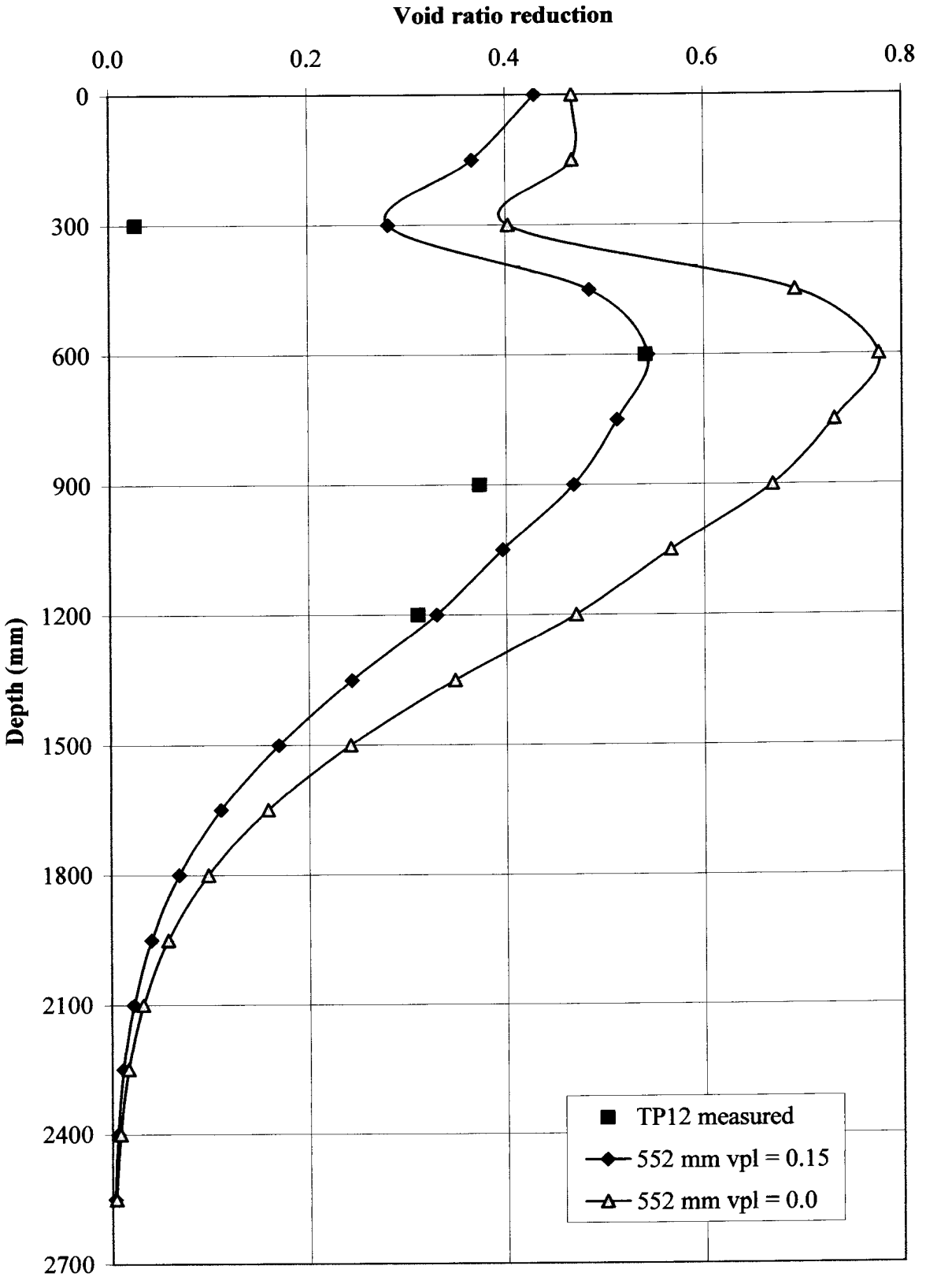

Figure 6.4 : Model verification - TP12 - Kriel, 1991

6.3.2 *Site No. 2 – Thubelethle Township, Kriel (1997)*

As part of an extensive research programme, Africon Engineering conducted further extensive trials for Landpac close to where the original 1991 trails were undertaken. The site was selected due to the fairly uniform conditions to allow comparison of the various models of impact compactors, using a conventional 11 ton vibratory compactor as a yardstick. A discussion of this trial has been presented by Berry (1998) and Strydom (1999).

Figures 6.5 shows the estimated void ratio reduction profile assuming an operative Poisson's ratio of 0.25. The surface settlement was typically 560mm in this trial, after 60 passes of a 25kJ Landpac impact compactor. The model underestimates the compaction below 1.5m at this site.

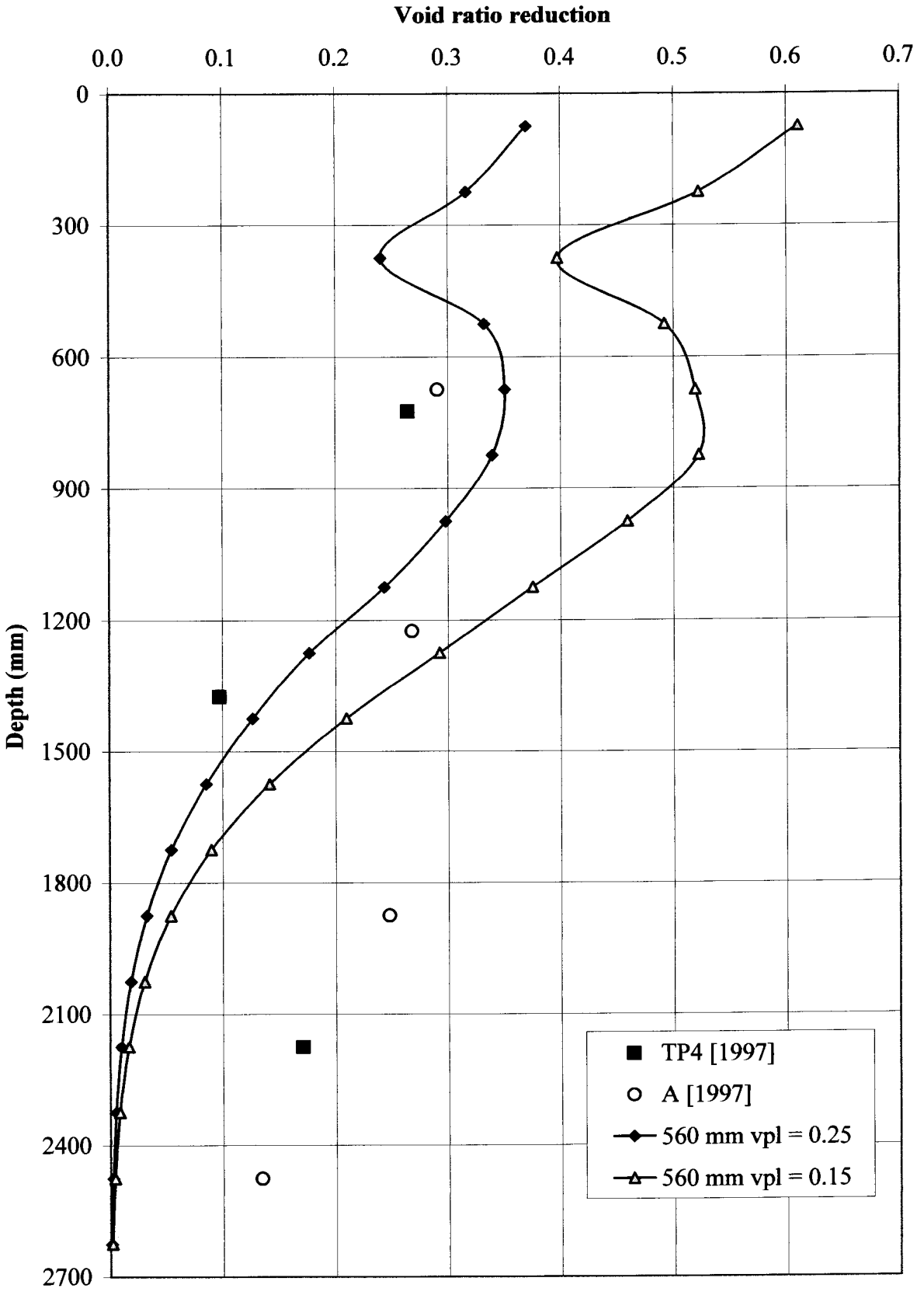

Figure 6.5 : Model verification - Kriel, 1997

6.3.3 *Site No. 3 – Highveld steel, Clegg (1969)*

The soil test results after impact compaction at this site are taken from a paper by Clegg et al (1969).

The measured void ratio reduction and the predicted values are given in Figure 6.6. Good correlation of actual and predicted data is found.

A notable correlation exists between vertical pressure transducer measurements at the site (Figure 6.7) and the predicted improvement profile given in Figure 6.6. The interesting feature of this measurement is the higher pressure at a depth of 0.95m. Theory would suggest that the pressure cannot be higher at a lower depth (a peak, theoretically only occurs in the vertical strain diagram, not the vertical stress diagram). The measurements indicate that under dynamic loading conditions this may not be the case. This behaviour warrants further investigation and analysis.

The vertical strain variation with depth was also measured by means of settlement plates. These strain are shown in Figure 6.8, where a double peak can be seen, as found in the numerical analysis in chapter 4. The magnitudes of the strains may be somewhat exaggerated as the material was placed in a trench and even though lightly re-compacted, it is likely that the soil in the trench was softer than the in-situ condition.

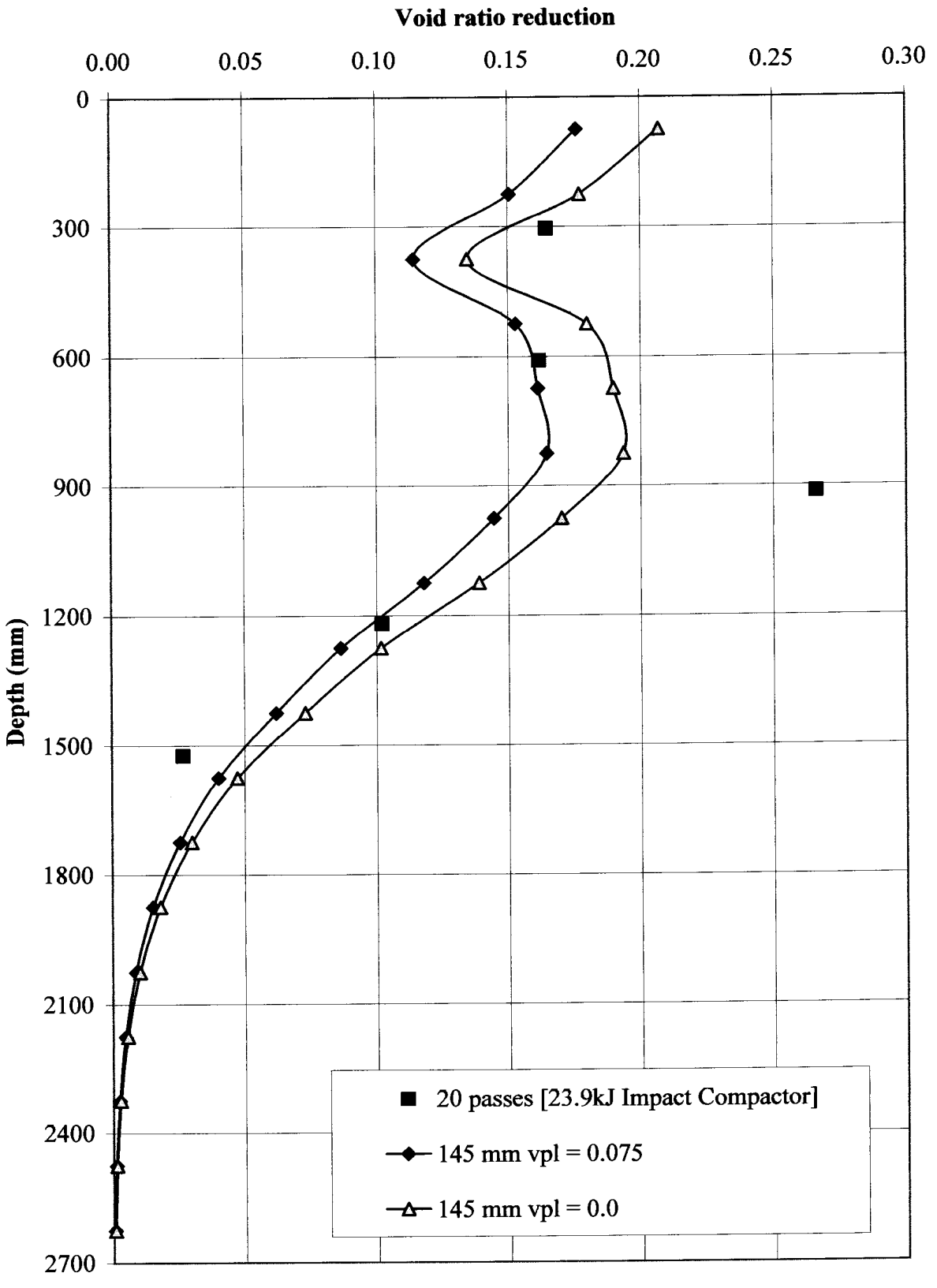

Figure 6.6 : Model verification - Highveld Steel, 1969

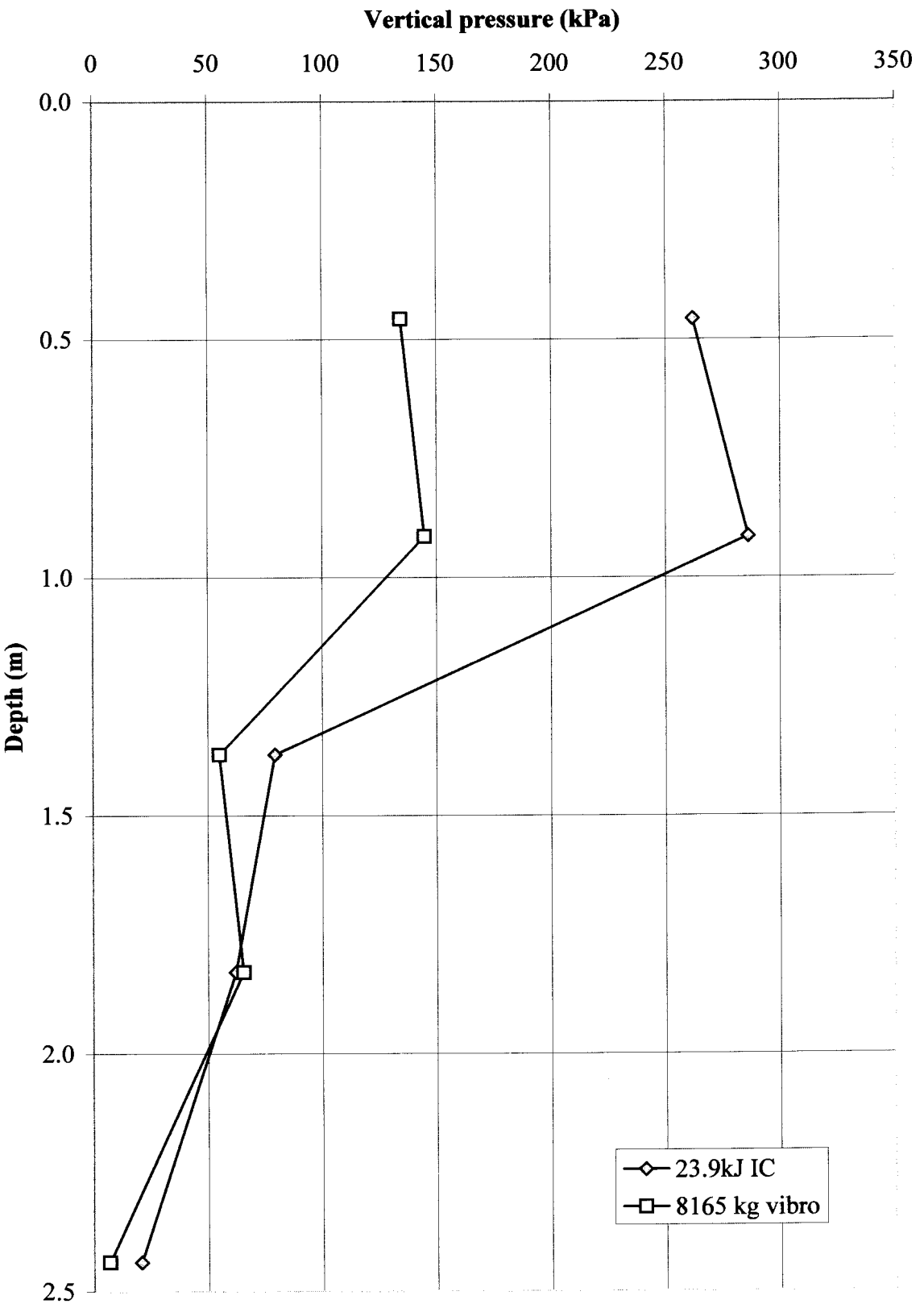

Figure 6.7 : Highveld Steel trial, 1969 : Pressure transducer measurements

(data after Clegg et al, 1969)

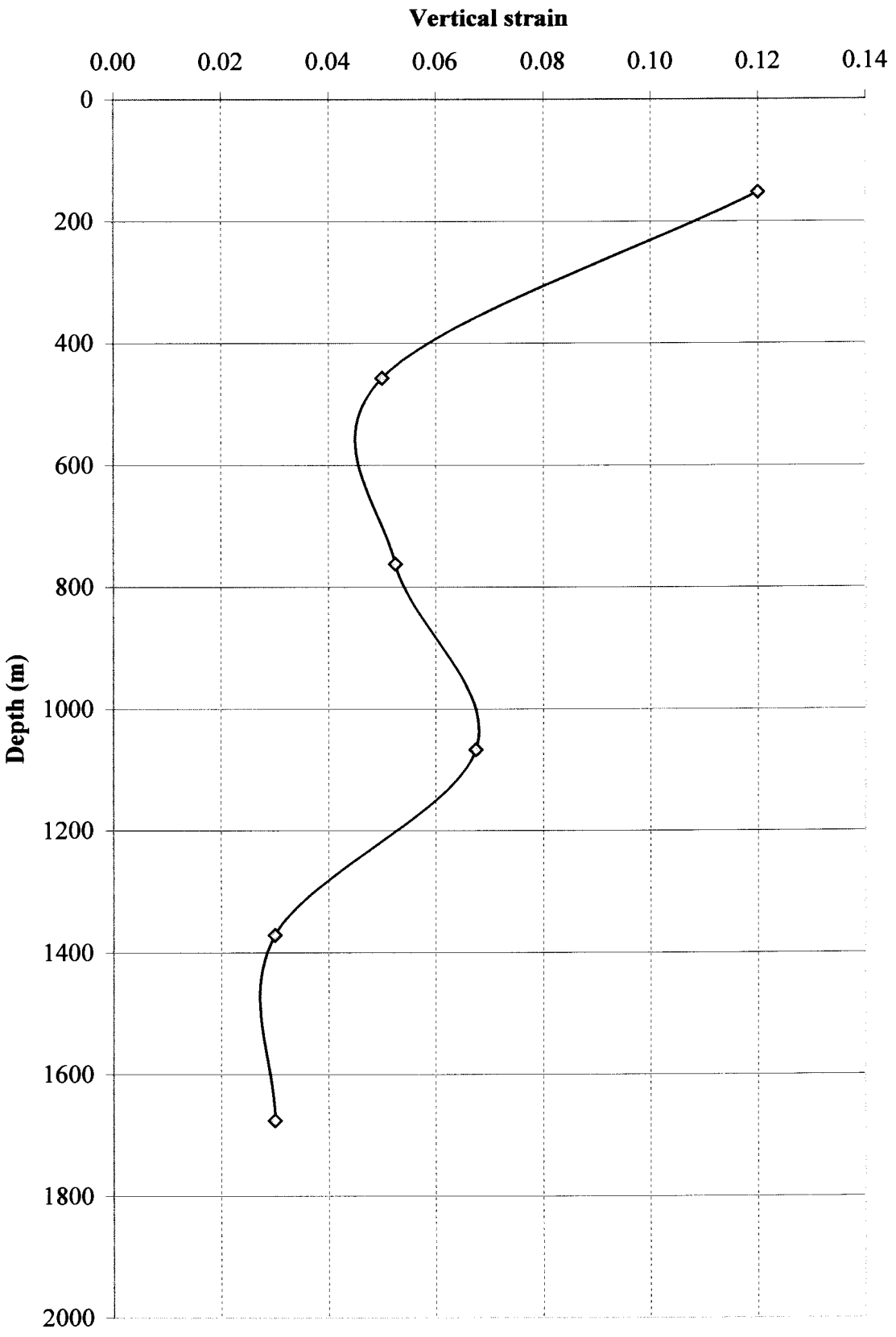

Figure 6.8 Highveld steel trial, Witbank 1969: Strain from settlement plates

(data recalculated from Clegg et al, 1969)

6.3.4 Site No. 4 – Middleburg, Barrett & Wrench (1984)

The results of impact compaction trials at Middleburg reported by Barrett & Wrench in 1984 showed little improvement in the silty materials compacted. Back analysis of the 87mm settlement at 20 passes and 112mm at 50 passes is shown in Figure 6.9. An operative Poisson's ratio of 0.3 was required to correlate the poor improvement achieved at 20 passes. The use of a higher operative Poisson's ratio may be required for clays and silts, where it is know that the elastic Poisson's ratio is about 0.4. At 50 passes the operative Poisson's ratio required to fit the data was about 0.1, indicating that strain hardening may have been taking place to some extent. The paper noted that settlements of up to 300mm occurred in certain areas. The model can be used to plot contours of improvement for different levels of settlement – the 200mm settlement contour is shown to demonstrate the predicted void ratio reduction .

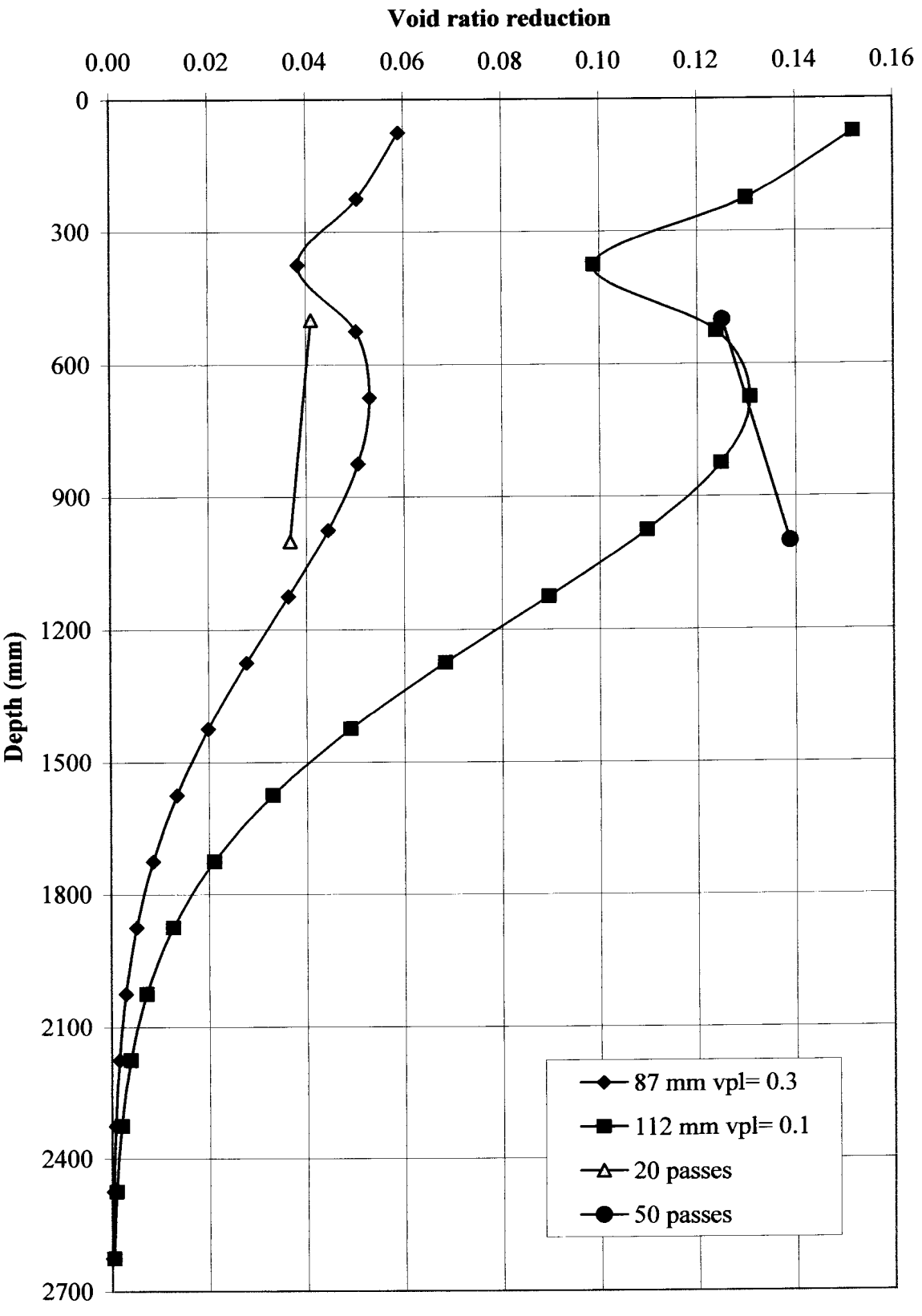

Figure 6.9 : Model verification - Barrett & Wrench trial, 1984

6.3.5 *Site No. 5 – Villa Lisa, Solesbury & Walker (1991)*

Figure 6.10 shows the predicted and measured void ratio reductions at Villa Lisa. Good correlation is found between the model and the measured results. There seems to be a tendency for the operative Poisson's ratio to decrease with increasing number of passes.

Although the theory does not support a distribution with a single peak below the surface (i.e similar to the Rayleigh distribution), much of the measured data seems to indicate a surface loosening, which would practically support such a distribution. The advice given after impact compaction is to finish off with a conventional compactor to rectify the common problem of surface loosening.

A simple Rayleigh distribution analysis is shown in Figure 6.11 for comparison purposes. The model fits well, but higher values of the operative Poisson's ratio are required to fit the data. It is suspected that finer grained and materials may require higher values of the operative Poisson's ratio to fit the data.

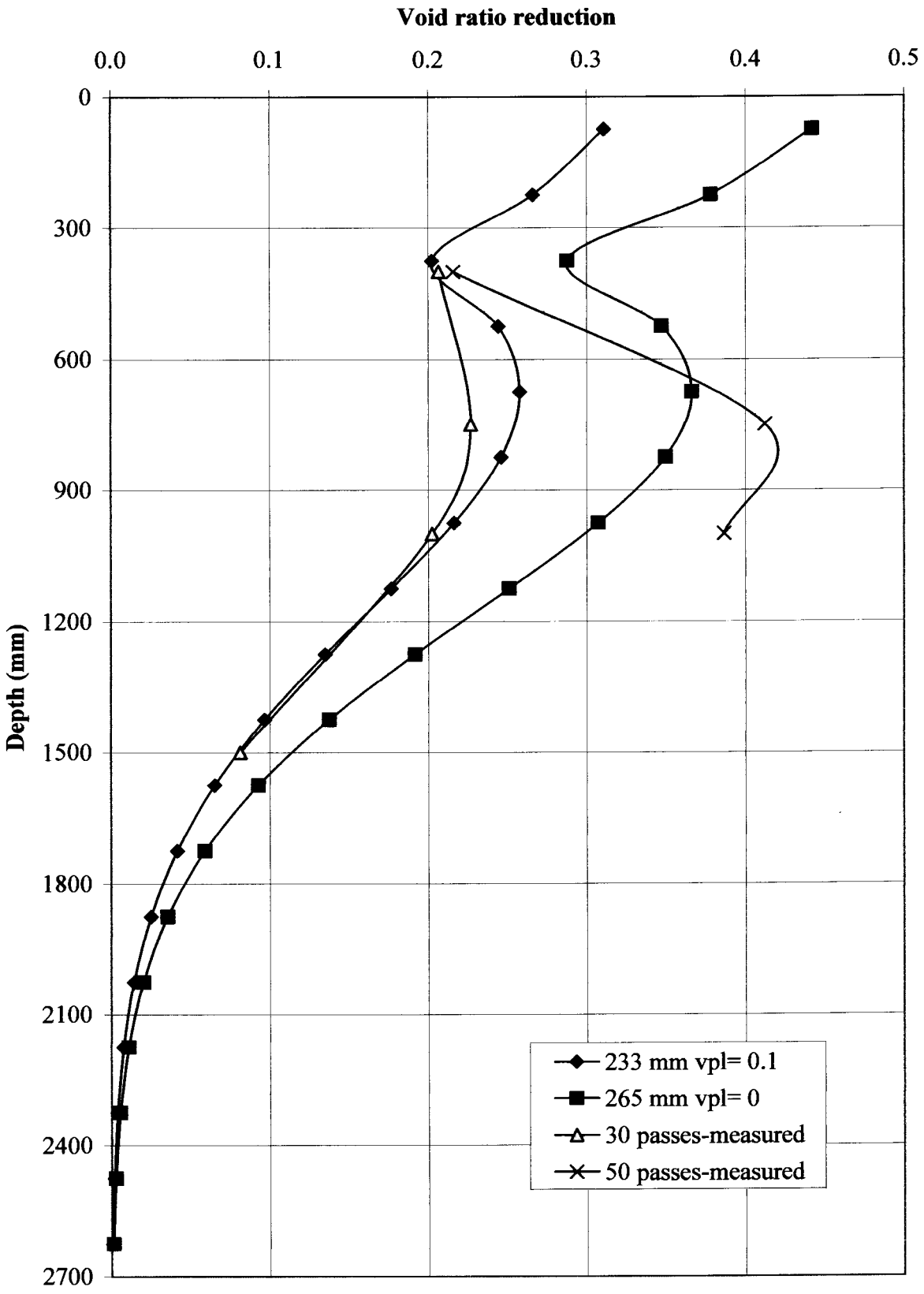

Figure 6.10 : Model verification - Villa Lisa, 1991

(data after Solesbury Walker, 1991)

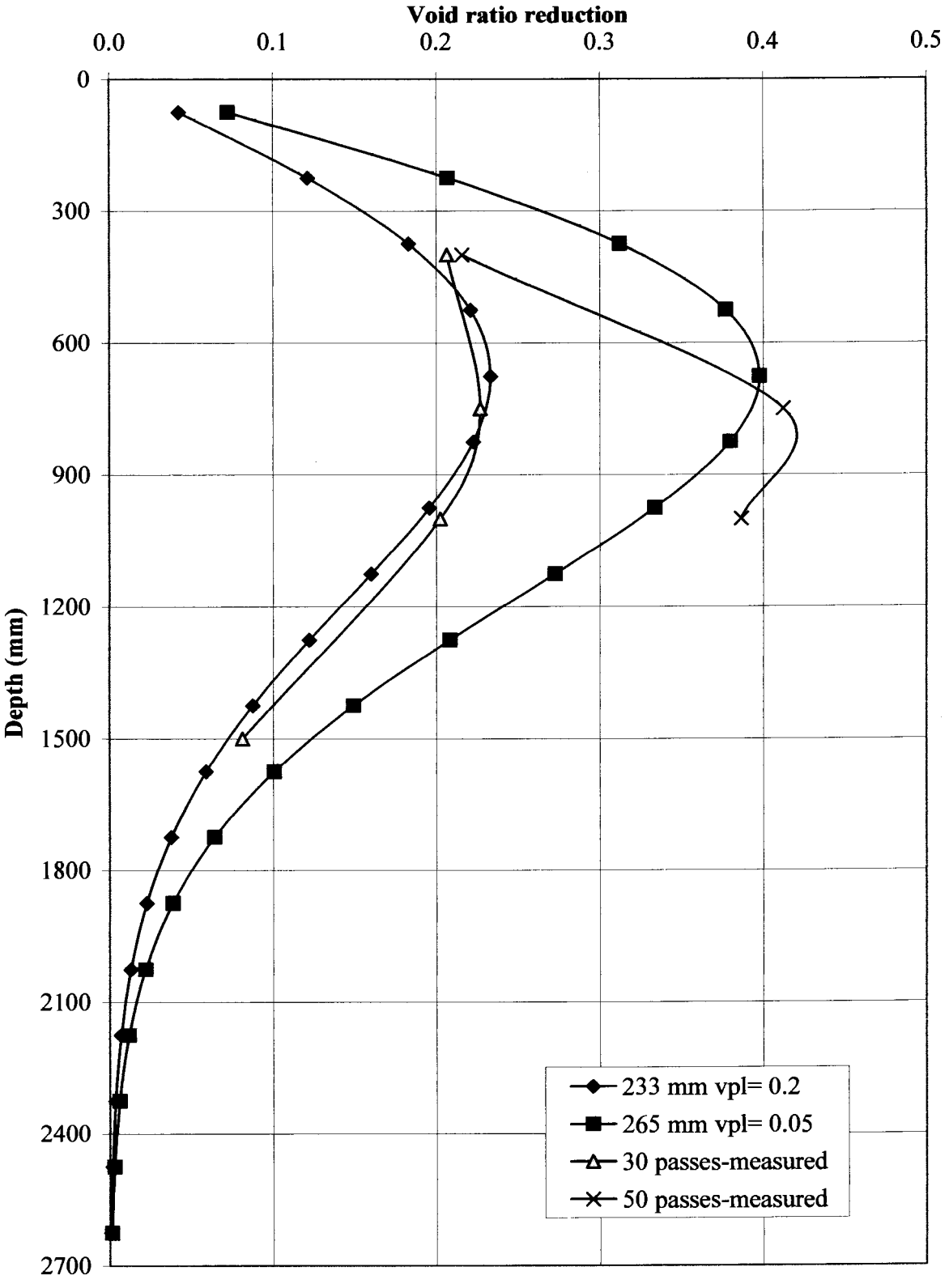

Figure 6.11 : Model verification - Villa Lisa, 1991 [Unmodified Rayleigh volumetric strain distribution]

6.3.6 Site No. 6 – Serowe-Orapa (1991)

Significant trials have also been undertaken in Botswana using mainly three sided 25kJ Landpac impact compactors. The model was checked against tests performed during the construction of the road between Serowe and Orapa, as presented by Pinard (1988).

Back-calculation of void ratios from the settlements recorded are shown in Figure 6.12, using the proposed volumetric strain influence distribution. The model underestimates the densities in the upper part of profile and gives better correlation lower down in the profile. This indicates that the assumed strain influence distribution over the upper portion is not accurate for the conditions at the site. A profile that more closely follows the elastic volumetric strain profiles appears more applicable here. Figure 6.13 shows the effect of modifying the assumed distribution so that the surface strains are twice that of the lower peak, and the depth of the lower peak is rased from the recommended 0.75B to 0.6B. This results is a depth of influence of 2.1m maximum and a volumetric strain influence distribution that more closely follows the shape of the elastic volumetric strain distribution. The result is a much better correlation in the back-calculated data. Further work is clearly warranted to investigate the variation of the volumetric strain profile with different materials, especially over the upper portion of the profile.

Some examples where the modified Rayleigh distribution is used to estimate the void ratio reduction achieved at a dynamic compaction site, where extensive testing was undertaken, are given next. This is done to illustrate that the principal mechanism of improvement is similar, no matter what kind of compactor is used: surface settlement is a good indicator of the improvements achieved, and can be used to estimate the void ratio reductions achieved.

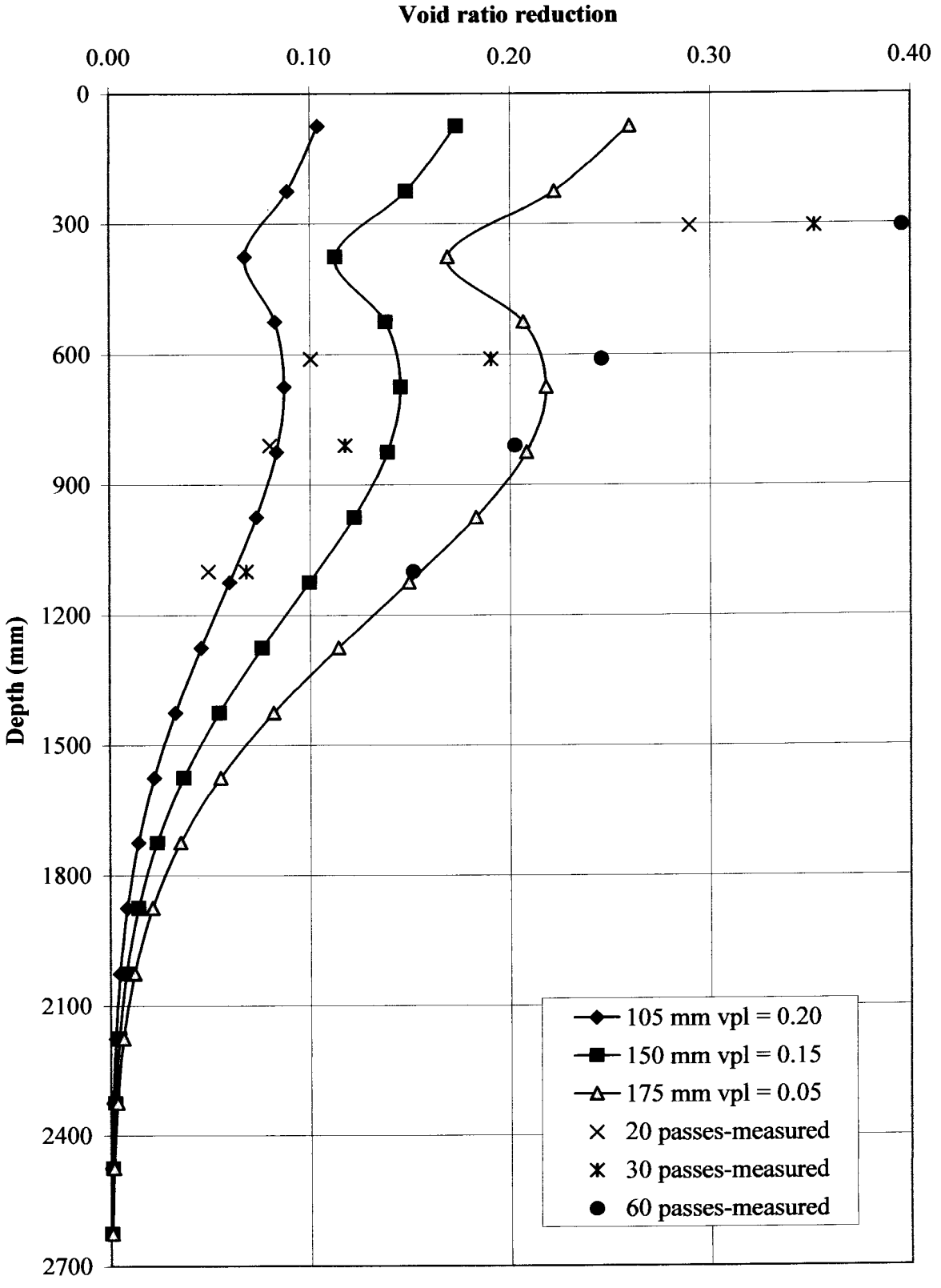

Figure 6.12 : Model verification - Serowe-Orapa, 1988

(data after Pinard, 1988)

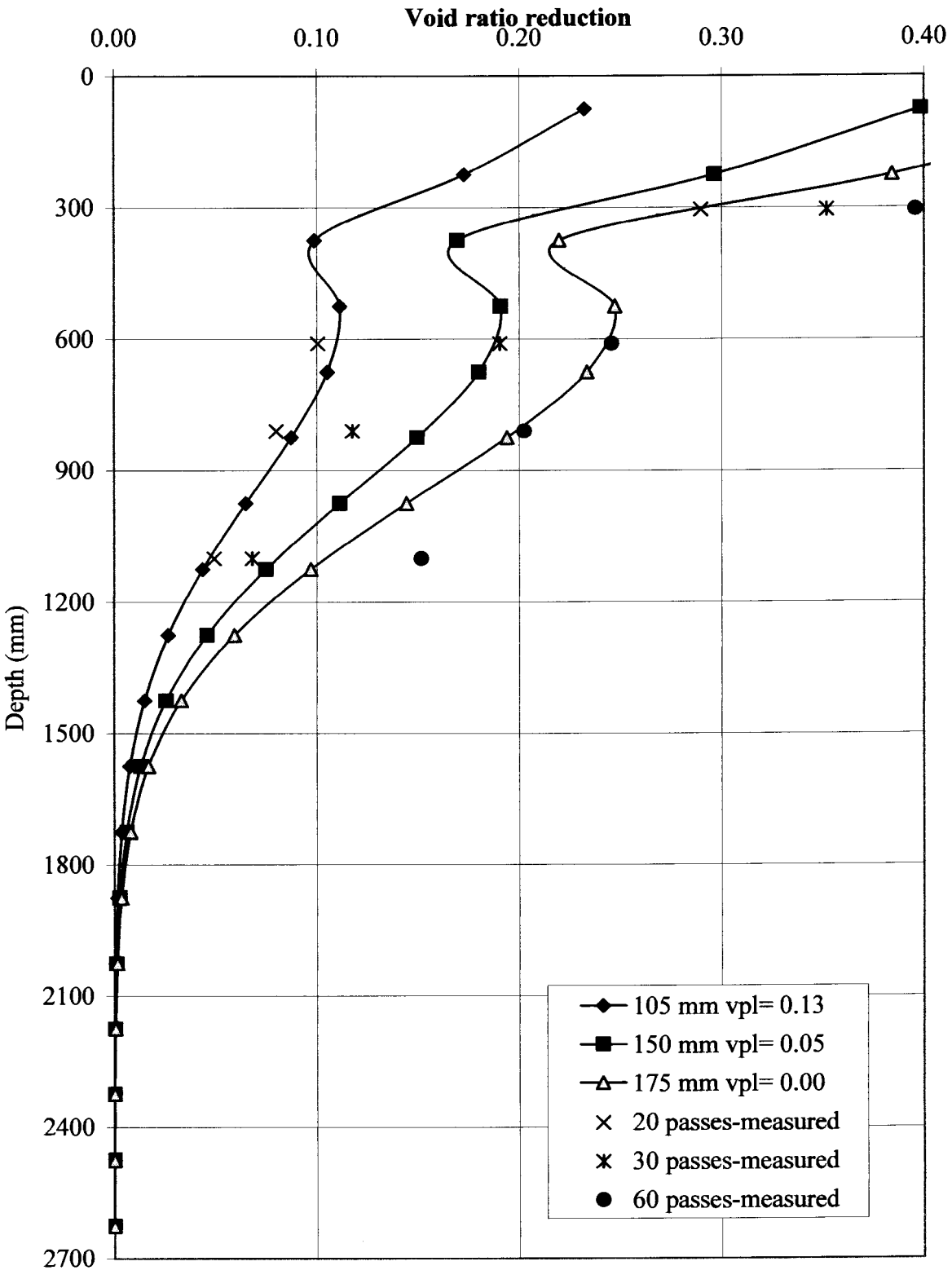

Figure 6.13 : Model verification - Serowe-Orapa, 1988 [Effect of a change in assumed volumetric strain influence distribution]

(data after Pinard, 1988

6.4 VERIFICATION ON DYNAMIC COMPACTION SITES

From the extensive dynamic compaction literature surveyed in the compilation of chapter 2, the patterns of improvement found for impact compactors appeared applicable to dynamic compaction as well. A few additional profiles are also given where the patterns of improvement are confirmed.

Table 6.2 : Dynamic compaction sites used in model verification

Site No.	Name	Reference	No. of profiles	Void ratio from:
7	Nefti, Utah	Rollins, 1998	6	Sand replacement

6.4.1 SITE No. 7 – Rollins (1998).

Extensive work at a site in Utah was undertaken by Rollins to determine whether there is a optimum moisture content for dynamic compaction. Void ratio and moisture content measurements were made throughout the soil profiles, before and after compaction. The use of the data was therefore ideal, especially as the surface settlements were also monitored.

Figures 6.14 to 6.19 show the measured and back-calculated void ratio reduction profiles as the moisture content was increased (to well in excess of optimum for cell 6). It is interesting to note that the operative Poisson's ratio also tended to increase with increasing moisture content. (It is well known that under saturated conditions (undrained behaviour), soil is incompressible and an elastic Poisson's ratio of 0.5 is applicable). [$\varepsilon_{vol}=(1-2\nu)\varepsilon_{vert}=(1-2x0.5)\varepsilon_{vert}=0$]

The modelling showed that for the higher energy levels of a dynamic compactor, a slightly deeper peak in the Rayleigh distribution is applicable (1.0xB compared to 0.67xB for impact compaction). Calculation of the modified distribution is given in Appendix H29, along with the calculations for all the Figures shown in this chapter.

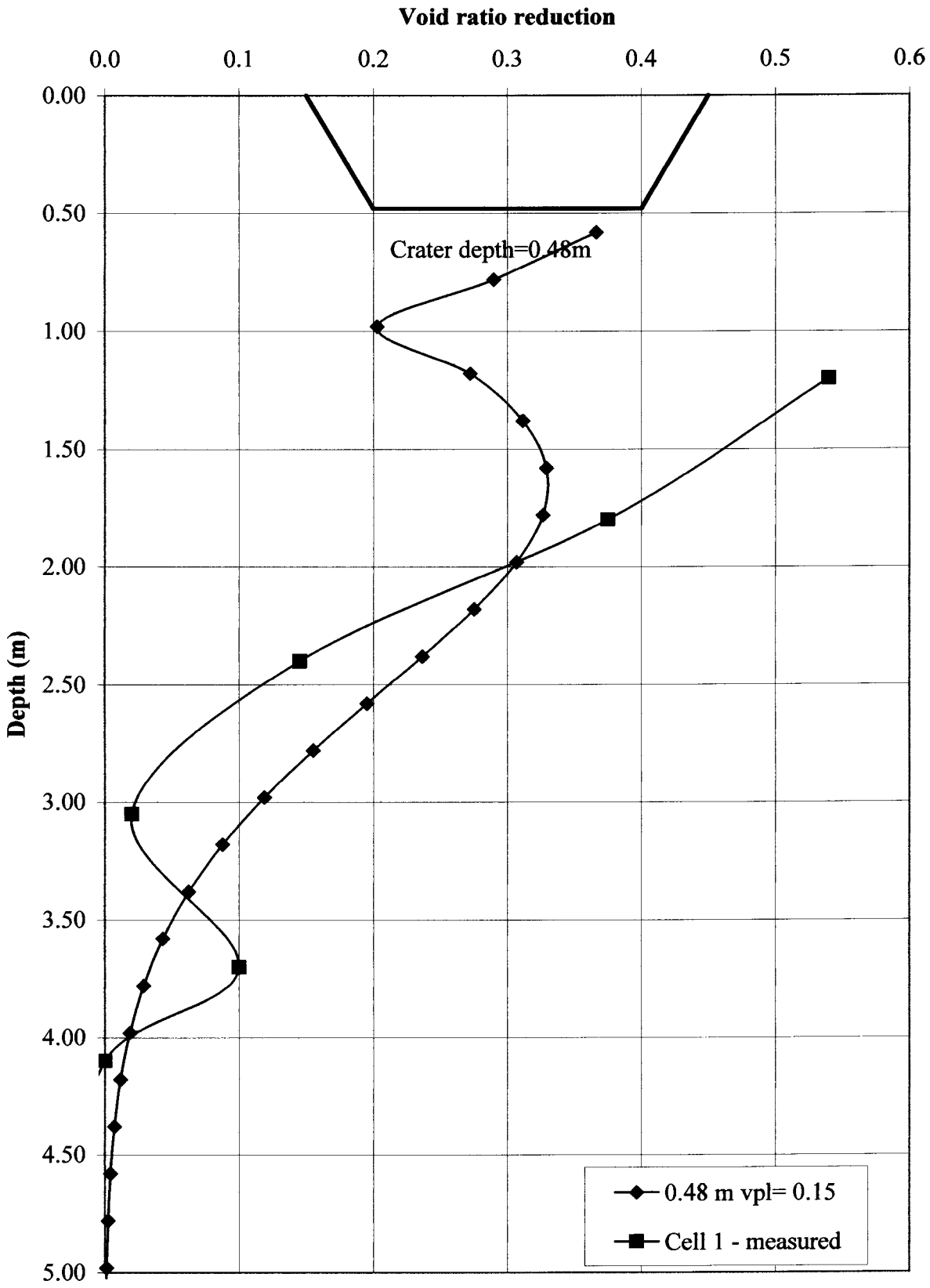

Figure 6.14 : Model verification [DC] - Cell1, Nefti, 1998

data after Rollins, 1998

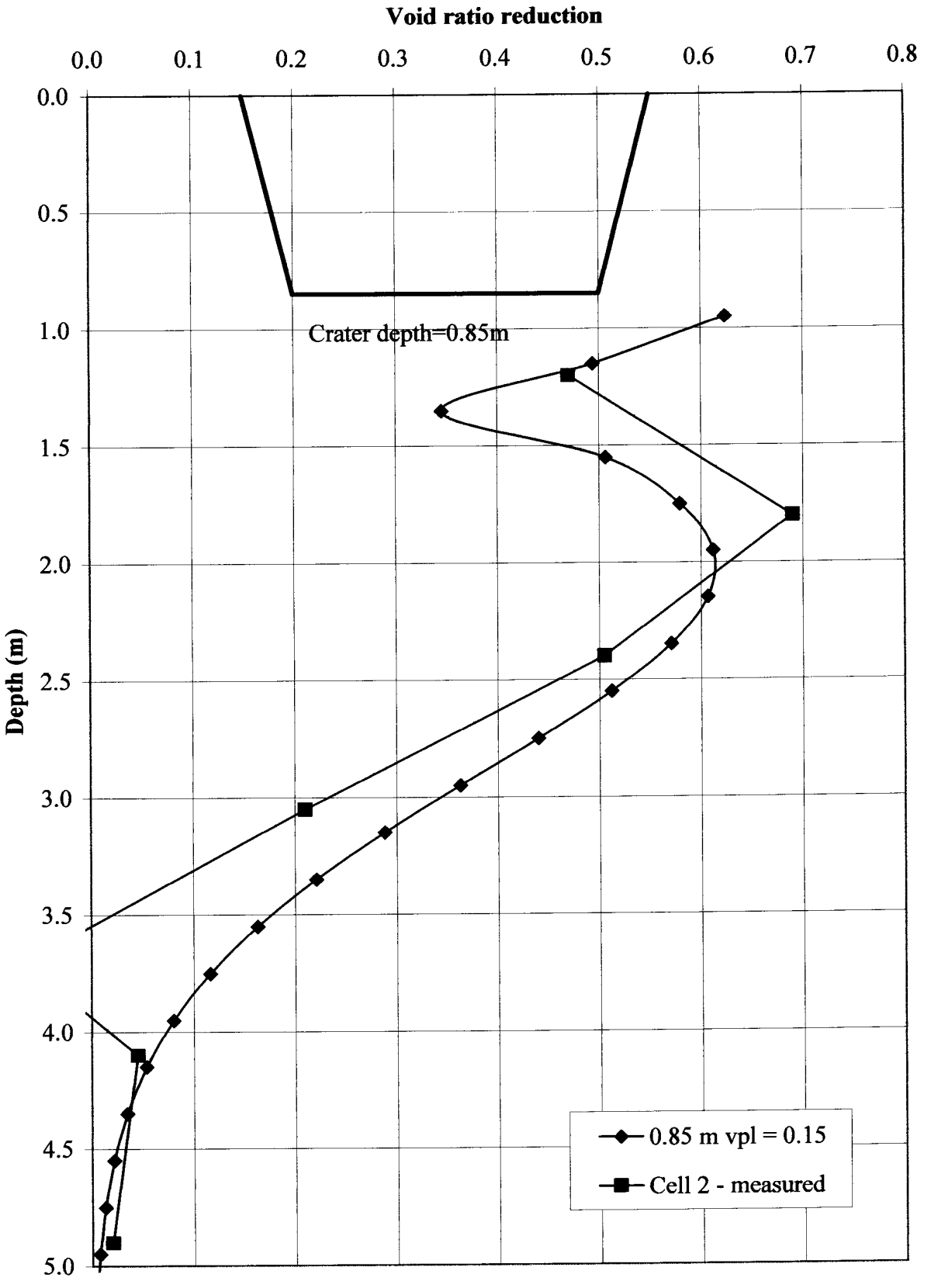

Figure 6.15 : Model verification [DC] - Cell2, Nefti, 1998

data after Rollins, 1998

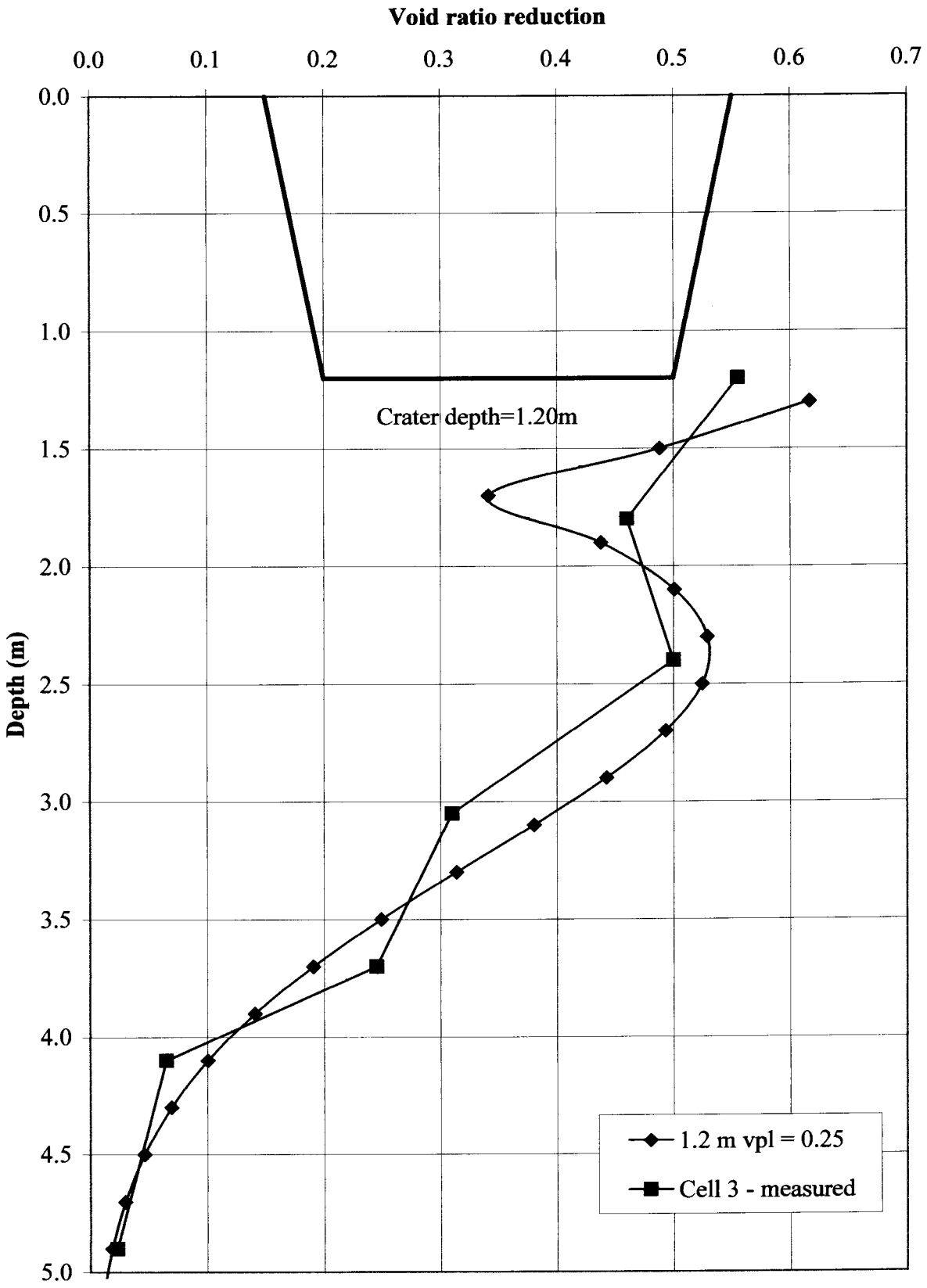

Figure 6.16 : Model verification [DC] - Cell3, Nefti, 1998

data after Rollins, 1998

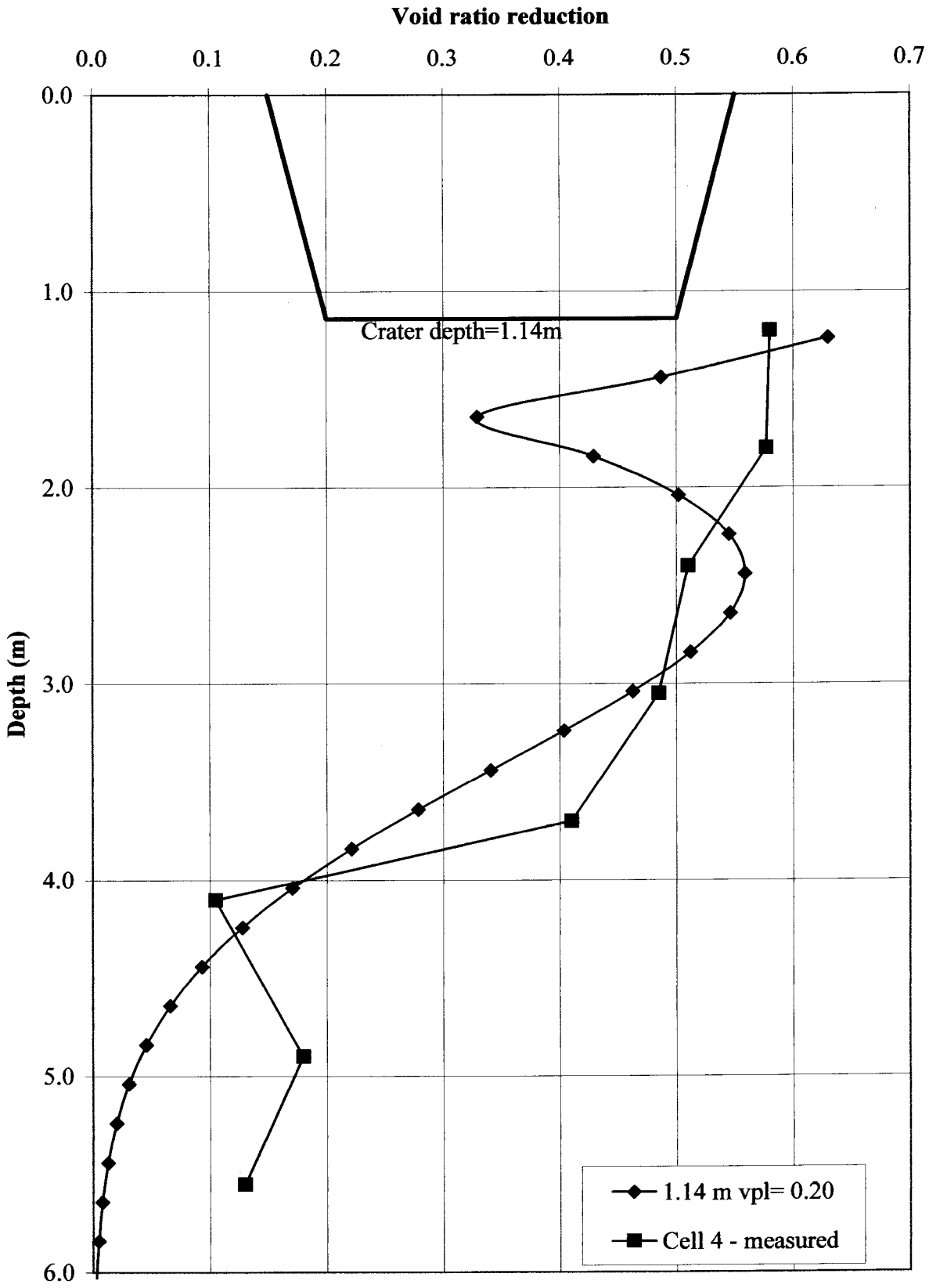

Figure 6.17 : Model verification [DC] - Cell4, Nefti, 1998

data after Rollins, 1998

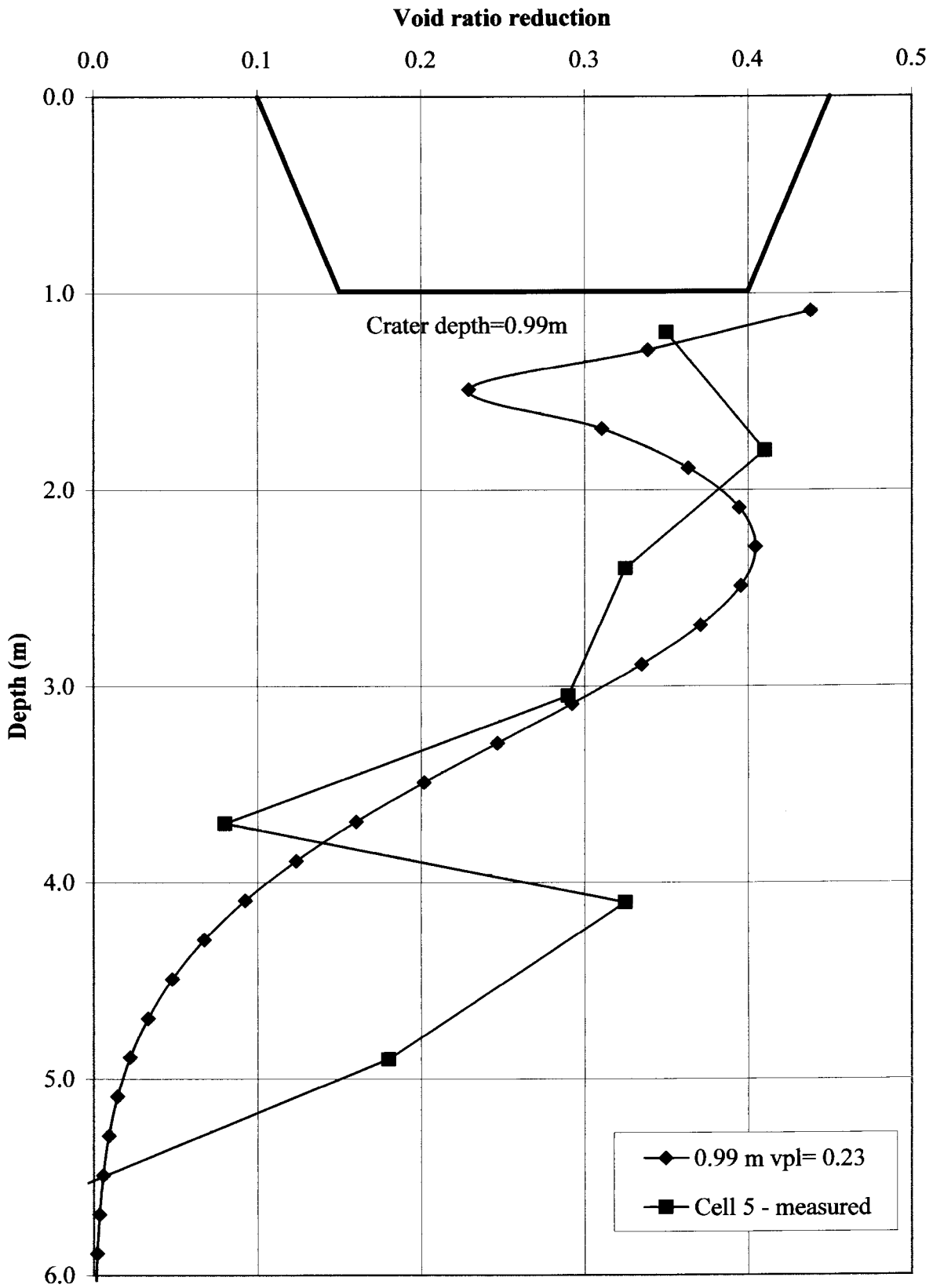

Figure 6.18 : Model verification [DC] - Cell5, Nefti, 1998

data after Rollins, 1998

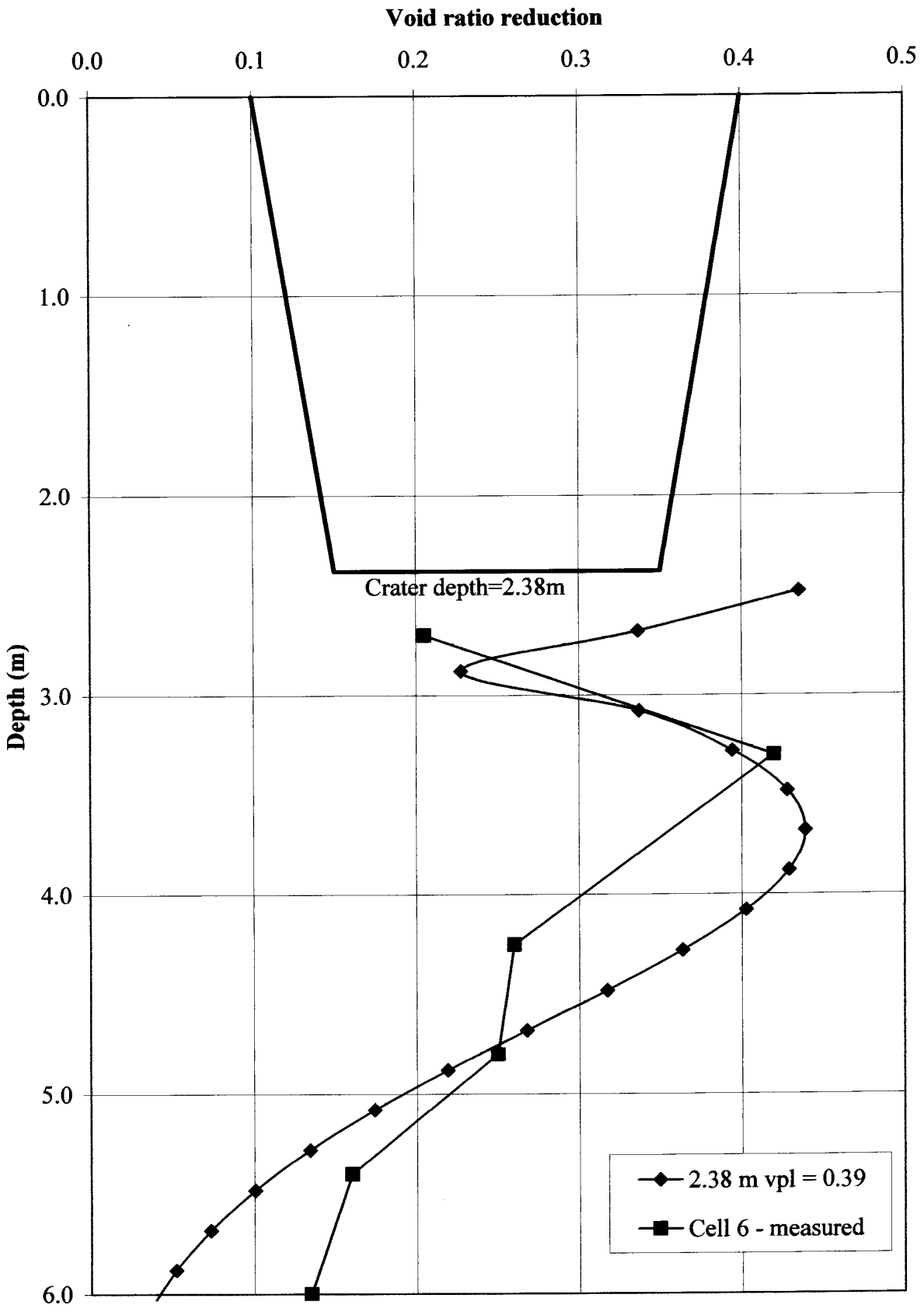

Figure 6.19 : Model verification [DC] - Cell 6, Nefti, 1998

data after Rollins, 1998

The results of the back-analysis of dynamic compaction data confirm that the patterns of improvement found for impact compactors have similarities to the improvement profile of dynamic compactor in un-saturated conditions.

The much higher dynamic forces generated by dynamic compactors further complicate the prediction of improvement, as a punching in quite often occurs when small diameter pounders are used. The initial predictions however, look promising.

6.5 APPLICATION OF MODEL TO CONVENTIONAL COMPACTION

At the International Conference on Compaction held in Paris in 1980, Forssblad presented a paper on the compactometer. In this paper results showing the density – settlement – compactometer accelerations were presented. The applicability of the use of surface settlement to conventional compaction density calculation is demonstrated using this data.

Table 6.3 : Vibratory compaction site used in model verification

Site No.	Name	Reference	No. of profiles	Void ratio from:
8	Compaction trial	Forssblad, 1980b	1	Sand replacement

The calculations for the back-calculation shown in Figure 6.20 and 6.21 are given in Appendix J.

The trial was conducted using a 300mm thick approximately subbase quality material, which was placed on top of a stiff rockfill layer. The strain distribution assumed was constant throughout the layer and assumed no strains in the underlying rock layer. If one-dimensional densification is assumed (1D calc), the surface settlements over-estimate the densification. However, if lateral strains are taken into account using the operative Poisson's ratio, a direct correlation can be achieved between settlement and density.

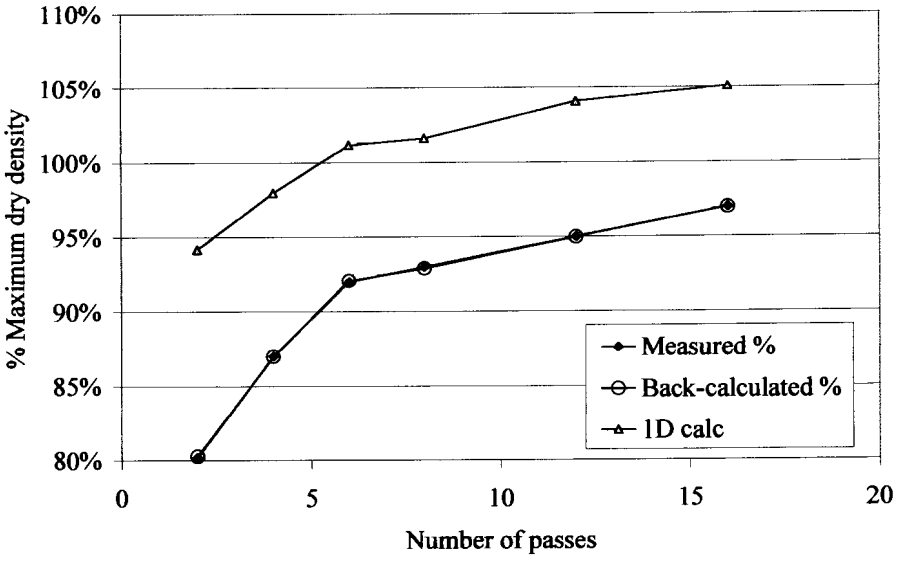

Figure 6.20 : Back-calculated change in densities

The required values of operative Poisson's ratio to achieve an exact correlation are shown in Figure 6.21.

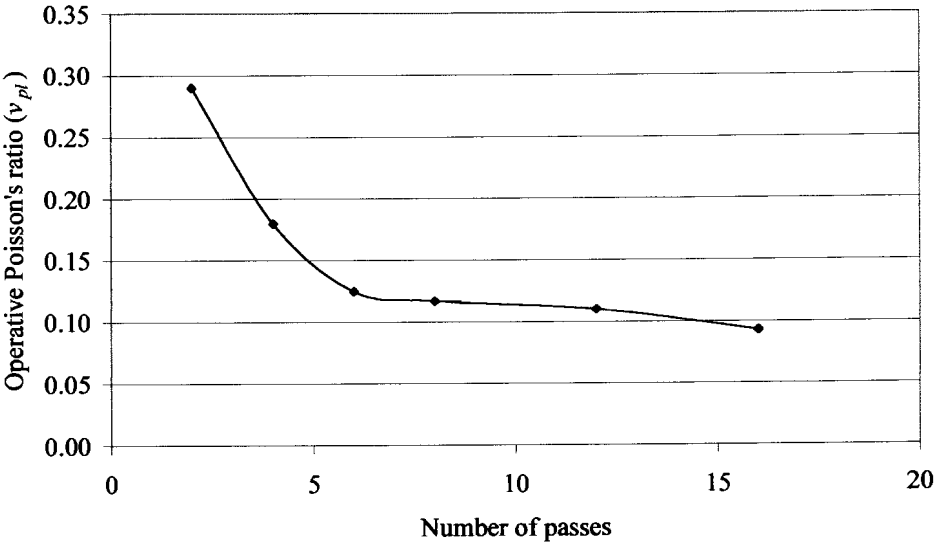

Figure 6.21 : Back-calculated operative Poisson's ratio

It is noteworthy that the back-calculated operative Poisson's ratio reduces from a value close to the typical elastic Poisson's ratio to a lower value during the compaction process. An intuitive explanation for this is that strain hardening is taking place and hence stiffening occurs in both the vertical and horizontal directions.

This warrants further investigation.

The use of surface settlement to estimate the densification during conventional compaction therefore also seems feasible if the operative Poisson's ratio is known.

6.6 VERIFICATION USING A 2 TON DROP MASS COMPACTOR

In order to simulate the compaction achieved by an impact compactor a 2 ton drop mass machine [DMM] was developed by Landpac with a view to simulation of the impact compaction process. The foot-plate of the compactor is of a similar size, while the energy could be varied up to a maximum of about 18kJ/blow. The details of this testing was reported by Berry (1999). A typical result of the soil improvement is shown in Figure 22. Reasonable agreement with the measured and back-calculated void ratio reduction is found, but a volumetric strain distribution that more closely follows the elastic volumetric strain profile would have been more appropriate. By decreasing the peak of the Rayleigh distribution, the depth of influence (DI) is decreased (DI=3.5σ, where σ=depth of the peak). A plot of this revised distribution is also shown in Figure 22 with the depth of the peak at 0.45m. The resulting distribution more closely fits the measured data. This seems to support the findings of the numerical analysis (see Figures 4.6 and 4.7), where materials with higher strength parameters such as the well-graded gravelly sands at the site, are less likely to dilate below the load. Below the Rayleigh peak the default strain distribution proposed yields reasonable results.

The volumetric strain influence profile appears to be a function the soil strength parameters, compactor geometry, mass and energy. Until a better understanding of the dynamic volumetric strain profile is obtained, a unique volumetric strain influence distribution, obtained form static analysis as proposed, appears adequate for initial estimates of improvement.

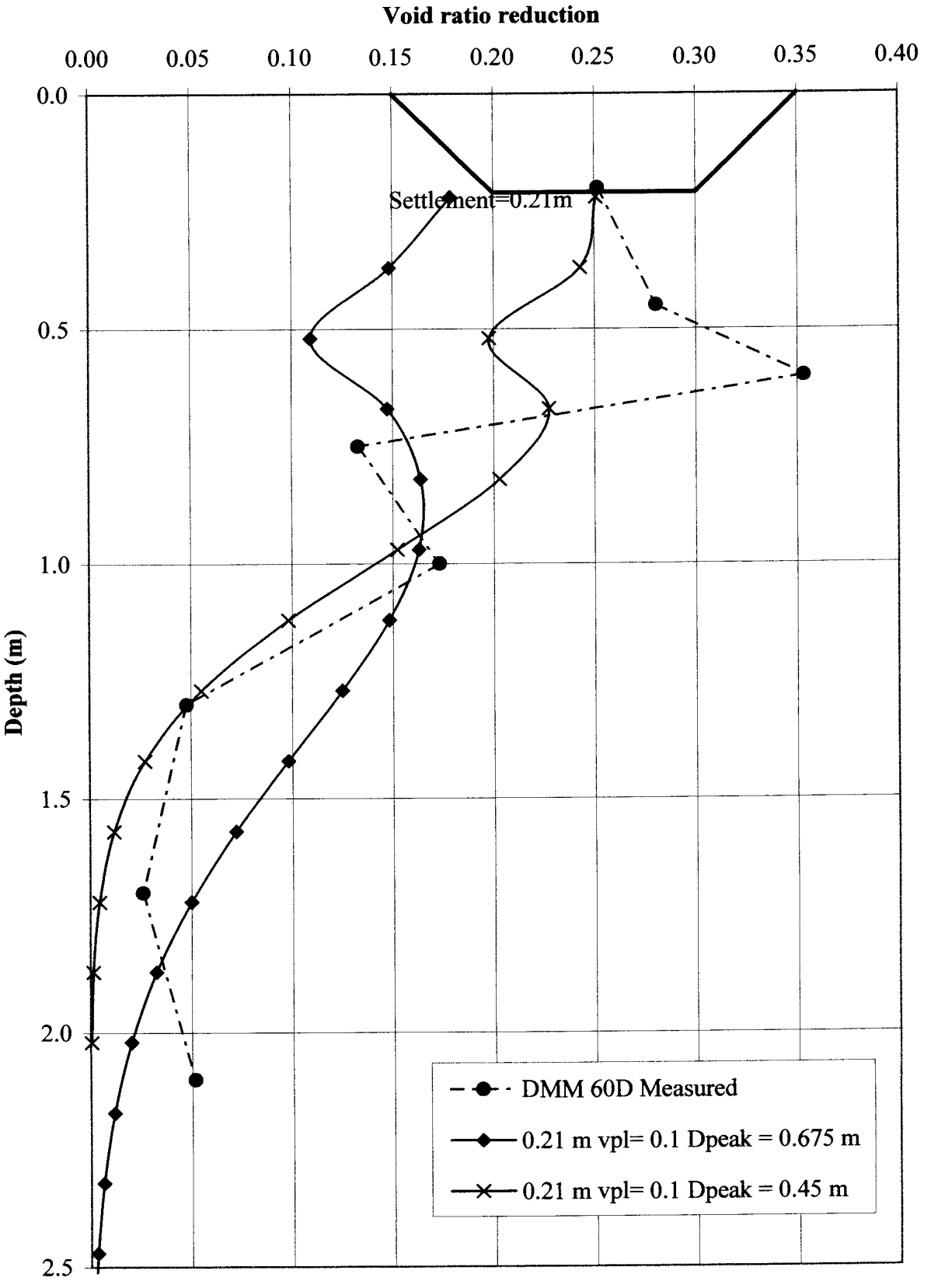

Figure 6.22 : Model verification [DMM-Midrand]

Report for Landpac, Berry (1999)

6.7 DISCUSSION

6.7.1 *Limitations of the proposed model*

6.7.1.1 *General*

The proposed void ratio reduction prediction model appears to be generally applicable to impact compaction, dynamic compaction and conventional compaction if the compactor contact dimensions are known and the surface settlement is measured. The model is not intended for use where the water table is present within the depth of influence of the compactive load (i.e marine conditions etc). Furthermore, a single volumetric strain influence distribution has been used throughout, with no allowance for layering of the soil, or changes in the soil strength parameters. These additional parameters could be built into a more comprehensive model. These limitations are common to most of the prediction models surveyed in the literature study. The factors that significantly affect the predictions of the proposed model are discussed below.

6.7.1.2 *Choice of volumetric strain influence diagram*

A limitation of the model is the selection of an representative volumetric strain influence diagram. This includes estimating the depth of influence at the end of compaction and an appropriate distribution of permanent volumetric strains. Static numerical analysis and field data confirmed a depth of influence of approximately 3 times the impact compactor contact width (B) gives a good estimate of the maximum depth of compaction. The proposed "S" shaped volumetric strain influence diagram appears to give a reasonable estimate of the average volumetric behaviour under the compactor. The current proposal that a single volumetric strain influence profile applies to all soil types and conditions, is clearly an over-simplification. Yet the model yielded acceptable results in most of the soil types encountered in this study (R^2=0.59 in Figure 6.23). The greatest deviations are often found over the top 0.75B meters below the compactor. Large variations in the volumetric strain profile were also found in this region in the numerical analysis in undertaken in chapter 4.

A model that accurately predicts the improvement close to the surface is therefore going to be difficult to achieve. In addition, verification testing at close vertical and horizontal intervals is not often undertaken, and changes in the soil improvement profile may therefore not be measured.

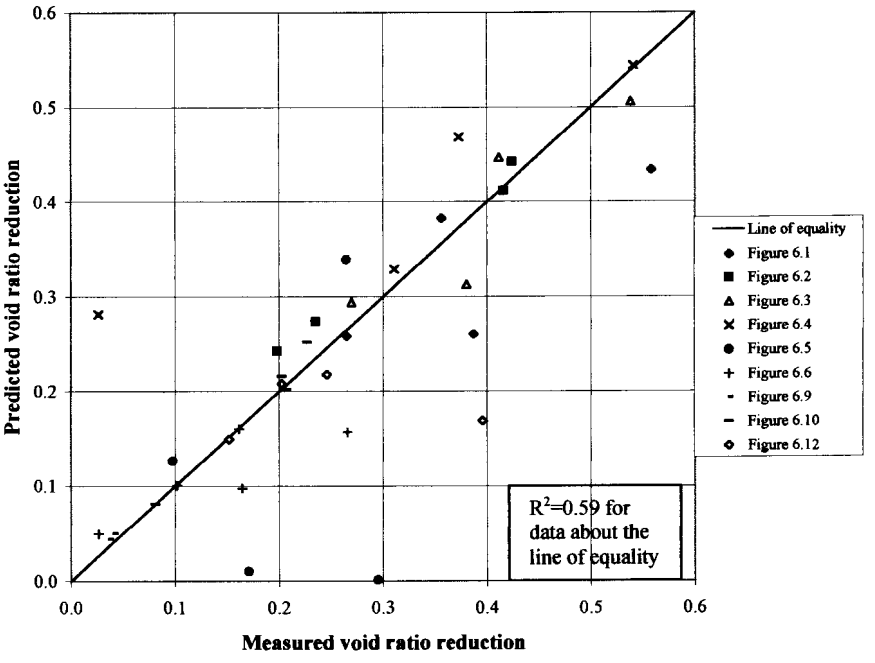

Figure 6.23 : Comparison of measured and predicted void ratio reduction for impact compaction

The use of the Rayleigh distribution limits the depth of influence of the compactive load to 3.5σ, where σ is the depth to the peak of the distribution. Possible alternative distributions can be used, but the proposed distribution is preferred as it highlights the complexity of the behaviour under the loaded area and, being continuous, allows for simple calculation in a spreadsheet.

To properly assess the permanent volumetric strains under a compactor, a dynamic analysis using the measured displacement-time plot as input is essential (Lourens, 2000). The soil constitutive model should allow for non-linear soil behaviour and preferably takes hysteresis into account.

Although a complex analysis may be preferable, Figure 6.24 shows that a good correlation was obtained when the model was applied to dynamic compaction.

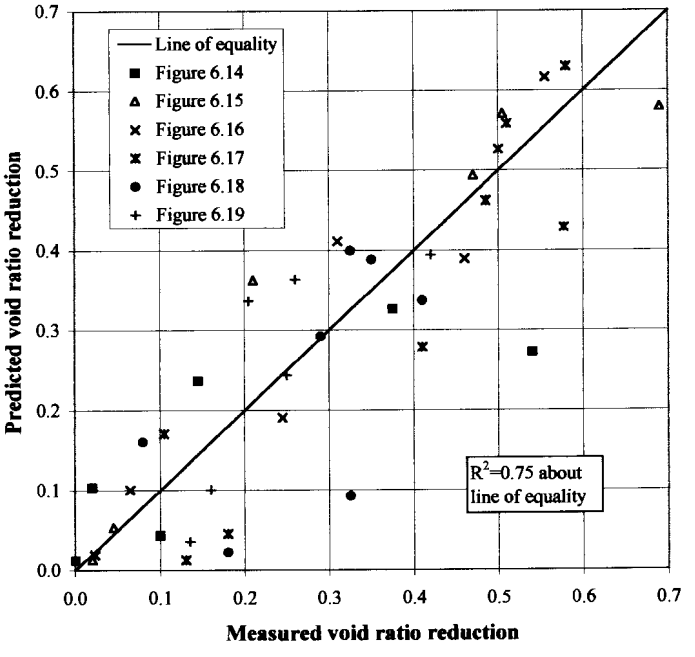

Figure 6.24 : Comparison between measured and predicted void ratio reduction for dynamic compaction

In addition to the good correlation obtained in Figure 6.24, the frequent presence of a peak in the improvement profile data appears to tie in with the presence of a peak in the residual horizontal stress profile.

The occurrence of residual horizontal stresses occurs because of elasto-plastic strains according to Smith and Yandell (1987). A plot of the residual horizontal stresses calculated in the FLAC numerical analysis is shown in Figure 6.25. The peak calculated by the intersection of the horizontal stresses and the passive pressure line (Kp=3.0) is slightly deeper than anticipated at 1,1m. However, if Kp>3.0, as noted is possible by Broms (1965), then the residual horizontal stress peak would increase to between 1.1m and 0.6m (Broms noted that Kp can vary between Kp and 3Kp for passive toe-in pressures for soldier-pile walls).

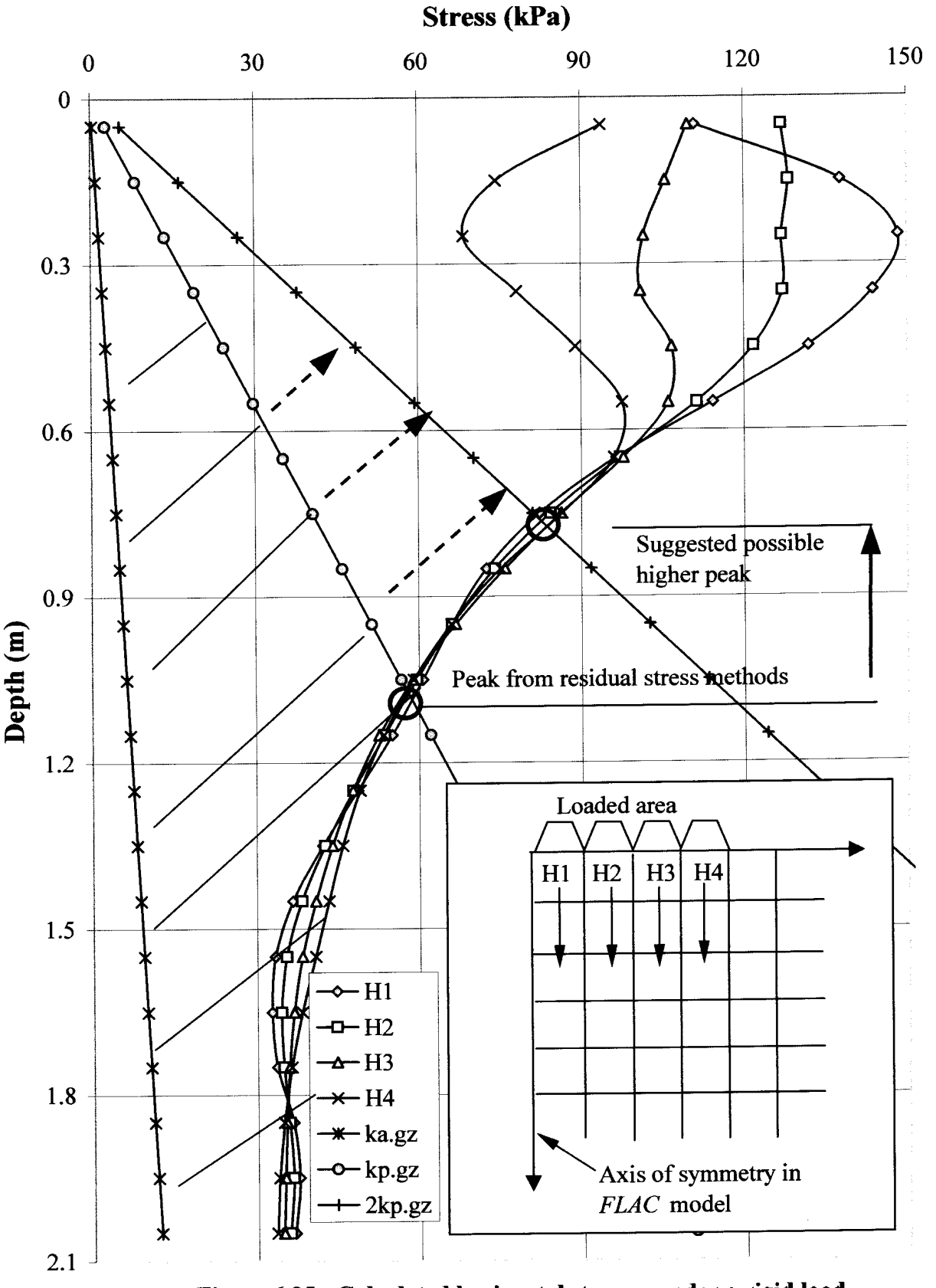

Figure 6.25 : Calculated horizontal stresses under a rigid load

Figure 6.25 shows the effect of an increase in the Kp line on the distribution of residual horizontal pressures. The common thread between the currently proposed volumetric strain influence profile and the residual compaction stress method appears to be the presence of permanent lateral strains and the presence of a peak in the improvement profile. Both these models are similar in principle to the patterns noted by Lukas (1986) and shown in Chapter 2, Figure 2.2. Patterns of improvement appear to be emerging using different approaches. Further research could therefore investigate these similarities further.

An empirical method is currently being investigated by the author, of estimating the improvement in stiffness of the soil after compaction, using the residual (locked in) horizontal stresses as a basis of the prediction.

What is interesting to note from Figure 6.25, it the variation in the horizontal stress profile immediately below the loaded area. Series H1 shows the stresses immediately adjacent the axis of symmetry in an axi-symmetric model, while H4 represents the stresses below the edge of the edge of the rigid loaded area. The elasto-plastic stress distributions do not necessarily follow the continuously decreasing profile of elastic theory. This behaviour could perhaps explain the pressure transducer measurements of Figure 6.7.

6.7.2 *Operative Poisson's ratio*

A further limitation of the model is in determining the value of the operative Poisson's ratio, ν_{pl}. The use of the operative Poisson's ratio is an attempt to correct the over-estimation in void ratio reduction initially found, when one-dimensional behaviour was assumed. The important effect of lateral strains in compaction was highlighted by Chow et al (1992).

The presence of permanent strains and the cumulative nature of these strains have been demonstrated by Wolff and Visser (1994). No literature can be cited where use is made of an operative Poisson's ratio to estimate permanent volumetric strains.

The hypothesis needs further verification and testing, but provides a simple tool for estimating permanent volumetric changes in the soil without the need for complex analyses. The approach is therefore pragmatic and semi-empirical as v_{pl} requires back-calculation to be quantified.

Initial indications are that the value of v_{pl} is about 0.15 at the end of the compaction process, as indicated in Table 6.4.

Table 6.4 : Summary of operative Poisson's ratios from back-calculation of impact compaction data

Figure No	v_{pl}	Type of compactor
6.1	0.075	23kJ IC
6.2	0.175	23kJ IC
6.3	0.175	23kJ IC
6.4	0.150	23kJ IC
6.5	0.250	25kJ IC
6.6	0.075	15kJ IC
6.9	0.100	23kJ IC
6.10	0.100	23kJ IC
6.11	0.200	23kJ IC
6.12	0.150	25kJ IC
6.13	0.075	23kJ IC
Average	*0.14*	*[Std dev=0.06]*

A summary of operative Poisson's ratios back-calculated in verifying the model for dynamic compaction, is given in Table 6.5. A value of approximately 0.25 appears an appropriate initial estimate for v_{pl} for dynamic compaction. As the database of back-calculated values increases, this initial estimate can be revised.

It is believed that the convention to compact on a grid (5.4m minimum spacing) leads to there being significant lateral strains during dynamic compaction, and larger values of v_{pl} are therefore hypothesised.

The argument for this is as follows: Current model impact compactors impact the ground between about 1.5m to 2.5m centres depending on the type of compactor.

Table 6.5 : Summary of operative Poisson's ratios from back-calculation of dynamic compaction data

Figure No	v_{pl}	m.c %	Type of compactor
6.14	0.15	7	DC
6.15	0.15	10	DC
6.16	0.25	15	DC
6.17	0.20	17	DC
6.18	0.23	18	DC
6.19	0.39	20	DC
Average	*0.23*	*Std. Dev.=0.09*	

With repeated passes of the compactor, the ground is usually compacted in different positions, resulting in a uniform distribution of compaction energy density (kJ/m^2) to the lane being compacted. In addition, split drum compactors compact in strips as shown below in Figure 6.26, alternating from one strip to the other in successive passes.

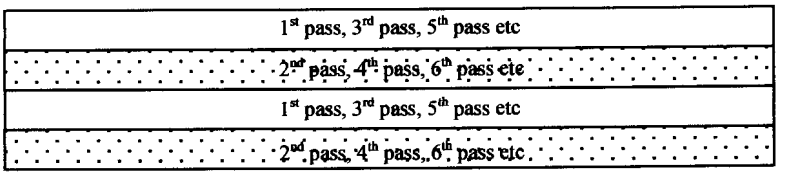

Figure 6.26 : Typical split drum impact compaction rolling procedure

The author believes that when compacting adjacent lanes, lateral strain hardening is occurring. This can be likened to bending a piece of wire, first in one direction and then back again. When compacting one lane lateral strains occur in the direction of the adjacent lane. When compacting the other lane, strains in the opposite direction occur, with an effect similar to bending back the wire. The close proximity of the compaction lanes, it is suggested, results in significant lateral stiffening. It is further suggested that this effect is not nearly as pronounced when the compaction blows are far

apart, as with dynamic compaction. A higher value of the operative Poisson's ratio is therefore hypothesised for increased compactor impact spacing. The effect of surface ironing after dynamic compaction does however, result in a more even application of applied energy. This should be investigated further.

From Figure 6.27, it appears possible that ν_{pl} increases with moisture content (Data from Figures 6.14-6.19).

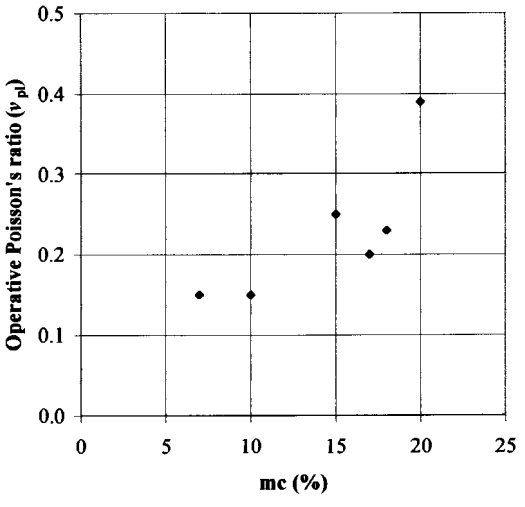

Figure 6.27 : Variation of ν_{pl} with moisture content at a dynamic compaction site

The saturation moisture content for the soils at the site was approximately 33%. The effect of moisture content on the plastic volumetric strains warrants further investigation.

In Figure 6.21 it was also demonstrated that the back-calculated ν_{pl} varied from about 0.3 at the beginning of compaction to 0.1 at the end of the compaction process, using an 11 ton vibratory compactor. This shows similarity in behaviour to the plasticity parameter, ε, proposed by Adam et al (2000), shown in Chapter 2, Figure 2.12. These authors noted that the soil becomes more elastic as compaction proceeds. The reduction in ν_{pl} from 0.3 to 0.1 can be explained by the build-up of residual horizontal stresses due to permanent lateral strains. In other words, a strain hardening appears to be

taking place as the horizontal stresses become "locked-in". It is suggested that further work in this regard be conducted, particularly with the aid of the Mechano-lattice software developed by Smith and Yandell (1987).

6.7.3 *Effect of layering*

The effect of a layering has not been included in the proposed model. A more comprehensive model could make allowance for changes in the soil's initial density and stiffness. It is proposed that if layering needs to be taken into account, the volumetric strain influence distribution be obtained from a numerical model. Stiff layers would show a reduced volumetric strain and softer layers an increased volumetric strain within each layer. In developing such a model, the effect of wave absorption and reflection would probable need to be considered. It is probable that layering only need be taken into account for sizeable projects, where the additional effort is warranted.

6.7.4 *Effect of the water table*

The current model is not applicable to compaction with the water table within the zone of influence of the compactor. A criticism levelled at most of the DC models currently available is that no clear differentiation is made between compaction with the water table absent or being present.

The presence of water completely changes the soils response to load and effective stresses and pore water and pore air pressures become significant.

The long-term volumetric effects in a saturated soil is complex, but from observation of field data where the water table is present, its appears that the Rayleigh distribution may be modified to include a longer tail. (see Appendix J). The explanation according to Varaksin (1981) is that the shock waves (Compression, shear and Rayleigh waves) are felt deeper due to the virtually incompressible water. If sufficiently permeable ($<10^{7}$m/s) the soil will consolidate in proportion to the permeability within the zone of increased pore water pressure. An example of the soil improvement profile with the water table near the surface is attached in Appendix J.

As impact compaction usually takes place unsaturated conditions, a model that considers saturated conditions is not essential.

6.7.5 *Suggested further research*

6.7.5.1 *Profile of work done on the soil*

In addition to the dynamic analysis suggested earlier, an investigation into the profile of work done in the soil under a dynamic load, taking hysteresis into account, is also suggested. It is suspected that there will be a correlation between the work done on the soil, once losses are taken into account and the improvement profile. This may then lead to a comparison between input energy of the pounder to the work done on the soil, highlighting where the energy losses occur. This could then result in more efficient compaction methods being proposed.

The dynamic analysis could also investigate the effect of compactor's impact load duration. It is commonly believed that a larger drop height (or total energy input) results in deeper and better compaction. The author suspects that above a certain contact stress, little if any benefit is gained as the energy is wasted in dilation of the soil near the surface.

6.7.5.2 *Investigation into the induced pore water and pore air pressure distributions*

It is believed that the distribution of pore air pressure, and possibly pore water pressures, increases in proportion to the volumetric strains induced during compaction. These effects should perhaps form part of a more comprehensive study.

6.7.5.3 *Prediction of surface settlement and energy requirements*

No attempt has been made to predict the energy requirements to achieve the surface settlement that is used as primary input into the proposed prediction model. This is a limitation to contractors, who have to estimate the energy requirements before making an offer. This limitation is usually overcome by undertaking a compaction trail once on site, from which both the surface settlement and energy requirements can be adjusted.

Never-the-less, the prediction of energy requirements for impact compaction is still based on experience. Many dynamic compaction models predict the energy requirements, but seldom settlement. It is unlikely that any model that does not consider the initial void ratio of the soil can predict the surface settlement after compaction. None of the dynamic compaction models are applicable to the prediction of impact compaction energy requirements and so further work in this area may be required.

6.8 CONCLUSIONS

A simplified volumetric strain influence model for predicting the profile of void ratio reduction for impact compaction has been proposed. The model was verified with reasonable success on 15 impact compact profiles. Further work is required to confirm the shape of the volumetric strain influence profile, particularly in the upper portions of the profile, but the proposed model appears adequate for initial estimation purposes, in unsaturated conditions.

The relative simplicity of the model is one of it's main limitations, but it is believed that this simplicity has highlighted patterns of behaviour that can serve as a starting point for further detailed research.

In addition, the principles of the model were also applied to both dynamic and conventional compaction with reasonable success.

CHAPTER 7

SUMMARY AND CONCLUSIONS

7.1 SUMMARY

The purpose of this dissertation was to show that the profile of improvement in the ground is predictable and proportional to the surface settlement of the compacted ground, provided lateral deformation is taken into account.

To accomplish this task, the pertinent literature was surveyed. No prediction model was found in compaction literature surveyed, which predicted the volumetric changes in the ground based on the surface settlement after compaction.

In order to estimate the volumetric changes in the ground using a numerical model, an estimate of the dynamic force of the compactor is required. This was achieved using an accelerometer attached to the tube axle of the compactor. Comparisons of measured and predicted decelerations were in good agreement and the dynamic force applied to a numerical model to estimate the volumetric strains in the ground. The numerical model highlighted the complexity of the strains. The average volumetric strain profile under the compactor was adopted for use in a simplified model.

Data from fifteen impact compaction profiles on six different sites was collected. In addition to this, measurement of the ground improvement using a two-ton drop mass compactor was undertaken. Data from dynamic compaction and vibratory compaction research was also used to demonstrate the principle of the model appears to be applicable to various types of compaction. Although actual predictions were not undertaken by virtue of the data being back-calculated, reasonable correlation of "predicted" against back-calculated data was achieved.

Some of the significant findings of this study were:

- Surface settlement can be used to estimate the void ratio reduction in the soil after impact compaction
- The proposed soil improvement model for impact compaction appears to be applicable to other forms of compaction
- The volume changes under dynamic loading are complex and a dynamic analysis is warranted to better understand the volumetric strain profile under impact loading. A more detailed analysis that can more accurately model the permanent strains should be used.
- The assumed volumetric strain influence diagram/distribution yields reasonable results considering the simplification of the complex problem at hand. Modification to the assumed volumetric strain influence distribution is likely as a better understanding of the factors affecting the distribution unfold.
- The simple numerical analysis performed in Chapter 4 indicated that the soil strength parameters have a major effect on the volume change characteristics of the soil, and could in future be built into a more rigorous model.
- Lateral strains appear to have a significant effect on the volume changes in the soil.
- Back-calculation is required to estimate operative Poisson's ratio, ν_{pl}, which is essentially a plastic soil volume change parameter. The model is therefore dependent of an accurate assessment of this parameter and therefore remains semi-empirical is nature. The soil volume changes are also very sensitive to the magnitude of ν_{pl}.
- Small settlements imply small void ratio reductions (little improvement achieved)
- Improvement of between 2 and 3 compactor diameters can typically be expected for an impact compactor, in unsaturated conditions
- Improvement of between 3 and 4 compactor diameters can typically be expected for dynamic compactors, in unsaturated conditions
- A peak in the improvement profile is often found at a depth of about 0.75B for impact compactors and 1.0B for dynamic compactors

7.2 CONCLUSIONS

A simplified volumetric strain influence ground improvement prediction model has been presented. Although in many respects, the model is over-simplified, initial indications are that the reduction is void ratio through-out the depth of influence of an impact compactor, can be estimated with a reasonable degree of confidence. The argument, that the plastic volumetric strains are proportional to the total volumetric strains produced by a compactive load, was (although possibly not proven beyond doubt) given substantial credibility. The proposal that the surface settlement is a direct measure of the improvement in the ground, provided lateral deformation is considered was confirmed. Of particular use to the practicing engineer, is the possibility of drawing contours of void ratio reduction profile possible with varying amounts of surface settlement. A predetermined minimum surface settlement could then be used as a quality control measure.

The model requires three input parameters: the volumetric strain distribution, the operative Poisson's ratio and the surface settlement. Initial proposals have been made for both the volumetric strain distribution and the operative Poisson's ratio. Only the surface settlement is unknown. As the surface settlement is dependent on the initial void ratio of the soil (amongst other parameters), it is recommended that a settlement trial be conducted to determine the magnitude of the settlement.

The study has unveiled patterns of improvement that appear to be predictable. It is recommended that the similarities between the proposed model improvement profile and the residual horizontal stress profile be further investigated, preferably with software capable of modelling dynamic effects as well as hysteresis in the soil constitutive model. The relationship between the void ratio reduction profile and the stiffness profile must also be researched, hopefully leading to a prediction of the stiffness improvement as an additional output to the model.

Similarities in the void ratio reduction profile and the stiffness profile were seen in some of the trials where stiffness was also measured (e.g Kriel, 1998). The relationship between the two is a challenging next step in the research started here.

In conclusion, it is hoped that some of the additional questions raised, will inspire further more detailed research.

REFERENCES

Adam D., & Kopf F. 2000. *Theoretical analysis of dynamiclly loaded soils.* European Workshop: Compaction of soils and granular materials. ETC 11 of ISSMGE. Paris-Nord-Villepinte, France, 19 May, LCPC.

Africon, 1998. Report on the trials at Kriel to access the effectiveness of impact compaction and to establish appropriate means of integrity testing. Report 50444AE/G1/98, Africon Engineering International.

Barrett A J, & Wrench B P, 1984. *Impact rolling trials on collapsing aeolian sand..* Proceedings on Eighth Regional Conference on Soil Mechanics and Foundation Engineering, Harare, p177-181.

Berry A., Strydom, J.H., & van Wijk, I. 1998. *Impact compaction as an effective means of subgrade improvement and the establishment of appropriate methods of integrity testing.* Annual Transport Conference, CSIR, Pretoria.

Berry A D, 1998. *Overview of an impact compaction design method.* Confidential internal report, IREP 016, Landpac, Nigel, South Africa.

Berry A D, 1999. *Drop Mass Machine compaction at Midrand..* Confidential internal report, IREP 025, Landpac, Nigel, South Africa.

Biarez, J. 1980. *General report: International Conference on Compaction.* Anciens Ecole Nationale des Ponts et Chaussees, Laboratoire Central, Paris, Vol III, p13-16.

Broch J.T. 1980. *Mechanical vibration and shock measurements*. Bruel & Kjaer, Denmark.

Broms, B. 1964. *Lateral resistance of piles in non-cohesive soils.* J. of Soil Mech. & Found. Engrg, ASCE, Vol 90, SM3, p27-63.

Charles J. A, Earle E. W. & Burford D. 1978. The treatment and subsequent performance of cohesive fill left by opencast ironstone mining at Snatchhill experimental housing site, Corby. Proc. Conf. Clay Fills, ICE, London, p63-72.

Chow Y. K, Yong D M, Yong K. Y & Lee S. L. 1992. *Dynamic compaction analysis*. Journal of Geotechnical Engineering, ASCE, Vol 118, No 8 [August], p1141-1157.

Chow Y. K, Yong D M, Yong K. Y & Lee S. L. 2000. *Improvement of granular soils by high-energy impact.* Ground Improvement, 4, 31-35.

Clegg B, Kuhn S H & Walker R N, 1969. Report on the field trial to investigate the performance of different types of roller for deep compaction of soil. CSIR report RC/3/69, April 1969.

Clifford J.M. 1978. *Evaluation of compaction plant and methods for the construction of earthworks in Southern Africa.* Submitted in partial fulfillment-MSc (Eng), Dept. of Civil Engineering, University of Natal, Durban.

Davies, T.G., & Karim, U.F. 1995. *An elastodynamic interpretation of impact test apparatus for soils.* Geotechnique, 45, No. 4, p 691-700.

Duncan J.M., & Chang C.Y. 1970. *Non-linear analysis of stress and strain in soils.* ASCE. Vol 96, No SM5, Proc. Paper 7513, p1629-1655.

Duncan J.M., & Seed R.B. 1986. *Compaction induced earth pressures under Ko conditions.* Journal of Geotechnical Engineering, ASCE, Vol 112, No 1 [January], p1-43.

Dunn, A. (2000). *Personal communication.* Svedala representative, Johannesburg, South Africa.

Forssblad, L. 1980a. *Discussion: International Conference on Compaction.* Anciens Ecole Nationale des Ponts et Chaussees, Laboratoire Central, Paris, Vol III, p27-28.

Forssblad, L. 1980b. *Compaction meter on vibrating rollers for improved compaction control.* International Conference on Compaction. Anciens Ecole Nationale des Ponts et Chaussees, Laboratoire Central, Paris, Vol II, p541-546.

Gere J.M. & Timoshenko S.P. 1984. *Mechanics of Materials.* Brooke Cole Engineering Division, Monterey, California, Ch 6, p326.

Hansbo S. 1979. *Dynamic consolidation of soil by a falling weight.* Ground Engineering, Emap Construct, Vol 12, No 1 [January], p 27-36.

Huang Y.H. 1993. *Pavement analysis and design.* Prentice hall.

Heulekom W., & Klomp A.J.G. 1962. *Dynamic testing as a means of controlling pavements during and after construction.* Proceedings, 1st International Conference on the Structural Design of Asphalt Pavements, pp667-685.

Heyns S. 1998. *Response analysis of an impact compactor.* Report LGI98/013, Project No 020-DP, Laboratory for Advanced Engineering (Pty) Ltd., University of Pretoria.

Hussein J.B., & Selig, E.T. 1980. *Predicting compactor performance.* International Conference on Compaction. Anciens Ecole Nationale des Ponts et Chaussees, Laboratoire Central, Paris, Session VII, Vol II, p639-645.

Jessberger H. L. & Beine R. A. 1981. *Heavy tamping: Theoretical and practical aspects.* Proceedings: 10th ICSMFE, AA Balkema, ISSMFE, Stockholm, Vol 3, Session 12 : Soil Improvement, p 695-699.

Kwang Wei Lo, Peng Lee Ooi, & Seng-Lip Lee. 1990. *Unified approach to ground improvement by heavy tamping.* Journal of Geotechnical Engineering, ASCE, Vol 116, No 3 [March], p 514-527.

Landpac, 1991. Unpublished field data on trials undertaken at the Thubelethle township, Kriel. Landpac, Nigel, South Africa.

LCPC, 1986. *Realisation des remblais et des couches de forme.* Fascicule 1, Principes gẽnẽraux, SETRA, prix de vente : 250 F, Paris, France.

Lewis W. A. 1957. *A study of some of the factors likely to affect the performance of impact compactors on soil.* Proceedings: 4th ICSMFE, AA Balkema, ISSMFE, Stockholm, Vol 3, Session 12 : Soil Improvement, p617-622.

Lourens J, 2000. *Personal conversation: Use of a Duncan and Chang model to simulate compaction and the volumetric strain profile.* BKS Consulting Engineers, Pretoria, September 2000.

Lotfi H.A, Schwartz C.W. & Witzak M.W. 1988. *Compaction specification for the control of pavement subgrade rutting.* Transportation Research Record 1196, p108-115.

Lukas R. G. 1986. *Dynamic compaction for highway construction. Vol 1: Design and construction guidelines.* FHWA report No RD-86/133, Washington DC.

Lukas R. G. 1979. *Densification of loose deposits by pounding.* Journal of Geotechnical Engineering, ASCE, Vol 106, No GT4 [April], p435-446.

Lytton R.L., 1999. *Hand written class notes for CVEN649.* Texas A & M University.

Lukas R. G. 1985. *Densification of a decomposed landfill deposit.* Proceedings: 11th ICSMFE, AA Balkema, ISSMFE, Stockholm, Vol 3, Session 12 : Soil Improvement, p617-622.

O'Reily M.P. & Brown S.F. 1981. *Cyclic loading of soils.* Blackie Press, London, p417.

Mayne P. W., Jones J. S. & Dumas J. C. 1984. *Ground response to dynamic compaction.* Journal of Geotechnical Engineering, ASCE, Vol 110, No 6 [June], p757-773.

Mayne P. W., Jones J. S. 1983. *Impact stresses during dynamic compaction.* Journal of Geotechnical Engineering, ASCE, Vol 109, No 10 [October], p 1342-1346.

Menard .L & Broise 1976. *Theoretical and practical aspects of dynamic consolidation.* Ground Treatment by Deep Compaction, ICE, London, p3-18.

Muir Wood D. 1991. *Approaches to modelling the cyclic stress-strain response of soils.* Ch 2 in "Cyclic Loading of Soils", p19-69, Eds: O'Reilly and Brown, Blackie Press, NY.

Novais Ferreira H. 1983. *The earth pressure of compacted soils.* Proc. 8th Intl. CSMFE, Helsinki, p279-282.

Oshima A. & Takada N. 1977. *Relation between compacted area and ram momentum.* Proceedings: 14th ICSMFE, ISSMFE, Hamburg, Vol 3, p1641-1644.

O'Riordan N.J. 1991.*Effects of cyclic loading on the long term settlement of structures.* Ch 9 in "Cyclic Loading of Soils", p19-69, Eds: O'Reilly and Brown, Blackie Press, NY.

Paige-Green P. 1998. *The use of impact compaction in ground improvement.* Report CR-97/098 (prepared for Landpac), CSIR, Pretoria.

Pinard M I, Ookeditse S & Fraser C, 1988. Evaluation of impact roller compaction trials on potentially collapsing sands in Botswana. Annual transport Convention, 1988, paper 3D/7.

Poran C. J. & Rodriguez J. A. 1992. *Design of dynamic compaction.* Canadian Geotechnical Journal, CISMFE, Vol 29, p796-802.

Rollins K M, Jorgensen S J & Ross T E, 1998. *Optimum moisture content for dynamic compaction of collapsible soils.* Journal of Geotechnical and Environmental Engineering, ASCE, Vol 124, No 8, p699-708.

Sawicki, A. & Swidzinski, W. 1990. *Compaction beneath flexible pavement due to traffic.* J. of Geotechnical Engineering, ASCE, Vol 116, No 11, p1738-1743.

Sawicki, A. & Swidzinski. W. (1989). *Mechanics of sandy soils subjected to cyclic loadings.* Int. J. of Num. & Anal. Methods in Geomech. Vol 13, 511-529.

Schmertmann J.H. (1970). *Static cone to compute settlement over sand.* J. of Geot. Engnr. ASCE, 96 (SM3), p0111-1043.

Schmertmann, J. H. Hartmann J.P. & Brown P.R. 1978. *Improved strain influence factor diagrams.* ASCE J. of Geotech. Engnrg. GT8, Vol 104, p1131-1135.

Scott R. A. & Pearce R. W. 1976. *Soil compaction by impact.* Ground treatment by deep compaction, ICE, London, p19-30.

Sears F. W., Zermanski M. W. & Young H. D. 1982. *University Physics.* 6th edition, Addison-Wesley, Massachusetts, p130.

Selig E. (1980). *Discussion: International Conference on Compaction.* Anciens Ecole Nationale des Ponts et Chaussees, Laboratoire Central, Paris, Vol III, p28.

Semmelink C.J. & Visser A.T. 1995. *Effect of material properties on compactability and bearing capacity.* J. of Transportation Engineering, ASCE, Vol 120, No 4, July/August, p570-589.

Smith R.B. & Yandel W. O. *Predicting performance of granular pavements.* Prediction and performance in geotechnical engineering. Calgary, 17-19 June, p219-225.

Smits M. & de Quelerij L. 1989. *The effect of dynamic compaction on dry granular soils.* Proceedings: 12th ICSMFE, ISSMFE, Rio de Janeiro, Vol 2, Session 18, p1419-1422.

Solesbury F W & Walker D G (1991). *The impact rolling of a large housing site Boksburg.* Geotechnics in the African enviroment, Blight et al (eds), Balkema, Rotterdam. p393-399.

Spangler M.G. & Handy R.L. 1982. *Soil Engineering.* 4th edition, Harper & Row, New York, Ch 18, p470-472.

Starfield A.M. & Cundall P.A. 1988. *Towards a methodology for rock mechanics modelling.* Int. J. of Rock Mech. MIn. Sci. & Geomech. 25 (3).

Strydom J.H. (1999). *Impact compaction trials : Assessment of depth and degree of improvement and methods of integrity testing.* Geotechnics for Developing Africa, AA Balkema, p603-611, Eds: Wardle G.R., Blight G.E. & Fourie A.B.

Terashi M. & Juran I. 2000. *Ground Improvement – State of the art.* GeoEng2000, Sydney.

Ullah, W., & Selig, E.T. 1980. *Test of a vibratory plate compactor.* International Conference on Compaction. Anciens Ecole Nationale des Ponts et Chaussees, Laboratoire Central, Paris, Session VII, Vol II, p689-694.

Van Impe W. F., de Kock F. & van der Cruyssen J. P. 1977. *Soil improvement experiences in Belgium: Part 1: Overview and dynamic compaction.* Ground Improvement, 1, 147-155.

Varaskin S. 1981. *Recent developments in soil improvement techniques and their practical applications.* Solcompact Sols/Soils, 38/39-1981, Techniques Louis Menard, 15, rue des Sablons, Paris.

Wallays M. 1983. *Speciality session 3 : Deep compaction.* Proc. 8th Int. Conf. Soil Mech & Found. Eng., AA Balkema , Helsinki, p1126-1128.

Wolff H. & Visser A.T. 1994. *Incorporating elasto-plasticity in granular pavement design.* Proc. ICE Transp., 105, Nov, Paper 10223, p259-272.

Yandel W. O. (1971). *Prediction of the behaviour of elastoplastic roads during repeated rolling using mechano-lattice analogy.* Highway Research record No. 374. Soil: Compaction and laterites. 7 reports, Washington.

Yoo, T.S., & Selig, E.T. 1979. *Dynamics of vibratory roller compaction.* J. Geotechnical Engineering, ASCE, Vol 105, GT10, p1211-1231.

Yoo, T.S., & Selig, E.T. 1980. *New concepts in vibratory compaction of soil.* International Conference on Compaction. Anciens Ecole Nationale des Ponts et Chaussees, Laboratoire Central, Paris, Session VII, Vol II, p703-707.

APPENDIX A

KRIEL VISUAL SETTLEMENT INDICATOR TRIAL

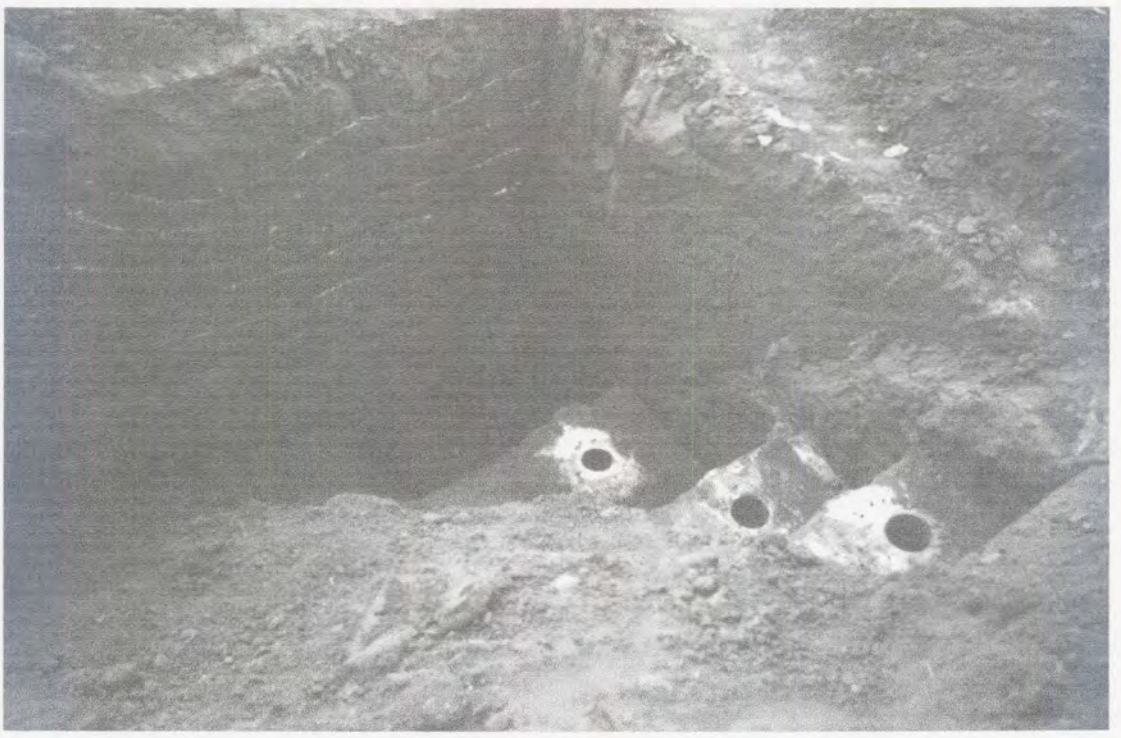

Plate A1 : Excavation after compaction of 25kJ compactor (Photo by Landpac)

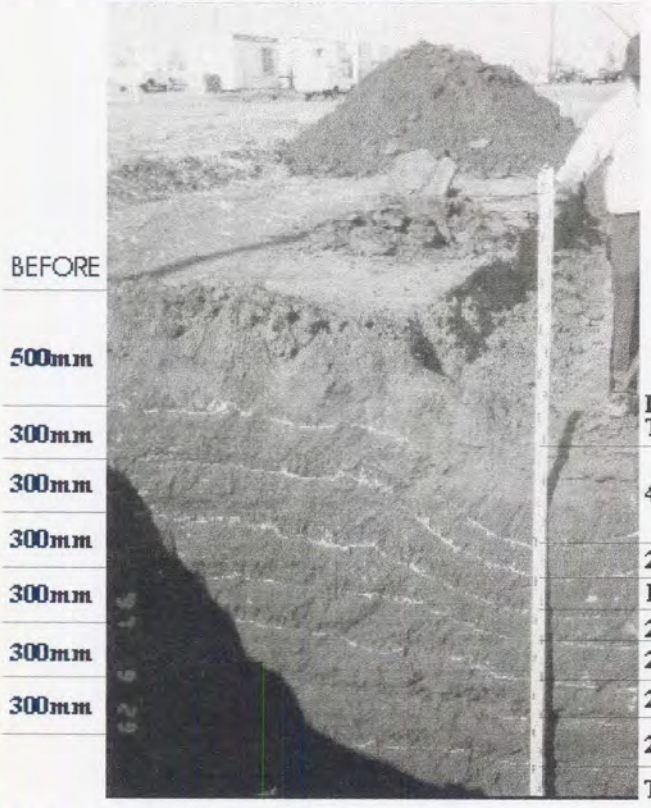

AFTER

Layer Thickness	Settlement (mm)	Strain (%)
425mm	75mm	13.6
200mm	100mm	18.2
175mm	125mm	22.7
200mm	100mm	18.2
225mm	75mm	13.6
250mm	50mm	9.1
275mm	25mm	4.5
Total	550mm	

Plate A2 : Excavation after compaction of 25kJ compactor (Photo by Landpac)

Table A1: Measured changes in layer thickness, Kriel, 1997 (after Africon, 1998)

Layer	Initial thickness (mm)	Final thickness (mm)	Compression (mm)	Strain
1	500	425	75	0.150
2	300	200	100	0.333
3	300	175	125	0.417
4	300	200	100	0.333
5	300	225	75	0.250
6	300	250	50	0.167
7	300	275	25	0.083

APPENDIX B

ESTIMATION OF DISPLACEMENTS, VELOCITIES AND ACCELERATIONS OF LANDPAC IMPACT COMPACTORS USING THE DAVIES & KARIM (1995) MODEL

APPENDIX B: OTHER EQUATIONS USED IN ANALYSIS (AFTER DAVIES & KARIM, 1995)

$$k = \frac{4G.r}{(1-v)} \qquad (1)$$

$c=\rho.A.V$ (2) V=compression-extension wave velocity

$$V = \frac{3.4.Vs}{\pi(1-v)} \qquad (3')$$

OR....

$$V = \sqrt{(\lambda + 2G)/\rho}$$

$$\lambda = \frac{2vG}{1-2v}$$

$$\therefore c = \frac{3.4.r^2\sqrt{\rho G}}{(1-v)} \qquad (3)$$

m.a+c.v+k.z = 0 (4)

$$c = \rho\pi r^2\sqrt{\frac{\lambda+2G}{\rho}}$$

$$\therefore c = \pi r^2\sqrt{\rho(\lambda+2G)}$$

$$z = \frac{V_o}{\varpi_d}e^{-\varpi_n D.t}.\sin(\varpi_d.t) \qquad (5)$$

$$\frac{dz}{dt} = v = \frac{V_o}{\varpi_d}e^{-\varpi_n D.t}.(-\varpi_n.D).\sin(\varpi_d.t) + \frac{V_o}{\varpi_d}e^{-\varpi_n D.t}.\cos(\varpi_d.t).\varpi_d$$

$$\therefore v = V_o e^{-\varpi_n D.t}.\cos(\varpi_d.t) - V_o D\frac{\varpi_n}{\varpi_d}e^{-\varpi_n D.t}.\sin(\varpi_d.t) \qquad (5a)$$

$$a = \frac{d^2 z}{dt^2} = \ddot{z} = V_o e^{-\varpi_n D.t}.(-\varpi_n D)\cos(\varpi_d.t) + V_o e^{-\varpi_n D.t}.-\sin(\varpi_d.t)\varpi_d$$

$$- V_o D\frac{\varpi_n}{\varpi_d}e^{-\varpi_n D.t}(-\varpi_n.D)\sin(\varpi_d.t) - V_o D\frac{\varpi_n}{\varpi_d}.e^{-\varpi_n D.t}\cos(\varpi_d.t)\varpi_d$$

$$\therefore a = V_o e^{-\varpi_n D.t}\left[\sin(\varpi_d.t)\left(\frac{\varpi_n^2.D^2}{\varpi_d} - \varpi_d\right) - 2\varpi_n.D.\cos(\varpi_d.t)\right] \qquad (5b)$$

$$D = \frac{c}{2}\sqrt{k.m} \qquad (6)$$

$$\varpi_d = F.\varpi_n \qquad (7)$$

$$F = \sqrt{1-D^2} \qquad (8)$$

Arrival times:

$$t_z = \frac{\alpha_z}{\varpi_n} \qquad (9a)$$

$$t_v = 2t_z \qquad (9b)$$

$$t_a = \frac{\alpha_a}{\varpi_n} \qquad (9c)$$

the dimensionless coefficients are

$$\alpha_z = \frac{\tan^{-1}\frac{F}{D}}{F} \qquad (10a)$$

$$\alpha_a = \frac{\tan^{-1}\frac{(1-4D^2)F}{3D-4D^3}}{F} \qquad (10b)$$

APPENDIX B: [DAVIES & KARIM, 1995]

The corresponding displacement (rebound) velocity and acceleration maxima are:

$$z_m = \beta \frac{V_o}{\varpi_n} \qquad (11a)$$

$$v_m = -\beta . V_o \qquad (11b)$$

$$a_m = -\beta_a . V_o \varpi_n \qquad (11c)$$

$$\beta_z = e^{-D.\alpha_z} \qquad (12a)$$

$$\beta_v = e^{-2D.\alpha_z} \qquad (12b)$$

$$\beta_a = e^{-D.\alpha_a} \qquad (12c)$$

10kJ Impact compactor elastodynamic prediction (after Davies & Karim, 1995)

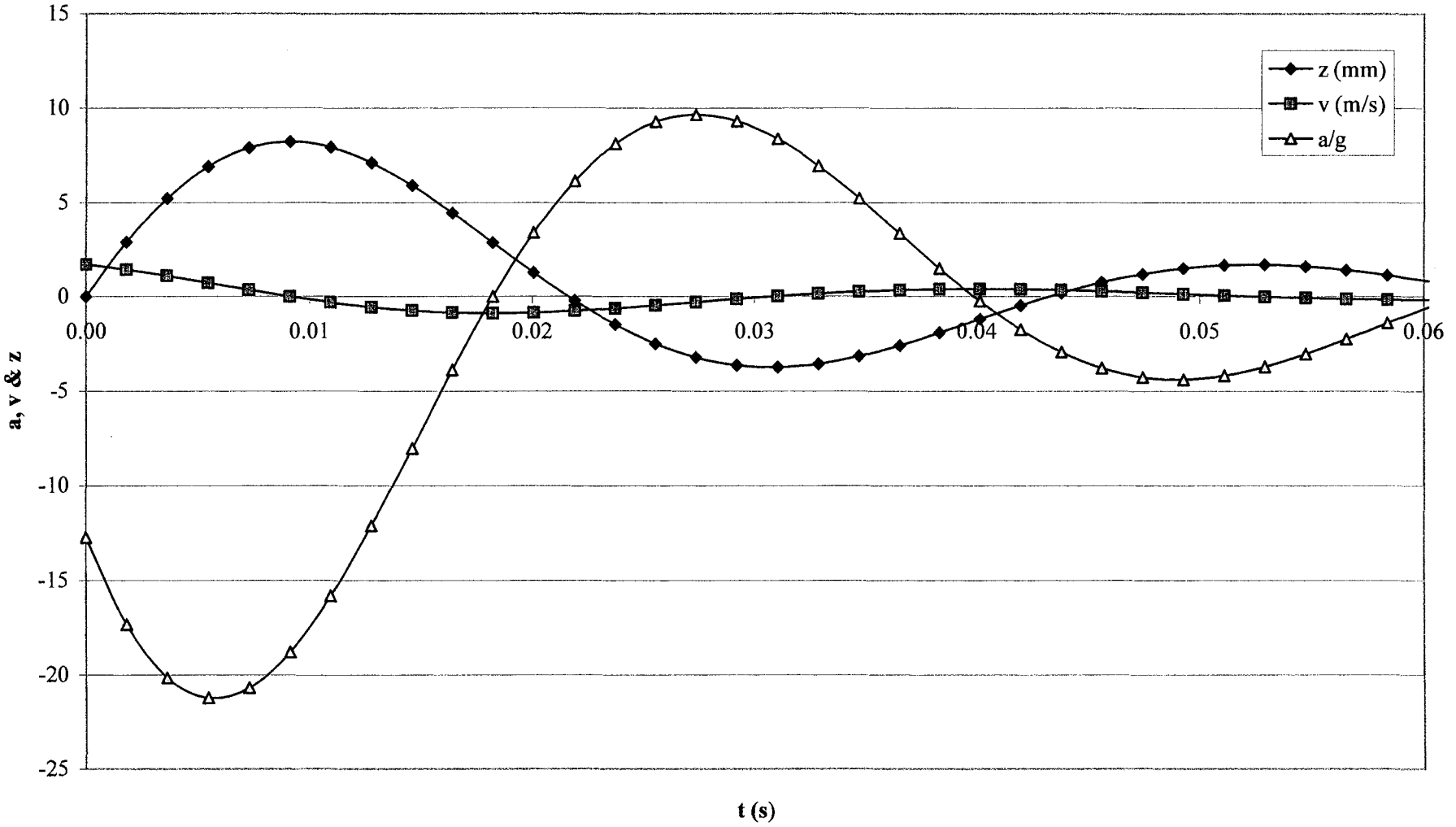

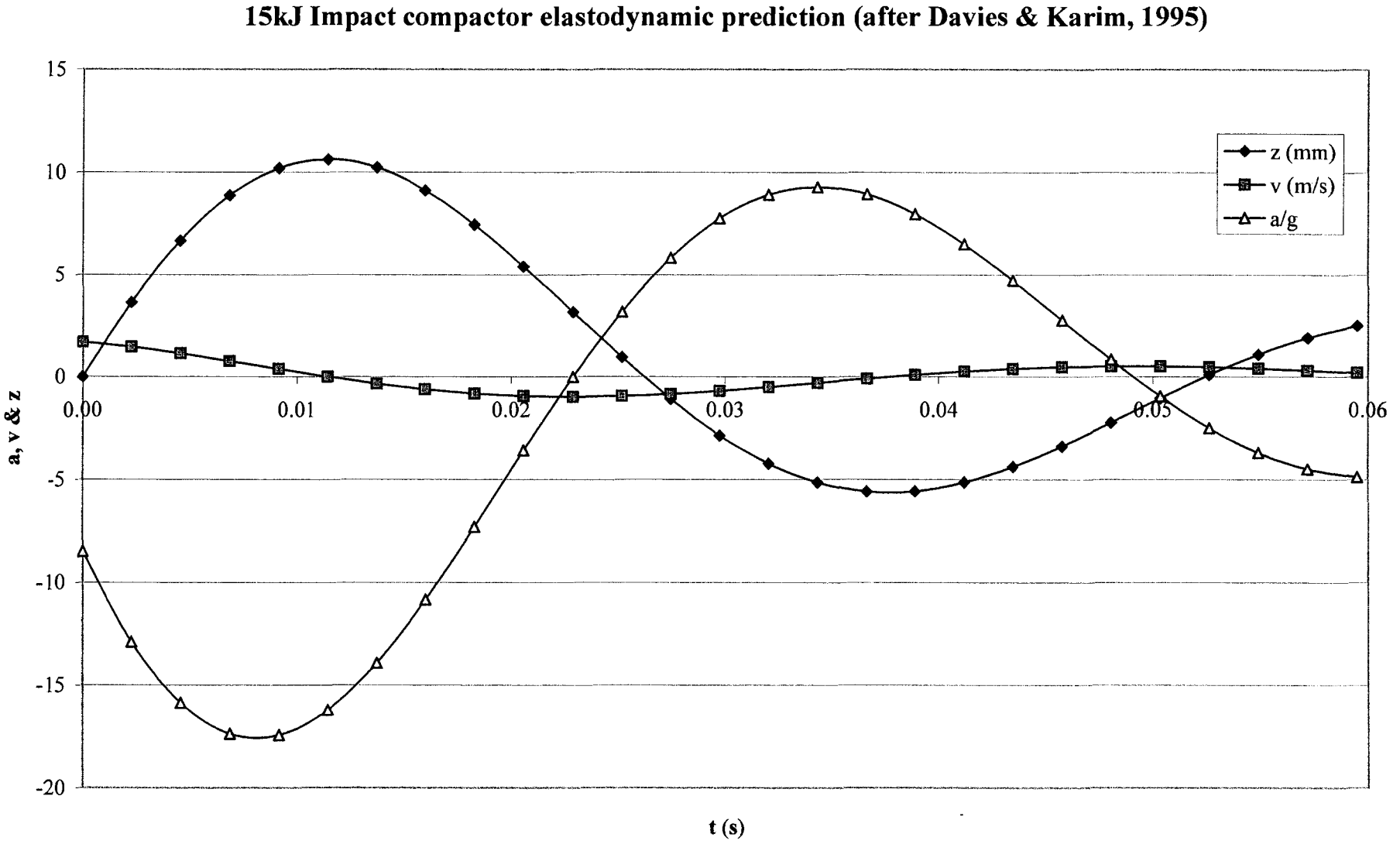

25kJ Impact compactor elastodynamic prediction (after Davies & Karim, 1995)

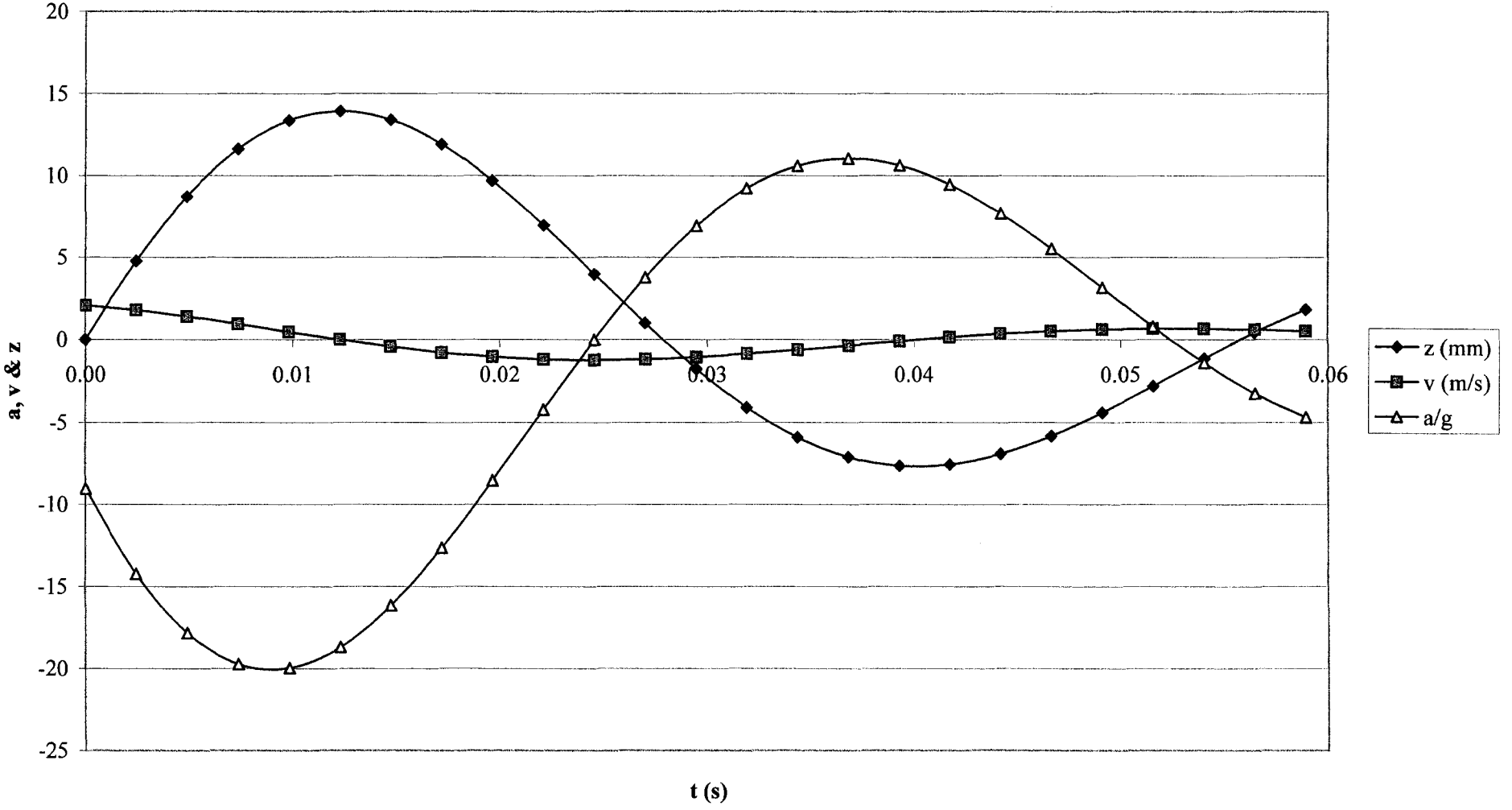

APPENDIX C

ACCELEROMETER DATA SHEET AND CALIBRATION CERTIFICATE

PCB CALIBRATION CARD:

PCB ELECTRONICS DATA CALIBRATION CARD:
SHEAR ACCELEROMETER
MODEL# 353B14
SERIAL # 58576

VOLTAGE SENSITIVITY 5.42mV/g
FREQUENCY RANGE 1-100000 Hz
OUTPUT BIAS LEVEL 8.6V
DATE : 06/28/99 BY S.S

PCB ELECTRONICS
Shock and Vibration Sensors Division
3425 Walden Ave, Depew, NY 14043
888-684-0013

10. Specifications

A/D Converter	12-Bit Version	16-Bit Version
Acquisition + Conversion	2 ms + 8 ms	2 ms + 8 ms
Monotonicity	No missing codes	No missing codes
Integral linearity error	± 1 LSB	± 3 LSB
Differential linearity error	± 1 LSB	+3/-2 LSB
Full scale error	± 0.5 %	± 0.5 %
Aperture delay	40 ns	40 ns

Analog Input		
Number of input channels	8 differential / 16 single-ended, expandable to 256	
Input range	±10, ±5, ±2.5, ±1.25V	(DAQP-12 and DAQP-16)
	±10, ±1, ±0.1, ±0.01V	(DAQP-12H)
Programmable gain	1, 2, 4, 8	(DAQP-12 and DAQP-16)
	1, 10, 100, 1000	(DAQP-12H)
Maximum over-voltage	±30 V	
Input impedance	100 MW (DC)	

A/D Miscellaneous Specifications	
Data FIFO depth	2048 samples
Scan list length	2048 entries
Scan speed	10 ms, 20 ms, 40 ms
Trigger source	Internal (Software) / External (TTL)
Trigger mode	Continuous / One-shot
External (TTL) trigger	0.8 V (low) / 2.2 V (high), Rising / Falling edges
	Latency to A/D scan < 1 ms
Sampling rate	0.006 Hz to 100 kHz (with internal clock source)
External clock rate	DC - 5 MHz

Digital I/O	
Digital input channels	4 (no latch)
Digital output channels	4 (latched)
Maximum source current	0.5 mA
Maximum sinking current	2.5 mA
Minimum logic '1' level	2.4 V
Maximum logic '0' level	0.8 V

General Specifications	
Power consumption	160 mA (full power), 40 mA (power down)
Operating temperature	0 °C to 50 °C
Storage temperature	0 °C to 70 °C
Humidity	0 to 95%, non-condensing
Size (cable not included)	Standard PCMCIA type II
Weight	1.5 oz (for reference only)

APPENDIX D

ESTIMATION OF ACCELERATIONS USING MAYNE (1983)

APPENDIX D : ESTIMATION OF DECELERATIONS

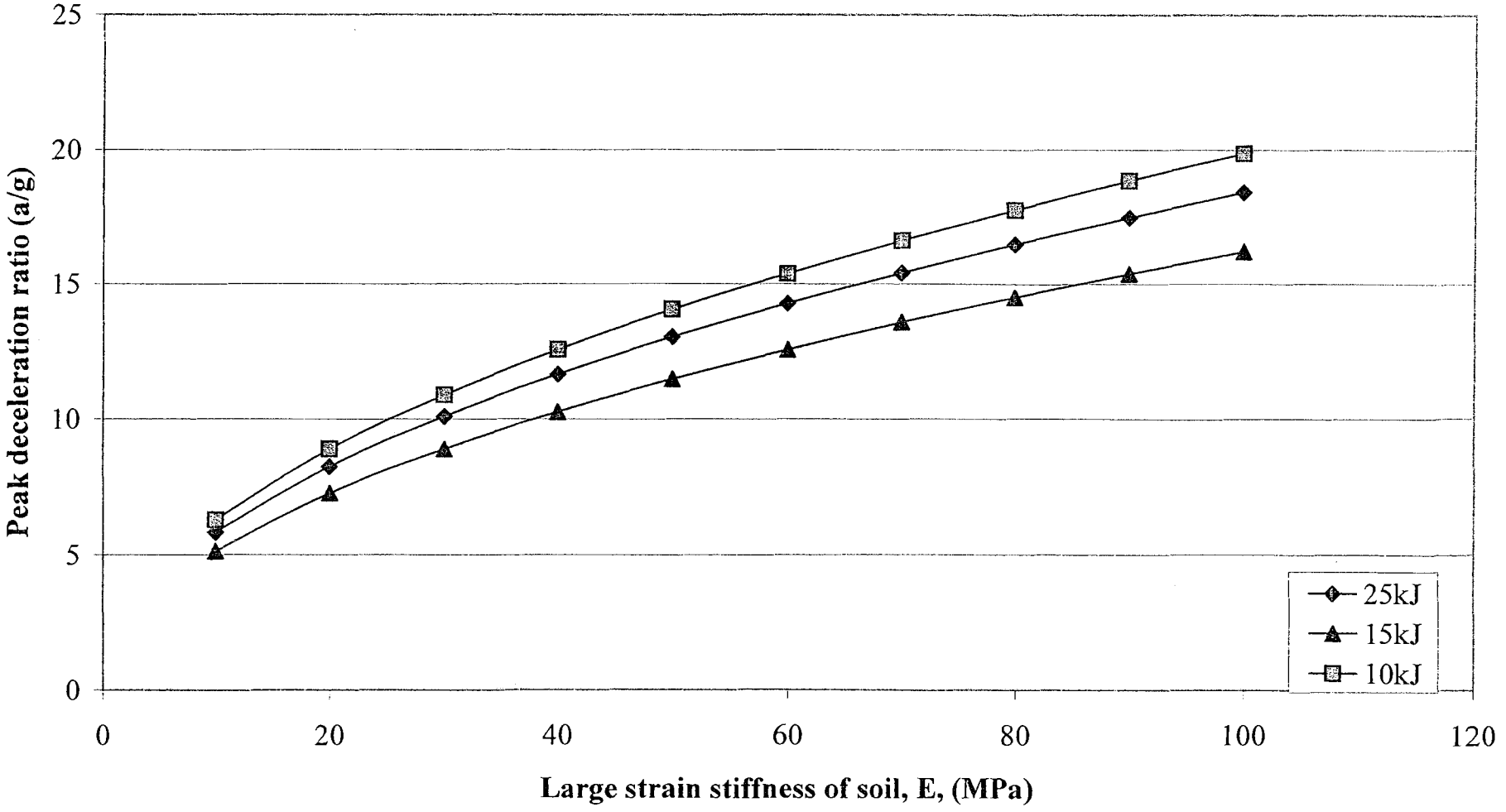

(after Mayne, 1983)

ADDPENDIX D : FORCE ESTIMATES ON VARIOUS MODEL IMPACT COMPACTORS

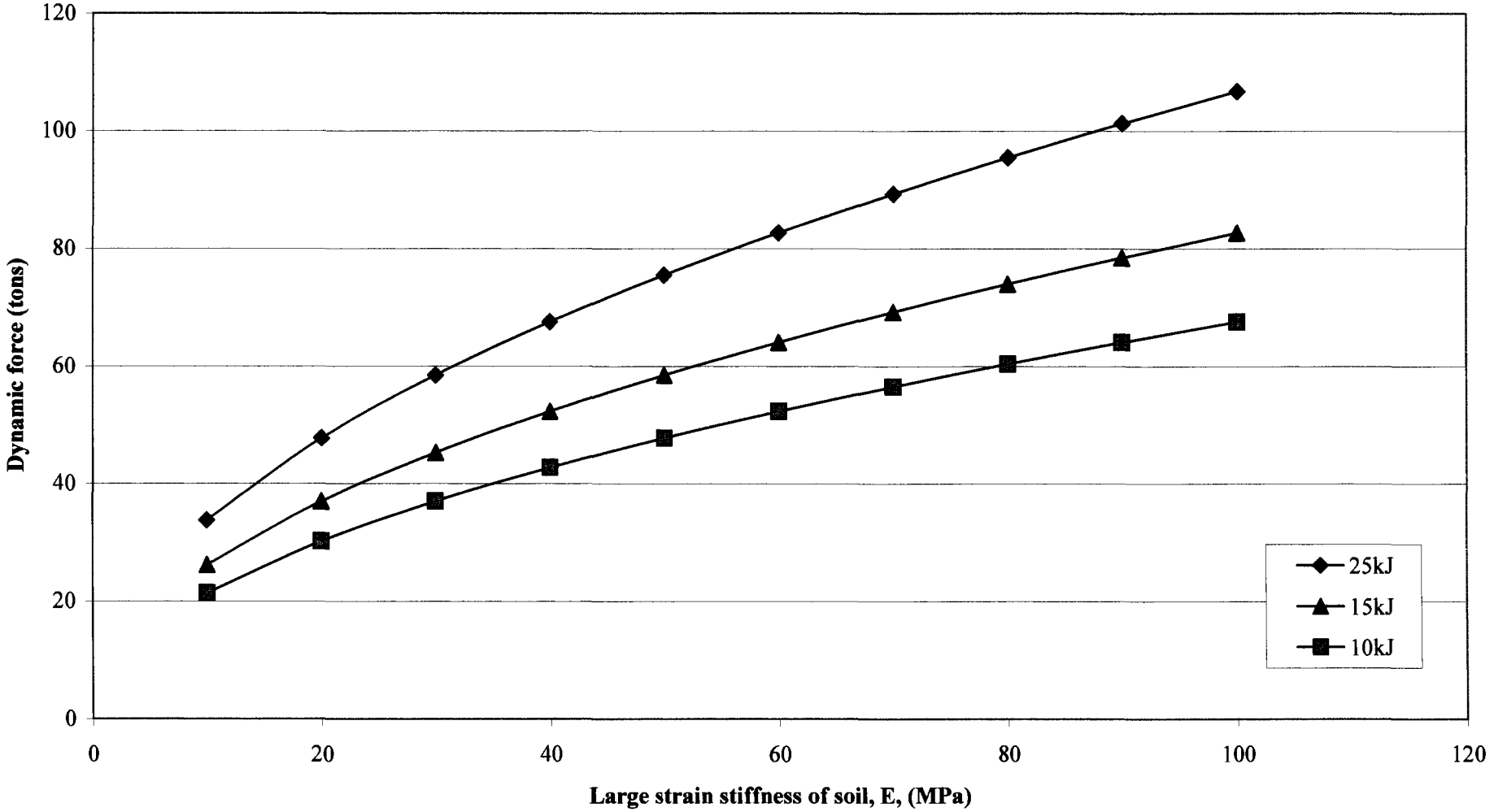

(after Mayne, 1983)

APPENDIX E

MEASURED ACCELERATIONS

Appendix E1 : 10kJ impact roller at normal operating speed on hard ground

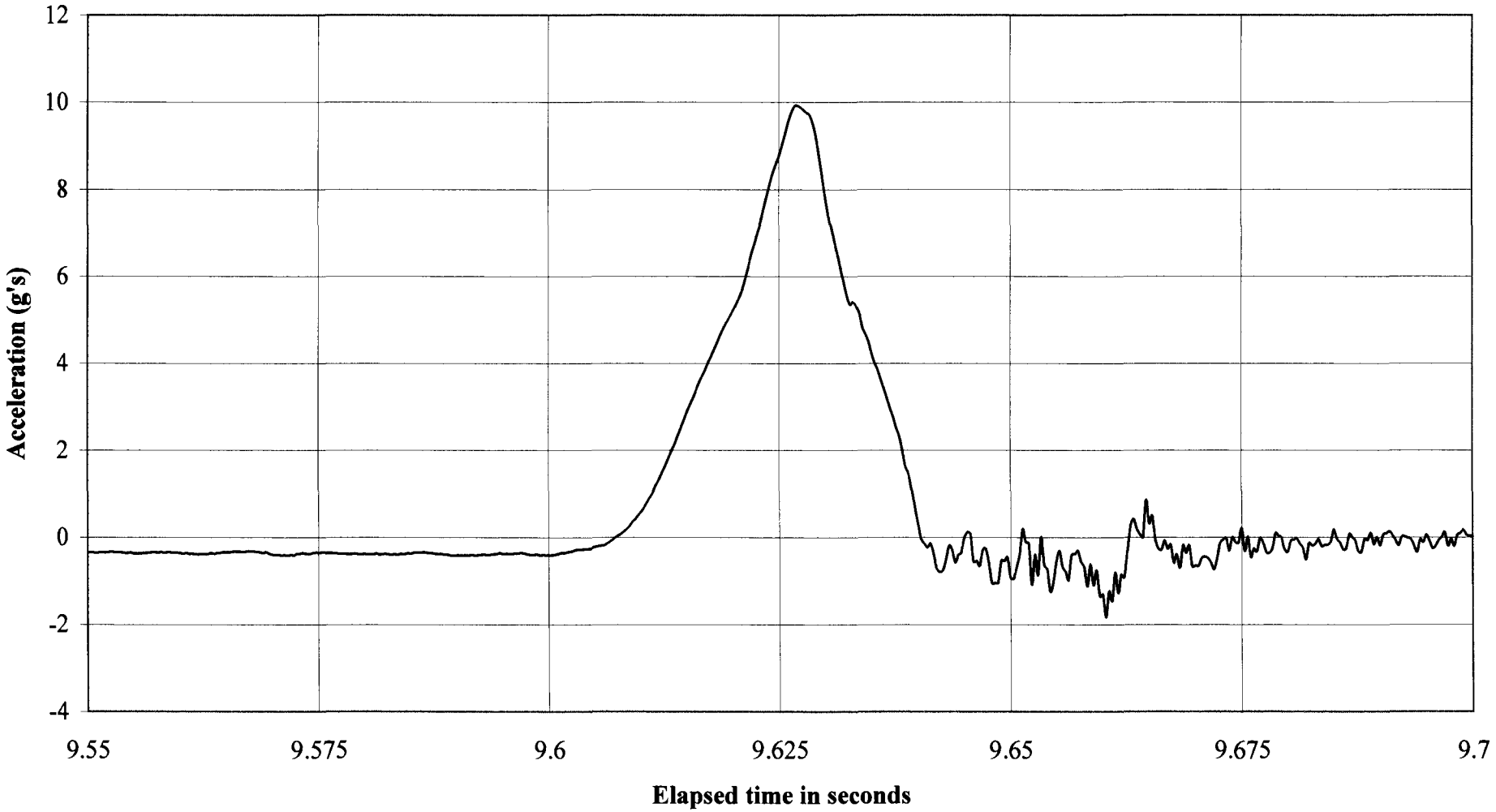

Appendix E2 : 15kJ impact roller at normal operating speed on hard ground

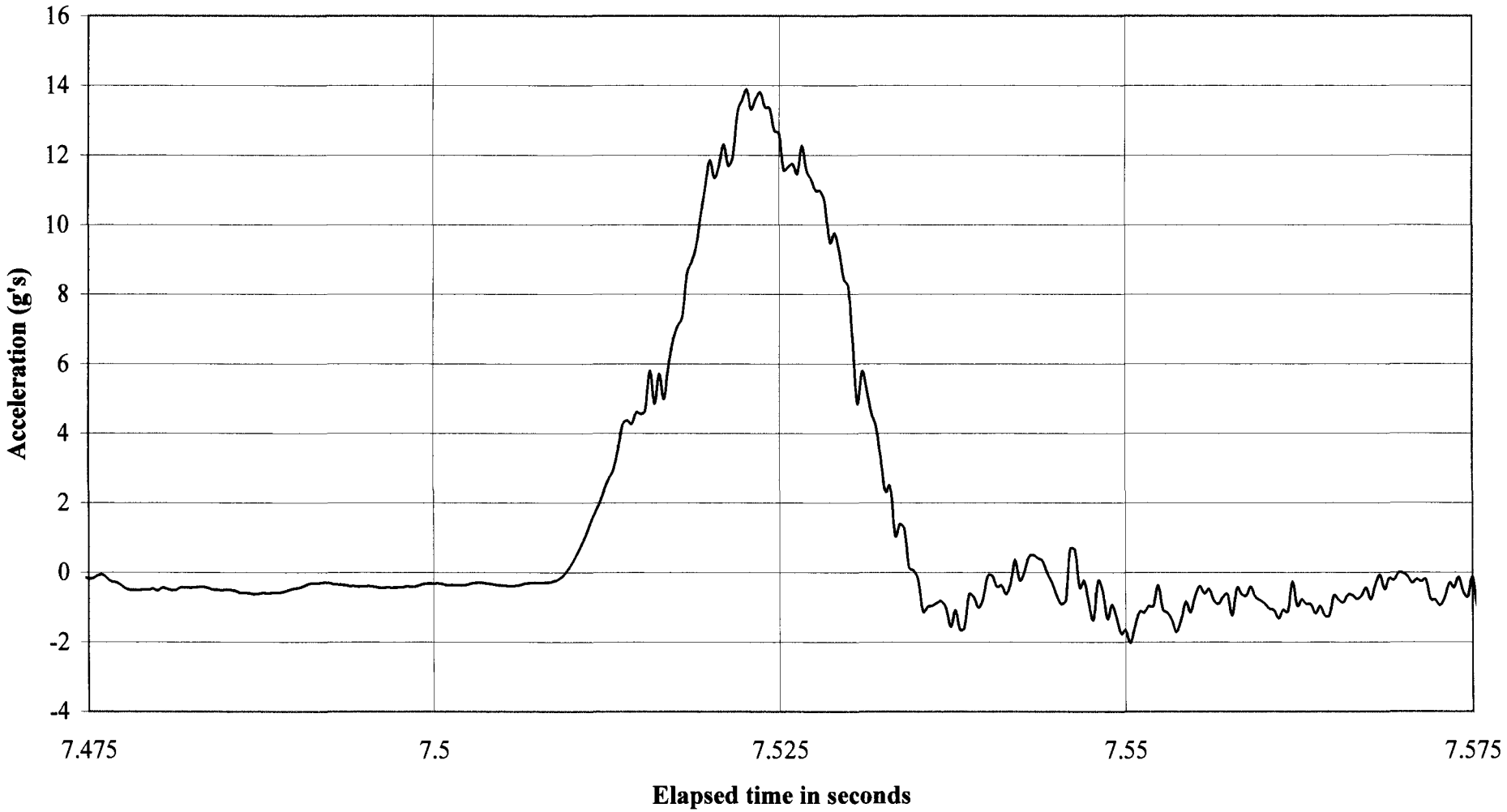

Appendix E3 : 25kJ impact roller at normal operating speed on hard ground

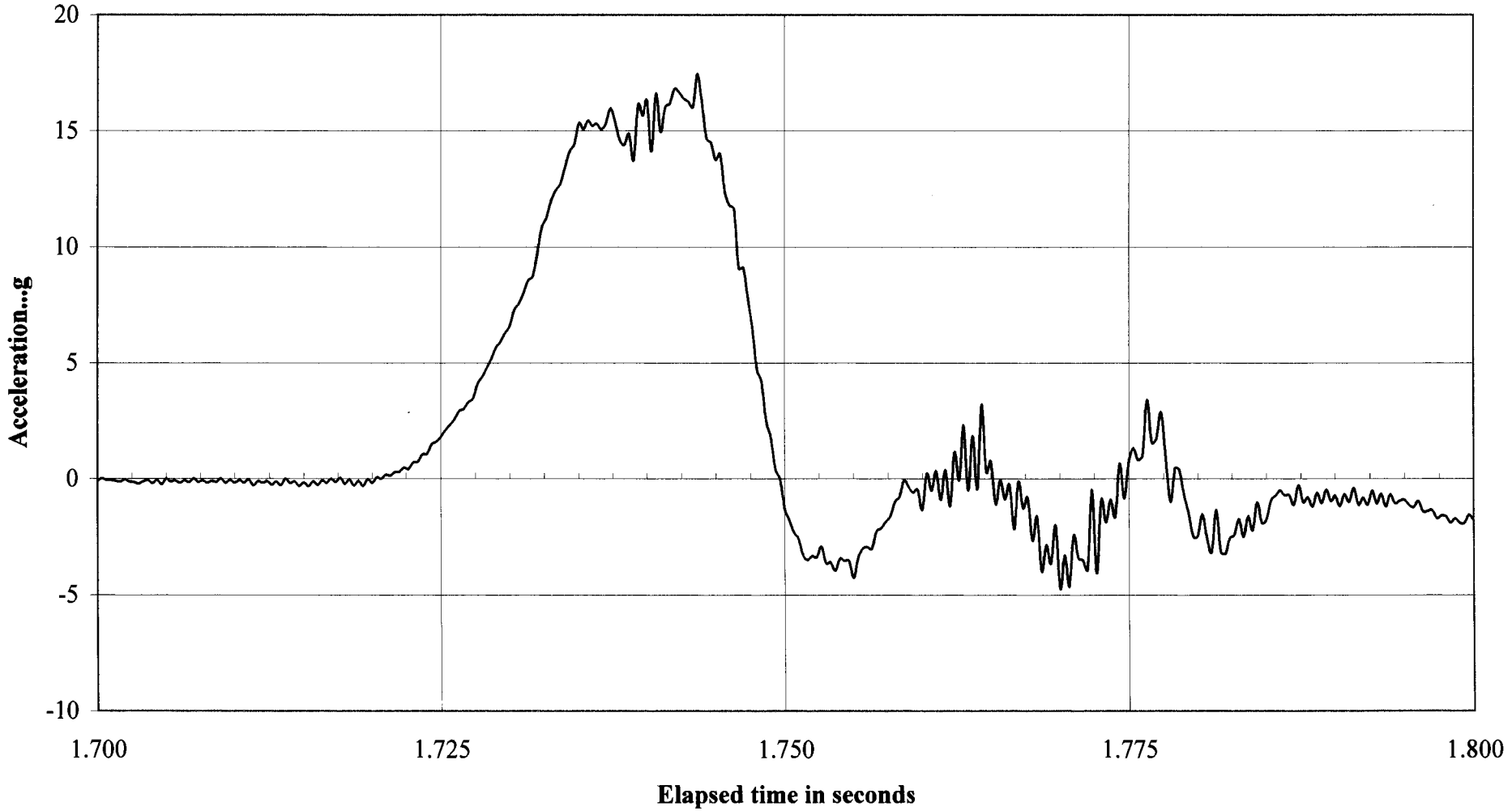

Appendix E4 : 10kJ impact roller on very soft soil at normal operating speed

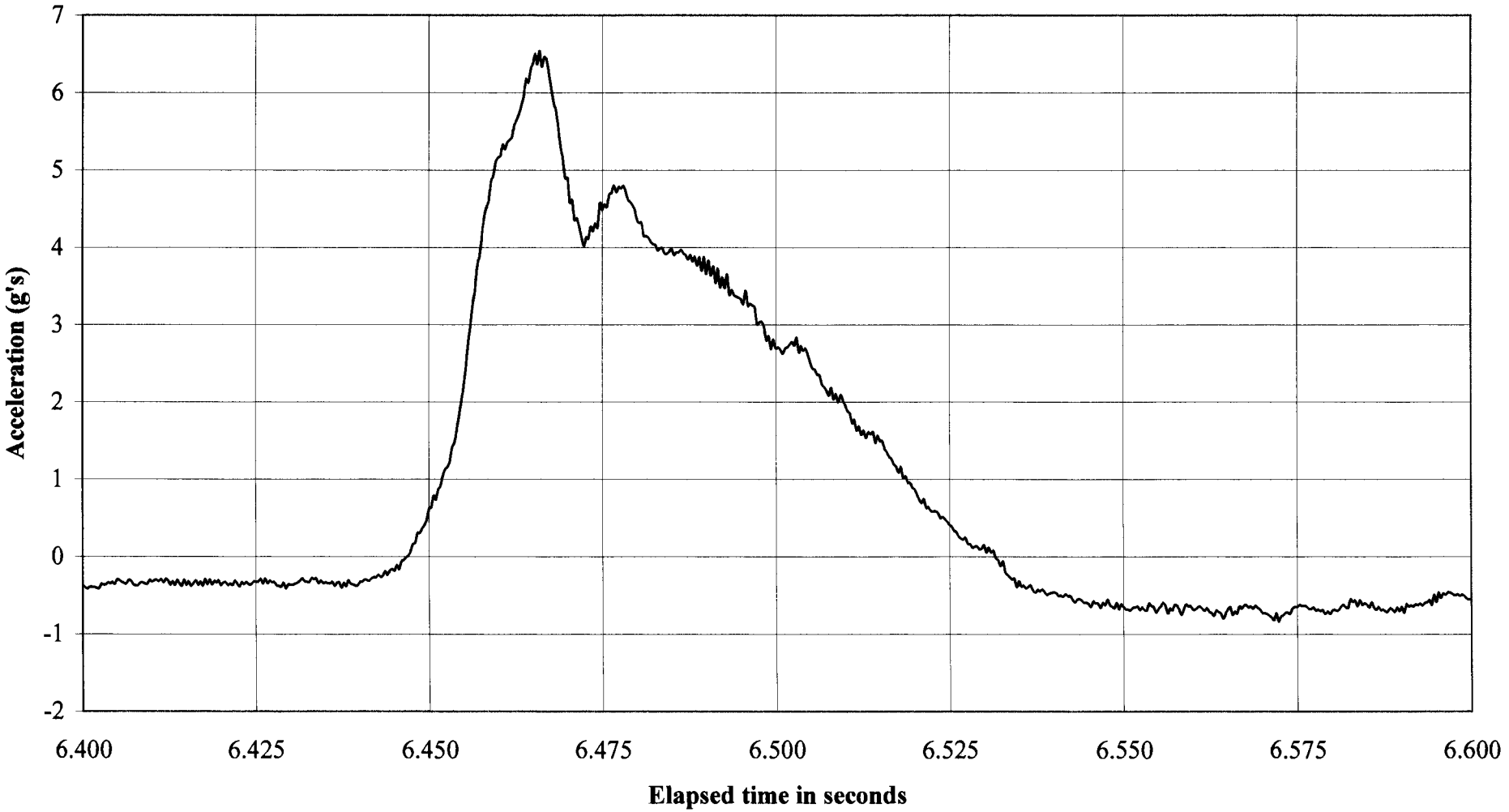

Appendix E5 : 15kJ impact roller on very soft ground at normal operating speed

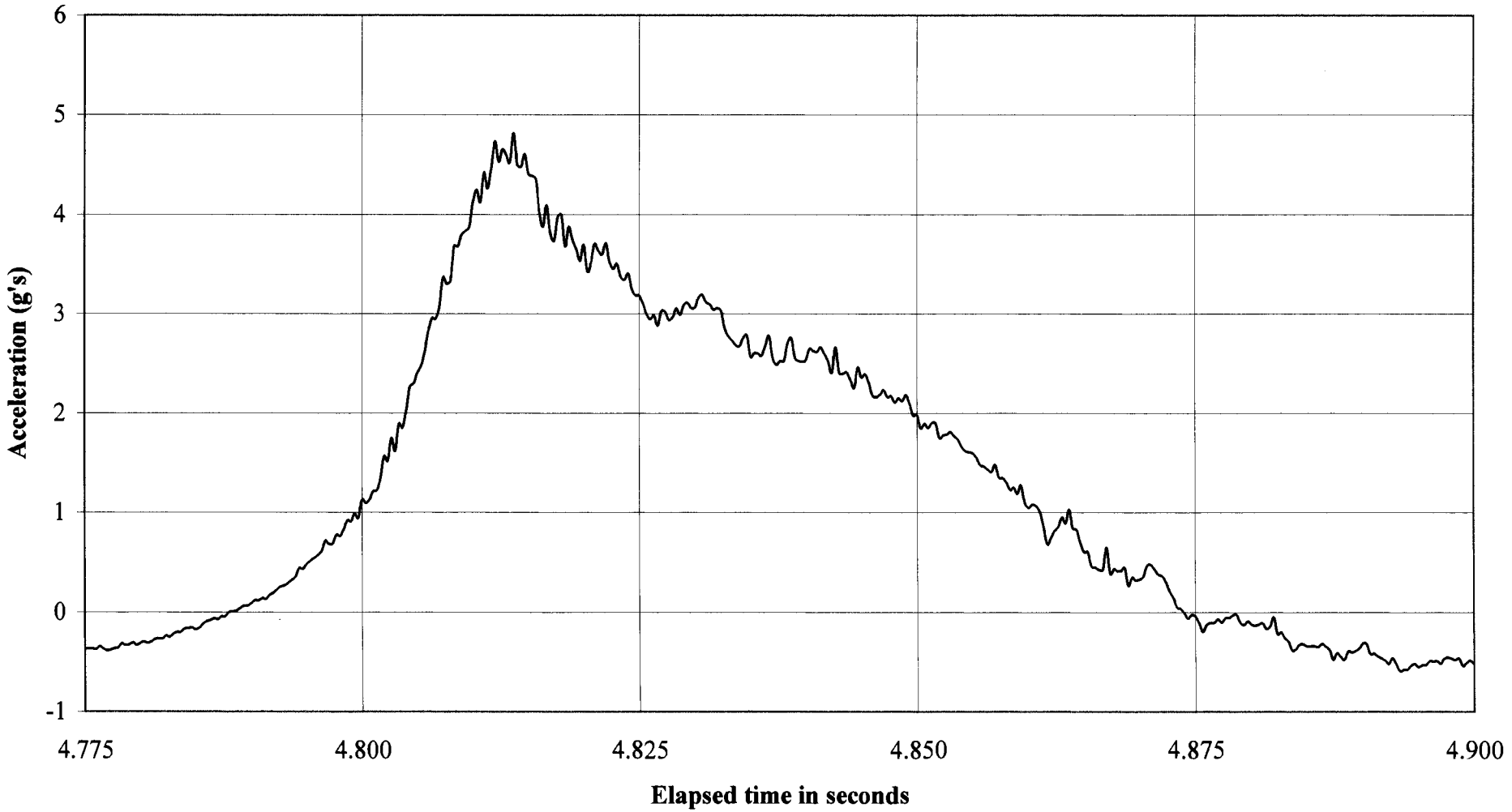

Appendix E6 : 25kJ impact compactor on very soft ground

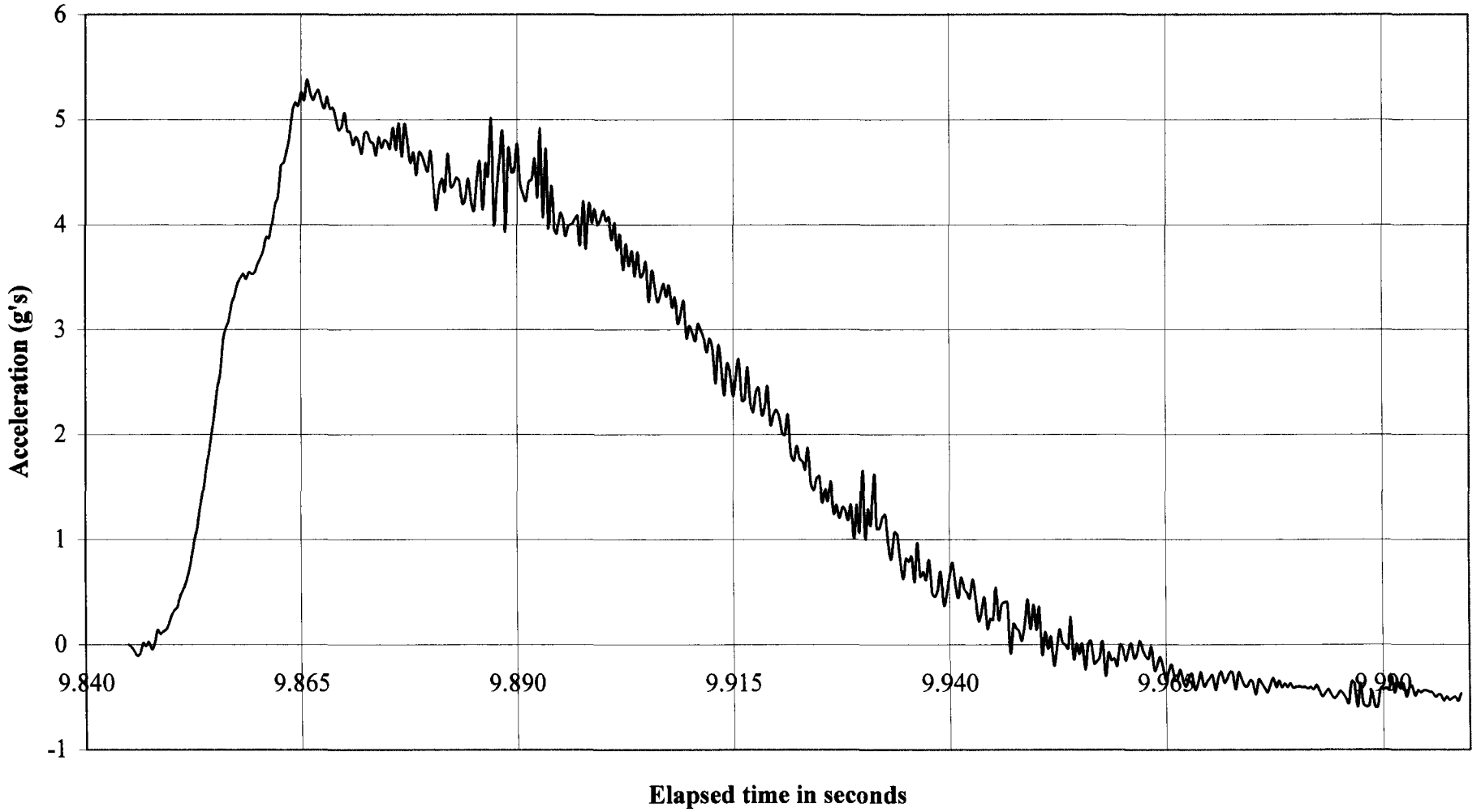

APPENDIX F

ELASTIC VOLUMETRIC STRAIN CALCULATIONS

Elastic strain under an impact compactor (Vertical, radial, volumetric)

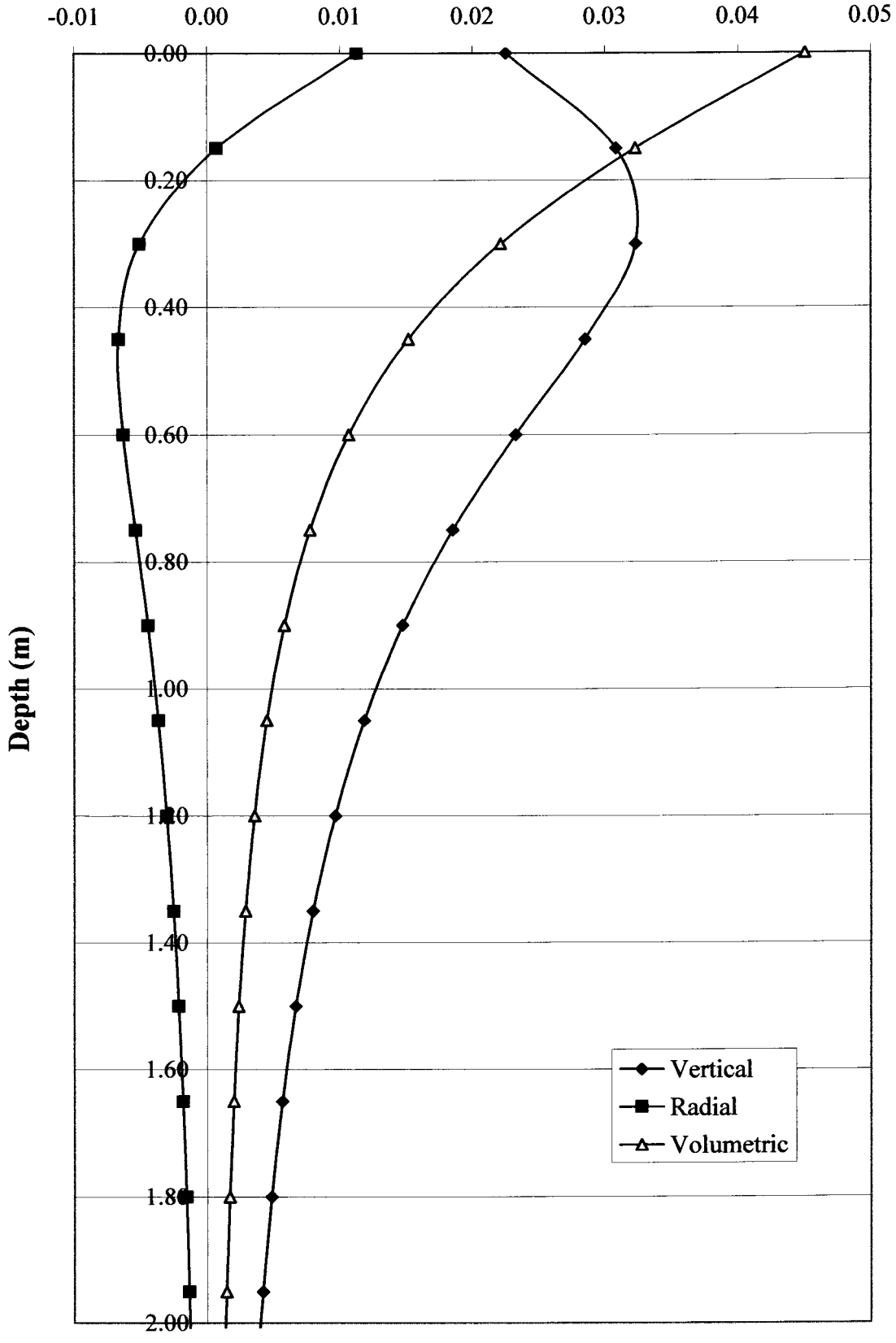

From Huang, Y.H Pavement analysis and design, Prentice Hall, 1993.

$$\sigma_z = q\left(1 - \frac{z^3}{\left(a^2 + z^2\right)^{1.5}}\right)$$

$$\sigma_r = \frac{q}{2}\left[1 + 2v - \frac{2(1+v)z}{\sqrt{a^2 + z^2}} + \frac{z^3}{\left(a^2 + z^2\right)^{1.5}}\right]$$

Note :The vertical stress is independan t of E and v, and the lateral stress independan t of E

$$\varepsilon_z = \frac{(1+v)q}{E}\left[1 - 2v + \frac{2vz}{\sqrt{a^2 + z^2}} - \frac{z^3}{\left(a^2 + z^2\right)^{1.5}}\right]$$

$$\varepsilon_r = \frac{(1+v)q}{2E}\left[1 - 2v - \frac{2(1-v)z}{\sqrt{a^2 + z^2}} + \frac{z^3}{\left(a^2 + z^2\right)^{1.5}}\right]$$

The deflection is given by :

$$w = \frac{(1+v)qa}{E}\left\{\frac{a}{\sqrt{a^2 + z^2}} + \frac{1-2v}{a}\left[\sqrt{a^2 + z^2} - z\right]\right\}$$

which at the suface is

$$w = \frac{2\left(1 - v^2\right)qa}{E}$$

Compared this with the rigid plate formula :

$$w = \frac{\pi\left(1 - v^2\right)qa}{2E}$$ i.e the pressure under a rigid plate is 79% of that under a flexible plate!

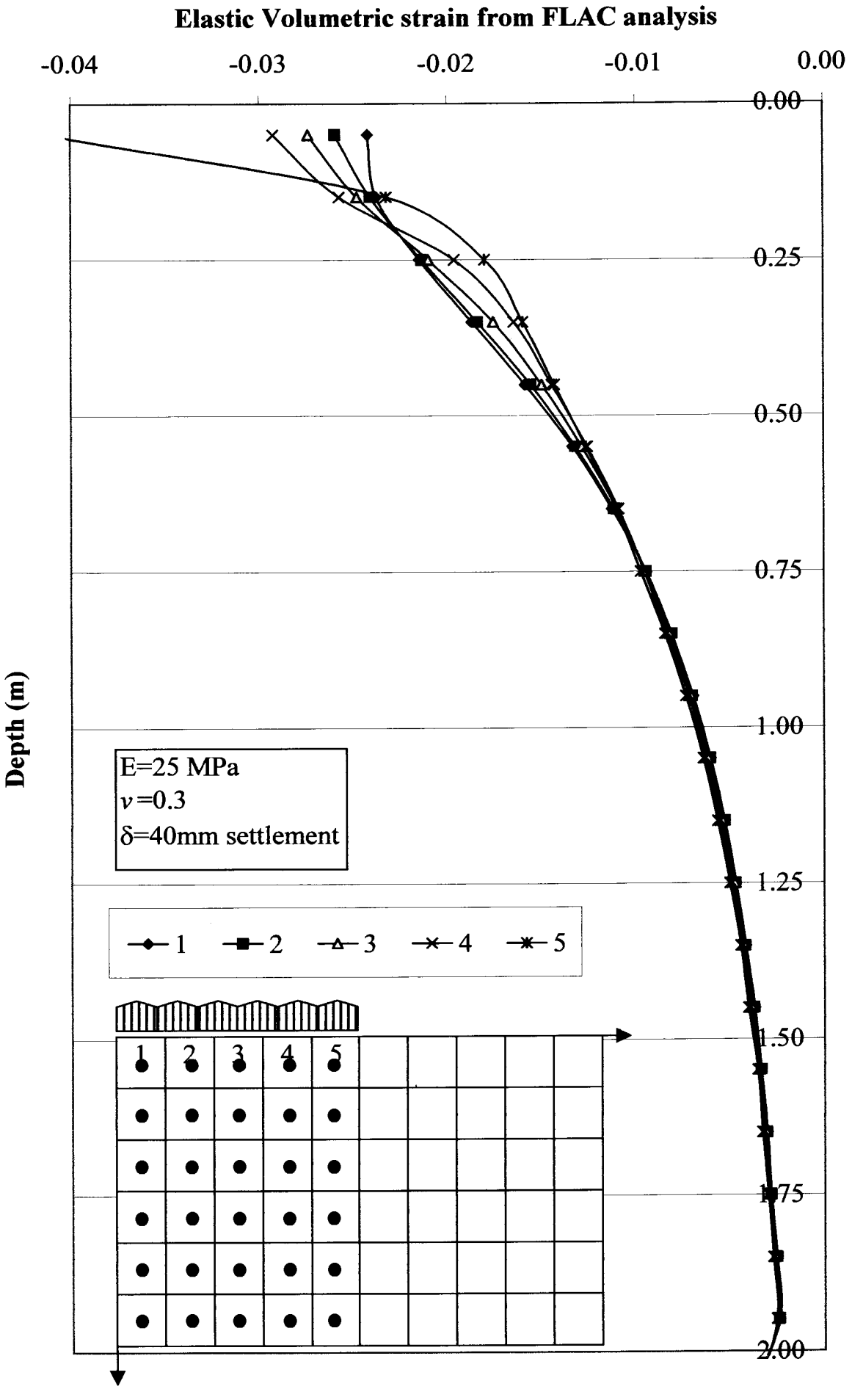

APPENDIX G

ELASTIC-PLASTIC ANALYSIS OF VOLUMETRIC STRAINS

CALCULATION POSITIONS FOR STRAINS IN *FLAC* ANALYSIS

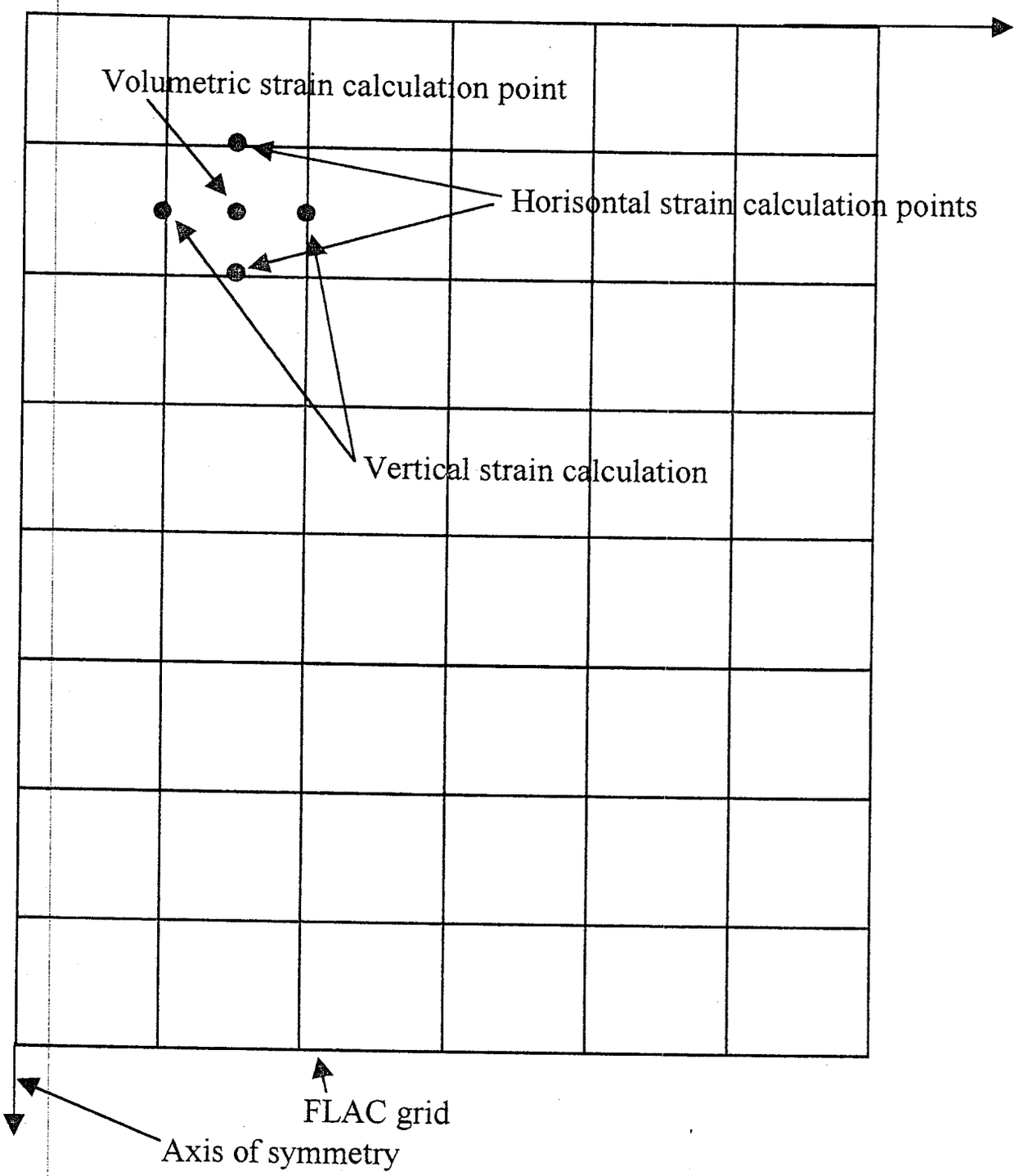

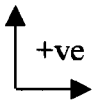

DATA FOR MC1 ANALYSIS: VERTICAL DEFLECTION

z (m)	x10^{-2} [Vertical displacements of grid points]					
0.0	-4.000	-4.000	-4.000	-4.000	-4.000	-4.000
0.1	-3.858	-3.826	-3.783	-3.602	-3.469	-2.695
0.2	-3.462	-3.413	-3.192	-2.933	-2.373	-1.318
0.3	-2.788	-2.656	-2.473	-2.126	-1.521	-0.820
0.4	-1.912	-1.898	-1.751	-1.477	-1.022	-0.609
0.5	-1.320	-1.304	-1.210	-1.025	-0.725	-0.499
0.6	-0.969	-0.952	-0.875	-0.754	-0.555	-0.433
0.7	-0.759	-0.741	-0.685	-0.595	-0.461	-0.381
0.8	-0.610	-0.597	-0.557	-0.488	-0.397	-0.338
0.9	-0.498	-0.489	-0.458	-0.405	-0.343	-0.297
1.0	-0.412	-0.405	-0.379	-0.339	-0.297	-0.260
1.1	-0.343	-0.336	-0.316	-0.287	-0.257	-0.226
1.2	-0.286	-0.280	-0.265	-0.245	-0.223	-0.196
1.3	-0.237	-0.234	-0.224	-0.210	-0.193	-0.169
1.4	-0.198	-0.196	-0.190	-0.181	-0.166	-0.146
1.5	-0.168	-0.167	-0.163	-0.155	-0.143	-0.124
1.6	-0.144	-0.143	-0.140	-0.133	-0.122	-0.105
1.7	-0.125	-0.124	-0.121	-0.114	-0.103	-0.088
1.8	-0.109	-0.108	-0.104	-0.097	-0.086	-0.073
1.9	-0.095	-0.094	-0.089	-0.082	-0.071	-0.060
2.0	-0.082	-0.080	-0.075	-0.068	-0.058	-0.049
2.1	-0.069	-0.067	-0.062	-0.055	-0.047	-0.042

DATA FOR MC1 ANALYSIS: HORIZONTAL DEFLECTION

z (m)	x10^{-2} [Horizon displacements of grid points]					
0.0	0.000	0.029	0.032	0.074	0.155	0.204
0.1	0.000	0.086	0.257	0.572	1.121	2.450
0.2	0.000	0.277	0.636	1.050	1.683	2.221
0.3	0.000	0.431	0.805	1.187	1.503	1.633
0.4	0.000	0.360	0.689	0.957	1.131	1.141
0.5	0.000	0.208	0.413	0.584	0.675	0.665
0.6	0.000	0.109	0.214	0.299	0.343	0.337
0.7	0.000	0.069	0.129	0.176	0.196	0.192
0.8	0.000	0.049	0.093	0.127	0.144	0.144
0.9	0.000	0.037	0.071	0.098	0.112	0.116
1.0	0.000	0.028	0.055	0.077	0.089	0.094
1.1	0.000	0.023	0.045	0.061	0.071	0.077
1.2	0.000	0.019	0.036	0.049	0.057	0.064
1.3	0.000	0.016	0.029	0.039	0.047	0.054
1.4	0.000	0.012	0.023	0.032	0.039	0.046
1.5	0.000	0.009	0.018	0.026	0.033	0.039
1.6	0.000	0.007	0.014	0.021	0.028	0.034
1.7	0.000	0.006	0.012	0.018	0.025	0.031
1.8	0.000	0.005	0.010	0.016	0.023	0.028
1.9	0.000	0.005	0.010	0.015	0.021	0.026
2.0	0.000	0.005	0.010	0.015	0.020	0.024
2.1	0.000	0.005	0.010	0.015	0.019	0.021

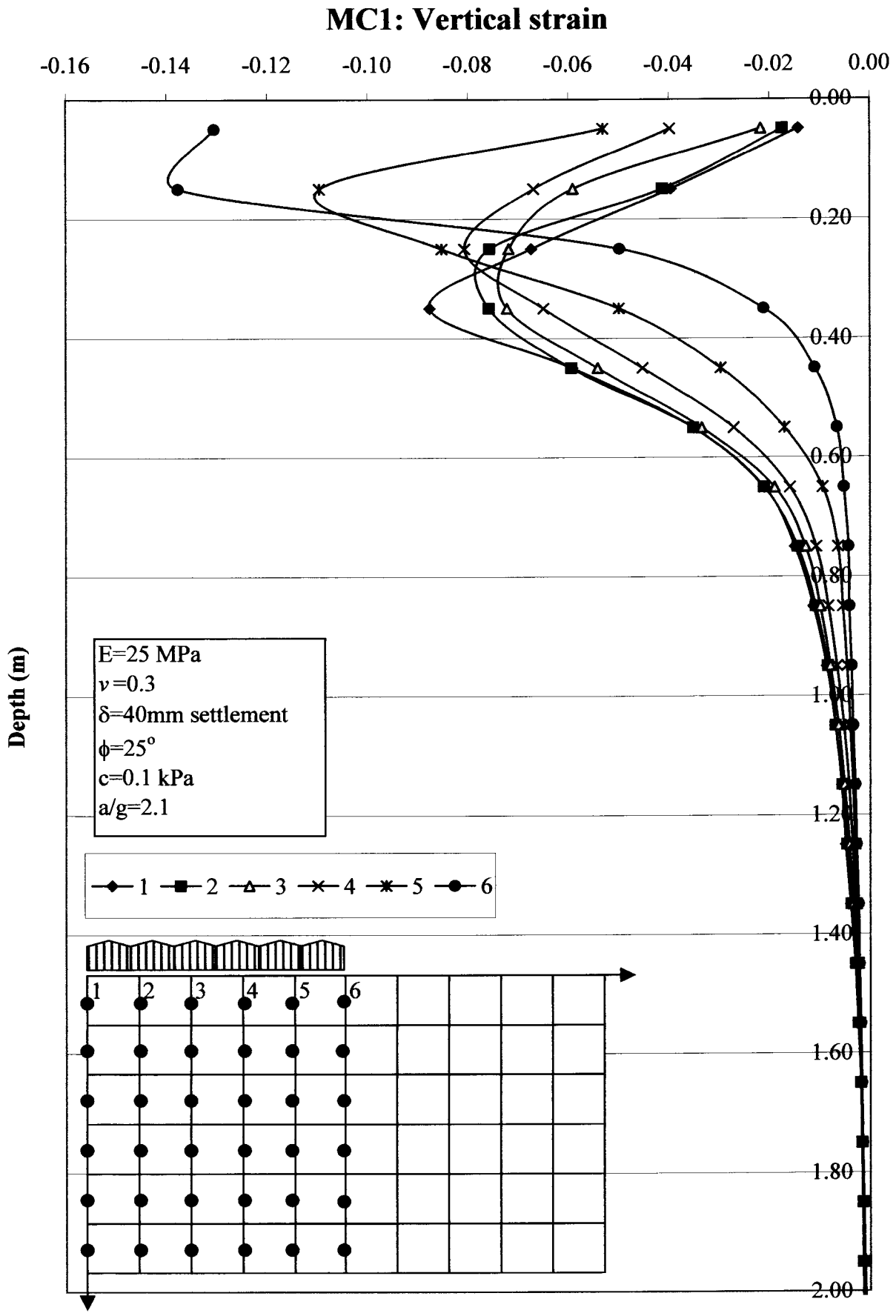
MC1: Vertical strain
-0.16
-0.14
-0.12
-0.10
-0.08
-0.06
-0.04
-0.02
0.00
0.00
0.20
0.40
0.60
0.80
1.00
1.20
1.40
1.60
1.80
2.00
Depth (m)
E=25 MPa
ν=0.3
δ=40mm settlement
ϕ=25°
c=0.1 kPa
a/g=2.1
1
2
3
4
5
6
1
2
3
4
5
6

MC 1 : Horizontal strains

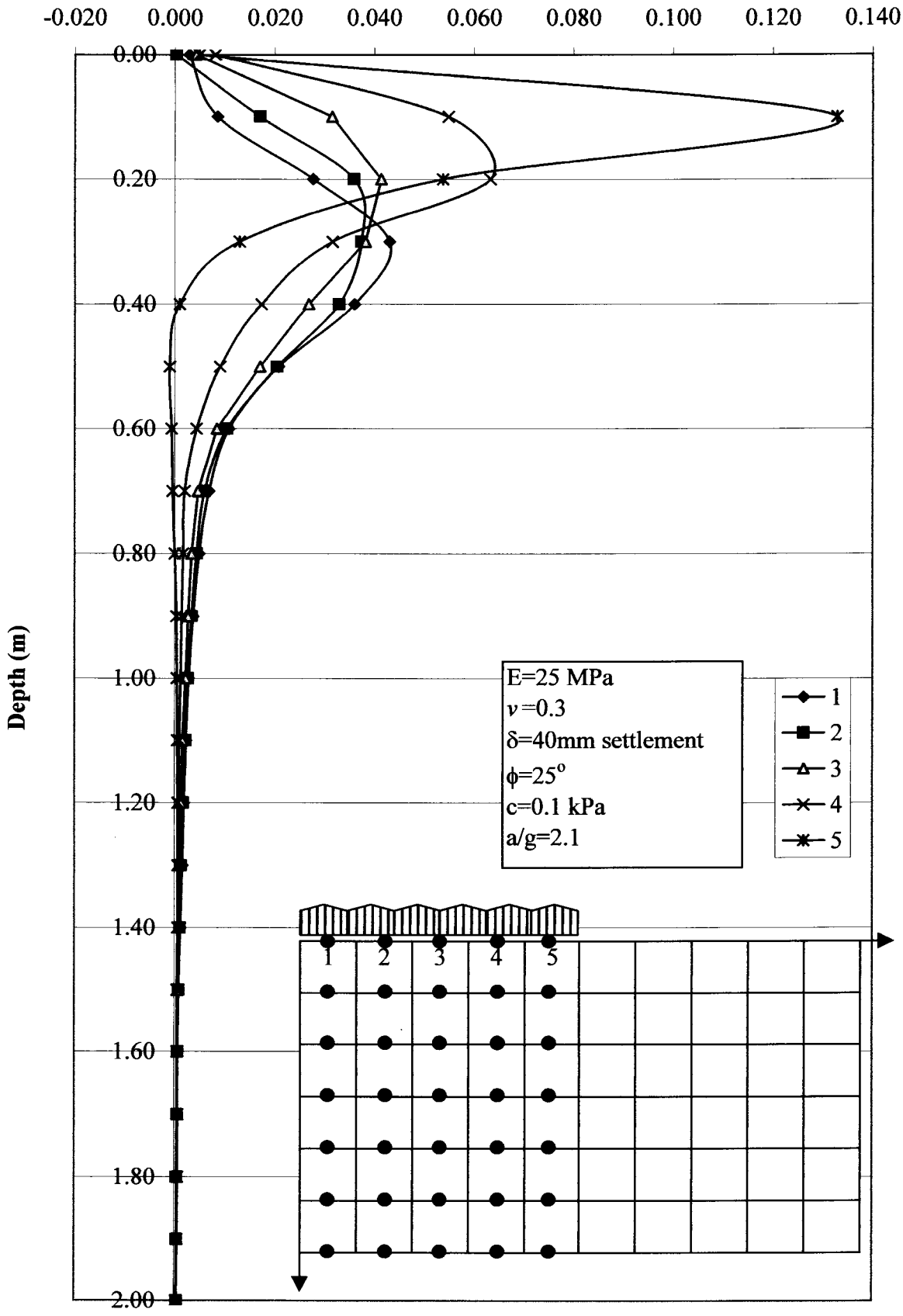

MC 1: Volumetric strain variation under rigid base

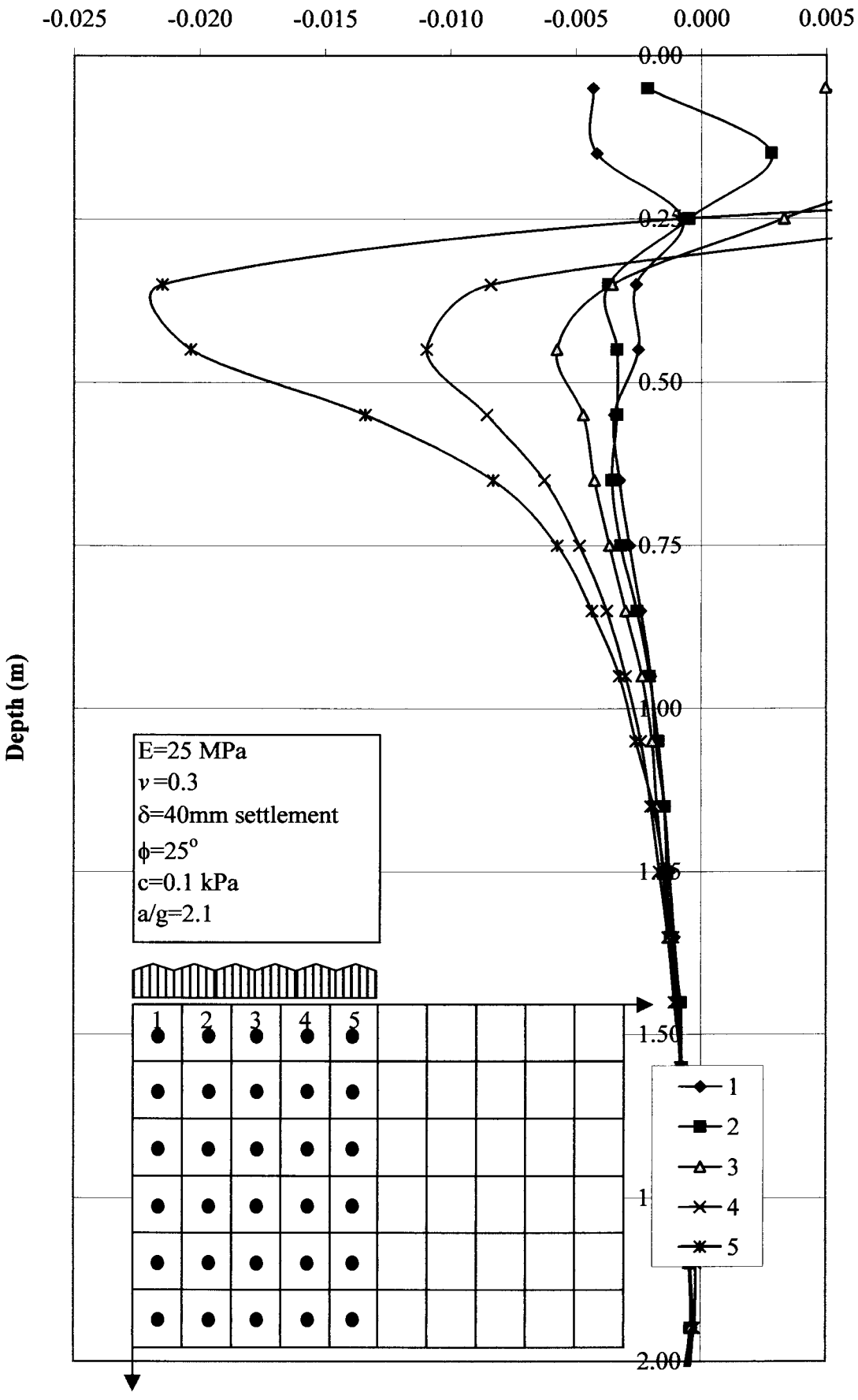

DATA FOR MC1 ANALYSIS: VERTICAL STRAIN CALCULATION

	y ordinate at center of zone		Δy/Yo			Xo=Yo=100mm =grid zone size		
Zone		z (m)	1	2	3	4	5	6
40	3.95	0.05	-0.0142	-0.0174	-0.0217	-0.0398	-0.0531	-0.1305
39	3.85	0.15	-0.0396	-0.0413	-0.0591	-0.0669	-0.1096	-0.1377
38	3.75	0.25	-0.0674	-0.0757	-0.0719	-0.0807	-0.0852	-0.0498
37	3.65	0.35	-0.0876	-0.0758	-0.0722	-0.0649	-0.0499	-0.0211
36	3.55	0.45	-0.0592	-0.0594	-0.0541	-0.0452	-0.0297	-0.011
35	3.45	0.55	-0.0351	-0.0352	-0.0335	-0.0271	-0.017	-0.0066
34	3.35	0.65	-0.021	-0.0211	-0.019	-0.0159	-0.0094	-0.0052
33	3.25	0.75	-0.0149	-0.0144	-0.0128	-0.0107	-0.0064	-0.0043
32	3.15	0.85	-0.0112	-0.0108	-0.0099	-0.0083	-0.0054	-0.0041
31	3.05	0.95	-0.0086	-0.0084	-0.0079	-0.0066	-0.0046	-0.0037
30	2.95	1.05	-0.0069	-0.0069	-0.0063	-0.0052	-0.004	-0.0034
29	2.85	1.15	-0.0057	-0.0056	-0.0051	-0.0042	-0.0034	-0.003
28	2.75	1.25	-0.0049	-0.0046	-0.0041	-0.0035	-0.003	-0.0027
27	2.65	1.35	-0.0039	-0.0038	-0.0034	-0.0029	-0.0027	-0.0023
26	2.55	1.45	-0.003	-0.0029	-0.0027	-0.0026	-0.0023	-0.0022
25	2.45	1.55	-0.0024	-0.0024	-0.0023	-0.0022	-0.0021	-0.0019
24	2.35	1.65	-0.0019	-0.0019	-0.0019	-0.0019	-0.0019	-0.0017
23	2.25	1.75	-0.0016	-0.0016	-0.0017	-0.0017	-0.0017	-0.0015
22	2.15	1.85	-0.0014	-0.0014	-0.0015	-0.0015	-0.0015	-0.0013
21	2.05	1.95	-0.0013	-0.0014	-0.0014	-0.0014	-0.0013	-0.0011
20	1.95	2.05	-0.0013	-0.0013	-0.0013	-0.0013	-0.0011	-0.0007

DATA FOR MC1 ANALYSIS: HORIZONTAL STRAIN CALC.

	Δx/Xo				
z	1	2	3	4	5
0.00	0.0029	0.0003	0.0042	0.0081	0.0049
0.10	0.0086	0.0171	0.0315	0.0549	0.1329
0.20	0.0277	0.0359	0.0414	0.0633	0.0538
0.30	0.0431	0.0374	0.0382	0.0316	0.0130
0.40	0.0360	0.0329	0.0268	0.0174	0.0010
0.50	0.0208	0.0205	0.0171	0.0091	-0.0010
0.60	0.0109	0.0105	0.0085	0.0044	-0.0006
0.70	0.0069	0.0060	0.0047	0.0020	-0.0004
0.80	0.0049	0.0044	0.0034	0.0017	0.0000
0.90	0.0037	0.0034	0.0027	0.0014	0.0004
1.00	0.0028	0.0027	0.0022	0.0012	0.0005
1.10	0.0023	0.0022	0.0016	0.0010	0.0006
1.20	0.0019	0.0017	0.0013	0.0008	0.0007
1.30	0.0016	0.0013	0.0010	0.0008	0.0007
1.40	0.0012	0.0011	0.0009	0.0007	0.0007
1.50	0.0009	0.0009	0.0008	0.0007	0.0006
1.60	0.0007	0.0007	0.0007	0.0007	0.0006
1.70	0.0006	0.0006	0.0006	0.0007	0.0006
1.80	0.0005	0.0005	0.0006	0.0007	0.0005
1.90	0.0005	0.0005	0.0005	0.0006	0.0005
2.00	0.0005	0.0005	0.0005	0.0005	0.0004

DATA FOR MC1 ANALYSIS: VOLUMETRIC STRAIN CALC.

	ε vol =ave(vert) +2(ave hor)					
z	1	2	3	4	5	Total
0.05	-0.00430	-0.00215	0.00495	0.01655	0.04600	0.01221
0.15	-0.00415	0.00280	0.00990	0.02995	0.06305	0.02031
0.25	-0.00075	-0.00050	0.00330	0.01195	-0.00070	0.00266
0.35	-0.00260	-0.00370	-0.00355	-0.00840	-0.02150	-0.00795
0.45	-0.00250	-0.00335	-0.00575	-0.01095	-0.02035	-0.00858
0.55	-0.00345	-0.00335	-0.00470	-0.00855	-0.01340	-0.00669
0.65	-0.00325	-0.00355	-0.00425	-0.00625	-0.00830	-0.00512
0.75	-0.00285	-0.00320	-0.00365	-0.00485	-0.00574	-0.00406
0.85	-0.00240	-0.00255	-0.00300	-0.00375	-0.00434	-0.00321
0.95	-0.00200	-0.00205	-0.00235	-0.00300	-0.00325	-0.00253
1.05	-0.00180	-0.00170	-0.00195	-0.00240	-0.00260	-0.00209
1.15	-0.00145	-0.00145	-0.00175	-0.00200	-0.00190	-0.00171
1.25	-0.00125	-0.00135	-0.00150	-0.00165	-0.00145	-0.00144
1.35	-0.00105	-0.00120	-0.00125	-0.00130	-0.00110	-0.00118
1.45	-0.00085	-0.00080	-0.00095	-0.00105	-0.00095	-0.00092
1.55	-0.00080	-0.00075	-0.00075	-0.00075	-0.00080	-0.00077
1.65	-0.00060	-0.00060	-0.00060	-0.00050	-0.00060	-0.00058
1.75	-0.00050	-0.00055	-0.00050	-0.00030	-0.00050	-0.00047
1.85	-0.00040	-0.00045	-0.00040	-0.00020	-0.00040	-0.00037
1.95	-0.00035	-0.00040	-0.00040	-0.00025	-0.00030	-0.00034
2.05	-0.00080	-0.00080	-0.00080	-0.00070	-0.00050	-0.00072

DATA FOR MC2 ANALYSIS: VERTICAL DISPLACEMENTS

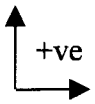

z (m)	x10^{-2} [Vertical displacements of grid points]					
0.0	-4.000	-4.000	-4.000	-4.000	-4.000	-4.000
0.1	-3.674	-3.724	-3.752	-3.717	-3.640	-3.098
0.2	-3.372	-3.379	-3.366	-3.273	-2.904	-2.022
0.3	-3.010	-2.981	-2.905	-2.708	-2.207	-1.458
0.4	-2.607	-2.567	-2.435	-2.195	-1.690	-1.180
0.5	-2.221	-2.172	-2.027	-1.797	-1.329	-1.014
0.6	-1.870	-1.825	-1.696	-1.497	-1.088	-0.905
0.7	-1.563	-1.529	-1.429	-1.256	-0.925	-0.818
0.8	-1.306	-1.282	-1.204	-1.052	-0.806	-0.740
0.9	-1.097	-1.079	-1.012	-0.878	-0.711	-0.665
1.0	-0.925	-0.908	-0.847	-0.734	-0.632	-0.594
1.1	-0.777	-0.760	-0.705	-0.618	-0.561	-0.528
1.2	-0.646	-0.631	-0.584	-0.528	-0.497	-0.466
1.3	-0.531	-0.518	-0.485	-0.456	-0.440	-0.408
1.4	-0.433	-0.425	-0.409	-0.398	-0.387	-0.353
1.5	-0.356	-0.354	-0.351	-0.349	-0.339	-0.300
1.6	-0.301	-0.304	-0.307	-0.308	-0.294	-0.251
1.7	-0.267	-0.269	-0.273	-0.270	-0.253	-0.208
1.8	-0.244	-0.244	-0.243	-0.236	-0.214	-0.172
1.9	-0.223	-0.222	-0.217	-0.205	-0.179	-0.144
2.0	-0.201	-0.199	-0.192	-0.175	-0.148	-0.121
2.1	-0.178	-0.175	-0.166	-0.147	-0.122	-0.103

DATA FOR MC2 ANALYSIS: HORIZONTAL DISPLACEMENTS

z (m)	x10^{-2} [Horizon displacements of grid points]					
0.0	0.000	0.108	0.133	0.194	0.216	0.298
0.1	0.000	0.104	0.227	0.367	0.676	1.503
0.2	0.000	0.127	0.307	0.568	1.008	1.543
0.3	0.000	0.153	0.354	0.636	0.973	1.209
0.4	0.000	0.158	0.345	0.561	0.789	0.905
0.5	0.000	0.145	0.296	0.443	0.576	0.623
0.6	0.000	0.127	0.245	0.347	0.425	0.435
0.7	0.000	0.108	0.204	0.285	0.336	0.332
0.8	0.000	0.088	0.168	0.239	0.279	0.272
0.9	0.000	0.071	0.139	0.201	0.233	0.229
1.0	0.000	0.059	0.118	0.170	0.194	0.194
1.1	0.000	0.052	0.103	0.144	0.160	0.164
1.2	0.000	0.046	0.090	0.120	0.131	0.139
1.3	0.000	0.041	0.076	0.097	0.106	0.116
1.4	0.000	0.034	0.059	0.074	0.084	0.097
1.5	0.000	0.025	0.042	0.054	0.065	0.082
1.6	0.000	0.015	0.028	0.039	0.052	0.070
1.7	0.000	0.008	0.017	0.029	0.043	0.061
1.8	0.000	0.005	0.012	0.024	0.039	0.055
1.9	0.000	0.005	0.012	0.023	0.037	0.050
2.0	0.000	0.006	0.014	0.024	0.037	0.046
2.1	0.000	0.007	0.016	0.026	0.037	0.042

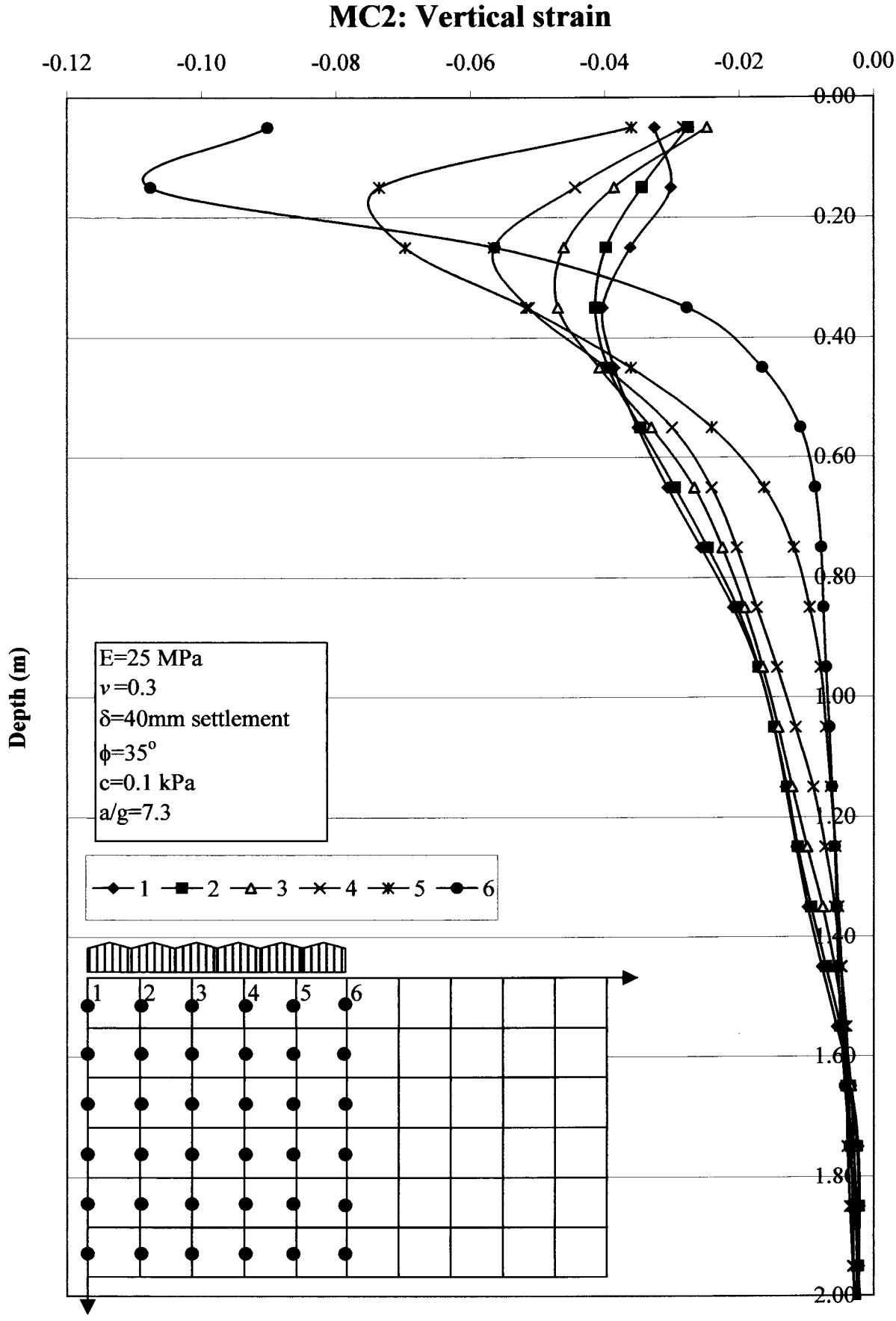
MC2: Vertical strain
-0.12
-0.10
-0.08
-0.06
-0.04
-0.02
0.00
0.00
0.20
0.40
0.60
0.80
1.00
1.20
1.40
1.60
1.80
2.00
Depth (m)
E=25 MPa
ν=0.3
δ=40mm settlement
ϕ=35°
c=0.1 kPa
a/g=7.3
1
2
3
4
5
6
1
2
3
4
5
6

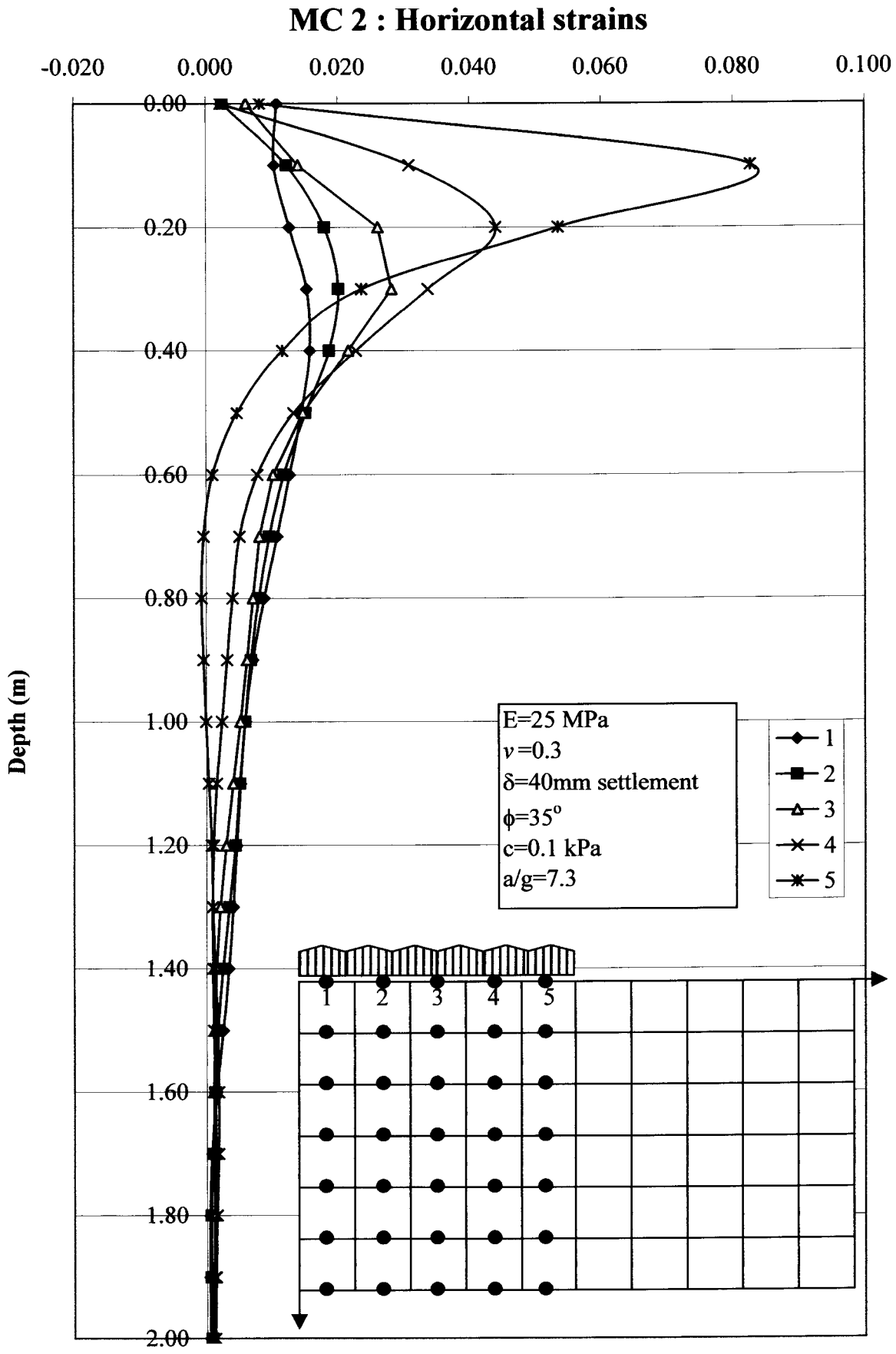
MC 2 : Horizontal strains
-0.020
0.000
0.020
0.040
0.060
0.080
0.100
0.00
0.20
0.40
0.60
0.80
1.00
1.20
1.40
1.60
1.80
2.00
Depth (m)
E=25 MPa
ν=0.3
δ=40mm settlement
ϕ=35°
c=0.1 kPa
a/g=7.3
1
2
3
4
5
1
2
3
4
5

MC2 : Volumetric strain

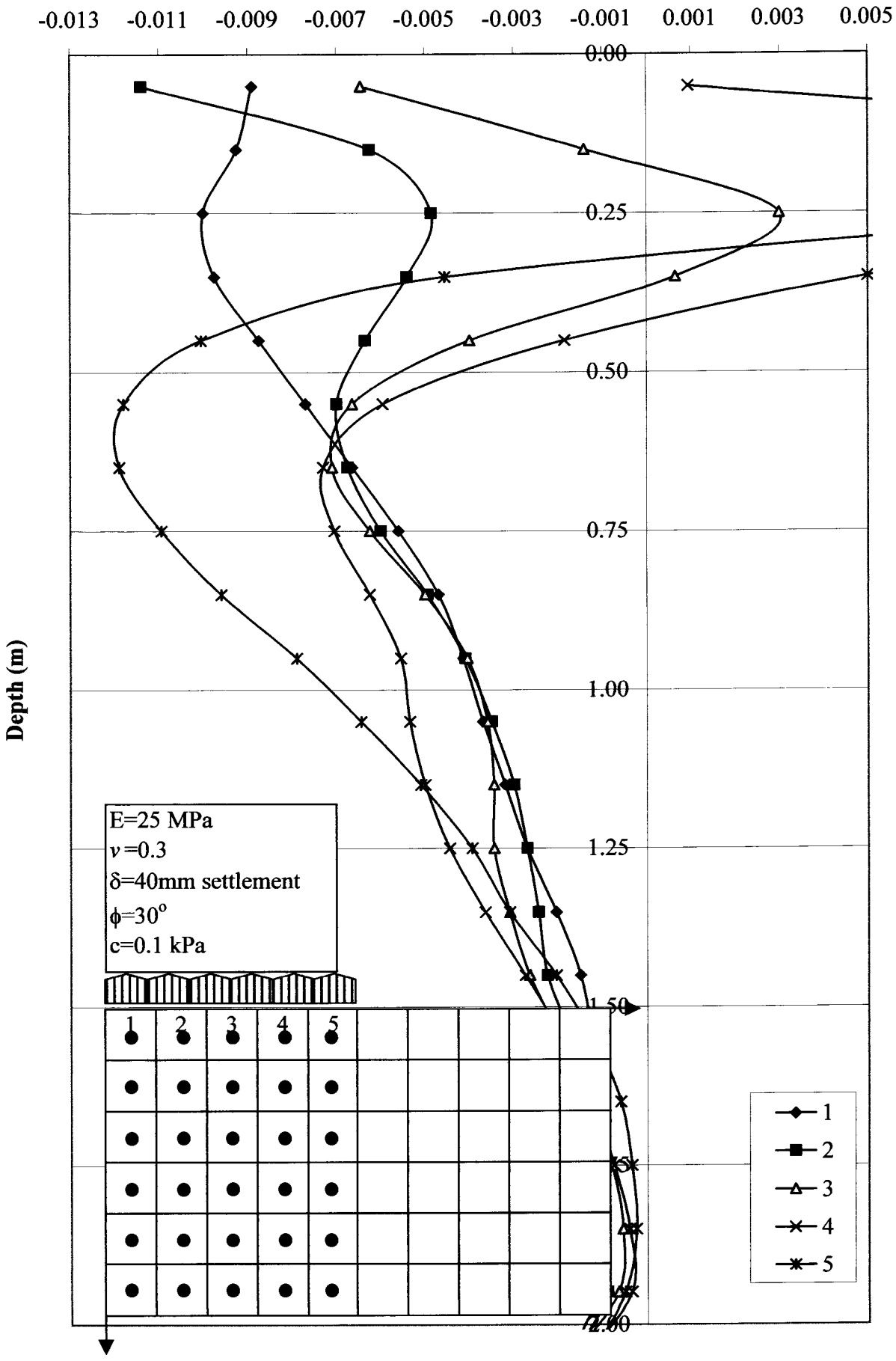

DATA FOR MC2 ANALYSIS: VERTICAL STRAIN CALCULATION

Zone	y ordinate at center of zone	z (m)	Δy/Yo 1	2	3	4	5	Xo=Yo=100mm =grid zone size 6
40	3.95	0.05	-0.0326	-0.0276	-0.0248	-0.0283	-0.036	-0.0902
39	3.85	0.15	-0.0302	-0.0345	-0.0386	-0.0444	-0.0736	-0.1076
38	3.75	0.25	-0.0362	-0.0398	-0.0461	-0.0565	-0.0697	-0.0564
37	3.65	0.35	-0.0403	-0.0414	-0.047	-0.0513	-0.0517	-0.0278
36	3.55	0.45	-0.0386	-0.0395	-0.0408	-0.0398	-0.0361	-0.0166
35	3.45	0.55	-0.0351	-0.0347	-0.0331	-0.03	-0.0241	-0.0109
34	3.35	0.65	-0.0307	-0.0296	-0.0267	-0.0241	-0.0163	-0.0087
33	3.25	0.75	-0.0257	-0.0247	-0.0225	-0.0204	-0.0119	-0.0078
32	3.15	0.85	-0.0209	-0.0203	-0.0192	-0.0174	-0.0095	-0.0075
31	3.05	0.95	-0.0172	-0.0171	-0.0165	-0.0144	-0.0079	-0.0071
30	2.95	1.05	-0.0148	-0.0148	-0.0142	-0.0116	-0.0071	-0.0066
29	2.85	1.15	-0.0131	-0.0129	-0.0121	-0.009	-0.0064	-0.0062
28	2.75	1.25	-0.0115	-0.0113	-0.0099	-0.0072	-0.0057	-0.0058
27	2.65	1.35	-0.0098	-0.0093	-0.0076	-0.0058	-0.0053	-0.0055
26	2.55	1.45	-0.0077	-0.0071	-0.0058	-0.0049	-0.0048	-0.0053
25	2.45	1.55	-0.0055	-0.005	-0.0044	-0.0041	-0.0045	-0.0049
24	2.35	1.65	-0.0034	-0.0035	-0.0034	-0.0038	-0.0041	-0.0043
23	2.25	1.75	-0.0023	-0.0025	-0.003	-0.0034	-0.0039	-0.0036
22	2.15	1.85	-0.0021	-0.0022	-0.0026	-0.0031	-0.0035	-0.0028
21	2.05	1.95	-0.0022	-0.0023	-0.0025	-0.003	-0.0031	-0.0023
20	1.95	2.05	-0.0023	-0.0024	-0.0026	-0.0028	-0.0026	-0.0018

DATA FOR MC2 ANALYSIS: HORIZONTAL STRAIN CALC.

z	Δx/Xo 1	2	3	4	5
0.00	0.0108	0.0025	0.0061	0.0022	0.0082
0.10	0.0104	0.0123	0.0140	0.0309	0.0827
0.20	0.0127	0.0180	0.0261	0.0440	0.0535
0.30	0.0153	0.0201	0.0282	0.0337	0.0236
0.40	0.0158	0.0187	0.0216	0.0228	0.0116
0.50	0.0145	0.0151	0.0147	0.0133	0.0047
0.60	0.0127	0.0118	0.0102	0.0078	0.0010
0.70	0.0108	0.0096	0.0081	0.0051	-0.0004
0.80	0.0088	0.0080	0.0071	0.0040	-0.0007
0.90	0.0071	0.0068	0.0062	0.0032	-0.0004
1.00	0.0059	0.0059	0.0052	0.0024	0.0000
1.10	0.0052	0.0051	0.0041	0.0016	0.0004
1.20	0.0046	0.0044	0.0030	0.0011	0.0008
1.30	0.0041	0.0035	0.0021	0.0009	0.0010
1.40	0.0034	0.0025	0.0015	0.0010	0.0013
1.50	0.0025	0.0017	0.0012	0.0011	0.0017
1.60	0.0015	0.0013	0.0011	0.0013	0.0018
1.70	0.0008	0.0009	0.0012	0.0014	0.0018
1.80	0.0005	0.0007	0.0012	0.0015	0.0016
1.90	0.0005	0.0007	0.0011	0.0014	0.0013
2.00	0.0006	0.0008	0.0010	0.0013	0.0009

DATA FOR MC3 ANALYSIS: VOLUMETRIC STRAIN CALC.

z	ε vol =ave(vert) +2(ave hor) 1	2	3	4	5	MC2
0.05	-0.00890	-0.01140	-0.00645	0.00095	0.02780	0.00040
0.15	-0.00925	-0.00625	-0.00140	0.01590	0.04560	0.00892
0.25	-0.01000	-0.00485	0.00300	0.01460	0.01405	0.00336
0.35	-0.00975	-0.00540	0.00065	0.00500	-0.00455	-0.00281
0.45	-0.00875	-0.00635	-0.00400	-0.00185	-0.01005	-0.00620
0.55	-0.00770	-0.00700	-0.00665	-0.00595	-0.01180	-0.00782
0.65	-0.00665	-0.00675	-0.00710	-0.00730	-0.01190	-0.00794
0.75	-0.00560	-0.00600	-0.00625	-0.00705	-0.01095	-0.00717
0.85	-0.00470	-0.00495	-0.00500	-0.00625	-0.00960	-0.00610
0.95	-0.00415	-0.00410	-0.00405	-0.00555	-0.00790	-0.00515
1.05	-0.00370	-0.00350	-0.00360	-0.00535	-0.00645	-0.00452
1.15	-0.00320	-0.00300	-0.00345	-0.00500	-0.00510	-0.00395
1.25	-0.00270	-0.00270	-0.00345	-0.00445	-0.00395	-0.00345
1.35	-0.00205	-0.00245	-0.00310	-0.00365	-0.00310	-0.00287
1.45	-0.00150	-0.00225	-0.00265	-0.00275	-0.00205	-0.00224
1.55	-0.00125	-0.00170	-0.00195	-0.00190	-0.00120	-0.00160
1.65	-0.00115	-0.00125	-0.00130	-0.00125	-0.00060	-0.00111
1.75	-0.00110	-0.00115	-0.00080	-0.00075	-0.00035	-0.00083
1.85	-0.00115	-0.00100	-0.00055	-0.00040	-0.00025	-0.00067
1.95	-0.00115	-0.00090	-0.00065	-0.00035	-0.00050	-0.00071
2.05	-0.00175	-0.00170	-0.00170	-0.00140	-0.00130	

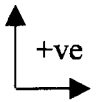

DATA FOR MC3 ANALYSIS: VERTICAL DISPLACEMENTS

z (m)	x10^{-2} [Vertical displacements of grid points]					
0.0	-4.000	-4.000	-4.000	-4.000	-4.000	-4.000
0.1	-3.597	-3.650	-3.678	-3.673	-3.699	-3.431
0.2	-3.316	-3.331	-3.345	-3.347	-3.229	-2.734
0.3	-3.066	-3.061	-3.051	-3.006	-2.770	-2.228
0.4	-2.837	-2.826	-2.791	-2.695	-2.372	-1.909
0.5	-2.621	-2.606	-2.553	-2.415	-2.037	-1.693
0.6	-2.410	-2.391	-2.323	-2.146	-1.763	-1.535
0.7	-2.201	-2.178	-2.093	-1.880	-1.546	-1.402
0.8	-1.993	-1.964	-1.859	-1.629	-1.376	-1.283
0.9	-1.782	-1.746	-1.624	-1.405	-1.239	-1.171
1.0	-1.564	-1.523	-1.397	-1.219	-1.120	-1.064
1.1	-1.339	-1.298	-1.186	-1.068	-1.012	-0.961
1.2	-1.114	-1.081	-1.004	-0.943	-0.910	-0.865
1.3	-0.903	-0.885	-0.853	-0.833	-0.815	-0.774
1.4	-0.725	-0.727	-0.731	-0.735	-0.725	-0.688
1.5	-0.599	-0.612	-0.632	-0.646	-0.642	-0.605
1.6	-0.525	-0.536	-0.554	-0.568	-0.565	-0.525
1.7	-0.483	-0.486	-0.494	-0.501	-0.495	-0.448
1.8	-0.448	-0.448	-0.447	-0.445	-0.431	-0.376
1.9	-0.413	-0.412	-0.408	-0.398	-0.374	-0.311
2.0	-0.377	-0.376	-0.370	-0.355	-0.323	-0.256
2.1	-0.342	-0.340	-0.332	-0.314	-0.276	-0.211

DATA FOR MC3 ANALYSIS: HORIZONTAL DISPLACEMENTS

z (m)	x10^{-3} [Horizon displacements of grid points]					
0.0	0.000	1.457	1.982	3.086	3.835	4.612
0.1	0.000	0.976	2.056	3.130	4.834	9.225
0.2	0.000	0.671	1.626	2.826	5.114	8.972
0.3	0.000	0.506	1.214	2.378	4.469	6.962
0.4	0.000	0.440	1.036	2.026	3.771	5.387
0.5	0.000	0.452	1.031	1.958	3.397	4.379
0.6	0.000	0.491	1.116	2.093	3.288	3.819
0.7	0.000	0.541	1.242	2.263	3.204	3.444
0.8	0.000	0.611	1.391	2.375	3.044	3.114
0.9	0.000	0.699	1.538	2.398	2.815	2.823
1.0	0.000	0.793	1.643	2.319	2.540	2.569
1.1	0.000	0.864	1.663	2.151	2.266	2.321
1.2	0.000	0.876	1.564	1.901	1.995	2.085
1.3	0.000	0.790	1.338	1.591	1.719	1.849
1.4	0.000	0.604	1.019	1.258	1.432	1.609
1.5	0.000	0.367	0.677	0.928	1.147	1.374
1.6	0.000	0.173	0.392	0.634	0.880	1.157
1.7	0.000	0.076	0.210	0.411	0.658	0.969
1.8	0.000	0.059	0.140	0.283	0.505	0.820
1.9	0.000	0.063	0.136	0.242	0.431	0.722
2.0	0.000	0.068	0.147	0.252	0.423	0.672
2.1	0.000	0.076	0.163	0.279	0.450	0.650

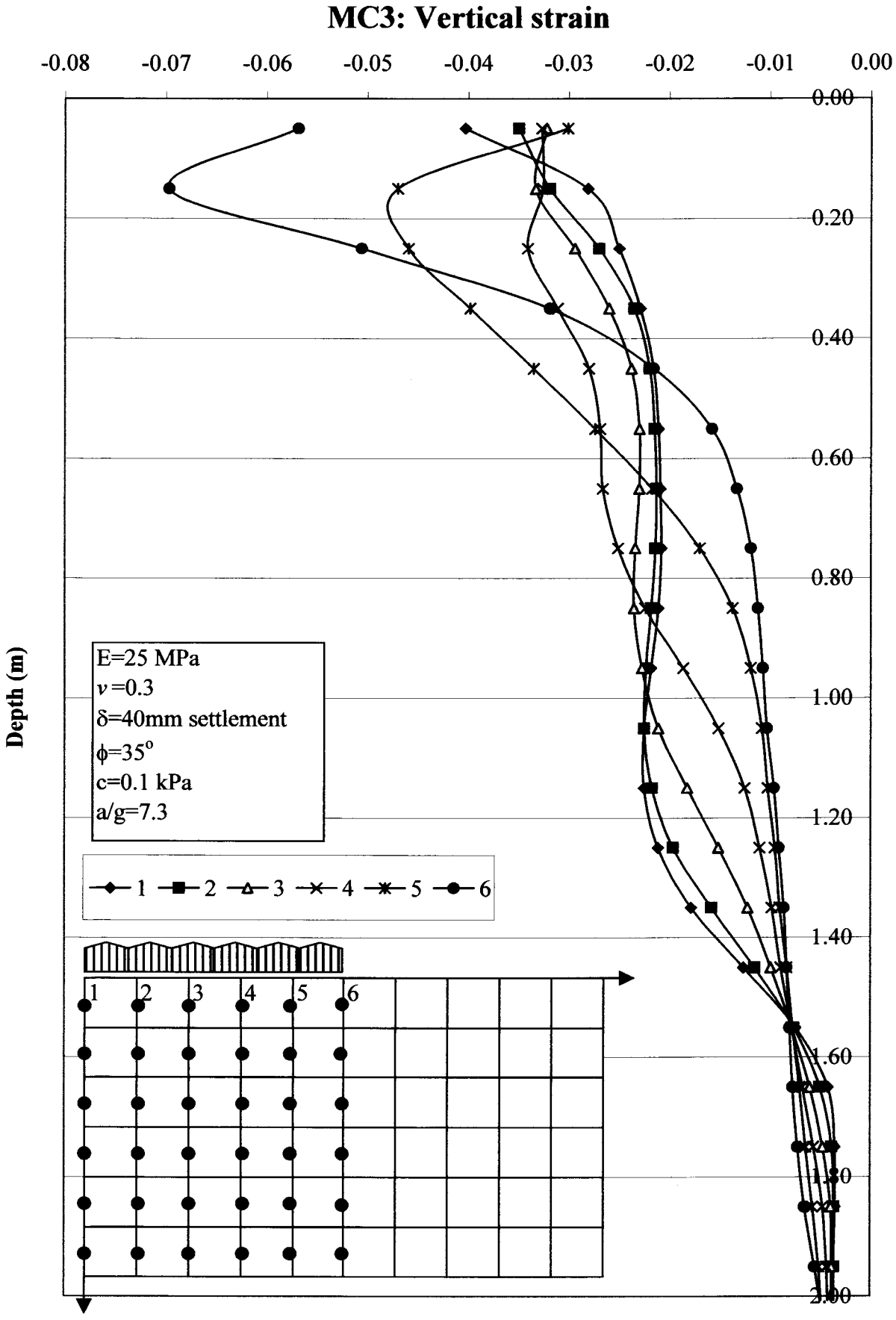
MC3: Vertical strain
-0.08
-0.07
-0.06
-0.05
-0.04
-0.03
-0.02
-0.01
0.00
Depth (m)
0.00
0.20
0.40
0.60
0.80
1.00
1.20
1.40
1.60
1.80
2.00
E=25 MPa
ν=0.3
δ=40mm settlement
ϕ=35°
c=0.1 kPa
a/g=7.3
1
2
3
4
5
6

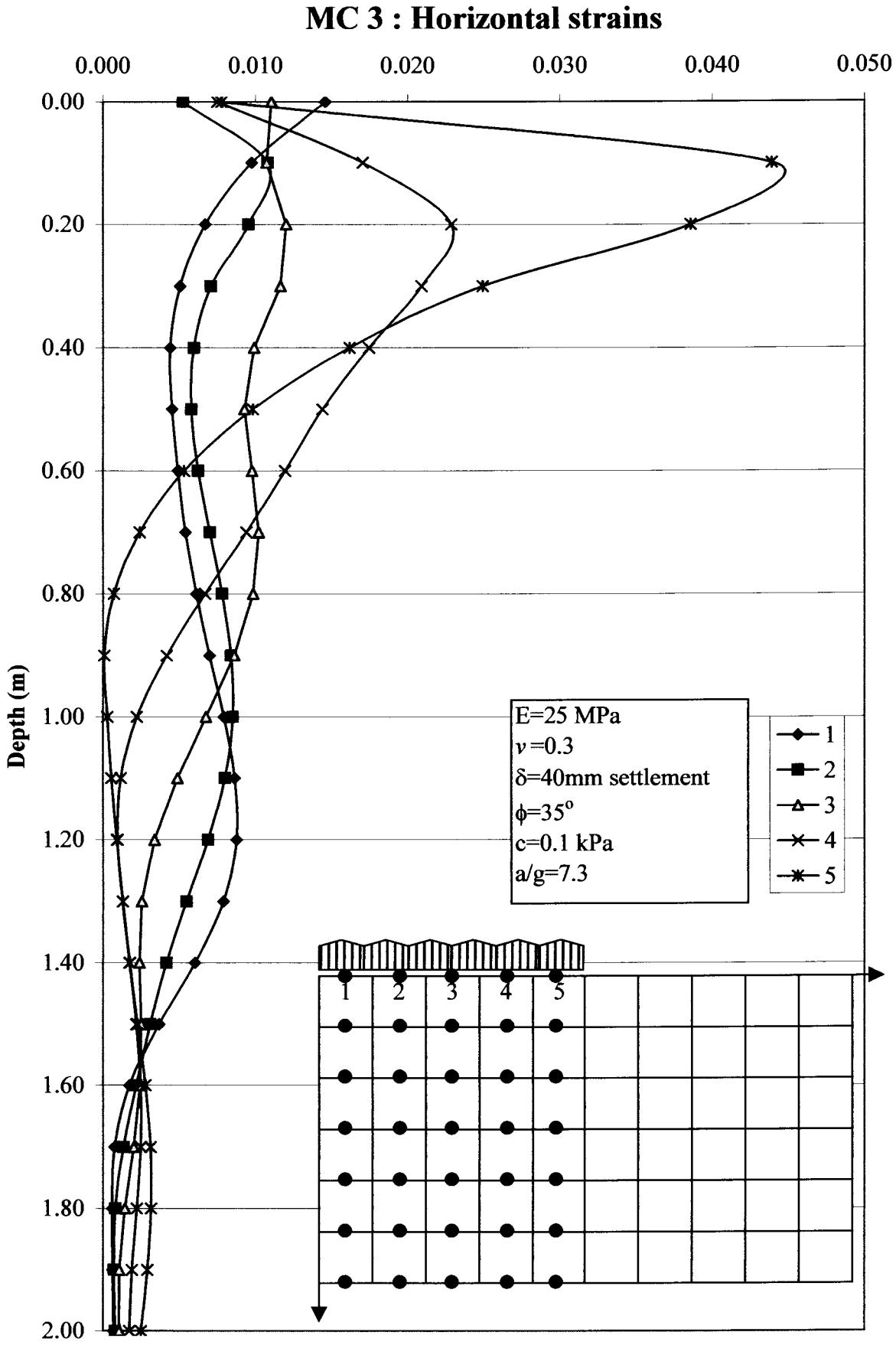
MC 3 : Horizontal strains
0.000
0.010
0.020
0.030
0.040
0.050
0.00
0.20
0.40
0.60
0.80
1.00
1.20
1.40
1.60
1.80
2.00
Depth (m)
E=25 MPa
ν=0.3
δ=40mm settlement
ϕ=35°
c=0.1 kPa
a/g=7.3
1
2
3
4
5
1
2
3
4
5

MC 3: Volumetric strain variation under rigid base

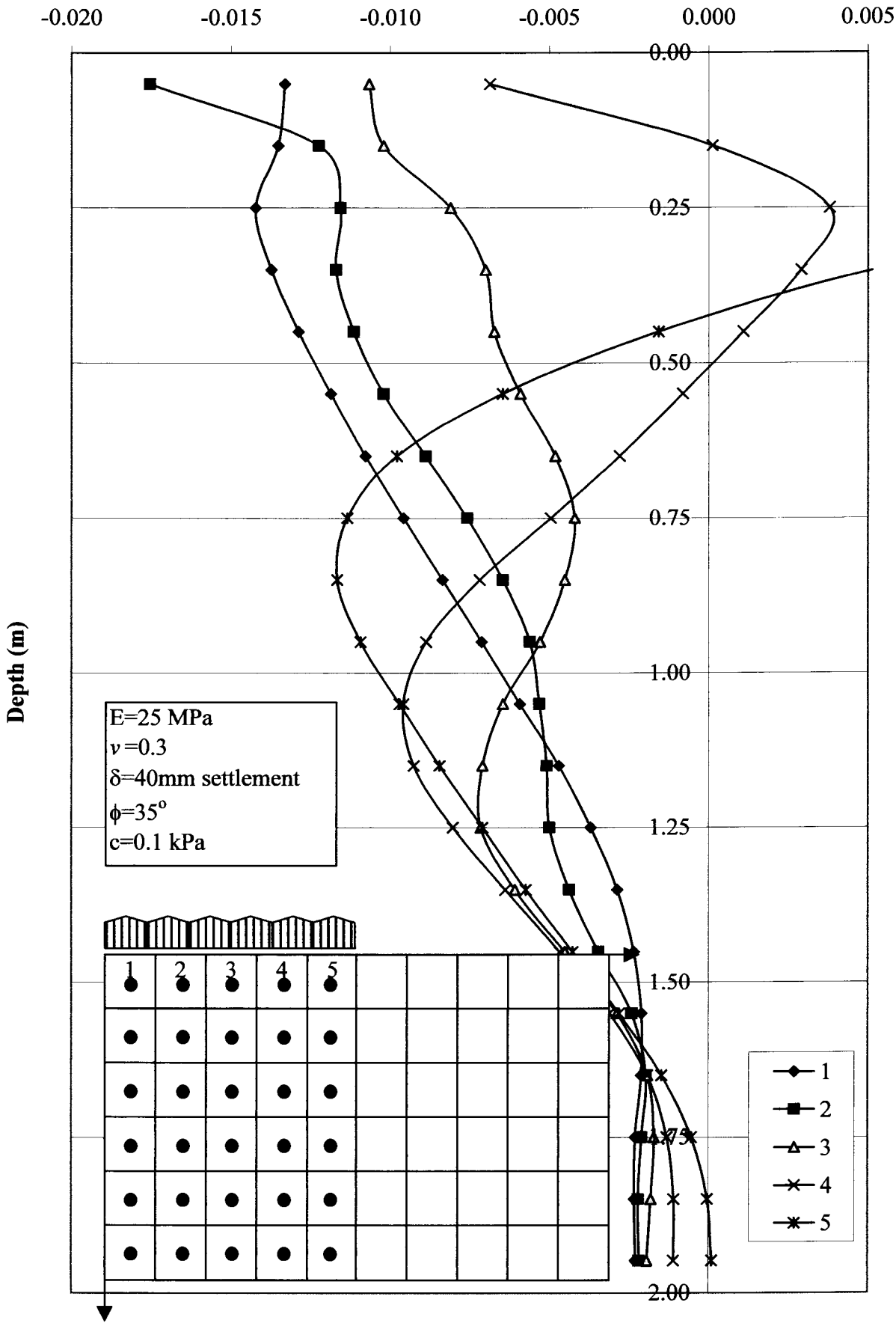

DATA FOR MC3 ANALYSIS: VERTICAL STRAIN CALCULATION

Zone	y ordinate at center of zone	z (m)	Δy/Yo 1	2	3	Xo=Yo=100mm =grid zone size 4	5	6
40	3.95	0.05	-0.0403	-0.035	-0.0322	-0.0327	-0.0301	-0.0569
39	3.85	0.15	-0.0281	-0.0319	-0.0333	-0.0326	-0.047	-0.0697
38	3.75	0.25	-0.025	-0.027	-0.0294	-0.0341	-0.0459	-0.0506
37	3.65	0.35	-0.0229	-0.0235	-0.026	-0.0311	-0.0398	-0.0319
36	3.55	0.45	-0.0216	-0.022	-0.0238	-0.028	-0.0335	-0.0216
35	3.45	0.55	-0.0211	-0.0215	-0.023	-0.0269	-0.0274	-0.0158
34	3.35	0.65	-0.0209	-0.0213	-0.023	-0.0266	-0.0217	-0.0133
33	3.25	0.75	-0.0208	-0.0214	-0.0234	-0.0251	-0.017	-0.0119
32	3.15	0.85	-0.0211	-0.0218	-0.0235	-0.0224	-0.0137	-0.0112
31	3.05	0.95	-0.0218	-0.0223	-0.0227	-0.0186	-0.0119	-0.0107
30	2.95	1.05	-0.0225	-0.0225	-0.0211	-0.0151	-0.0108	-0.0103
29	2.85	1.15	-0.0225	-0.0217	-0.0182	-0.0125	-0.0102	-0.0096
28	2.75	1.25	-0.0211	-0.0196	-0.0151	-0.011	-0.0095	-0.0091
27	2.65	1.35	-0.0178	-0.0158	-0.0122	-0.0098	-0.009	-0.0086
26	2.55	1.45	-0.0126	-0.0115	-0.0099	-0.0089	-0.0083	-0.0083
25	2.45	1.55	-0.0074	-0.0076	-0.0078	-0.0078	-0.0077	-0.008
24	2.35	1.65	-0.0042	-0.005	-0.006	-0.0067	-0.007	-0.0077
23	2.25	1.75	-0.0035	-0.0038	-0.0047	-0.0056	-0.0064	-0.0072
22	2.15	1.85	-0.0035	-0.0036	-0.0039	-0.0047	-0.0057	-0.0065
21	2.05	1.95	-0.0036	-0.0036	-0.0038	-0.0043	-0.0051	-0.0055
20	1.95	2.05	-0.0035	-0.0036	-0.0038	-0.0041	-0.0047	-0.0045

DATA FOR MC3 ANALYSIS: HORIZONTAL STRAIN CALCULATION

z	Δx/Xo 1	2	3	4	5
0.00	0.0146	0.0053	0.0110	0.0075	0.0078
0.10	0.0098	0.0108	0.0107	0.0170	0.0439
0.20	0.0067	0.0096	0.0120	0.0229	0.0386
0.30	0.0051	0.0071	0.0116	0.0209	0.0249
0.40	0.0044	0.0060	0.0099	0.0175	0.0162
0.50	0.0045	0.0058	0.0093	0.0144	0.0098
0.60	0.0049	0.0063	0.0098	0.0120	0.0053
0.70	0.0054	0.0070	0.0102	0.0094	0.0024
0.80	0.0061	0.0078	0.0098	0.0067	0.0007
0.90	0.0070	0.0084	0.0086	0.0042	0.0001
1.00	0.0079	0.0085	0.0068	0.0022	0.0003
1.10	0.0086	0.0080	0.0049	0.0012	0.0006
1.20	0.0088	0.0069	0.0034	0.0009	0.0009
1.30	0.0079	0.0055	0.0025	0.0013	0.0013
1.40	0.0060	0.0042	0.0024	0.0017	0.0018
1.50	0.0037	0.0031	0.0025	0.0022	0.0023
1.60	0.0017	0.0022	0.0024	0.0025	0.0028
1.70	0.0008	0.0013	0.0020	0.0025	0.0031
1.80	0.0006	0.0008	0.0014	0.0022	0.0032
1.90	0.0006	0.0007	0.0011	0.0019	0.0029
2.00	0.0007	0.0008	0.0011	0.0017	0.0025

DATA FOR MC3 ANALYSIS: VOLUMETRIC STRAIN CALCULATION

z	ε vol =ave(vert) +2(ave hor) 1	2	3	4	5	Total
0.05	-0.01332	-0.01755	-0.01067	-0.00687	0.00818	-0.00805
0.15	-0.01353	-0.01225	-0.01021	0.00012	0.02414	-0.00235
0.25	-0.01423	-0.01157	-0.00811	0.00379	0.01526	-0.00297
0.35	-0.01374	-0.01171	-0.00701	0.00291	0.00524	-0.00486
0.45	-0.01288	-0.01115	-0.00673	0.00109	-0.00157	-0.00625
0.55	-0.01187	-0.01021	-0.00591	-0.00081	-0.00647	-0.00705
0.65	-0.01078	-0.00889	-0.00482	-0.00279	-0.00979	-0.00741
0.75	-0.00958	-0.00759	-0.00420	-0.00495	-0.01135	-0.00753
0.85	-0.00835	-0.00646	-0.00451	-0.00719	-0.01167	-0.00764
0.95	-0.00713	-0.00561	-0.00529	-0.00887	-0.01093	-0.00757
1.05	-0.00593	-0.00531	-0.00646	-0.00959	-0.00971	-0.00740
1.15	-0.00470	-0.00508	-0.00710	-0.00926	-0.00845	-0.00692
1.25	-0.00369	-0.00499	-0.00715	-0.00803	-0.00710	-0.00619
1.35	-0.00286	-0.00437	-0.00608	-0.00638	-0.00573	-0.00508
1.45	-0.00234	-0.00345	-0.00450	-0.00467	-0.00426	-0.00384
1.55	-0.00210	-0.00241	-0.00287	-0.00310	-0.00281	-0.00266
1.65	-0.00211	-0.00197	-0.00192	-0.00192	-0.00147	-0.00188
1.75	-0.00230	-0.00210	-0.00171	-0.00131	-0.00054	-0.00159
1.85	-0.00233	-0.00221	-0.00181	-0.00109	-0.00004	-0.00150
1.95	-0.00229	-0.00218	-0.00194	-0.00110	0.00010	-0.00148

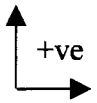

DATA FOR MC4 ANALYSIS: VERTICAL DISPLACEMENTS

z (m)	x10^{-2} [Vertical displacements of grid points]					
0.0	-4.000	-4.000	-4.000	-4.000	-4.000	-4.000
0.1	-3.815	-3.806	-3.738	-3.698	-3.803	-3.662
0.2	-3.592	-3.556	-3.501	-3.487	-3.447	-3.131
0.3	-3.315	-3.303	-3.291	-3.250	-3.088	-2.666
0.4	-3.066	-3.075	-3.068	-2.987	-2.750	-2.312
0.5	-2.866	-2.863	-2.829	-2.707	-2.432	-2.031
0.6	-2.674	-2.654	-2.583	-2.422	-2.137	-1.799
0.7	-2.465	-2.432	-2.332	-2.147	-1.875	-1.600
0.8	-2.229	-2.190	-2.078	-1.889	-1.646	-1.429
0.9	-1.975	-1.937	-1.826	-1.651	-1.448	-1.278
1.0	-1.718	-1.684	-1.584	-1.435	-1.275	-1.143
1.1	-1.470	-1.442	-1.359	-1.242	-1.124	-1.021
1.2	-1.241	-1.219	-1.157	-1.072	-0.990	-0.908
1.3	-1.038	-1.023	-0.980	-0.925	-0.871	-0.803
1.4	-0.865	-0.856	-0.831	-0.800	-0.766	-0.705
1.5	-0.724	-0.721	-0.710	-0.695	-0.672	-0.612
1.6	-0.614	-0.615	-0.614	-0.608	-0.588	-0.524
1.7	-0.533	-0.535	-0.538	-0.534	-0.512	-0.443
1.8	-0.475	-0.476	-0.478	-0.471	-0.443	-0.371
1.9	-0.431	-0.431	-0.428	-0.415	-0.379	-0.310
2.0	-0.393	-0.391	-0.383	-0.364	-0.322	-0.260
2.1	-0.356	-0.353	-0.341	-0.315	-0.271	-0.222

DATA FOR MC4 ANALYSIS: HORIZONTAL DISPLACEMENTS

z (m)	x10^{-3} [Horizon displacements of grid points]					
0.0	0.000	0.204	0.552	2.373	3.127	1.649
0.1	0.000	0.349	1.080	1.792	2.723	5.507
0.2	0.000	0.671	1.184	1.538	2.857	5.853
0.3	0.000	0.688	1.112	1.676	3.054	5.269
0.4	0.000	0.498	1.045	1.903	3.311	4.959
0.5	0.000	0.402	1.061	2.101	3.485	4.760
0.6	0.000	0.474	1.211	2.286	3.540	4.521
0.7	0.000	0.643	1.456	2.476	3.521	4.236
0.8	0.000	0.810	1.684	2.620	3.449	3.947
0.9	0.000	0.912	1.815	2.661	3.311	3.654
1.0	0.000	0.940	1.827	2.582	3.097	3.345
1.1	0.000	0.908	1.739	2.402	2.817	3.016
1.2	0.000	0.832	1.577	2.146	2.489	2.675
1.3	0.000	0.725	1.364	1.839	2.131	2.328
1.4	0.000	0.600	1.120	1.505	1.763	1.990
1.5	0.000	0.469	0.869	1.174	1.414	1.676
1.6	0.000	0.340	0.634	0.879	1.113	1.402
1.7	0.000	0.225	0.438	0.645	0.880	1.183
1.8	0.000	0.138	0.296	0.481	0.722	1.017
1.9	0.000	0.093	0.217	0.390	0.632	0.893
2.0	0.000	0.085	0.195	0.363	0.593	0.800
2.1	0.000	0.094	0.212	0.380	0.584	0.729

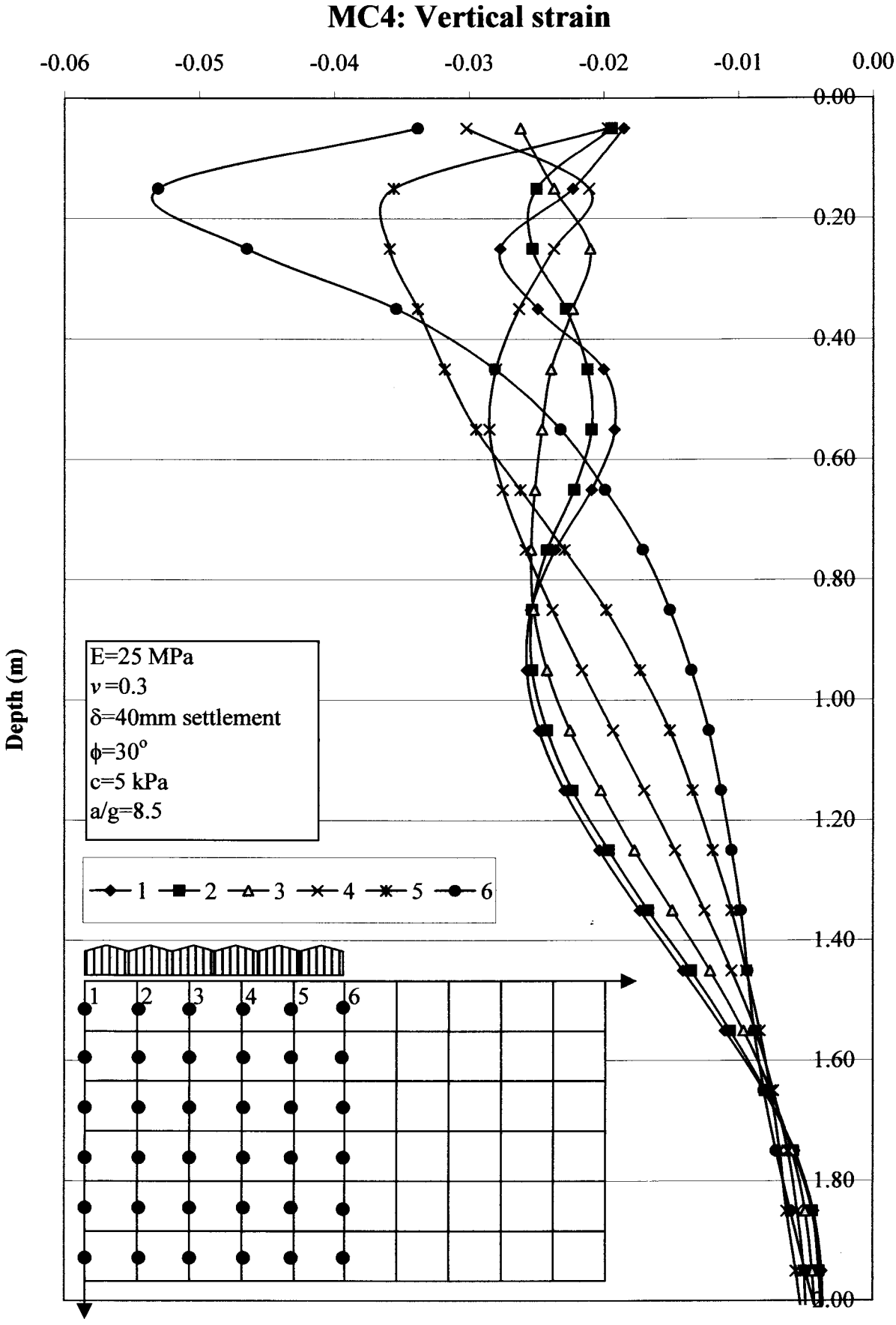

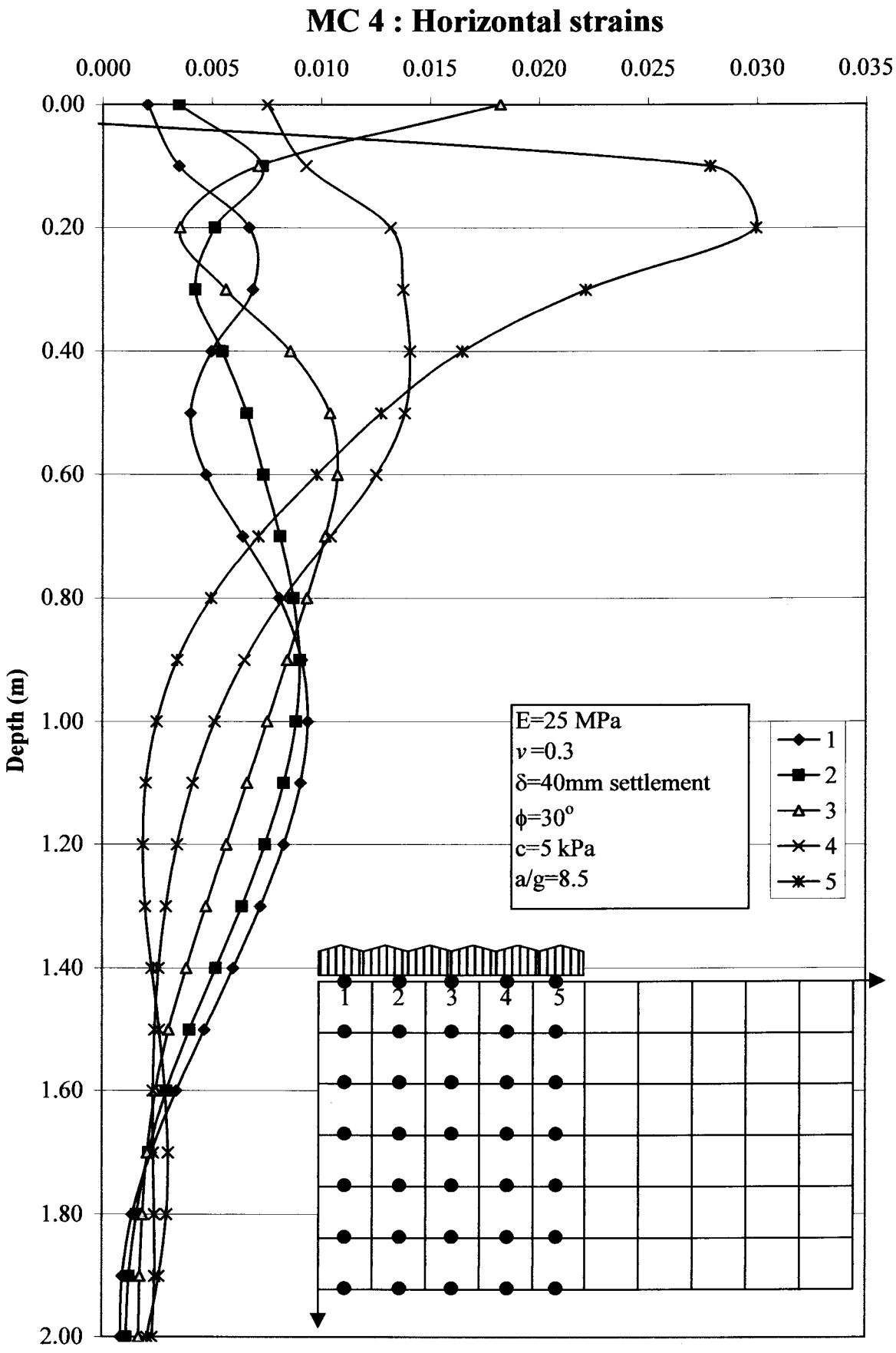
MC 4 : Horizontal strains
0.000
0.005
0.010
0.015
0.020
0.025
0.030
0.035
0.00
0.20
0.40
0.60
0.80
1.00
1.20
1.40
1.60
1.80
2.00
Depth (m)
E=25 MPa
ν=0.3
δ=40mm settlement
ϕ=30°
c=5 kPa
a/g=8.5
1
2
3
4
5
1
2
3
4
5

MC4 : Volumetric strain variation under rigid base

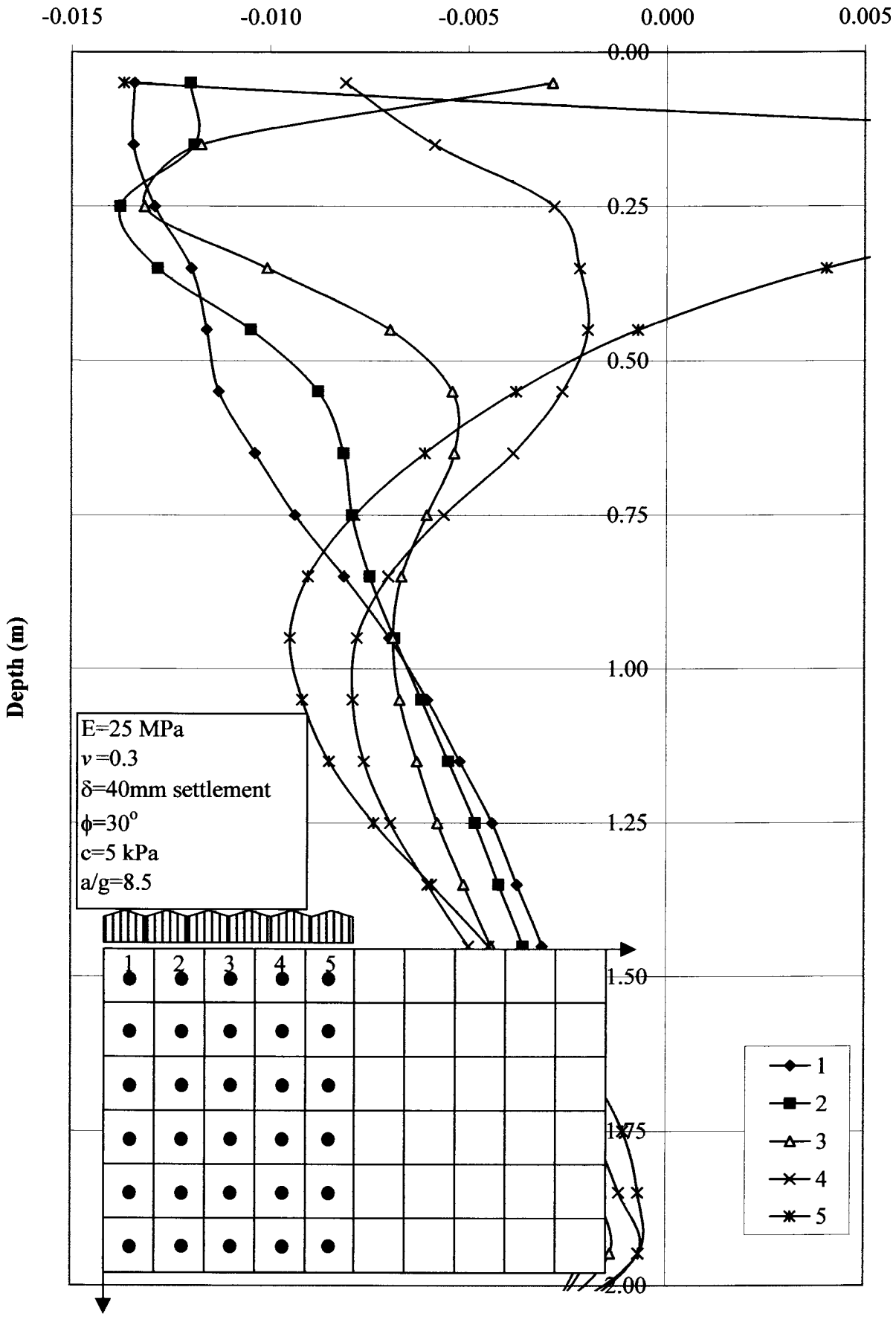

DATA FOR MC4 ANALYSIS: VERTICAL STRAIN CALCULATION

Zone	y ordinate at center of zone	z (m)	Δy/Yo 1	2	3	4	5	6
			Xo=Yo=100mm =grid zone size					
40	3.95	0.05	-0.0185	-0.0194	-0.0262	-0.0302	-0.0197	-0.0338
39	3.85	0.15	-0.0223	-0.025	-0.0237	-0.0211	-0.0356	-0.0531
38	3.75	0.25	-0.0277	-0.0253	-0.021	-0.0237	-0.0359	-0.0465
37	3.65	0.35	-0.0249	-0.0228	-0.0223	-0.0263	-0.0338	-0.0354
36	3.55	0.45	-0.02	-0.0212	-0.0239	-0.028	-0.0318	-0.0281
35	3.45	0.55	-0.0192	-0.0209	-0.0246	-0.0285	-0.0295	-0.0232
34	3.35	0.65	-0.0209	-0.0222	-0.0251	-0.0275	-0.0262	-0.0199
33	3.25	0.75	-0.0236	-0.0242	-0.0254	-0.0258	-0.0229	-0.0171
32	3.15	0.85	-0.0254	-0.0253	-0.0252	-0.0238	-0.0198	-0.0151
31	3.05	0.95	-0.0257	-0.0253	-0.0242	-0.0216	-0.0173	-0.0135
30	2.95	1.05	-0.0248	-0.0242	-0.0225	-0.0193	-0.0151	-0.0122
29	2.85	1.15	-0.0229	-0.0223	-0.0202	-0.017	-0.0134	-0.0113
28	2.75	1.25	-0.0203	-0.0196	-0.0177	-0.0147	-0.0119	-0.0105
27	2.65	1.35	-0.0173	-0.0167	-0.0149	-0.0125	-0.0105	-0.0098
26	2.55	1.45	-0.0141	-0.0135	-0.0121	-0.0105	-0.0094	-0.0093
25	2.45	1.55	-0.011	-0.0106	-0.0096	-0.0087	-0.0084	-0.0088
24	2.35	1.65	-0.0081	-0.008	-0.0076	-0.0074	-0.0076	-0.0081
23	2.25	1.75	-0.0058	-0.0059	-0.006	-0.0063	-0.0069	-0.0072
22	2.15	1.85	-0.0044	-0.0045	-0.005	-0.0056	-0.0064	-0.0061
21	2.05	1.95	-0.0038	-0.004	-0.0045	-0.0051	-0.0057	-0.005
20	1.95	2.05	-0.0037	-0.0038	-0.0042	-0.0049	-0.0051	-0.0038

DATA FOR MC4 ANALYSIS: HORIZONTAL STRAIN CALC.

z	Δx/Xo 1	2	3	4	5
0.00	0.0020	0.0035	0.0182	0.0075	-0.0148
0.10	0.0035	0.0073	0.0071	0.0093	0.0278
0.20	0.0067	0.0051	0.0035	0.0132	0.0300
0.30	0.0069	0.0042	0.0056	0.0138	0.0222
0.40	0.0050	0.0055	0.0086	0.0141	0.0165
0.50	0.0040	0.0066	0.0104	0.0138	0.0128
0.60	0.0047	0.0074	0.0108	0.0125	0.0098
0.70	0.0064	0.0081	0.0102	0.0105	0.0072
0.80	0.0081	0.0087	0.0094	0.0083	0.0050
0.90	0.0091	0.0090	0.0085	0.0065	0.0034
1.00	0.0094	0.0089	0.0076	0.0052	0.0025
1.10	0.0091	0.0083	0.0066	0.0042	0.0020
1.20	0.0083	0.0075	0.0057	0.0034	0.0019
1.30	0.0073	0.0064	0.0048	0.0029	0.0020
1.40	0.0060	0.0052	0.0039	0.0026	0.0023
1.50	0.0047	0.0040	0.0031	0.0024	0.0026
1.60	0.0034	0.0029	0.0025	0.0023	0.0029
1.70	0.0023	0.0021	0.0021	0.0024	0.0030
1.80	0.0014	0.0016	0.0019	0.0024	0.0030
1.90	0.0009	0.0012	0.0017	0.0024	0.0026
2.00	0.0009	0.0011	0.0017	0.0023	0.0021

DATA FOR MC4 ANALYSIS: VOLUMETRIC STRAIN CALC.

z	ε vol =ave(vert) +2(ave hor) 1	2	3	4	5	Total
0.05	-0.01342	-0.01201	-0.00287	-0.00810	-0.01369	-0.01002
0.15	-0.01345	-0.01191	-0.01174	-0.00585	0.01345	-0.00590
0.25	-0.01291	-0.01378	-0.01317	-0.00283	0.01091	-0.00636
0.35	-0.01199	-0.01284	-0.01008	-0.00219	0.00403	-0.00661
0.45	-0.01160	-0.01049	-0.00697	-0.00198	-0.00072	-0.00635
0.55	-0.01129	-0.00879	-0.00540	-0.00262	-0.00379	-0.00638
0.65	-0.01038	-0.00815	-0.00535	-0.00386	-0.00609	-0.00677
0.75	-0.00937	-0.00793	-0.00604	-0.00561	-0.00787	-0.00736
0.85	-0.00813	-0.00748	-0.00668	-0.00701	-0.00904	-0.00767
0.95	-0.00698	-0.00685	-0.00689	-0.00780	-0.00949	-0.00760
1.05	-0.00602	-0.00617	-0.00672	-0.00790	-0.00918	-0.00720
1.15	-0.00520	-0.00549	-0.00628	-0.00762	-0.00850	-0.00662
1.25	-0.00438	-0.00481	-0.00576	-0.00695	-0.00737	-0.00585
1.35	-0.00375	-0.00421	-0.00510	-0.00600	-0.00591	-0.00499
1.45	-0.00311	-0.00360	-0.00440	-0.00497	-0.00446	-0.00411
1.55	-0.00271	-0.00316	-0.00365	-0.00381	-0.00309	-0.00328
1.65	-0.00240	-0.00273	-0.00298	-0.00281	-0.00193	-0.00257
1.75	-0.00222	-0.00224	-0.00223	-0.00184	-0.00107	-0.00192
1.85	-0.00214	-0.00193	-0.00172	-0.00117	-0.00069	-0.00153
1.95	-0.00212	-0.00191	-0.00139	-0.00068	-0.00067	-0.00135
2.05	-0.00290	-0.00290	-0.00287	-0.00270	-0.00238	-0.00275

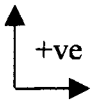

DATA FOR MC5 ANALYSIS: VERTICAL DISPLACEMENTS

z (m)	x10^{-2} [Vertical displacements of grid points]					
0.0	-4.000	-4.000	-4.000	-4.000	-4.000	-4.000
0.1	-3.851	-3.844	-3.842	-3.840	-3.835	-3.644
0.2	-3.674	-3.672	-3.668	-3.657	-3.565	-3.171
0.3	-3.496	-3.494	-3.487	-3.437	-3.230	-2.763
0.4	-3.318	-3.315	-3.289	-3.177	-2.882	-2.429
0.5	-3.143	-3.129	-3.064	-2.889	-2.550	-2.159
0.6	-2.951	-2.918	-2.810	-2.586	-2.248	-1.935
0.7	-2.719	-2.671	-2.530	-2.285	-1.982	-1.742
0.8	-2.443	-2.388	-2.235	-1.999	-1.752	-1.571
0.9	-2.135	-2.082	-1.938	-1.738	-1.553	-1.416
1.0	-1.818	-1.774	-1.655	-1.505	-1.378	-1.272
1.1	-1.513	-1.482	-1.400	-1.303	-1.222	-1.137
1.2	-1.243	-1.226	-1.180	-1.128	-1.080	-1.008
1.3	-1.021	-1.016	-0.999	-0.980	-0.952	-0.886
1.4	-0.855	-0.858	-0.858	-0.854	-0.837	-0.771
1.5	-0.741	-0.745	-0.750	-0.750	-0.733	-0.665
1.6	-0.664	-0.666	-0.668	-0.664	-0.641	-0.569
1.7	-0.607	-0.606	-0.603	-0.592	-0.561	-0.483
1.8	-0.556	-0.554	-0.546	-0.529	-0.490	-0.408
1.9	-0.507	-0.504	-0.493	-0.471	-0.426	-0.346
2.0	-0.458	-0.454	-0.442	-0.415	-0.366	-0.295
2.1	-0.410	-0.405	-0.391	-0.361	-0.311	-0.253

DATA FOR MC5 ANALYSIS: HORIZONTAL DISPLACEMENTS

z (m)	x10^{-3} [Horizon displacements of grid points]					
0.0	0.000	-0.246	-0.111	-0.248	-0.029	-0.169
0.1	0.000	0.070	0.129	0.271	0.631	3.000
0.2	0.000	0.135	0.282	0.509	1.584	4.090
0.3	0.000	0.158	0.340	0.860	2.315	4.451
0.4	0.000	0.165	0.482	1.322	2.883	4.528
0.5	0.000	0.236	0.785	1.862	3.350	4.546
0.6	0.000	0.455	1.227	2.405	3.689	4.497
0.7	0.000	0.753	1.709	2.864	3.874	4.381
0.8	0.000	1.021	2.102	3.153	3.891	4.188
0.9	0.000	1.188	2.311	3.225	3.749	3.925
1.0	0.000	1.231	2.310	3.079	3.463	3.602
1.1	0.000	1.153	2.113	2.748	3.059	3.221
1.2	0.000	0.977	1.770	2.290	2.579	2.792
1.3	0.000	0.740	1.348	1.777	2.071	2.347
1.4	0.000	0.496	0.929	1.283	1.588	1.918
1.5	0.000	0.294	0.585	0.872	1.175	1.538
1.6	0.000	0.165	0.355	0.583	0.867	1.232
1.7	0.000	0.112	0.246	0.426	0.680	1.023
1.8	0.000	0.098	0.218	0.373	0.602	0.906
1.9	0.000	0.103	0.223	0.379	0.597	0.854
2.0	0.000	0.113	0.242	0.407	0.623	0.829
2.1	0.000	0.124	0.265	0.440	0.648	0.801

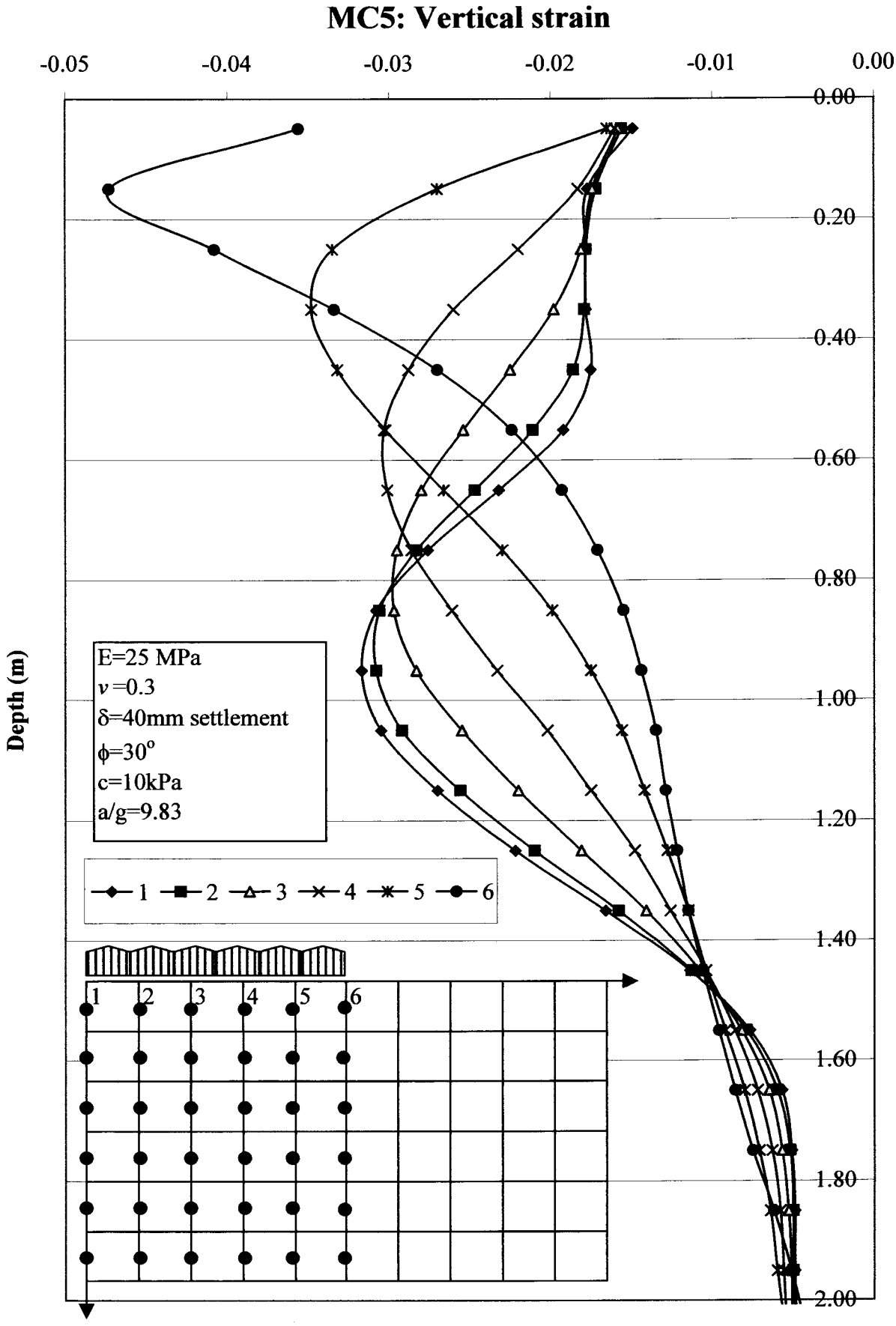
MC5: Vertical strain
-0.05
-0.04
-0.03
-0.02
-0.01
0.00
0.00
0.20
0.40
0.60
0.80
1.00
1.20
1.40
1.60
1.80
2.00
Depth (m)
E=25 MPa
ν=0.3
δ=40mm settlement
ϕ=30°
c=10kPa
a/g=9.83
1
2
3
4
5
6

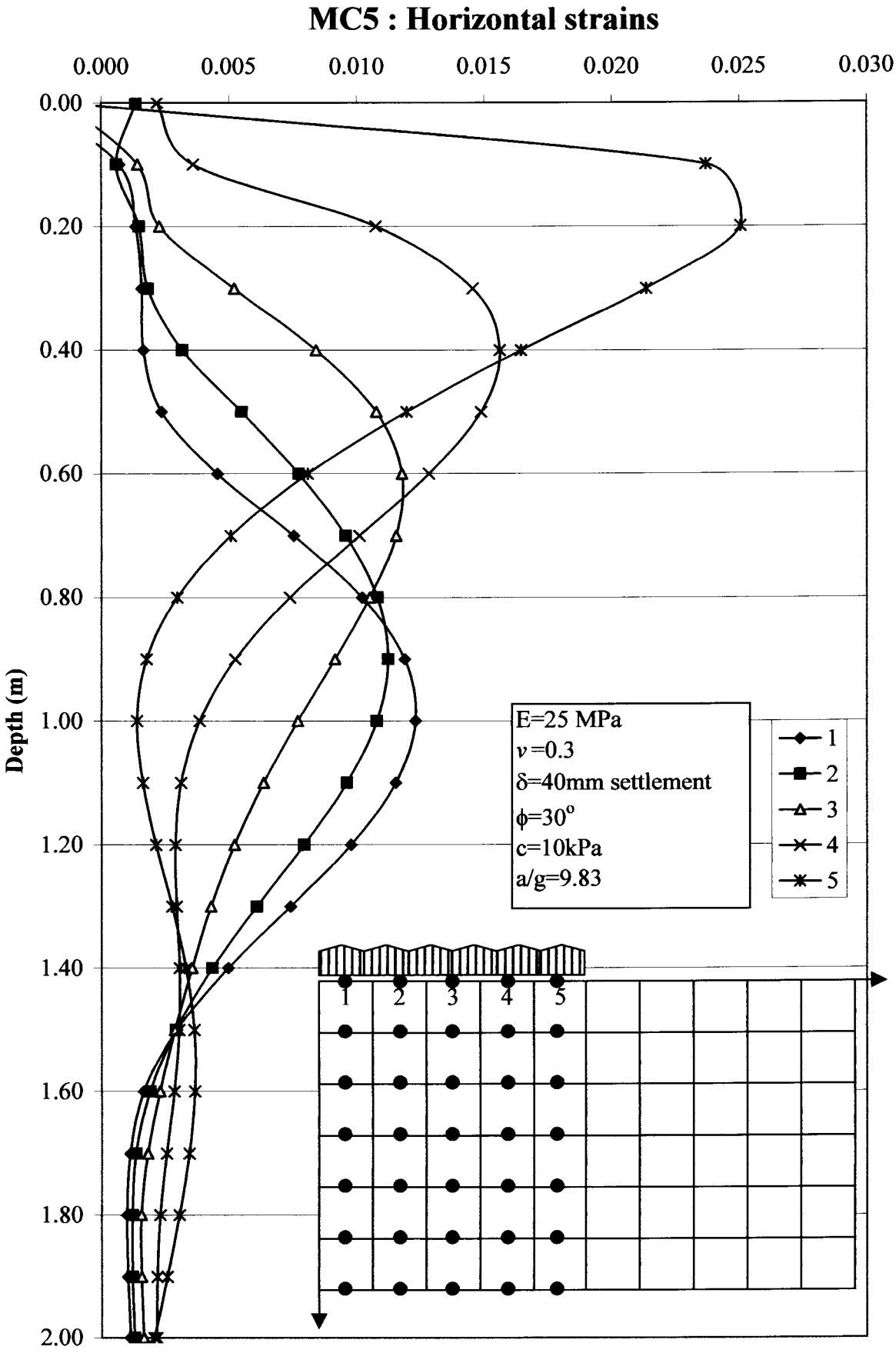
MC5 : Horizontal strains
0.000
0.005
0.010
0.015
0.020
0.025
0.030
0.00
0.20
0.40
0.60
0.80
1.00
1.20
1.40
1.60
1.80
2.00
Depth (m)
E=25 MPa
v=0.3
δ=40mm settlement
ϕ=30°
c=10kPa
a/g=9.83
1
2
3
4
5
1
2
3
4
5

MC5 : Volumetric strain variation under rigid base

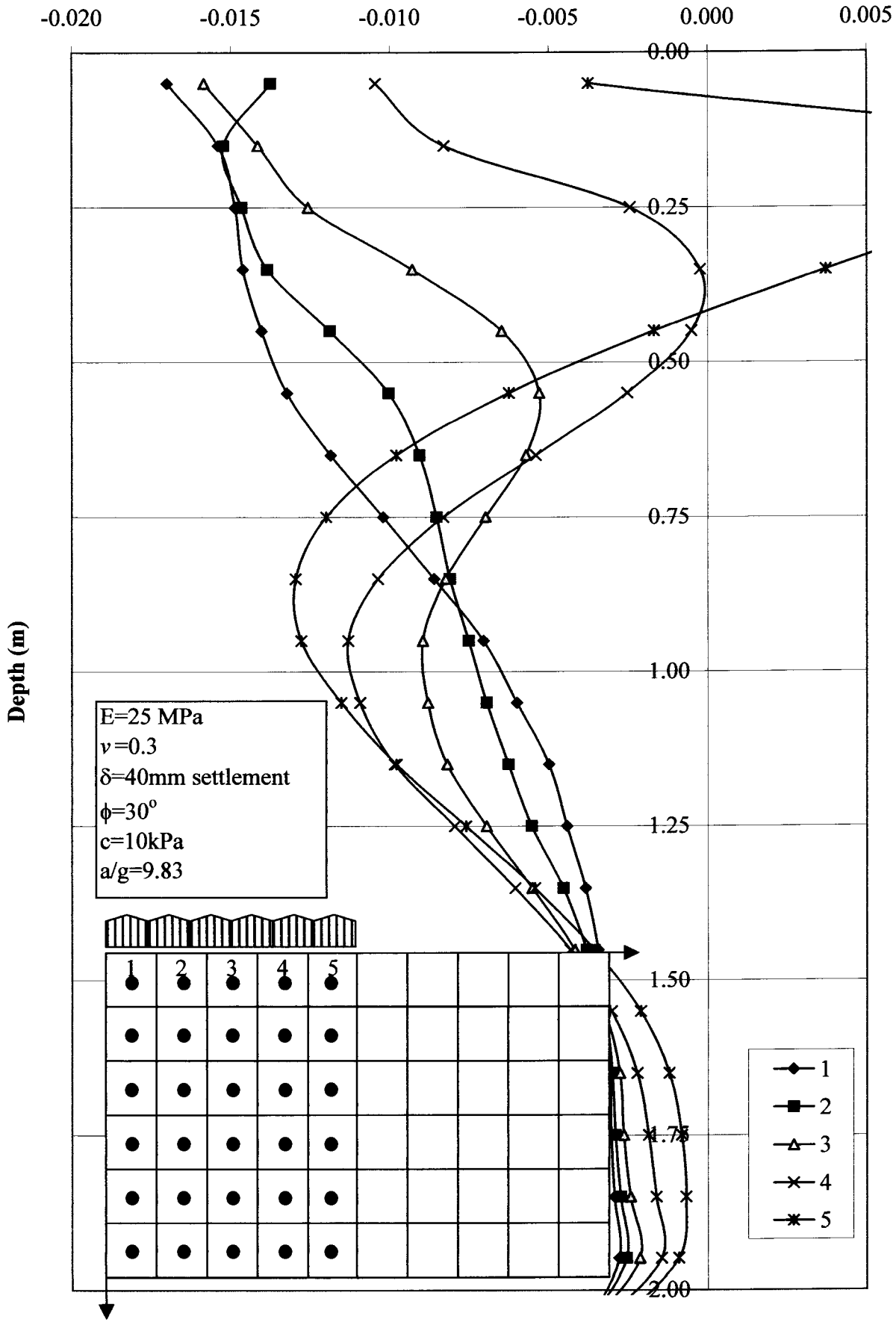

DATA FOR MC5 ANALYSIS: VERTICAL STRAIN CALCULATION

Zone	y ordinate at center of zone	z (m)	Δy/Yo 1	2	3	4	5	Xo=Yo=100mm =grid zone size 6
40	3.95	0.05	-0.0149	-0.0156	-0.0158	-0.016	-0.0165	-0.0356
39	3.85	0.15	-0.0177	-0.0172	-0.0174	-0.0183	-0.027	-0.0473
38	3.75	0.25	-0.0178	-0.0178	-0.0181	-0.022	-0.0335	-0.0408
37	3.65	0.35	-0.0178	-0.0179	-0.0198	-0.026	-0.0348	-0.0334
36	3.55	0.45	-0.0175	-0.0186	-0.0225	-0.0288	-0.0332	-0.027
35	3.45	0.55	-0.0192	-0.0211	-0.0254	-0.0303	-0.0302	-0.0224
34	3.35	0.65	-0.0232	-0.0247	-0.028	-0.0301	-0.0266	-0.0193
33	3.25	0.75	-0.0276	-0.0283	-0.0295	-0.0286	-0.023	-0.0171
32	3.15	0.85	-0.0308	-0.0306	-0.0297	-0.0261	-0.0199	-0.0155
31	3.05	0.95	-0.0317	-0.0308	-0.0283	-0.0233	-0.0175	-0.0144
30	2.95	1.05	-0.0305	-0.0292	-0.0255	-0.0202	-0.0156	-0.0135
29	2.85	1.15	-0.027	-0.0256	-0.022	-0.0175	-0.0142	-0.0129
28	2.75	1.25	-0.0222	-0.021	-0.0181	-0.0148	-0.0128	-0.0122
27	2.65	1.35	-0.0166	-0.0158	-0.0141	-0.0126	-0.0115	-0.0115
26	2.55	1.45	-0.0114	-0.0113	-0.0108	-0.0104	-0.0104	-0.0106
25	2.45	1.55	-0.0077	-0.0079	-0.0082	-0.0086	-0.0092	-0.0096
24	2.35	1.65	-0.0057	-0.006	-0.0065	-0.0072	-0.008	-0.0086
23	2.25	1.75	-0.0051	-0.0052	-0.0057	-0.0063	-0.0071	-0.0075
22	2.15	1.85	-0.0049	-0.005	-0.0053	-0.0058	-0.0064	-0.0062
21	2.05	1.95	-0.0049	-0.005	-0.0051	-0.0056	-0.006	-0.0051
20	1.95	2.05	-0.0048	-0.0049	-0.0051	-0.0054	-0.0055	-0.0042

DATA FOR MC5 ANALYSIS: HORIZONTAL STRAIN CALC.

z	Δx/Xo 1	2	3	4	5
0.00	-0.0025	0.0014	-0.0014	0.0022	-0.0014
0.10	0.0007	0.0006	0.0014	0.0036	0.0237
0.20	0.0014	0.0015	0.0023	0.0108	0.0251
0.30	0.0016	0.0018	0.0052	0.0146	0.0214
0.40	0.0017	0.0032	0.0084	0.0156	0.0165
0.50	0.0024	0.0055	0.0108	0.0149	0.0120
0.60	0.0046	0.0077	0.0118	0.0128	0.0081
0.70	0.0075	0.0096	0.0116	0.0101	0.0051
0.80	0.0102	0.0108	0.0105	0.0074	0.0030
0.90	0.0119	0.0112	0.0091	0.0052	0.0018
1.00	0.0123	0.0108	0.0077	0.0038	0.0014
1.10	0.0115	0.0096	0.0064	0.0031	0.0016
1.20	0.0098	0.0079	0.0052	0.0029	0.0021
1.30	0.0074	0.0061	0.0043	0.0029	0.0028
1.40	0.0050	0.0043	0.0035	0.0031	0.0033
1.50	0.0029	0.0029	0.0029	0.0030	0.0036
1.60	0.0017	0.0019	0.0023	0.0028	0.0037
1.70	0.0011	0.0013	0.0018	0.0025	0.0034
1.80	0.0010	0.0012	0.0016	0.0023	0.0030
1.90	0.0010	0.0012	0.0016	0.0022	0.0026
2.00	0.0011	0.0013	0.0017	0.0022	0.0021

DATA FOR MC5 ANALYSIS: VOLUMETRIC STRAIN CALC.

z	ε vol =ave(vert) +2(ave hor) 1	2	3	4	5	Total
0.05	-0.01701	-0.01376	-0.01585	-0.01046	-0.00376	-0.01217
0.15	-0.01540	-0.01524	-0.01416	-0.00830	0.01160	-0.00830
0.25	-0.01487	-0.01466	-0.01258	-0.00245	0.00927	-0.00706
0.35	-0.01462	-0.01386	-0.00930	-0.00024	0.00371	-0.00686
0.45	-0.01404	-0.01189	-0.00648	-0.00051	-0.00169	-0.00692
0.55	-0.01324	-0.01004	-0.00530	-0.00253	-0.00626	-0.00747
0.65	-0.01187	-0.00907	-0.00572	-0.00541	-0.00980	-0.00837
0.75	-0.01021	-0.00853	-0.00699	-0.00832	-0.01201	-0.00921
0.85	-0.00861	-0.00811	-0.00825	-0.01038	-0.01297	-0.00966
0.95	-0.00706	-0.00753	-0.00897	-0.01132	-0.01280	-0.00954
1.05	-0.00601	-0.00696	-0.00881	-0.01095	-0.01154	-0.00885
1.15	-0.00500	-0.00627	-0.00820	-0.00985	-0.00980	-0.00782
1.25	-0.00443	-0.00554	-0.00696	-0.00797	-0.00761	-0.00650
1.35	-0.00384	-0.00454	-0.00552	-0.00606	-0.00544	-0.00508
1.45	-0.00345	-0.00381	-0.00419	-0.00432	-0.00357	-0.00387
1.55	-0.00321	-0.00324	-0.00325	-0.00303	-0.00212	-0.00297
1.65	-0.00308	-0.00301	-0.00277	-0.00222	-0.00122	-0.00246
1.75	-0.00305	-0.00291	-0.00265	-0.00187	-0.00083	-0.00226
1.85	-0.00294	-0.00275	-0.00244	-0.00163	-0.00069	-0.00209
1.95	-0.00279	-0.00256	-0.00214	-0.00146	-0.00092	-0.00197
2.05	-0.00372	-0.00371	-0.00360	-0.00329	-0.00279	

APPENDIX H

VOLUMETRIC STRAIN INFLUENCE MODEL CALCULATIONS

APPENDIX H1 : Calculation of strain influence diagram for impact compaction:

Compactor contact dimension, B=	0.9	m
Assuming depth of influence, D =	2.7	m, =3B say
Asuming peak strain at of	0.75	B
which is equal to…	675	mm
Upper peak is how many times larger	1.025	x lower peak

Depth (mm)	ε ord.	Surface peak	Nett curve	Normalised ε ord.
0	0.00000	0.00091	0.00091	0.113663
150	0.00032	0.00045	0.00078	0.096982
300	0.00060	0.00000	0.00060	0.074567
450	0.00079		0.00079	0.098860
600	0.00089		0.00089	0.110891
750	0.00089		0.00089	0.110993
900	0.00081		0.00081	0.101513
1050	0.00069		0.00069	0.085914
1200	0.00054		0.00054	0.067796
1350	0.00040		0.00040	0.050126
1500	0.00028		0.00028	0.034840
1650	0.00018		0.00018	0.022818
1800	0.00011		0.00011	0.014107
1950	0.00007		0.00007	0.008244
2100	0.00004		0.00004	0.004558
2250	0.00002		0.00002	0.002386
2400	0.00001		0.00001	0.001184
2550	0.00000		0.00000	0.000557
	0.00664		0.00800	1.00

$$f(z) = \frac{z}{\sigma^2}.e^{-\frac{z^2}{2.\sigma^2}}$$

APPENDIX H2 : Normalised strain influence diagram

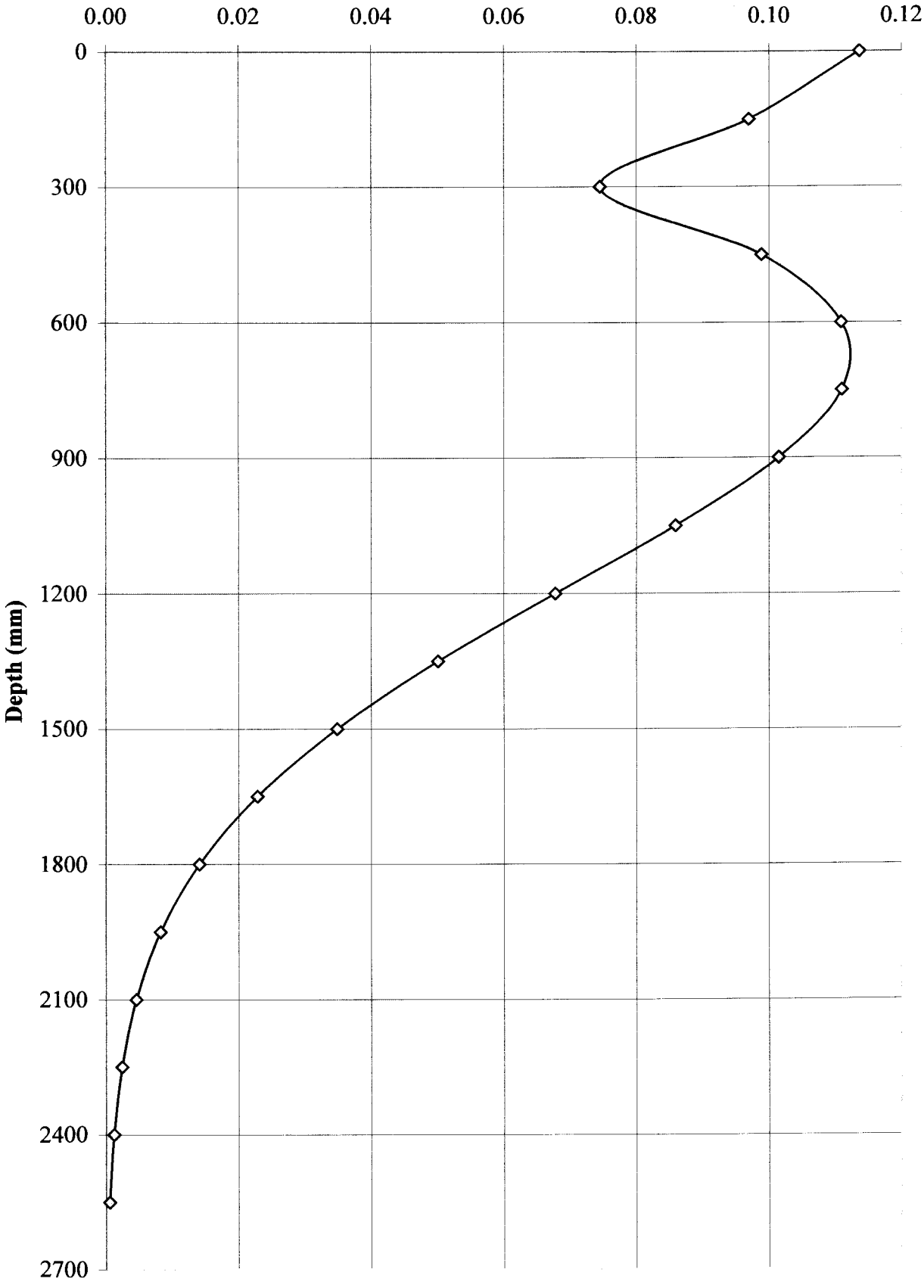

APPENDIX H3: Strain influence calculation : TP3 - Kriel 1991 [25 passes]

[Figure 6.1]

$$\Delta V = V_o.\varepsilon_{vol} = V_o.(1-2v_{pl})\varepsilon_v = (1+e_o)(1-2v_{pl})\varepsilon_v$$

$$\rho = \frac{G_s}{(V_o - \Delta V)}$$

δ (settlement)=	356	mm	v_{pl} =	0.075	Gs =	2650	(kg/m^3)

Depth (mm)	ρ_o	e_o	ΔH	ε_v=ΔH/H	Depth (mm)	ΔV=Δe	ρ_f(kg/m^3)
0	1531	0.731	40.5	0.26976	0	0.397	1986
150	1531	0.731	34.5	0.23017	150	0.339	1903
300	1531	0.731	26.5	0.17697	300	0.260	1802
450	1366	0.940	35.2	0.23463	450	0.387	1706
600	1366	0.940	39.5	0.26318	600	0.434	1760
750	1418	0.869	39.5	0.26342	750	0.418	1827
900	1418	0.869	36.1	0.24092	900	0.383	1783
1050	1418	0.869	30.6	0.20390	1050	0.324	1715
1200	1403	0.889	24.1	0.16090	1200	0.258	1625
1350	1403	0.889	17.8	0.11897	1350	0.191	1561
1500	1403	0.889	12.4	0.08269	1500	0.133	1509
1650	1403	0.889	8.1	0.05416	1650	0.087	1471
1800	1403	0.889	5.0	0.03348	1800	0.054	1444
1950	1403	0.889	2.9	0.01956	1950	0.031	1427
2100	1403	0.889	1.6	0.01082	2100	0.017	1416
2250	1403	0.889	0.8	0.00566	2250	0.009	1410
2400	1403	0.889	0.4	0.00281	2400	0.005	1406
2550	1403	0.889	0.2	0.00132	2550	0.002	1405
			Sum 356	mm			

TP3 measured	Before	After
d (mm)	ρ_o (kg/m^3)	ρ_f(kg/m^3)
300	1531	1972
600	1366	1918
900	1418	1752
1200	1403	1632

TP3 measured	Before	After	
d (mm)	e_o	e_f	Δe
300	0.731	0.344	0.387
600	0.940	0.382	0.558
900	0.869	0.513	0.356
1200	0.889	0.624	0.265

Measured densities from reference: Landpac (1991).

APPENDIX H4: Strain influence calculation : TP3 - Kriel 1991 [25 passes]

(one dimensional case-no allowance for lateral strains) [Figure 6.1]

$$\Delta V = V_o.\varepsilon_{vol} = V_o.(1-2\nu_{pl})\varepsilon_v = (1+e_o)(1-2\nu_{pl})\varepsilon_v$$

$$\rho = \frac{G_s}{(V_o - \Delta V)}$$

δ (settlement)=	356	mm	ν_{pl}=	0.0	Gs =	2650	(kg/m^3)

Depth (mm)	ρ_o	e_o	ΔH	ε_v=ΔH/H	Depth (mm)	ΔV=Δe	ρ_f(kg/m^3)
0	1531	0.731	40.5	0.26976	0	0.467	2097
150	1531	0.731	34.5	0.23017	150	0.398	1989
300	1531	0.731	26.5	0.17697	300	0.306	1860
450	1366	0.940	35.2	0.23463	450	0.455	1785
600	1366	0.940	39.5	0.26318	600	0.511	1854
750	1418	0.869	39.5	0.26342	750	0.492	1925
900	1418	0.869	36.1	0.24092	900	0.450	1868
1050	1418	0.869	30.6	0.20390	1050	0.381	1781
1200	1403	0.889	24.1	0.16090	1200	0.304	1672
1350	1403	0.889	17.8	0.11897	1350	0.225	1592
1500	1403	0.889	12.4	0.08269	1500	0.156	1529
1650	1403	0.889	8.1	0.05416	1650	0.102	1483
1800	1403	0.889	5.0	0.03348	1800	0.063	1452
1950	1403	0.889	2.9	0.01956	1950	0.037	1431
2100	1403	0.889	1.6	0.01082	2100	0.020	1418
2250	1403	0.889	0.8	0.00566	2250	0.011	1411
2400	1403	0.889	0.4	0.00281	2400	0.005	1407
2550	1403	0.889	0.2	0.00132	2550	0.002	1405
		Sum	356	mm			

TP3 measured	Before	After
d (mm)	ρ_o (kg/m^3)	ρ_f (kg/m^3)
300	1531	1972
600	1366	1918
900	1418	1752
1200	1403	1632

TP3 measured	Before	After	
d (mm)	e_o	e_f	Δe
300	0.731	0.344	0.387
600	0.940	0.382	0.558
900	0.869	0.513	0.356
1200	0.889	0.624	0.265

Measured densities from reference: Landpac (1991).

H5 : Measured - predicted density TP3

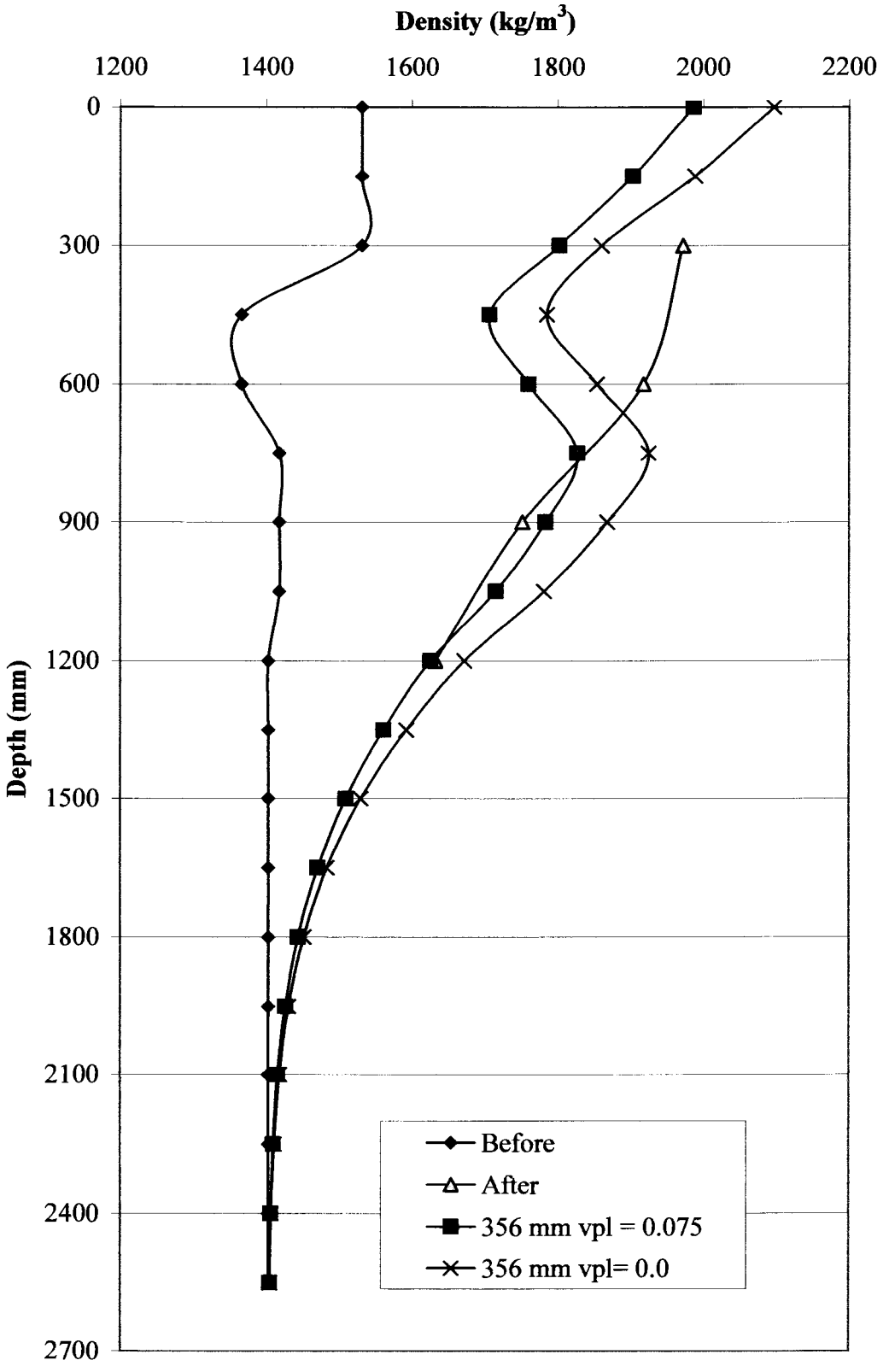

APPENDIX H6: Strain influence calculation : TP13 - Kriel 1991 [45 passes]

[Figure 6.3]

$$\Delta V = V_o.\varepsilon_{vol} = V_o.(1-2\nu_{pl})\varepsilon_v = (1+e_o)(1-2\nu_{pl})\varepsilon_v$$

$$\rho = \frac{G_s}{(V_o - \Delta V)}$$

δ (settlement)=	488	mm	ν_{pl} =	0.175	Gs =	2650	(kg/m^3)

Depth (mm)	ρ_o	e_o	ΔH	ε_v=ΔH/H	Depth (mm)	ΔV=Δe	ρ_f(kg/m^3)
0	1722	0.539	55.5	0.36978	0	0.370	2267
150	1722	0.539	47.3	0.31551	150	0.316	2166
300	1722	0.539	36.4	0.24259	300	0.243	2044
450	1404	0.887	48.2	0.32162	450	0.395	1775
600	1404	0.887	54.1	0.36077	600	0.443	1834
750	1380	0.920	54.2	0.36110	750	0.451	1803
900	1380	0.920	49.5	0.33026	900	0.412	1757
1050	1380	0.920	41.9	0.27951	1050	0.349	1686
1200	1386	0.912	33.1	0.22056	1200	0.274	1618
1350	1386	0.912	24.5	0.16308	1350	0.203	1550
1500	1386	0.912	17.0	0.11335	1500	0.141	1496
1650	1386	0.912	11.1	0.07424	1650	0.092	1456
1800	1386	0.912	6.9	0.04589	1800	0.057	1429
1950	1386	0.912	4.0	0.02682	1950	0.033	1411
2100	1386	0.912	2.2	0.01483	2100	0.018	1399
2250	1386	0.912	1.2	0.00776	2250	0.010	1393
2400	1386	0.912	0.6	0.00385	2400	0.005	1389
2550	1386	0.912	0.3	0.00181	2550	0.002	1388
			Sum 488 mm				

TP13 measured	Before	After
d (mm)	ρ_o (kg/m^3)	ρ_f(kg/m^3)
300	1722	1976
600	1404	1811
900	1380	1761
1200	1386	1580

TP13 measured	Before	After	
d (mm)	e_o	e_f	Δe
300	0.539	0.341	0.198
600	0.887	0.463	0.424
900	0.920	0.505	0.415
1200	0.912	0.677	0.235

Measured densities from reference: Landpac (1991).

APPENDIX H7: Strain influence calculation : TP13 - Kriel 1991 [45 passes]

(one dimensional case-no allowance for lateral strains) [Figure 6.3]

$$\Delta V = V_o.\varepsilon_{vol} = V_o.(1-2\nu_{pl})\varepsilon_v = (1+e_o)(1-2\nu_{pl})\varepsilon_v$$

$$\rho = \frac{G_s}{(V_o - \Delta V)}$$

δ (settlement)=	488	mm	ν_{pl} =	0.0	Gs =	2650	(kg/m^3)

Depth (mm)	ρ_o	e_o	ΔH	ε_v=ΔH/H	Depth (mm)	ΔV=Δe	ρ_f(kg/m^3)
0	1531	0.731	55.5	0.36978	0	0.640	2429
150	1531	0.731	47.3	0.31551	150	0.546	2237
300	1531	0.731	36.4	0.24259	300	0.420	2021
450	1366	0.940	48.2	0.32162	450	0.624	2014
600	1366	0.940	54.1	0.36077	600	0.700	2137
750	1418	0.869	54.2	0.36110	750	0.675	2219
900	1418	0.869	49.5	0.33026	900	0.617	2117
1050	1418	0.869	41.9	0.27951	1050	0.522	1968
1200	1403	0.889	33.1	0.22056	1200	0.417	1800
1350	1403	0.889	24.5	0.16308	1350	0.308	1676
1500	1403	0.889	17.0	0.11335	1500	0.214	1582
1650	1403	0.889	11.1	0.07424	1650	0.140	1516
1800	1403	0.889	6.9	0.04589	1800	0.087	1470
1950	1403	0.889	4.0	0.02682	1950	0.051	1442
2100	1403	0.889	2.2	0.01483	2100	0.028	1424
2250	1403	0.889	1.2	0.00776	2250	0.015	1414
2400	1403	0.889	0.6	0.00385	2400	0.007	1408
2550	1403	0.889	0.3	0.00181	2550	0.003	1406
		Sum	488	mm			

TP13 measured	Before	After
d (mm)	ρ_o (kg/m^3)	ρ_f(kg/m^3)
300	1722	1976
600	1404	1811
900	1380	1761
1200	1386	1580

TP13 measured	Before	After	
d (mm)	e_o	e_f	Δe
300	0.539	0.341	0.198
600	0.887	0.463	0.424
900	0.920	0.505	0.415
1200	0.912	0.677	0.235

Measured densities from reference: Landpac (1991).

APPENDIX H8: Strain influence calculation : TP11 - Kriel 1991 [55 passes]

[Figure 6.3]

$$\Delta V = V_o.\varepsilon_{vol} = V_o.(1-2\nu_{pl})\varepsilon_v = (1+e_o)(1-2\nu_{pl})\varepsilon_v$$

$$\rho = \frac{G_s}{(V_o - \Delta V)}$$

δ (settlement)=	552	mm	ν_{pl} =	0.175	Gs =	2650	(kg/m^3)

Depth (mm)	ρ_o	e_o	ΔH	ε_v=ΔH/H	Depth (mm)	ΔV=Δe	ρ_f(kg/m^3)
0	1511	0.754	62.7	0.41828	0	0.477	2075
150	1511	0.754	53.5	0.35689	150	0.407	1967
300	1511	0.754	41.2	0.27441	300	0.313	1839
450	1389	0.908	54.6	0.36381	450	0.451	1819
600	1389	0.908	61.2	0.40808	600	0.506	1890
750	1439	0.842	61.3	0.40846	750	0.489	1959
900	1439	0.842	56.0	0.37357	900	0.447	1900
1050	1439	0.842	47.4	0.31616	1050	0.378	1811
1200	1461	0.814	37.4	0.24949	1200	0.294	1744
1350	1461	0.814	27.7	0.18446	1350	0.217	1660
1500	1461	0.814	19.2	0.12821	1500	0.151	1594
1650	1461	0.814	12.6	0.08397	1650	0.099	1545
1800	1461	0.814	7.8	0.05191	1800	0.061	1512
1950	1461	0.814	4.6	0.03034	1950	0.036	1490
2100	1461	0.814	2.5	0.01677	2100	0.020	1477
2250	1461	0.814	1.3	0.00878	2250	0.010	1469
2400	1461	0.814	0.7	0.00436	2400	0.005	1465
2550	1461	0.814	0.3	0.00205	2550	0.002	1463
			Sum 552	mm			

TP11 measured	Before	After
d (mm)	ρ_o (kg/m^3)	ρ_f(kg/m^3)
300	1511	1929
600	1389	1935
900	1439	1853
1200	1461	1716

TP11 measured	Before	After	
d (mm)	e_o	e_f	Δe
300	0.754	0.374	0.380
600	0.908	0.370	0.538
900	0.842	0.430	0.411
1200	0.814	0.544	0.270

Measured densities from reference: Landpac (1991).

APPENDIX H9: Strain influence calculation : TP11 - Kriel 1991 [55 passes]

(one dimensional case-no allowance for lateral strains) [Figure 6.3]

$$\Delta V = V_o.\varepsilon_{vol} = V_o.(1-2v_{pl})\varepsilon_v = (1+e_o)(1-2v_{pl})\varepsilon_v$$

$$\rho = \frac{G_s}{(V_o - \Delta V)}$$

δ (settlement)=	552	mm	v_{pl} =	0.0	Gs =	2650	(kg/m^3)

Depth (mm)	ρ_o	e_o	ΔH	ε_v=ΔH/H	Depth (mm)	ΔV=Δe	ρ_f(kg/m^3)
0	1511	0.754	62.7	0.41828	0	0.734	2597
150	1511	0.754	53.5	0.35689	150	0.626	2350
300	1511	0.754	41.2	0.27441	300	0.481	2082
450	1389	0.908	54.6	0.36381	450	0.694	2183
600	1389	0.908	61.2	0.40808	600	0.779	2347
750	1439	0.842	61.3	0.40846	750	0.752	2433
900	1439	0.842	56.0	0.37357	900	0.688	2297
1050	1439	0.842	47.4	0.31616	1050	0.582	2104
1200	1461	0.814	37.4	0.24949	1200	0.453	1947
1350	1461	0.814	27.7	0.18446	1350	0.335	1791
1500	1461	0.814	19.2	0.12821	1500	0.233	1676
1650	1461	0.814	12.6	0.08397	1650	0.152	1595
1800	1461	0.814	7.8	0.05191	1800	0.094	1541
1950	1461	0.814	4.6	0.03034	1950	0.055	1507
2100	1461	0.814	2.5	0.01677	2100	0.030	1486
2250	1461	0.814	1.3	0.00878	2250	0.016	1474
2400	1461	0.814	0.7	0.00436	2400	0.008	1467
2550	1461	0.814	0.3	0.00205	2550	0.004	1464
			Sum 552 mm				

TP11 measured	Before	After
d (mm)	ρ_o (kg/m^3)	ρ_f(kg/m^3)
300	1511	1929
600	1389	1935
900	1439	1853
1200	1461	1716

TP11 measured	Before	After	
d (mm)	e_o	e_f	Δe
300	0.754	0.374	0.380
600	0.908	0.370	0.538
900	0.842	0.430	0.411
1200	0.814	0.544	0.270

Measured densities from reference: Landpac (1991).

APPENDIX H10: Strain influence calculation : TP12 - Kriel 1991 [55 passes]

[Figure 6.4]

$$\Delta V = V_o.\varepsilon_{vol} = V_o.(1-2\nu_{pl})\varepsilon_v = (1+e_o)(1-2\nu_{pl})\varepsilon_v$$

$$\rho = \frac{G_s}{(V_o - \Delta V)}$$

δ (settlement)=	552	mm	ν_{pl} =	0.15	Gs =	2650	(kg/m^3)

Depth (mm)	ρ_o	e_o	ΔH	ε_v=ΔH/H	Depth (mm)	ΔV=Δe	ρ_f(kg/m^3)
0	1806	0.467	62.7	0.41828	0	0.430	2554
150	1806	0.467	53.5	0.35689	150	0.367	2407
300	1806	0.467	41.2	0.27441	300	0.282	2235
450	1392	0.904	54.6	0.36381	450	0.485	1868
600	1392	0.904	61.2	0.40808	600	0.544	1949
750	1479	0.792	61.3	0.40846	750	0.512	2071
900	1479	0.792	56.0	0.37357	900	0.469	2003
1050	1479	0.792	47.4	0.31616	1050	0.397	1899
1200	1405	0.886	37.4	0.24949	1200	0.329	1702
1350	1405	0.886	27.7	0.18446	1350	0.244	1613
1500	1405	0.886	19.2	0.12821	1500	0.169	1544
1650	1405	0.886	12.6	0.08397	1650	0.111	1493
1800	1405	0.886	7.8	0.05191	1800	0.069	1458
1950	1405	0.886	4.6	0.03034	1950	0.040	1435
2100	1405	0.886	2.5	0.01677	2100	0.022	1422
2250	1405	0.886	1.3	0.00878	2250	0.012	1414
2400	1405	0.886	0.7	0.00436	2400	0.006	1409
2550	1405	0.886	0.3	0.00205	2550	0.003	1407
			Sum 552	mm			

TP12 measured	Before	After
d (mm)	ρ_o (kg/m^3)	ρ_f(kg/m^3)
300	1806	1839
600	1392	1945
900	1479	1868
1200	1405	1682

TP12 measured	Before	After	
d (mm)	e_o	e_f	Δe
300	0.467	0.441	0.026
600	0.904	0.362	0.541
900	0.792	0.419	0.373
1200	0.886	0.576	0.311

Measured densities from reference: Landpac (1991).

APPENDIX H11: Strain influence calculation : TP12 - Kriel 1991 [55 passes]

(one dimensional case-no allowance for lateral strains) [Figure 6.4]

$$\Delta V = V_o.\varepsilon_{vol} = V_o.(1-2\nu_{pl})\varepsilon_v = (1+e_o)(1-2\nu_{pl})\varepsilon_v$$

$$\rho = \frac{G_s}{(V_o - \Delta V)}$$

δ (settlement)=	552	mm	ν_{pl} =	0.0	Gs =	2650	(kg/m^3)

Depth (mm)	ρ_o	e_o	ΔH	ε_v=ΔH/H	Depth (mm)	ΔV=Δe	ρ_f(kg/m^3)
0	1806	0.467	62.7	0.41828	0	0.467	2650
150	1806	0.467	53.5	0.35689	150	0.467	2650
300	1806	0.467	41.2	0.27441	300	0.403	2489
450	1392	0.904	54.6	0.36381	450	0.693	2188
600	1392	0.904	61.2	0.40808	600	0.777	2352
750	1479	0.792	61.3	0.40846	750	0.732	2500
900	1479	0.792	56.0	0.37357	900	0.669	2361
1050	1479	0.792	47.4	0.31616	1050	0.566	2163
1200	1405	0.886	37.4	0.24949	1200	0.471	1872
1350	1405	0.886	27.7	0.18446	1350	0.348	1723
1500	1405	0.886	19.2	0.12821	1500	0.242	1612
1650	1405	0.886	12.6	0.08397	1650	0.158	1534
1800	1405	0.886	7.8	0.05191	1800	0.098	1482
1950	1405	0.886	4.6	0.03034	1950	0.057	1449
2100	1405	0.886	2.5	0.01677	2100	0.032	1429
2250	1405	0.886	1.3	0.00878	2250	0.017	1417
2400	1405	0.886	0.7	0.00436	2400	0.008	1411
2550	1405	0.886	0.3	0.00205	2550	0.004	1408
		Sum	552	mm			

TP12 measured	Before	After
d (mm)	ρ_o (kg/m^3)	ρ_f(kg/m^3)
300	1806	1839
600	1392	1945
900	1479	1868
1200	1405	1682

TP12 measured	Before	After	
d (mm)	e_o	e_f	Δe
300	0.467	0.441	0.026
600	0.904	0.362	0.541
900	0.792	0.419	0.373
1200	0.886	0.576	0.311

Measured densities from reference: Landpac (1991).

APPENDIX H12: Strain influence calculation : TP4 - Kriel 1997 [60 passes]

[Figure 6.5]

$$\Delta V = V_o.\varepsilon_{vol} = V_o.(1-2v_{pl})\varepsilon_v = (1+e_o)(1-2v_{pl})\varepsilon_v$$

$$\rho = \frac{G_s}{(V_o - \Delta V)}$$

δ (settlement)=	560	mm	v_{pl} =	0.25	Gs =	2650	(kg/m^3)

Depth (mm)	ρ_o	e_o	ΔH	ε_v=ΔH/H	Depth (mm)	ΔV=Δe	ρ_f(kg/m^3)
75	1800	0.472	75.4	0.50240	75	0.370	2404
225	1800	0.472	64.5	0.42969	225	0.316	2293
375	1800	0.472	49.0	0.32672	375	0.241	2151
525	1573	0.685	59.2	0.39442	525	0.332	1959
675	1573	0.685	62.4	0.41622	675	0.351	1986
825	1552	0.707	59.6	0.39741	825	0.339	1937
975	1552	0.707	52.4	0.34923	975	0.298	1880
1125	1552	0.707	42.8	0.28519	1125	0.243	1810
1275	1632	0.624	32.7	0.21773	1275	0.177	1831
1425	1632	0.624	23.4	0.15603	1425	0.127	1770
1575	1632	0.624	15.8	0.10524	1575	0.085	1723
1725	1632	0.624	10.0	0.06696	1725	0.054	1689
1875	1632	0.624	6.0	0.04024	1875	0.033	1666
2025	1632	0.624	3.4	0.02287	2025	0.019	1651
2175	1632	0.624	1.8	0.01230	2175	0.010	1642
2325	1632	0.624	0.9	0.00627	2325	0.005	1637
2475	1632	0.624	0.5	0.00303	2475	0.002	1634
2625	1632	0.624	0.2	0.00139	2625	0.001	1633
			Sum 560 mm				

TP3 measured	Before	
d (mm)	ρ_f(kg/m^3)	e_o
855	1526	0.737
1455	1487	0.782
2105	1411	0.878
2805	1381	0.919

TP3 measured	After		
d (mm)	ρ_o (kg/m^3)	e_f	Δe
725	1800	0.472	0.264
1375	1573	0.685	0.097
2175	1552	0.707	0.171
2875	1632	0.624	0.295

Measured densities from reference: AFRICON (1998).

APPENDIX H13: Strain influence calculation : TP A - Kriel 1997 [60 passes]

(one dimensional case-no allowance for lateral strains) [Figure 6.5]

$$\Delta V = V_o \varepsilon_{vol} = V_o.(1-2\nu_{pl})\varepsilon_v = (1+e_o)(1-2\nu_{pl})\varepsilon_v$$

$$\rho = \frac{G_s}{(V_o - \Delta V)}$$

δ (settlement)=	560	mm	ν_{pl} =	0.15	Gs =	2650	(kg/m^3)

Depth (mm)	ρ_o	e_o	ΔH	ε_v=ΔH/H	Depth (mm	ΔV=Δe	ρ_f(kg/m^3)
75	1526	0.737	75.4	0.50240	75	0.611	2354
225	1526	0.737	64.5	0.42969	225	0.522	2182
375	1526	0.737	49.0	0.32672	375	0.397	1978
525	1487	0.782	59.2	0.39442	525	0.492	2054
675	1487	0.782	62.4	0.41622	675	0.519	2098
825	1411	0.878	59.6	0.39741	825	0.522	1955
975	1411	0.878	52.4	0.34923	975	0.459	1868
1125	1411	0.878	42.8	0.28519	1125	0.375	1763
1275	1381	0.919	32.7	0.21773	1275	0.292	1629
1425	1381	0.919	23.4	0.15603	1425	0.210	1550
1575	1381	0.919	15.8	0.10524	1575	0.141	1491
1725	1381	0.919	10.0	0.06696	1725	0.090	1449
1875	1381	0.919	6.0	0.04024	1875	0.054	1421
2025	1381	0.919	3.4	0.02287	2025	0.031	1403
2175	1381	0.919	1.8	0.01230	2175	0.017	1393
2325	1381	0.919	0.9	0.00627	2325	0.008	1387
2475	1381	0.919	0.5	0.00303	2475	0.004	1384
2625	1381	0.919	0.2	0.00139	2625	0.002	1382
			Sum 560	mm			

TP3 measured	Before	
d (mm)	ρ_f(kg/m^3)	e_o
855	1526	0.737
1455	1487	0.782
2105	1411	0.878
2805	1381	0.919

TP3 measured	After		
d (mm)	ρ_o (kg/m^3)	e_f	Δe
725	1800	0.472	0.264
1375	1573	0.685	0.097
2175	1552	0.707	0.171
2875	1632	0.624	0.295

Measured densities from reference: AFRICON (1998).

APPENDIX H14: Strain influence calculation : Highveld Steel, 1969

[Figure 6.6]

$$\Delta V = V_o.\varepsilon_{vol} = V_o.(1-2\nu_{pl})\varepsilon_v = (1+e_o)(1-2\nu_{pl})\varepsilon_v$$

$$\rho = \frac{G_s}{(V_o - \Delta V)}$$

δ (settlement)=	145	mm	ν_{pl} =	0.075	Gs =	2650	(kg/m^3)

Depth (mm)	ρ_o	e_o	ΔH	ε_v=ΔH/H	Depth (mm)	ΔV=Δe	ρ_f(kg/m^3)
75	1665	0.591	19.5	0.13009	75	0.176	1872
225	1665	0.591	16.7	0.11126	225	0.150	1839
375	1665	0.591	12.7	0.08460	375	0.114	1794
525	1505	0.761	15.3	0.10213	525	0.153	1648
675	1505	0.761	16.2	0.10777	675	0.161	1657
825	1409	0.881	15.4	0.10290	825	0.164	1544
975	1409	0.881	13.6	0.09042	975	0.145	1526
1125	1409	0.881	11.1	0.07384	1125	0.118	1504
1275	1469	0.804	8.5	0.05638	1275	0.086	1543
1425	1469	0.804	6.1	0.04040	1425	0.062	1521
1575	1529	0.733	4.1	0.02725	1575	0.040	1565
1725	1529	0.733	2.6	0.01734	1725	0.026	1552
1875	1529	0.733	1.6	0.01042	1875	0.015	1543
2025	1529	0.733	0.9	0.00592	2025	0.009	1537
2175	1529	0.733	0.5	0.00319	2175	0.005	1533
2325	1529	0.733	0.2	0.00162	2325	0.002	1531
2475	1529	0.733	0.1	0.00078	2475	0.001	1530
2625	1529	0.733	0.1	0.00036	2625	0.001	1530
			Sum	145 mm			

20 passes [23.9	Before	
d (mm)	ρ_f(kg/m^3)	e_o
305	1665.3	0.591
610	1505.2	0.761
914	1409.1	0.881
1219	1469.2	0.804
1524	1529.2	0.733
1829	1529.2	0.733

20 passes [23.9	After		
d (mm)	ρ_o (kg/m^3)	e_f	Δe
305	1857.5	0.427	0.165
610	1657.3	0.599	0.162
914	1641.3	0.615	0.266
1219	1557.3	0.702	0.102
1524	1553.3	0.706	0.027

Measured densities from reference: by Clegg B, Kuhn S H & Walker R N. (1969)

APPENDIX H15: Strain influence calculation : Highveld Steel, 1969

[Figure 6.6]

$$\Delta V = V_o.\varepsilon_{vol} = V_o.(1-2\nu_{pl})\varepsilon_v = (1+e_o)(1-2\nu_{pl})\varepsilon_v$$

$$\rho = \frac{G_s}{(V_o - \Delta V)}$$

δ (settlement)=	145	mm	ν_{pl} =	0.0	Gs =	2650	(kg/m^3)

Depth (mm)	ρ_o	e_o	ΔH	ε_v=ΔH/H	Depth (mm)	ΔV=Δe	ρ_f(kg/m^3)
75	1665	0.591	19.5	0.13009	75	0.207	1914
225	1665	0.591	16.7	0.11126	225	0.177	1874
375	1665	0.591	12.7	0.08460	375	0.135	1819
525	1505	0.761	15.3	0.10213	525	0.180	1676
675	1505	0.761	16.2	0.10777	675	0.190	1687
825	1409	0.881	15.4	0.10290	825	0.194	1571
975	1409	0.881	13.6	0.09042	975	0.170	1549
1125	1409	0.881	11.1	0.07384	1125	0.139	1521
1275	1469	0.804	8.5	0.05638	1275	0.102	1557
1425	1469	0.804	6.1	0.04040	1425	0.073	1531
1575	1529	0.733	4.1	0.02725	1575	0.047	1572
1725	1529	0.733	2.6	0.01734	1725	0.030	1556
1875	1529	0.733	1.6	0.01042	1875	0.018	1545
2025	1529	0.733	0.9	0.00592	2025	0.010	1538
2175	1529	0.733	0.5	0.00319	2175	0.006	1534
2325	1529	0.733	0.2	0.00162	2325	0.003	1532
2475	1529	0.733	0.1	0.00078	2475	0.001	1530
2625	1529	0.733	0.1	0.00036	2625	0.001	1530
		Sum	145	mm			

20 passes [23.9kJ I	Before	
d (mm)	ρ_f(kg/m^3)	e_o
305	1665.3	0.591
610	1505.2	0.761
914	1409.1	0.881
1219	1469.2	0.804
1524	1529.2	0.733
1829	1529.2	0.733

20 passes [23.9kJ	After		
d (mm)	ρ_o (kg/m^3)	e_f	Δe
305	1857.5	0.427	0.165
610	1657.3	0.599	0.162
914	1641.3	0.615	0.266
1219	1557.3	0.702	0.102
1524	1553.3	0.706	0.027

Measured densities from reference: by Clegg B, Kuhn S H & Walker R N. (1969)

APPENDIX H16: Strain influence calculation : Middleberg, 1984 [20 passes]

[Figure 6.9]

$$\Delta V = V_o.\varepsilon_{vol} = V_o.(1-2\nu')\varepsilon_v = (1+e_o)(1-2\nu')\varepsilon_v$$

$$\rho = \frac{G_s}{(V_o - \Delta V)}$$

δ (settlement)=	87	mm	ν_{pl}=	0.3	Gs =	2650	(kg/m^3)

Depth (mm)	ρ_o	e_o	ΔH	ε_v=ΔH/H	Depth (mm)	ΔV=Δe	ρ_f(kg/m^3)
75	1402	0.890	11.7	0.07805	75	0.059	1447
225	1402	0.890	10.0	0.06676	225	0.050	1441
375	1402	0.890	7.6	0.05076	375	0.038	1431
525	1293	1.050	9.2	0.06128	525	0.050	1325
675	1293	1.050	9.7	0.06466	675	0.053	1327
825	1293	1.050	9.3	0.06174	825	0.051	1325
975	1293	1.050	8.1	0.05425	975	0.044	1321
1125	1293	1.050	6.6	0.04431	1125	0.036	1316
1275	1293	1.050	5.1	0.03383	1275	0.028	1310
1425	1293	1.050	3.6	0.02424	1425	0.020	1305
1575	1293	1.050	2.5	0.01635	1575	0.013	1301
1725	1293	1.050	1.6	0.01040	1725	0.009	1298
1875	1293	1.050	0.9	0.00625	1875	0.005	1296
2025	1293	1.050	0.5	0.00355	2025	0.003	1295
2175	1293	1.050	0.3	0.00191	2175	0.002	1294
2325	1293	1.050	0.1	0.00097	2325	0.001	1293
2475	1293	1.050	0.1	0.00047	2475	0.000	1293
2625	1293	1.050	0.0	0.00022	2625	0.000	1293
			Sum 87	mm			

20 passes	Before	
d (mm)	ρ_f(kg/m^3)	e_o
500	1402	0.890
1000	1293	1.050

20 passes	After		
d (mm)	ρ_o (kg/m^3)	e_f	Δe
500	1433	0.849	0.041
1000	1316	1.013	0.037

Measured densities from reference: Barrett & Wrench (1984).

APPENDIX H17: Strain influence calculation : Middleberg, 1984 [50 passes]

[Figure 6.9]

$$\Delta V = V_o \varepsilon_{vol} = V_o.(1-2\nu')\varepsilon_v = (1+e_o)(1-2\nu')\varepsilon_v$$

$$\rho = \frac{G_s}{(V_o - \Delta V)}$$

δ (settlement)=	112	mm	v_{pl}=	0.1	Gs =	2650	(kg/m^3)

Depth (mm)	ρ_o	e_o	ΔH	ε_v=ΔH/H	Depth (mm)	ΔV=Δe	ρ_f(kg/m^3)
75	1402	0.890	15.1	0.10048	75	0.152	1525
225	1402	0.890	12.9	0.08594	225	0.130	1506
375	1402	0.890	9.8	0.06534	375	0.099	1479
525	1350	0.963	11.8	0.07888	525	0.124	1441
675	1350	0.963	12.5	0.08324	675	0.131	1446
825	1350	0.963	11.9	0.07948	825	0.125	1442
975	1350	0.963	10.5	0.06985	975	0.110	1430
1125	1350	0.963	8.6	0.05704	1125	0.090	1415
1275	1350	0.963	6.5	0.04355	1275	0.068	1399
1425	1350	0.963	4.7	0.03121	1425	0.049	1385
1575	1350	0.963	3.2	0.02105	1575	0.033	1373
1725	1350	0.963	2.0	0.01339	1725	0.021	1365
1875	1350	0.963	1.2	0.00805	1875	0.013	1359
2025	1350	0.963	0.7	0.00457	2025	0.007	1355
2175	1350	0.963	0.4	0.00246	2175	0.004	1353
2325	1350	0.963	0.2	0.00125	2325	0.002	1351
2475	1350	0.963	0.1	0.00061	2475	0.001	1351
2625	1350	0.963	0.0	0.00028	2625	0.000	1350
			Sum	112 mm			

50 passes	Before	
d (mm)	ρ_f(kg/m^3)	e_o
500	1402	0.890
1000	1350	0.963

50 passes	After		
d (mm)	ρ_o (kg/m^3)	e_f	Δe
500	1502	0.765	0.125
1000	1453	0.824	0.139

Measured densities from reference: Barrett & Wrench (1984).

APPENDIX H18: Strain influence calculation : Villa Lisa, 1991 [30 passes]

$$\Delta V = V_o.\varepsilon_{vol} = V_o.(1-2v_{pl})\varepsilon_v = (1+e_o)(1-2v_{pl})\varepsilon_v$$

$$\rho = \frac{G_s}{(V_o - \Delta V)}$$

δ (settlement)=	233	mm	v_{pl}=	0.1	Gs =	2650	(kg/m^3)

Depth (mm)	ρ_o	e_o	ΔH	ε_v=ΔH/H	Depth (mm)	ΔV=Δe	ρ_f(kg/m^3)
75	1425	0.860	31.4	0.20903	75	0.311	1711
225	1425	0.860	26.8	0.17878	225	0.266	1663
375	1425	0.860	20.4	0.13594	375	0.202	1599
525	1425	0.860	24.6	0.16411	525	0.244	1640
675	1425	0.860	26.0	0.17318	675	0.258	1654
825	1425	0.860	24.8	0.16535	825	0.246	1642
975	1425	0.860	21.8	0.14530	975	0.216	1612
1125	1425	0.860	17.8	0.11866	1125	0.177	1574
1275	1425	0.860	13.6	0.09059	1275	0.135	1536
1425	1425	0.860	9.7	0.06492	1425	0.097	1503
1575	1425	0.860	6.6	0.04379	1575	0.065	1477
1725	1425	0.860	4.2	0.02786	1725	0.041	1457
1875	1425	0.860	2.5	0.01674	1875	0.025	1444
2025	1425	0.860	1.4	0.00952	2025	0.014	1436
2175	1425	0.860	0.8	0.00512	2175	0.008	1431
2325	1425	0.860	0.4	0.00261	2325	0.004	1428
2475	1425	0.860	0.2	0.00126	2475	0.002	1426
2625	1425	0.860	0.1	0.00058	2625	0.001	1426
			Sum 233	mm			

30 passes-meas	Before	
d (mm)	ρ_f(kg/m^3)	e_o
400	1425	0.860
750	1425	0.860
1000	1425	0.860
1500	1425	0.860

20 passes	After		
d (mm)	ρ_o (kg/m^3)	e_f	Δe
400	1603	0.653	0.206
750	1623	0.633	0.227
1000	1599	0.657	0.202
1500	1490	0.779	0.081

after Solesbury F W & Walker D G (1991). *The impact rolling of a large housing site Boksburg.* Geotechnics in the African enviroment, Blight et al (eds), Balkema, Rotterdam. p393-399.

APPENDIX H18a: Strain influence calculation : Villa Lisa, 1991 [30 passes]

[Unmodified Rayleigh distribution calculation for Figure 6.11]

$$\Delta V = V_o.\varepsilon_{vol} = V_o.(1-2\nu')\varepsilon_v = (1+e_o)(1-2\nu')\varepsilon_v$$

$$\rho = \frac{G_s}{(V_o - \Delta V)}$$

δ (settlement)=	233	mm	ν_{pl}=	0.2	Gs =	2650	(kg/m^3)

Depth (mm)	ρ_o	e_o	ΔH	ε_v=ΔH/H	Depth (mm)	ΔV=Δe	ρ_f(kg/m^3)
75	1425	0.860	5.7	0.03805	75	0.042	1458
225	1425	0.860	16.3	0.10865	225	0.121	1524
375	1425	0.860	24.6	0.16406	375	0.183	1581
525	1425	0.860	29.7	0.19806	525	0.221	1617
675	1425	0.860	31.4	0.20900	675	0.233	1629
825	1425	0.860	29.9	0.19956	825	0.223	1619
975	1425	0.860	26.3	0.17536	975	0.196	1593
1125	1425	0.860	21.5	0.14321	1125	0.160	1559
1275	1425	0.860	16.4	0.10933	1275	0.122	1525
1425	1425	0.860	11.8	0.07835	1425	0.087	1495
1575	1425	0.860	7.9	0.05285	1575	0.059	1472
1725	1425	0.860	5.0	0.03362	1725	0.038	1454
1875	1425	0.860	3.0	0.02021	1875	0.023	1442
2025	1425	0.860	1.7	0.01148	2025	0.013	1435
2175	1425	0.860	0.9	0.00618	2175	0.007	1430
2325	1425	0.860	0.5	0.00315	2325	0.004	1428
2475	1425	0.860	0.2	0.00152	2475	0.002	1426
2625	1425	0.860	0.1	0.00070	2625	0.001	1426
			Sum 233	mm			

30 passes-meas	Before	
d (mm)	ρ_f(kg/m^3)	e_o
400	1425	0.860
750	1425	0.860
1000	1425	0.860
1500	1425	0.860

20 passes	After		
d (mm)	ρ_o (kg/m^3)	e_f	Δe
400	1603	0.653	0.206
750	1623	0.633	0.227
1000	1599	0.657	0.202
1500	1490	0.779	0.081

after Solesbury F W & Walker D G (1991). *The impact rolling of a large housing site Boksburg.* Geotechnics in the African enviroment, Blight et al (eds), Balkema, Rotterdam. p393-399.

APPENDIX H19: Strain influence calculation : Villa Lisa, 1991 [50 passes]

$$\Delta V = V_o.\varepsilon_{vol} = V_o.(1-2\nu_{pl})\varepsilon_v = (1+e_o)(1-2\nu_{pl})\varepsilon_v$$

$$\rho = \frac{G_s}{(V_o - \Delta V)}$$

δ (settlement)=	265	mm	ν_{pl}=	0	Gs =	2650	(kg/m^3)

Depth (mm)	ρ_o	e_o	ΔH	ε_v=ΔH/H	Depth (mm)	ΔV=Δe	ρ_f(kg/m^3)
75	1425	0.860	35.7	0.23774	75	0.442	1869
225	1425	0.860	30.5	0.20334	225	0.378	1789
375	1425	0.860	23.2	0.15461	375	0.288	1686
525	1425	0.860	28.0	0.18665	525	0.347	1752
675	1425	0.860	29.5	0.19696	675	0.366	1775
825	1425	0.860	28.2	0.18806	825	0.350	1755
975	1425	0.860	24.8	0.16526	975	0.307	1707
1125	1425	0.860	20.2	0.13495	1125	0.251	1647
1275	1425	0.860	15.5	0.10303	1275	0.192	1589
1425	1425	0.860	11.1	0.07383	1425	0.137	1539
1575	1425	0.860	7.5	0.04980	1575	0.093	1500
1725	1425	0.860	4.8	0.03168	1725	0.059	1472
1875	1425	0.860	2.9	0.01904	1875	0.035	1453
2025	1425	0.860	1.6	0.01082	2025	0.020	1441
2175	1425	0.860	0.9	0.00582	2175	0.011	1433
2325	1425	0.860	0.4	0.00297	2325	0.006	1429
2475	1425	0.860	0.2	0.00143	2475	0.003	1427
2625	1425	0.860	0.1	0.00066	2625	0.001	1426
			Sum 265	mm			

50 passes	Before	
d (mm)	ρ_f(kg/m^3)	e_o
400	1425	0.860
750	1425	0.860
1000	1425	0.860
1500	1425	0.860

50 passes-meas	After		
d (mm)	ρ_o (kg/m^3)	e_f	Δe
400	1612	0.644	0.216
750	1831	0.447	0.412
1000	1799	0.473	0.387
1500			

after Solesbury F W & Walker D G (1991). *The impact rolling of a large housing site Boksburg.* Geotechnics in the African enviroment, Blight et al (eds), Balkema, Rotterdam. p393-399.

APPENDIX H19a: Strain influence calculation : Villa Lisa, 1991 [50 passes]

[Unmodified Rayleigh distribution calculation for Figure 6.11]

$$\Delta V = V_o \varepsilon_{vol} = V_o.(1-2\nu')\varepsilon_v = (1+e_o)(1-2\nu')\varepsilon_v$$

$$\rho = \frac{G_s}{(V_o - \Delta V)}$$

δ (settlement)=	265	mm	v_{pl}=	0.05	Gs =	2650	(kg/m^3)

Depth (mm)	ρ_o	e_o	ΔH	ε_v=ΔH/H	Depth (mm)	ΔV=Δe	ρ_f(kg/m^3)
75	1425	0.860	6.5	0.04328	75	0.072	1483
225	1425	0.860	18.5	0.12358	225	0.207	1603
375	1425	0.860	28.0	0.18659	375	0.312	1713
525	1425	0.860	33.8	0.22526	525	0.377	1787
675	1425	0.860	35.7	0.23771	675	0.398	1813
825	1425	0.860	34.0	0.22696	825	0.380	1791
975	1425	0.860	29.9	0.19945	975	0.334	1737
1125	1425	0.860	24.4	0.16287	1125	0.273	1670
1275	1425	0.860	18.7	0.12435	1275	0.208	1605
1425	1425	0.860	13.4	0.08911	1425	0.149	1549
1575	1425	0.860	9.0	0.06011	1575	0.101	1506
1725	1425	0.860	5.7	0.03824	1725	0.064	1476
1875	1425	0.860	3.4	0.02298	1875	0.038	1455
2025	1425	0.860	2.0	0.01306	2025	0.022	1442
2175	1425	0.860	1.1	0.00703	2175	0.012	1434
2325	1425	0.860	0.5	0.00358	2325	0.006	1430
2475	1425	0.860	0.3	0.00173	2475	0.003	1427
2625	1425	0.860	0.1	0.00079	2625	0.001	1426
		Sum	265	mm			

50 passes	Before	
d (mm)	ρ_f(kg/m^3)	e_o
400	1425	0.860
750	1425	0.860
1000	1425	0.860
1500	1425	0.860

50 passes-meas	After		
d (mm)	ρ_o (kg/m^3)	e_f	Δe
400	1612	0.644	0.216
750	1831	0.447	0.412
1000	1799	0.473	0.387
1500			

after Solesbury F W & Walker D G (1991). *The impact rolling of a large housing site Boksburg.* Geotechnics in the African enviroment, Blight et al (eds), Balkema, Rotterdam. p393-399.

APPENDIX H20: Strain influence calculation : Pinard, 1988 [20 passes]

[Figure 6.12]

$$\Delta V = V_o.\varepsilon_{vol} = V_o.(1-2\nu_{pl})\varepsilon_v = (1+e_o)(1-2\nu_{pl})\varepsilon_v$$

$$\rho = \frac{G_s}{(V_o - \Delta V)}$$

δ (settlement)=	105	mm	ν_{pl} =	0.20	Gs =	2650	(kg/m^3)

Depth (mm)	ρ_o	e_o	ΔH	ε_v=ΔH/H	Depth (mm)	ΔV=Δe	ρ_f(kg/m^3)
75	1441	0.839	14.1	0.09420	75	0.104	1527
225	1441	0.839	12.1	0.08057	225	0.089	1514
375	1441	0.839	9.2	0.06126	375	0.068	1496
525	1422	0.864	11.1	0.07395	525	0.083	1488
675	1422	0.864	11.7	0.07804	675	0.087	1492
825	1422	0.864	11.2	0.07451	825	0.083	1489
975	1422	0.864	9.8	0.06548	975	0.073	1480
1125	1422	0.864	8.0	0.05347	1125	0.060	1469
1275	1422	0.864	6.1	0.04082	1275	0.046	1458
1425	1422	0.864	4.4	0.02926	1425	0.033	1447
1575	1422	0.864	3.0	0.01973	1575	0.022	1439
1725	1422	0.864	1.9	0.01255	1725	0.014	1433
1875	1422	0.864	1.1	0.00754	1875	0.008	1428
2025	1422	0.864	0.6	0.00429	2025	0.005	1426
2175	1422	0.864	0.3	0.00231	2175	0.003	1424
2325	1422	0.864	0.2	0.00118	2325	0.001	1423
2475	1422	0.864	0.1	0.00057	2475	0.001	1422
2625	1422	0.864	0.0	0.00026	2625	0.000	1422
			Sum 105	mm			

20 passes-meas	Before	
d (mm)	ρ_f(kg/m^3)	e_o
305	1441	0.839
610	1422	0.864
810	1413	0.875
1100	1422	0.864

20 passes	After		
d (mm)	ρ_o (kg/m^3)	e_f	Δe
305	1710	0.549	0.290
610	1503	0.763	0.100
810	1476	0.795	0.080
1100	1461	0.814	0.049

Annual transport Convention, 1988, paper 3D/7

Evaluation of impact roller compaction trials on potentially collapsing sands in Botswana

Pinard M I, Ookeditse S & Fraser C

APPENDIX H20a: Strain influence calculation : Pinard, 1988 [20 passes]

[Figure 6.13]

$$\Delta V = V_o.\varepsilon_{vol} = V_o.(1-2\nu_{pl})\varepsilon_v = (1+e_o)(1-2\nu_{pl})\varepsilon_v$$

$$\rho = \frac{G_s}{(V_o - \Delta V)}$$

δ (settlement)=	105	mm	ν_{pl}=	0.13	Gs =	2650	(kg/m^3)

Depth (mm)	ρ_o	e_o	ΔH	ε_v=ΔH/H	Depth (mm)	ΔV=Δe	ρ_f(kg/m^3)
75	1441	0.839	25.3	0.16843	75	0.232	1649
225	1441	0.839	18.8	0.12537	225	0.173	1590
375	1441	0.839	10.8	0.07168	375	0.099	1523
525	1422	0.864	11.9	0.07962	525	0.111	1512
675	1422	0.864	11.3	0.07518	675	0.105	1507
825	1422	0.864	9.4	0.06248	825	0.087	1492
975	1422	0.864	7.0	0.04647	975	0.065	1473
1125	1422	0.864	4.7	0.03124	1125	0.044	1456
1275	1422	0.864	2.9	0.01910	1275	0.027	1443
1425	1422	0.864	1.6	0.01066	1425	0.015	1433
1575	1422	0.864	0.8	0.00545	1575	0.008	1428
1725	1422	0.864	0.4	0.00255	1725	0.004	1425
1875	1422	0.864	0.2	0.00110	1875	0.002	1423
2025	1422	0.864	0.1	0.00044	2025	0.001	1422
2175	1422	0.864	0.0	0.00016	2175	0.000	1422
2325	1422	0.864	0.0	0.00005	2325	0.000	1422
2475	1422	0.864	0.0	0.00002	2475	0.000	1422
2625	1422	0.864	0.0	0.00000	2625	0.000	1422
			Sum	105 mm			

20 passes-meas	Before	
d (mm)	ρ_f(kg/m^3)	e_f
305	1441	0.839
610	1422	0.864
810	1413	0.875
1100	1422	0.864

20 passes	After		
d (mm)	ρ_o (kg/m^3)	e_o	Δe
305	1710	0.549	0.290
610	1503	0.763	0.100
810	1476	0.795	0.080
1100	1461	0.814	0.049

Annual transport Convention, 1988, paper 3D/7

Evaluation of impact roller compaction trials on potentially collapsing sands in Botswana

Pinard M I, Ookeditse S & Fraser C

APPENDIX H21: Strain influence calculation : Pinard, 1988 [30 passes]

[Figure 6.12]

$$\Delta V = V_o.\varepsilon_{vol} = V_o.(1-2\nu_{pl})\varepsilon_v = (1+e_o)(1-2\nu_{pl})\varepsilon_v$$

$$\rho = \frac{G_s}{(V_o - \Delta V)}$$

δ (settlement)=	150	mm	ν_{pl} =	0.15	Gs =	2650	(kg/m^3)

Depth (mm)	ρ_o	e_o	ΔH	ε_v=ΔH/H	Depth (mm)	ΔV=Δe	ρ_f(kg/m^3)
75	1441	0.839	20.2	0.13457	75	0.173	1591
225	1441	0.839	17.3	0.11510	225	0.148	1567
375	1441	0.839	13.1	0.08751	375	0.113	1535
525	1422	0.864	15.8	0.10565	525	0.138	1536
675	1422	0.864	16.7	0.11149	675	0.145	1542
825	1422	0.864	16.0	0.10645	825	0.139	1536
975	1422	0.864	14.0	0.09354	975	0.122	1522
1125	1422	0.864	11.5	0.07639	1125	0.100	1502
1275	1422	0.864	8.7	0.05832	1275	0.076	1483
1425	1422	0.864	6.3	0.04179	1425	0.055	1465
1575	1422	0.864	4.2	0.02819	1575	0.037	1451
1725	1422	0.864	2.7	0.01793	1725	0.023	1440
1875	1422	0.864	1.6	0.01078	1875	0.014	1433
2025	1422	0.864	0.9	0.00613	2025	0.008	1428
2175	1422	0.864	0.5	0.00330	2175	0.004	1425
2325	1422	0.864	0.3	0.00168	2325	0.002	1424
2475	1422	0.864	0.1	0.00081	2475	0.001	1423
2625	1422	0.864	0.1	0.00037	2625	0.000	1422
			Sum 150	mm			

30 passes-meas	Before	
d (mm)	ρ_f(kg/m^3)	e_o
305	1441	0.839
610	1422	0.864
810	1413	0.875
1100	1422	0.864

30 passes	After		
d (mm)	ρ_o (kg/m^3)	e_f	Δe
305	1782	0.487	0.352
610	1584	0.673	0.191
810	1508	0.758	0.118
1100	1476	0.795	0.068

Annual transport Convention, 1988, paper 3D/7

Evaluation of impact roller compaction trials on potentially collapsing sands in Botswana

Pinard M I, Ookeditse S & Fraser C

APPENDIX H21a: Strain influence calculation : Pinard, 1988 [30 passes]

[Figure 6.13]

$$\Delta V = V_o.\varepsilon_{vol} = V_o.(1-2\nu_{pl})\varepsilon_v = (1+e_o)(1-2\nu_{pl})\varepsilon_v$$

$$\rho = \frac{G_s}{(V_o - \Delta V)}$$

δ (settlement)=	150	mm	ν_{pl}=	0.05	Gs =	2650	(kg/m^3)

Depth (mm)	ρ_o	e_o	ΔH	ε_v=ΔH/H	Depth (mm)	ΔV=Δe	ρ_f(kg/m^3)
75	1441	0.839	36.1	0.24062	75	0.398	1839
225	1441	0.839	26.9	0.17910	225	0.296	1718
375	1441	0.839	15.4	0.10240	375	0.169	1587
525	1422	0.864	17.1	0.11374	525	0.191	1584
675	1422	0.864	16.1	0.10740	675	0.180	1574
825	1422	0.864	13.4	0.08925	825	0.150	1546
975	1422	0.864	10.0	0.06639	975	0.111	1512
1125	1422	0.864	6.7	0.04463	1125	0.075	1482
1275	1422	0.864	4.1	0.02729	1275	0.046	1458
1425	1422	0.864	2.3	0.01523	1425	0.026	1442
1575	1422	0.864	1.2	0.00778	1575	0.013	1432
1725	1422	0.864	0.5	0.00365	1725	0.006	1427
1875	1422	0.864	0.2	0.00157	1875	0.003	1424
2025	1422	0.864	0.1	0.00062	2025	0.001	1423
2175	1422	0.864	0.0	0.00023	2175	0.000	1422
2325	1422	0.864	0.0	0.00008	2325	0.000	1422
2475	1422	0.864	0.0	0.00002	2475	0.000	1422
2625	1422	0.864	0.0	0.00001	2625	0.000	1422
			Sum	150 mm			

30 passes-meas	Before	
d (mm)	ρ_f(kg/m^3)	e_f
305	1441	0.839
610	1422	0.864
810	1413	0.875
1100	1422	0.864

30 passes	After		
d (mm)	ρ_o (kg/m^3)	e_o	Δe
305	1782	0.487	0.352
610	1584	0.673	0.191
810	1508	0.758	0.118
1100	1476	0.795	0.068

Annual transport Convention, 1988, paper 3D/7

Evaluation of impact roller compaction trials on potentially collapsing sands in Botswana

Pinard M I, Ookeditse S & Fraser C

APPENDIX H22: Strain influence calculation : Pinard, 1988 [60 passes]

[Figure 6.12]

$$\Delta V = V_o.\varepsilon_{vol} = V_o.(1-2v_{pl})\varepsilon_v = (1+e_o)(1-2v_{pl})\varepsilon_v$$

$$\rho = \frac{G_s}{(V_o - \Delta V)}$$

δ (settlement)=	175	mm	v_{pl} =	0.05	Gs =	2650	(kg/m^3)

Depth (mm)	ρ_o	e_o	ΔH	ε_v=ΔH/H	Depth (mm)	ΔV=Δe	ρ_f(kg/m^3)
75	1441	0.839	23.6	0.15700	75	0.260	1678
225	1441	0.839	20.1	0.13428	225	0.222	1639
375	1441	0.839	15.3	0.10210	375	0.169	1587
525	1422	0.864	18.5	0.12326	525	0.207	1599
675	1422	0.864	19.5	0.13007	675	0.218	1611
825	1422	0.864	18.6	0.12419	825	0.208	1601
975	1422	0.864	16.4	0.10913	975	0.183	1577
1125	1422	0.864	13.4	0.08912	1125	0.149	1546
1275	1422	0.864	10.2	0.06804	1275	0.114	1515
1425	1422	0.864	7.3	0.04876	1425	0.082	1487
1575	1422	0.864	4.9	0.03289	1575	0.055	1465
1725	1422	0.864	3.1	0.02092	1725	0.035	1449
1875	1422	0.864	1.9	0.01257	1875	0.021	1438
2025	1422	0.864	1.1	0.00715	2025	0.012	1431
2175	1422	0.864	0.6	0.00384	2175	0.006	1427
2325	1422	0.864	0.3	0.00196	2325	0.003	1425
2475	1422	0.864	0.1	0.00095	2475	0.002	1423
2625	1422	0.864	0.1	0.00043	2625	0.001	1423
			Sum 175	mm			

60 passes-meas	Before	
d (mm)	ρ_f(kg/m^3)	e_o
305	1441	0.839
610	1422	0.864
810	1413	0.875
1100	1422	0.864

60 passes	After		
d (mm)	ρ_o (kg/m^3)	e_f	Δe
305	1836	0.443	0.396
610	1638	0.618	0.246
810	1584	0.673	0.202
1100	1548	0.712	0.152

Annual transport Convention, 1988, paper 3D/7

Evaluation of impact roller compaction trials on potentially collapsing sands in Botswana

Pinard M I, Ookeditse S & Fraser C

APPENDIX H22a: Strain influence calculation : Pinard, 1988 [60 passes]

[Figure 6.13]

$$\Delta V = V_o.\varepsilon_{vol} = V_o.(1-2\nu_{pl})\varepsilon_v = (1+e_o)(1-2\nu_{pl})\varepsilon_v$$

$$\rho = \frac{G_s}{(V_o - \Delta V)}$$

δ (settlement)=	175	mm	ν_{pl}=	0.00	Gs =	2650	(kg/m^3)

Depth (mm)	ρ_o	e_o	ΔH	ε_v=ΔH/H	Depth (mm)	ΔV=Δe	ρ_f(kg/m^3)
75	1441	0.839	42.1	0.28072	75	0.516	2003
225	1441	0.839	31.3	0.20895	225	0.384	1821
375	1441	0.839	17.9	0.11947	375	0.220	1636
525	1422	0.864	19.9	0.13270	525	0.247	1640
675	1422	0.864	18.8	0.12530	675	0.234	1626
825	1422	0.864	15.6	0.10413	825	0.194	1587
975	1422	0.864	11.6	0.07745	975	0.144	1541
1125	1422	0.864	7.8	0.05207	1125	0.097	1500
1275	1422	0.864	4.8	0.03183	1275	0.059	1469
1425	1422	0.864	2.7	0.01777	1425	0.033	1448
1575	1422	0.864	1.4	0.00908	1575	0.017	1435
1725	1422	0.864	0.6	0.00425	1725	0.008	1428
1875	1422	0.864	0.3	0.00183	1875	0.003	1425
2025	1422	0.864	0.1	0.00073	2025	0.001	1423
2175	1422	0.864	0.0	0.00026	2175	0.000	1422
2325	1422	0.864	0.0	0.00009	2325	0.000	1422
2475	1422	0.864	0.0	0.00003	2475	0.000	1422
2625	1422	0.864	0.0	0.00001	2625	0.000	1422
			Sum 175	mm			

60 passes-meas	Before	
d (mm)	ρ_f(kg/m^3)	e_f
305	1441	0.839
610	1422	0.864
810	1413	0.875
1100	1422	0.864

60 passes	After		
d (mm)	ρ_o (kg/m^3)	e_o	Δe
305	1836	0.443	0.396
610	1638	0.618	0.246
810	1584	0.673	0.202
1100	1548	0.712	0.152

Annual transport Convention, 1988, paper 3D/7

Evaluation of impact roller compaction trials on potentially collapsing sands in Botswana

Pinard M I, Ookeditse S & Fraser C

APPENDIX H23: Strain influence calculation : Cell 1, Rollins, 1998

[Figure 6.14]

$$\Delta V = V_o.\varepsilon_{vol} = V_o.(1-2\nu_{pl})\varepsilon_v = (1+e_o)(1-2\nu_{pl})\varepsilon_v$$

$$\rho = \frac{G_s}{(V_o - \Delta V)}$$

(settlement)	0.48	m	ν_{pl}=	0.15	Gs =	2650	(kg/m^3)

Depth (m)	ρ_o	e_o	ΔH	$\varepsilon_v=\Delta H/H$	Depth (m)	$\Delta V=\Delta e$	ρ_f(kg/m^3)
0.10	1262	1.100	0.050	0.24918	0.58	0.366	1529
0.30	1262	1.100	0.039	0.19728	0.78	0.290	1464
0.50	1262	1.100	0.028	0.13795	0.98	0.203	1397
0.70	1205	1.200	0.035	0.17692	1.18	0.272	1375
0.90	1205	1.200	0.040	0.20237	1.38	0.312	1403
1.10	1205	1.200	0.043	0.21372	1.58	0.329	1416
1.30	1205	1.200	0.042	0.21196	1.78	0.326	1414
1.50	1205	1.200	0.040	0.19933	1.98	0.307	1400
1.70	1205	1.200	0.036	0.17882	2.18	0.275	1377
1.90	1205	1.200	0.031	0.15364	2.38	0.237	1350
2.10	1205	1.200	0.025	0.12678	2.58	0.195	1322
2.30	1205	1.200	0.020	0.10069	2.78	0.155	1296
2.50	1205	1.200	0.015	0.07707	2.98	0.119	1273
2.70	1205	1.200	0.011	0.05693	3.18	0.088	1255
2.90	1205	1.200	0.008	0.04062	3.38	0.063	1240
3.10	1205	1.200	0.006	0.02801	3.58	0.043	1229
3.30	1205	1.200	0.004	0.01868	3.78	0.029	1221
3.50	1205	1.200	0.002	0.01206	3.98	0.019	1215
3.70	1205	1.200	0.002	0.00753	4.18	0.012	1211
3.90	1205	1.200	0.001	0.00456	4.38	0.007	1208
4.10	1205	1.200	0.001	0.00267	4.58	0.004	1207
4.30	1205	1.200	0.000	0.00152	4.78	0.002	1206
4.50	1205	1.200	0.000	0.00083	4.98	0.001	1205
4.70	1205	1.200	0.000	0.00045	5.18	0.001	1205
4.90	1205	1.200	0.000	0.00023	5.38	0.000	1205
5.10	1205	1.200	0.000	0.00012	5.58	0.000	1205
5.30	1205	1.200	0.000	0.00006	5.78	0.000	1205
5.50	1205	1.200	0.000	0.00003	5.98	0.000	1205
		Sum	0.480	m			

Cell 1 - meas	Before	
d (mm)	ρ_o (kg/m^3)	e_o
1.20	1262	1.10
1.80	1205	1.20
2.40	1283	1.07
3.05	1312	1.02
3.70	1262	1.10
4.10	1305	1.03
4.90	1325	1.00
5.55	1274	1.08
Ave	1278	1.07

Cell 1 - measur	After		
d (mm)	ρ_f(kg/m^3)	e_f	Δe
1.20	1699	0.560	0.540
1.80	1452	0.825	0.375
2.40	1380	0.920	0.145
3.05	1325	1.000	0.020
3.70	1325	1.000	0.100
4.10	1305	1.030	0.000
4.90	1312	1.020	-0.020
5.55			

Based on a paper by Rollins, K.M., Jorgebsen, S.J., & Ross T.E.:
Optimum moisture content for dynamic compaction of collapsible soils.
Journal of Geotechnical Engineering, Vol 124, No 8, August 1998.

APPENDIX H24: Strain influence calculation : Cell 2, Rollins, 1998

$$\Delta V = V_o.\varepsilon_{vol} = V_o.(1-2v_{pl})\varepsilon_v = (1+e_o)(1-2v_{pl})\varepsilon_v$$

$$\rho = \frac{G_s}{(V_o - \Delta V)}$$

(settlement)=	0.85	m	v_{pl} =	0.15	Gs =	2650	(kg/m^3)

Depth (m)	ρ_o	e_o	ΔH	$\varepsilon_v = \Delta H/H$	Depth (m)	$\Delta V = \Delta e$	ρ_f (kg/m^3)
0.10	1312	1.020	0.088	0.44126	0.95	0.624	1898
0.30	1312	1.020	0.070	0.34935	1.15	0.494	1737
0.50	1312	1.020	0.049	0.24428	1.35	0.345	1582
0.70	1147	1.310	0.063	0.31329	1.55	0.507	1469
0.90	1147	1.310	0.072	0.35837	1.75	0.579	1531
1.10	1147	1.310	0.076	0.37847	1.95	0.612	1561
1.30	1147	1.310	0.075	0.37535	2.15	0.607	1556
1.50	1147	1.310	0.071	0.35298	2.35	0.571	1524
1.70	1147	1.310	0.063	0.31665	2.55	0.512	1474
1.90	1147	1.310	0.054	0.27207	2.75	0.440	1417
2.10	1147	1.310	0.045	0.22451	2.95	0.363	1361
2.30	1147	1.310	0.036	0.17830	3.15	0.288	1311
2.50	1147	1.310	0.027	0.13648	3.35	0.221	1268
2.70	1147	1.310	0.020	0.10082	3.55	0.163	1234
2.90	1147	1.310	0.014	0.07193	3.75	0.116	1208
3.10	1147	1.310	0.010	0.04960	3.95	0.080	1188
3.30	1147	1.310	0.007	0.03308	4.15	0.053	1174
3.50	1147	1.310	0.004	0.02135	4.35	0.035	1165
3.70	1147	1.310	0.003	0.01334	4.55	0.022	1158
3.90	1147	1.310	0.002	0.00807	4.75	0.013	1154
4.10	1147	1.310	0.001	0.00473	4.95	0.008	1151
4.30	1147	1.310	0.001	0.00269	5.15	0.004	1149
4.50	1147	1.310	0.000	0.00148	5.35	0.002	1148
4.70	1147	1.310	0.000	0.00079	5.55	0.001	1148
4.90	1147	1.310	0.000	0.00041	5.75	0.001	1148
5.10	1147	1.310	0.000	0.00020	5.95	0.000	1147
5.30	1147	1.310	0.000	0.00010	6.15	0.000	1147
5.50	1147	1.310	0.000	0.00005	6.35	0.000	1147
		Sum	0.850	m			

Cell 2 - meas	Before	
d (mm)	ρ_o (kg/m^3)	e_o
1.20	1312	1.02
1.80	1147	1.31
2.40	1188	1.23
3.05	1262	1.10
3.70	1432	0.85
4.10	1406	0.89
4.90	1425	0.86
5.55	1345	0.97
Ave	1315	1.03

Cell 2 - measur	After		
d (mm)	ρ_f (kg/m^3)	e_f	Δe
1.20	1710	0.550	0.470
1.80	1636	0.620	0.690
2.40	1536	0.725	0.505
3.05	1402	0.890	0.210
3.70	1384	0.915	-0.065
4.10	1440	0.840	0.045
4.90	1440	0.840	0.020
5.55			

Based on a paper by Rollins, K.M., Jorgebsen, S.J., & Ross T.E.:
Optimum moisture content for dynamic compaction of collapsible soils.
Journal of Geotechnical Engineering, Vol 124, No 8, August 1998.

APPENDIX H25: Strain influence calculation : Cell 3, Rollins, 1998

[Figure 6.16]

$$\Delta V = V_o.\varepsilon_{vol} = V_o.(1-2\nu_{pl})\varepsilon_v = (1+e_o)(1-2\nu_{pl})\varepsilon_v$$

$$\rho = \frac{G_s}{(V_o - \Delta V)}$$

(settlement)=	1.2	m	ν_{pl} =	0.25	Gs =	2650	(kg/m^3)

Depth (m)	ρ_o	e_o	ΔH	ε_v=ΔH/H	Depth (m)	ΔV=Δe	ρ_f(kg/m^3)
0.10	1338	0.980	0.125	0.62295	1.30	0.617	1944
0.30	1338	0.980	0.099	0.49320	1.50	0.488	1776
0.50	1338	0.980	0.069	0.34487	1.70	0.341	1617
0.70	1338	0.980	0.088	0.44229	1.90	0.438	1718
0.90	1338	0.980	0.101	0.50593	2.10	0.501	1792
1.10	1338	0.980	0.107	0.53430	2.30	0.529	1826
1.30	1338	0.980	0.106	0.52990	2.50	0.525	1821
1.50	1338	0.980	0.100	0.49833	2.70	0.493	1783
1.70	1338	0.980	0.089	0.44704	2.90	0.443	1724
1.90	1338	0.980	0.077	0.38410	3.10	0.380	1657
2.10	1338	0.980	0.063	0.31696	3.30	0.314	1590
2.30	1338	0.980	0.050	0.25172	3.50	0.249	1531
2.50	1338	0.980	0.039	0.19268	3.70	0.191	1481
2.70	1338	0.980	0.028	0.14233	3.90	0.141	1441
2.90	1338	0.980	0.020	0.10155	4.10	0.101	1410
3.10	1338	0.980	0.014	0.07003	4.30	0.069	1387
3.30	1338	0.980	0.009	0.04671	4.50	0.046	1370
3.50	1338	0.980	0.006	0.03014	4.70	0.030	1359
3.70	1338	0.980	0.004	0.01883	4.90	0.019	1351
3.90	1338	0.980	0.002	0.01139	5.10	0.011	1346
4.10	1338	0.980	0.001	0.00668	5.30	0.007	1343
4.30	1338	0.980	0.001	0.00379	5.50	0.004	1341
4.50	1338	0.980	0.000	0.00209	5.70	0.002	1340
4.70	1338	0.980	0.000	0.00111	5.90	0.001	1339
4.90	1338	0.980	0.000	0.00058	6.10	0.001	1339
5.10	1338	0.980	0.000	0.00029	6.30	0.000	1339
5.30	1338	0.980	0.000	0.00014	6.50	0.000	1338
5.50	1338	0.980	0.000	0.00007	6.70	0.000	1338
			Sum	1.200	m		

Cell 3 - meas	Before		Cell 3 - measur	After		
d (mm)	ρ_o (kg/m^3)	e_o	d (mm)	ρ_f(kg/m^3)	e_f	Δe
1.20	1338	0.98	1.20	1860	0.425	0.555
1.80	1338	0.98	1.80	1743	0.520	0.460
2.40	1268	1.09	2.40	1667	0.590	0.500
3.05	1312	1.02	3.05	1550	0.710	0.310
3.70	1296	1.05	3.70	1472	0.800	0.245
4.10	1342	0.98	4.10	1387	0.910	0.065
4.90	1326	1.00	4.90	1342	0.975	0.023
5.55	2650	0.00	5.55			
Ave	1484	0.89				

Based on a paper by Rollins, K.M., Jorgebsen, S.J., & Ross T.E.:
Optimum moisture content for dynamic compaction of collapsible soils.
Journal of Geotechnical Engineering, Vol 124, No 8, August 1998.

APPENDIX H26: Strain influence calculation : Cell 4, Rollins, 1998

$$\Delta V = V_o.\varepsilon_{vol} = V_o.(1-2v_{pl})\varepsilon_v = (1+e_o)(1-2v_{pl})\varepsilon_v$$

$$\rho = \frac{G_s}{(V_o - \Delta V)}$$

(settlement)=	1.14	m	v_{pl}=	0.20	Gs =	2650	(kg/m^3)

Depth (m)	ρ_o	e_o	ΔH	ε_v=ΔH/H	Depth (m)	ΔV=Δe	ρ_f(kg/m^3)
0.10	1325	1.000	0.105	0.52502	1.24	0.630	1934
0.30	1325	1.000	0.081	0.40576	1.44	0.487	1751
0.50	1325	1.000	0.055	0.27457	1.64	0.329	1586
0.70	1327	0.997	0.072	0.35805	1.84	0.429	1690
0.90	1327	0.997	0.084	0.41876	2.04	0.502	1772
1.10	1327	0.997	0.091	0.45470	2.24	0.545	1825
1.30	1327	0.997	0.093	0.46623	2.44	0.559	1842
1.50	1327	0.997	0.091	0.45582	2.64	0.546	1827
1.70	1327	0.997	0.085	0.42748	2.84	0.512	1785
1.90	1327	0.997	0.077	0.38611	3.04	0.463	1727
2.10	1327	0.997	0.067	0.33681	3.24	0.404	1663
2.30	1327	0.997	0.057	0.28433	3.44	0.341	1600
2.50	1327	0.997	0.047	0.23264	3.64	0.279	1542
2.70	1327	0.997	0.037	0.18470	3.84	0.221	1492
2.90	1327	0.997	0.028	0.14243	4.04	0.171	1451
3.10	1327	0.997	0.021	0.10675	4.24	0.128	1418
3.30	1327	0.997	0.016	0.07782	4.44	0.093	1392
3.50	1327	0.997	0.011	0.05519	4.64	0.066	1372
3.70	1327	0.997	0.008	0.03811	4.84	0.046	1358
3.90	1327	0.997	0.005	0.02562	5.04	0.031	1348
4.10	1327	0.997	0.003	0.01678	5.24	0.020	1340
4.30	1327	0.997	0.002	0.01070	5.44	0.013	1336
4.50	1327	0.997	0.001	0.00665	5.64	0.008	1332
4.70	1327	0.997	0.001	0.00403	5.84	0.005	1330
4.90	1327	0.997	0.000	0.00238	6.04	0.003	1329
5.10	1327	0.997	0.000	0.00137	6.24	0.002	1328
5.30	1327	0.997	0.000	0.00077	6.44	0.001	1328
5.50	1327	0.997	0.000	0.00042	6.64	0.001	1327
			Sum	1.140	m		

Cell 4 - meas	Before	
d (mm)	ρ_o (kg/m^3)	e_o
1.20	1325	1.00
1.80	1327	1.00
2.40	1359	0.95
3.05	1362	0.95
3.70	1268	1.09
4.10	1352	0.96
4.90	1286	1.06
5.55	1274	1.08
Ave	1319	1.01

Cell 4 - measur	After		
d (mm)	ρ_f(kg/m^3)	e_f	Δe
1.20	1866	0.420	0.580
1.80	1866	0.420	0.577
2.40	1840	0.440	0.510
3.05	1815	0.460	0.485
3.70	1577	0.680	0.410
4.10	1429	0.855	0.105
4.90	1410	0.880	0.180
5.55	1359	0.950	0.130

Based on a paper by Rollins, K.M., Jorgebsen, S.J., & Ross T.E.:
Optimum moisture content for dynamic compaction of collapsible soils.
Journal of Geotechnical Engineering, Vol 124, No 8, August 1998.

APPENDIX H27: Strain influence calculation : Cell 5, Rollins, 1998

$$\Delta V = V_o.\varepsilon_{vol} = V_o.(1-2\nu_{pl})\varepsilon_v = (1+e_o)(1-2\nu_{pl})\varepsilon_v$$

$$\rho = \frac{G_s}{(V_o - \Delta V)}$$

(settlement)=	0.99	m	ν_{pl}=	0.23	Gs =	2650	(kg/m^3)

Depth (m)	ρ_o	e_o	ΔH	$\varepsilon_v=\Delta H/H$	Depth (m)	$\Delta V=\Delta e$	ρ_f(kg/m^3)
0.10	1489	0.780	0.091	0.45594	1.09	0.438	1975
0.30	1489	0.780	0.070	0.35237	1.29	0.339	1839
0.50	1489	0.780	0.048	0.23844	1.49	0.229	1709
0.70	1432	0.850	0.062	0.31094	1.69	0.311	1721
0.90	1432	0.850	0.073	0.36366	1.89	0.363	1782
1.10	1432	0.850	0.079	0.39487	2.09	0.394	1821
1.30	1432	0.850	0.081	0.40488	2.29	0.404	1833
1.50	1432	0.850	0.079	0.39584	2.49	0.395	1822
1.70	1432	0.850	0.074	0.37123	2.69	0.371	1792
1.90	1432	0.850	0.067	0.33530	2.89	0.335	1749
2.10	1432	0.850	0.058	0.29249	3.09	0.292	1701
2.30	1432	0.850	0.049	0.24692	3.29	0.247	1653
2.50	1432	0.850	0.040	0.20203	3.49	0.202	1608
2.70	1432	0.850	0.032	0.16040	3.69	0.160	1568
2.90	1432	0.850	0.025	0.12369	3.89	0.124	1535
3.10	1432	0.850	0.019	0.09271	4.09	0.093	1508
3.30	1432	0.850	0.014	0.06758	4.29	0.068	1487
3.50	1432	0.850	0.010	0.04793	4.49	0.048	1470
3.70	1432	0.850	0.007	0.03309	4.69	0.033	1458
3.90	1432	0.850	0.004	0.02225	4.89	0.022	1450
4.10	1432	0.850	0.003	0.01457	5.09	0.015	1444
4.30	1432	0.850	0.002	0.00929	5.29	0.009	1440
4.50	1432	0.850	0.001	0.00578	5.49	0.006	1437
4.70	1432	0.850	0.001	0.00350	5.69	0.003	1435
4.90	1432	0.850	0.000	0.00207	5.89	0.002	1434
5.10	1432	0.850	0.000	0.00119	6.09	0.001	1433
5.30	1432	0.850	0.000	0.00067	6.29	0.001	1433
5.50	1432	0.850	0.000	0.00037	6.49	0.000	1433
		Sum	0.990	m			

Cell 5 - meas	Before	
d (mm)	ρ_o (kg/m^3)	e_o
1.20	1489	0.78
1.80	1432	0.85
2.40	1373	0.93
3.05	1402	0.89
3.70	1440	0.84
4.10	1452	0.83
4.90	1373	0.93
5.55	1380	0.92
Ave	1418	0.87

Cell 5 - measur	After		
d (mm)	ρ_f(kg/m^3)	e_f	Δe
1.20	1853	0.430	0.350
1.80	1840	0.440	0.410
2.40	1651	0.605	0.325
3.05	1656	0.600	0.290
3.70	1506	0.760	0.080
4.10	1767	0.500	0.325
4.90	1514	0.750	0.180
5.55	1373	0.930	-0.010

Based on a paper by Rollins, K.M., Jorgebsen, S.J., & Ross T.E.:
Optimum moisture content for dynamic compaction of collapsible soils.
Journal of Geotechnical Engineering, Vol 124, No 8, August 1998.

APPENDIX H28: Strain influence calculation : Cell 6, Rollins, 1998

$\Delta V = V_o.\varepsilon_{vol} = V_o.(1-2\nu_{pl})\varepsilon_v = (1+e_o)(1-2\nu_{pl})\varepsilon_v$ [Figure 6.19]

$$\rho = \frac{G_s}{(V_o - \Delta V)}$$

(settlement)=	2.38	m	ν_{pl} =	0.39	Gs =	2650	(kg/m^3)

Depth (m)	ρ_o	e_o	ΔH	$\varepsilon_v = \Delta H/H$	Depth (m)	$\Delta V = \Delta e$	ρ_f (kg/m^3)
0.10	1468	0.805	0.219	1.09609	2.48	0.435	1935
0.30	1468	0.805	0.169	0.84711	2.68	0.336	1804
0.50	1468	0.805	0.115	0.57322	2.88	0.228	1680
0.70	1293	1.050	0.150	0.74750	3.08	0.337	1547
0.90	1293	1.050	0.175	0.87426	3.28	0.394	1601
1.10	1293	1.050	0.190	0.94928	3.48	0.428	1634
1.30	1293	1.050	0.195	0.97335	3.68	0.439	1645
1.50	1293	1.050	0.190	0.95162	3.88	0.429	1635
1.70	1293	1.050	0.178	0.89246	4.08	0.402	1608
1.90	1293	1.050	0.161	0.80609	4.28	0.364	1571
2.10	1293	1.050	0.141	0.70316	4.48	0.317	1529
2.30	1293	1.050	0.119	0.59360	4.68	0.268	1487
2.50	1293	1.050	0.097	0.48569	4.88	0.219	1447
2.70	1293	1.050	0.077	0.38561	5.08	0.174	1413
2.90	1293	1.050	0.059	0.29736	5.28	0.134	1383
3.10	1293	1.050	0.045	0.22287	5.48	0.101	1359
3.30	1293	1.050	0.032	0.16246	5.68	0.073	1341
3.50	1293	1.050	0.023	0.11522	5.88	0.052	1326
3.70	1293	1.050	0.016	0.07955	6.08	0.036	1316
3.90	1293	1.050	0.011	0.05348	6.28	0.024	1308
4.10	1293	1.050	0.007	0.03502	6.48	0.016	1303
4.30	1293	1.050	0.004	0.02234	6.68	0.010	1299
4.50	1293	1.050	0.003	0.01389	6.88	0.006	1297
4.70	1293	1.050	0.002	0.00842	7.08	0.004	1295
4.90	1293	1.050	0.001	0.00497	7.28	0.002	1294
5.10	1293	1.050	0.001	0.00286	7.48	0.001	1293
5.30	1293	1.050	0.000	0.00161	7.68	0.001	1293
5.50	1293	1.050	0.000	0.00088	7.88	0.000	1293
			Sum 2.380	m			

Cell 6 - meas	Before		Cell 6 - measur	After		
d (mm)	ρ_o (kg/m^3)	e_o	d (mm)	ρ_f (kg/m^3)	e_f	Δe
2.70	1468	0.81	2.70	1656	0.600	0.205
3.30	1293	1.05	3.30	1626	0.630	0.420
4.25	1366	0.94	4.25	1577	0.680	0.260
4.80	1342	0.98	4.80	1536	0.725	0.250
5.40	1380	0.92	5.40	1506	0.760	0.160
6.00	1370	0.94	6.00	1472	0.800	0.135
Ave	1370	0.94				

Based on a paper by Rollins, K.M., Jorgebsen, S.J., & Ross T.E.:
Optimum moisture content for dynamic compaction of collapsible soils.
Journal of Geotechnical Engineering, Vol 124, No 8, August 1998.

APPENDIX H29 : Calculation of strain influence diagram:

Compactor contact dimension, B=	1.3	m
Assuming depth of influence, D =	3.9	m, =3B say
Asuming peak strain at a depth of	1	B
which is equal to…	1.300	m
Upper peak is how many times larger	1.025	x lower peak

Depth (mm)	ε ord.	Surface peak	Nett curve	Normalised ε ord.
0.10	0.05900	0.46640	0.52540	0.092109
0.30	0.17285	0.23320	0.40605	0.071186
0.50	0.27476	0.00000	0.27476	0.048170
0.70	0.35830		0.35830	0.062815
0.90	0.41906		0.41906	0.073467
1.10	0.45502		0.45502	0.079772
1.30	0.46656		0.46656	0.081794
1.50	0.45615		0.45615	0.079968
1.70	0.42779		0.42779	0.074997
1.90	0.38638		0.38638	0.067738
2.10	0.33705		0.33705	0.059089
2.30	0.28453		0.28453	0.049882
2.50	0.23281		0.23281	0.040814
2.70	0.18484		0.18484	0.032404
2.90	0.14253		0.14253	0.024988
3.10	0.10683		0.10683	0.018729
3.30	0.07787		0.07787	0.013652
3.50	0.05523		0.05523	0.009683
3.70	0.03813		0.03813	0.006685
3.90	0.02564		0.02564	0.004494
4.10	0.01679		0.01679	0.002943
4.30	0.01071		0.01071	0.001878
4.50	0.00666		0.00666	0.001167
4.70	0.00404		0.00404	0.000707
4.90	0.00238		0.00238	0.000418
5.10	0.00137		0.00137	0.000241
5.30	0.00077		0.00077	0.000135
5.50	0.00042		0.00042	0.000074
	5.00448		5.70408	1.00

APPENDIX H30 : Calculation of strain influence diagram: D_{peak}=0.675m
[Fig 6.22]

Compactor contact dimension, B=	0.9	m
Assuming depth of influence, D =	1.8	m, =3B say
Asuming peak strain at a depth of	0.75	B
which is equal to…	***0.675***	m
Upper peak is how many times larger	1.1	x lower peak

Depth (mm)	ε ord.	Surface peak	Nett curve	Normalised ε ord.
0.01	0.02195	0.97898	1.00093	0.123299
0.16	0.34144	0.48949	0.83093	0.102358
0.31	0.61229	0.00000	0.61229	0.075424
0.46	0.80039		0.80039	0.098596
0.61	0.88998		0.88998	0.109633
0.76	0.88497		0.88497	0.109014
0.91	0.80495		0.80495	0.099157
1.06	0.67795		0.67795	0.083513
1.21	0.53260		0.53260	0.065608
1.36	0.39213		0.39213	0.048304
1.51	0.27145		0.27145	0.033439
1.66	0.17709		0.17709	0.021815
1.81	0.10907		0.10907	0.013436
1.96	0.06350		0.06350	0.007822
2.11	0.03498		0.03498	0.004309
2.26	0.01825		0.01825	0.002248
2.41	0.00902		0.00902	0.001111
2.56	0.00423		0.00423	0.000521
2.71	0.00188		0.00188	0.000232
2.86	0.00079		0.00079	0.000098
3.01	0.00032		0.00032	0.000039
3.16	0.00012		0.00012	0.000015
3.31	0.00004		0.00004	0.000005
3.46	0.00001		0.00001	0.000002
3.61	0.00000		0.00000	0.000001
3.76	0.00000		0.00000	0.000000
3.91	0.00000		0.00000	0.000000
4.06	0.00000		0.00000	0.000000
	6.64941		8.11789	1.00

APPENDIX H31 : Calculation of strain influence diagram: D_{peak}=0.450m
[Fig 6.22]

Compactor contact dimension, B=	0.9	m
Assuming depth of influence, D =	1.8	m, =3B say
Asuming peak strain at a depth of	0.5	B
which is equal to…	***0.450***	m
Upper peak is how many times larger	1.1	x lower peak

Depth (mm)	ε ord.	Surface peak	Nett curve	Normalised ε ord.
0.01	0.04937	1.48190	1.53127	0.173015
0.16	0.74173	0.74095	1.48268	0.167524
0.31	1.20750	0.00000	1.20750	0.136432
0.46	1.34719		1.34719	0.152215
0.61	1.20196		1.20196	0.135807
0.76	0.90159		0.90159	0.101869
0.91	0.58159		0.58159	0.065713
1.06	0.32659		0.32659	0.036901
1.21	0.16083		0.16083	0.018171
1.36	0.06978		0.06978	0.007884
1.51	0.02676		0.02676	0.003024
1.66	0.00909		0.00909	0.001028
1.81	0.00274		0.00274	0.000310
1.96	0.00074		0.00074	0.000083
2.11	0.00018		0.00018	0.000020
2.26	0.00004		0.00004	0.000004
2.41	0.00001		0.00001	0.000001
2.56	0.00000		0.00000	0.000000
2.71	0.00000		0.00000	0.000000
2.86	0.00000		0.00000	0.000000
3.01	0.00000		0.00000	0.000000
3.16	0.00000		0.00000	0.000000
3.31	0.00000		0.00000	0.000000
3.46	0.00000		0.00000	0.000000
3.61	0.00000		0.00000	0.000000
3.76	0.00000		0.00000	0.000000
3.91	0.00000		0.00000	0.000000
4.06	0.00000		0.00000	0.000000
	6.62768		8.85053	1.00

APPENDIX H32 : Correlation calculation for impact compaction data

[Figure 6.23]

X	Y			
Measured	Predicted	$\underline{Y}$	$(Y-\underline{Y})^2$	$(X-Y)^2$
0.387	0.260	0.244	0.0003	0.01606
0.558	0.434	0.244	0.0363	0.01546
0.356	0.383	0.244	0.0194	0.0007
0.265	0.258	0.244	0.0002	4.5E-05
0.198	0.243	0.244	7E-07	0.00201
0.424	0.443	0.244	0.0396	0.00034
0.415	0.412	0.244	0.0285	1.1E-05
0.235	0.274	0.244	0.0009	0.00155
0.380	0.313	0.244	0.0048	0.00452
0.538	0.506	0.244	0.0689	0.00104
0.411	0.447	0.244	0.0415	0.00128
0.270	0.294	0.244	0.0026	0.00061
0.026	0.282	0.244	0.0015	0.06529
0.541	0.544	0.244	0.0902	6.5E-06
0.373	0.469	0.244	0.0506	0.0091
0.311	0.329	0.244	0.0074	0.00035
0.264	0.339	0.244	0.0092	0.00562
0.097	0.127	0.244	0.0136	0.00086
0.171	0.010	0.244	0.0545	0.0258
0.295	0.001	0.244	0.0587	0.08643
0.165	0.097	0.244	0.0213	0.0045
0.162	0.160	0.244	0.0069	1.4E-06
0.266	0.157	0.244	0.0075	0.01192
0.102	0.100	0.244	0.0205	2.3E-06
0.027	0.050	0.244	0.0376	0.00052
0.041	0.050	0.244	0.0374	8E-05
0.037	0.044	0.244	0.0398	5.3E-05
0.206	0.202	0.244	0.0017	1.8E-05
0.227	0.252	0.244	7E-05	0.00062
0.202	0.216	0.244	0.0007	0.00019
0.081	0.081	0.244	0.0265	6.9E-08
0.396	0.169	0.244	0.0056	0.05143
0.246	0.218	0.244	0.0006	0.00076
0.202	0.208	0.244	0.0012	3.4E-05
0.152	0.149	0.244	0.0088	4.9E-06

Mean Y	Sum (St)	Sum (Sr)	$R^2=(St-Sr)/St$	$S_{y/x}=(Sr/(n-2))^{0.5}$
0.244	0.745	0.307	0.59	0.10
	n=	35		

APPENDIX H33 : Correlation calculation : Dynamic compaction data

[Figure 6.24]

X	Y			
Measured	Predicted	$\underline{Y}$	$(Y-\underline{Y})^2$	$(X-Y)^2$
0.540	0.272	0.260	0.0001	0.0716
0.375	0.326	0.260	0.0043	0.0024
0.145	0.237	0.260	0.0006	0.0084
0.020	0.103	0.260	0.0247	0.0069
0.100	0.043	0.260	0.0472	0.0032
0.000	0.012	0.260	0.0619	0.0001
-0.020	0.002	0.260	0.0666	0.0005
0.470	0.494	0.260	0.0545	0.0006
0.690	0.579	0.260	0.1018	0.0122
0.505	0.571	0.260	0.0963	0.0043
0.210	0.363	0.260	0.0105	0.0234
-0.065	0.116	0.260	0.0208	0.0329
0.045	0.053	0.260	0.0428	0.0001
0.020	0.013	0.260	0.0612	0.0000
0.555	0.617	0.260	0.1269	0.0038
0.460	0.390	0.260	0.0167	0.0050
0.500	0.527	0.260	0.0709	0.0007
0.310	0.411	0.260	0.0228	0.0103
0.245	0.191	0.260	0.0049	0.0029
0.065	0.101	0.260	0.0256	0.0013
0.023	0.019	0.260	0.0585	0.0000
0.580	0.630	0.260	0.1366	0.0025
0.577	0.429	0.260	0.0284	0.0219
0.510	0.559	0.260	0.0889	0.0024
0.485	0.463	0.260	0.0409	0.0005
0.410	0.279	0.260	0.0003	0.0172
0.105	0.171	0.260	0.0081	0.0043
0.180	0.046	0.260	0.0462	0.0180
0.130	0.013	0.260	0.0613	0.0137
0.350	0.388	0.260	0.0164	0.0015
0.410	0.337	0.260	0.0058	0.0053
0.325	0.400	0.260	0.0195	0.0056
0.290	0.292	0.260	0.0010	0.0000
0.080	0.160	0.260	0.0100	0.0064
0.325	0.093	0.260	0.0282	0.0540
0.180	0.022	0.260	0.0568	0.0249
-0.010	0.006	0.260	0.0649	0.0002
0.205	0.336	0.260	0.0058	0.0173
0.420	0.394	0.260	0.0179	0.0007
0.260	0.364	0.260	0.0106	0.0107
0.250	0.243	0.260	0.0003	0.0000
0.160	0.101	0.260	0.0256	0.0035
0.135	0.036	0.260	0.0504	0.0098

Average Y	0.260	Sum (St	Sum (Sr)	$R^2=(St-Sr)/St$	$S_{y/x}=(Sr/(n-2))^{0.5}$
		1.644	0.411	0.750	0.10
		n=	43		

APPENDIX H34 : Calculation of void ratios from surface settlements of a vibro compactor: (data from Forssblad, 1980) [Figure 6.20 & 6.21]

Assumed MDD = 2000 kg/m^3 $\gamma_d=G_s/(1+e)$

Calculation of v_{pl} to achieve measured density: $\Delta V/V_o=(1-2v_{pl}).\varepsilon$

No. of passes	Density	e	Vo=1+e	Δe	δ (mm)	H	δh/H	v_{pl}	$(1-2v_{pl})$	$=(\delta h/H)(1-2v_{pl})$	ΔV	V	ρ=G/V
0	1450	0.828	1.828										
2	1604	0.652		-0.175	69	300	0.230	0.290	0.42	0.097	0.177	1.651	1605
4	1740	0.523		-0.305	78	300	0.260	0.180	0.64	0.166	0.304	1.523	1739
6	1840	0.440		-0.387	85	300	0.283	0.125	0.75	0.213	0.388	1.439	1841
8	1860	0.425		-0.403	86	300	0.287	0.117	0.77	0.220	0.401	1.426	1858
12	1900	0.395		-0.433	91	300	0.303	0.110	0.78	0.237	0.432	1.395	1899
16	1940	0.366		-0.462	93	300	0.310	0.093	0.81	0.252	0.461	1.366	1939

Assumed MDD = 2000 kg/m^3 $\gamma d=Gs/(1+e)$

Calculation with v_{pl} = 0 $\Delta V/V_o=(1-2v_{pl}).\varepsilon$

No. of passes	Density	e	Vo=1+e	Δe	δ (mm)	H	δh/H	v_{pl}	$(1-2v_{pl})$	$=(\delta h/H)(1-2v_{pl})$	ΔV	V	ρ=G/V
0	1450	0.828	1.828										
2	1604	0.652		-0.175	69	300	0.230	0	1.00	0.230	0.420	1.407	1883
4	1740	0.523		-0.305	78	300	0.260	0	1.00	0.260	0.475	1.352	1959
6	1840	0.440		-0.387	85	300	0.283	0	1.00	0.283	0.518	1.310	2023
8	1860	0.425		-0.403	86	300	0.287	0	1.00	0.287	0.524	1.304	2033
12	1900	0.395		-0.433	91	300	0.303	0	1.00	0.303	0.554	1.273	2081
16	1940	0.366		-0.462	93	300	0.310	0	1.00	0.310	0.567	1.261	2101

(after: Forsblad L *Compaction meter on vibrating follers for improved compaction control*, Dynapac Maskin AB Suede, Int.Conf. on Compaction, Paris, Vol II, p543-546, LCPC.)

No. of passes	Percent compaction	Settlement (mm)
2	80.2%	69
4	87.0%	78
6	92.0%	85
8	93.0%	86
12	95.0%	91
16	97.0%	93

From Fig 6.3 From Fig 6.4

APPENDIX I

ADDITIONAL EVIDENCE OF PATTERNS OF IMPROVEMENT IN DYNAMIC COMPACTION MEASUREMENTS

Dynamic Compaction Improvement : Average of 22 results at Karlstad Terminal

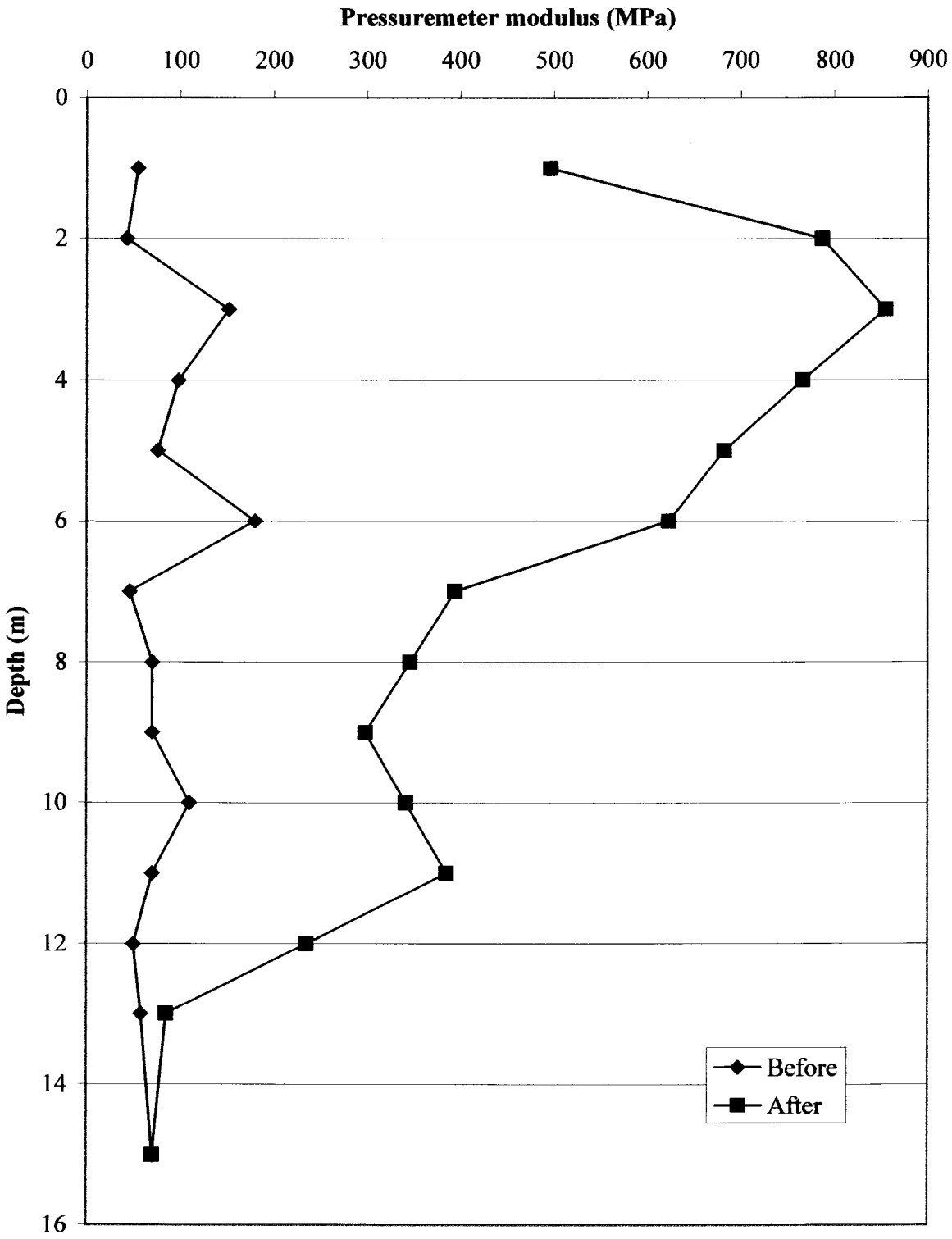

(After Menard and Broise, 1976)

DPSH results [Building S Mozal]

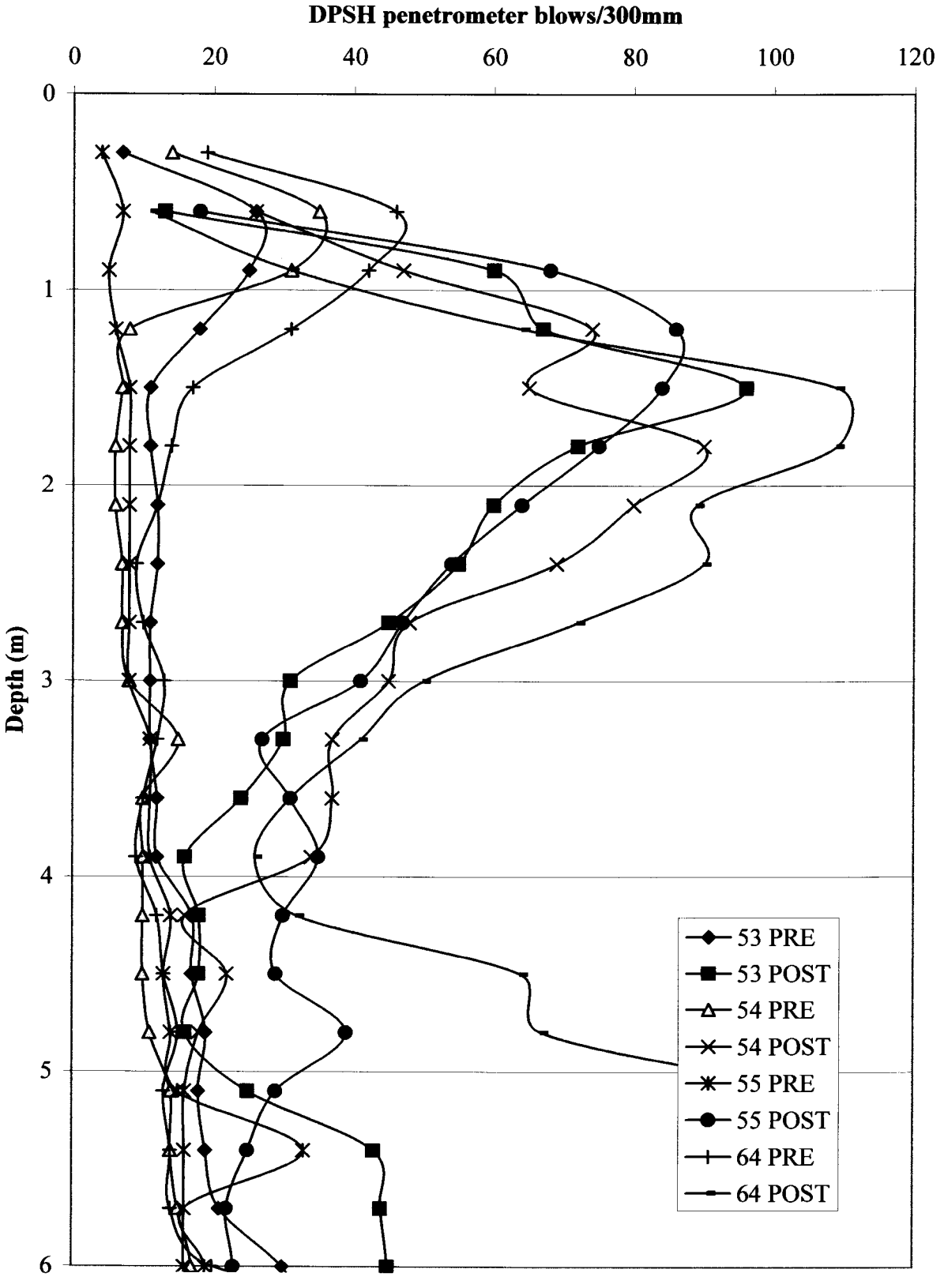

(with permission of Franki Africa)

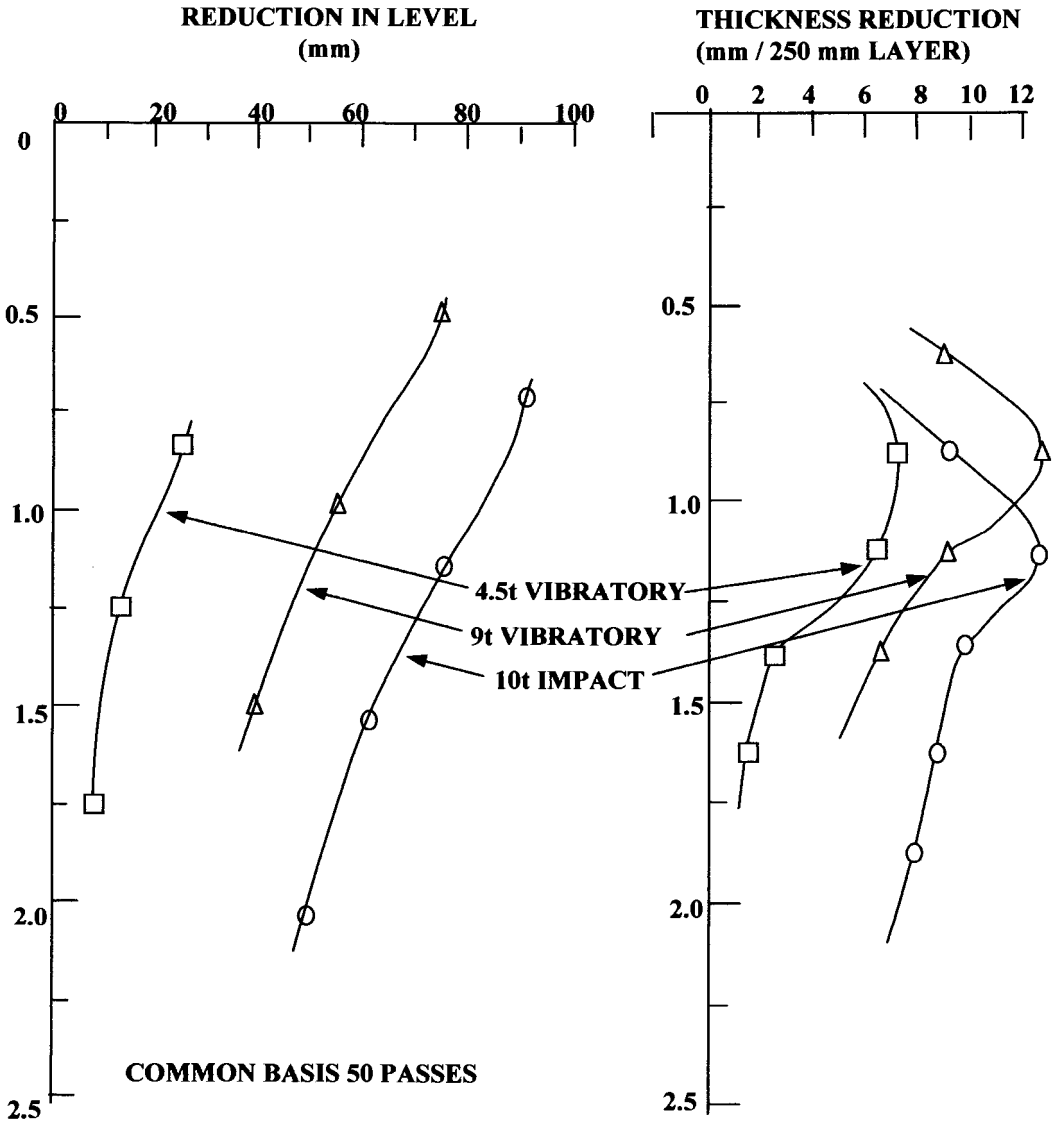

COMPARISON OF ROLLERS ON REDUCTION IN LEVELS AND THICKNESS : PIER 2, DURBAN, 1975

(from CSIR report by Van Vuuren, D.J, Paterson W.D.O & de Wet H, April 1975, *Pavement design recommendations for container terminals with special reference to Pier 2, Durban Harbour*)

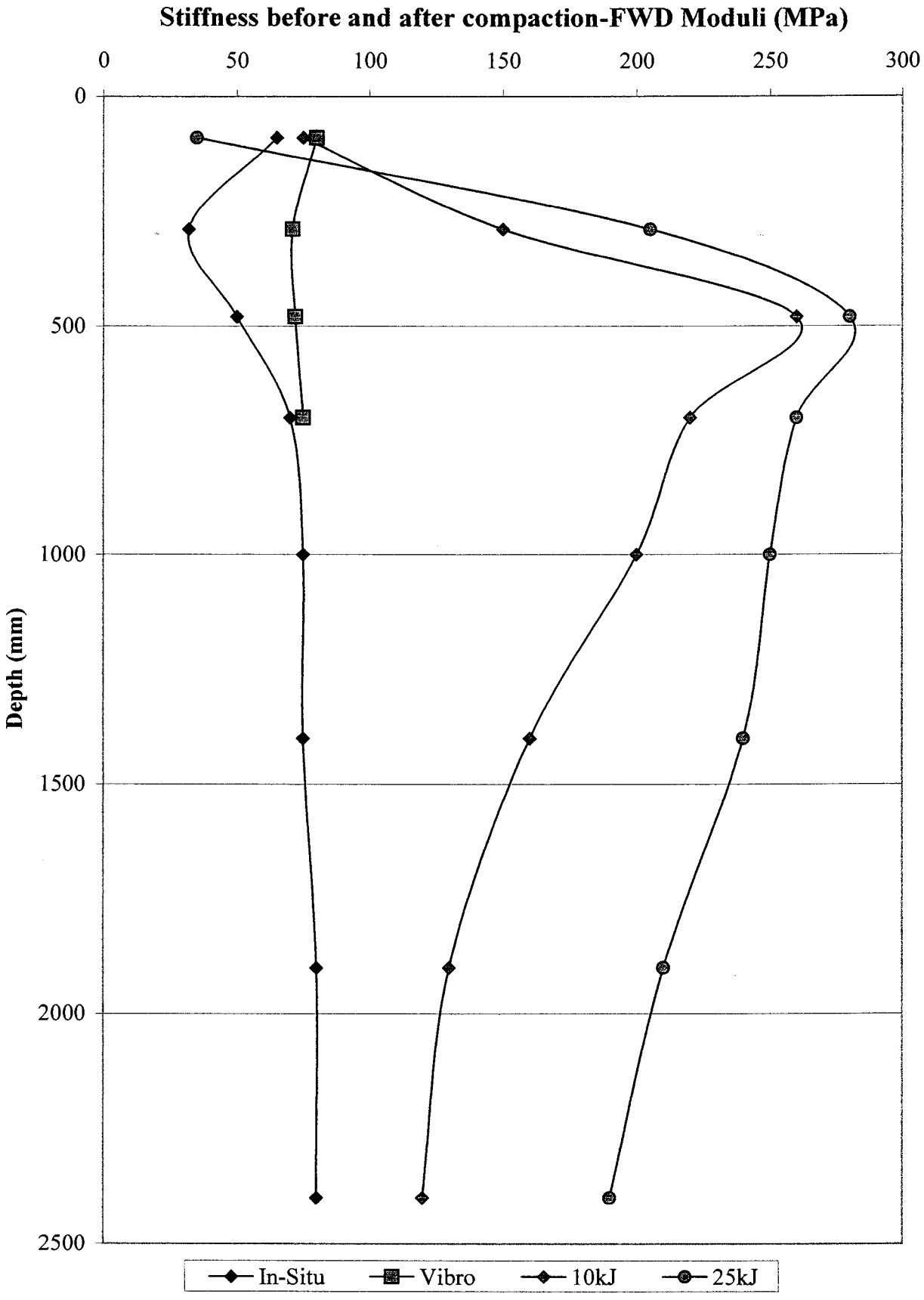

These trials were conducted on red aeolian sand in the Kriel area [Africon, 1998]

APPENDIX J

TYPICAL SOIL IMPROVEMENT PROFILE IN SATURATED CONDITIONS - NICE AIRPORT

FRENCH RIVERA AIRPORT IN NICE
IMPROVEMENT OF THE RECLAIMED LAND FOR
THE PROPOSED NEW RUN-WAY

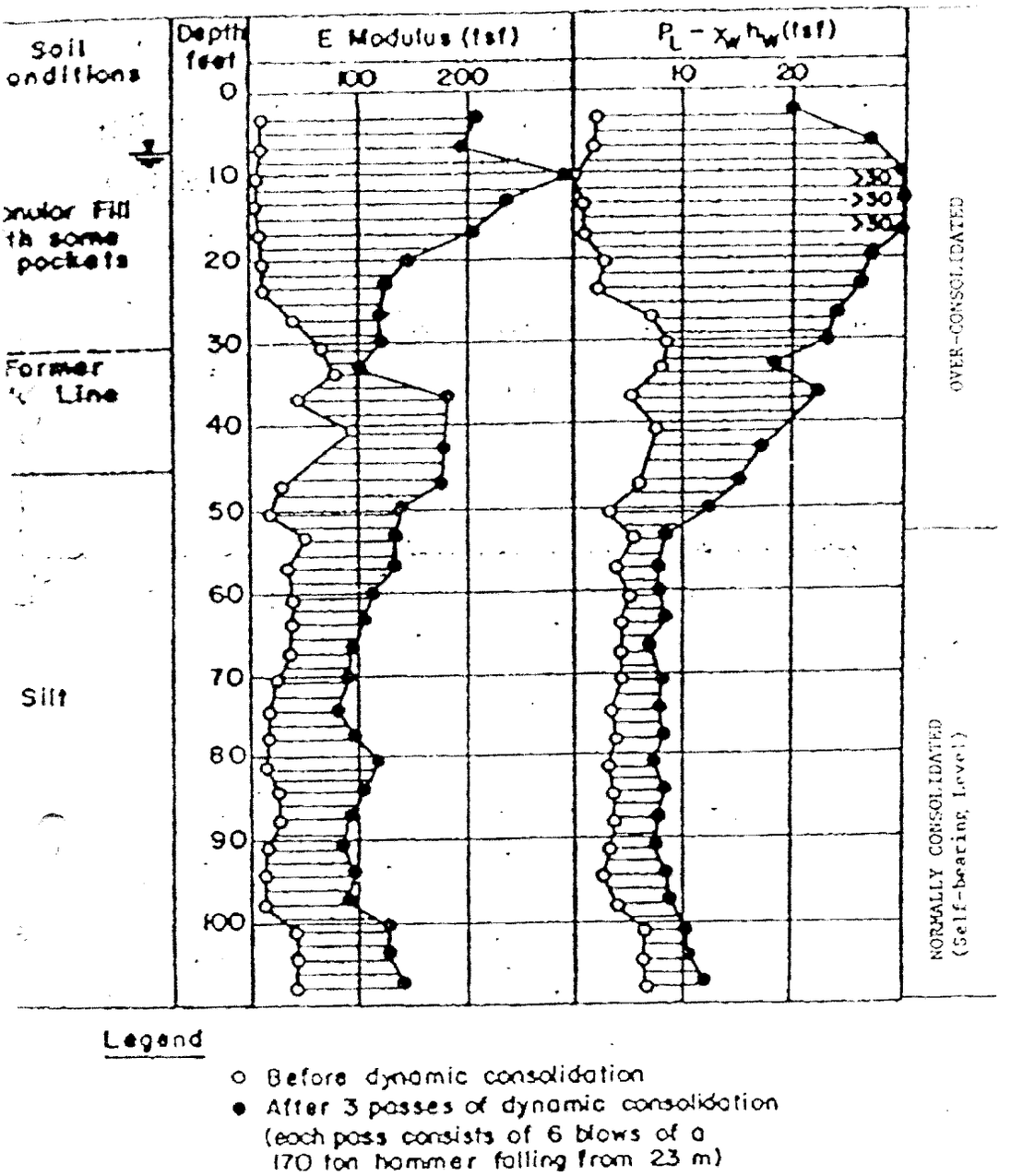

Variation in Pressuremeter Modulus and Limit Pressure with Depth at Nice Airport

(AFTER VARAKSIN, 1981)

APPENDIX K

CURVE FITTING USING A NEGATIVE EXPONENTIAL CURVE

Use of a negative exponential curve to fit settlement data [Kriel 1991]

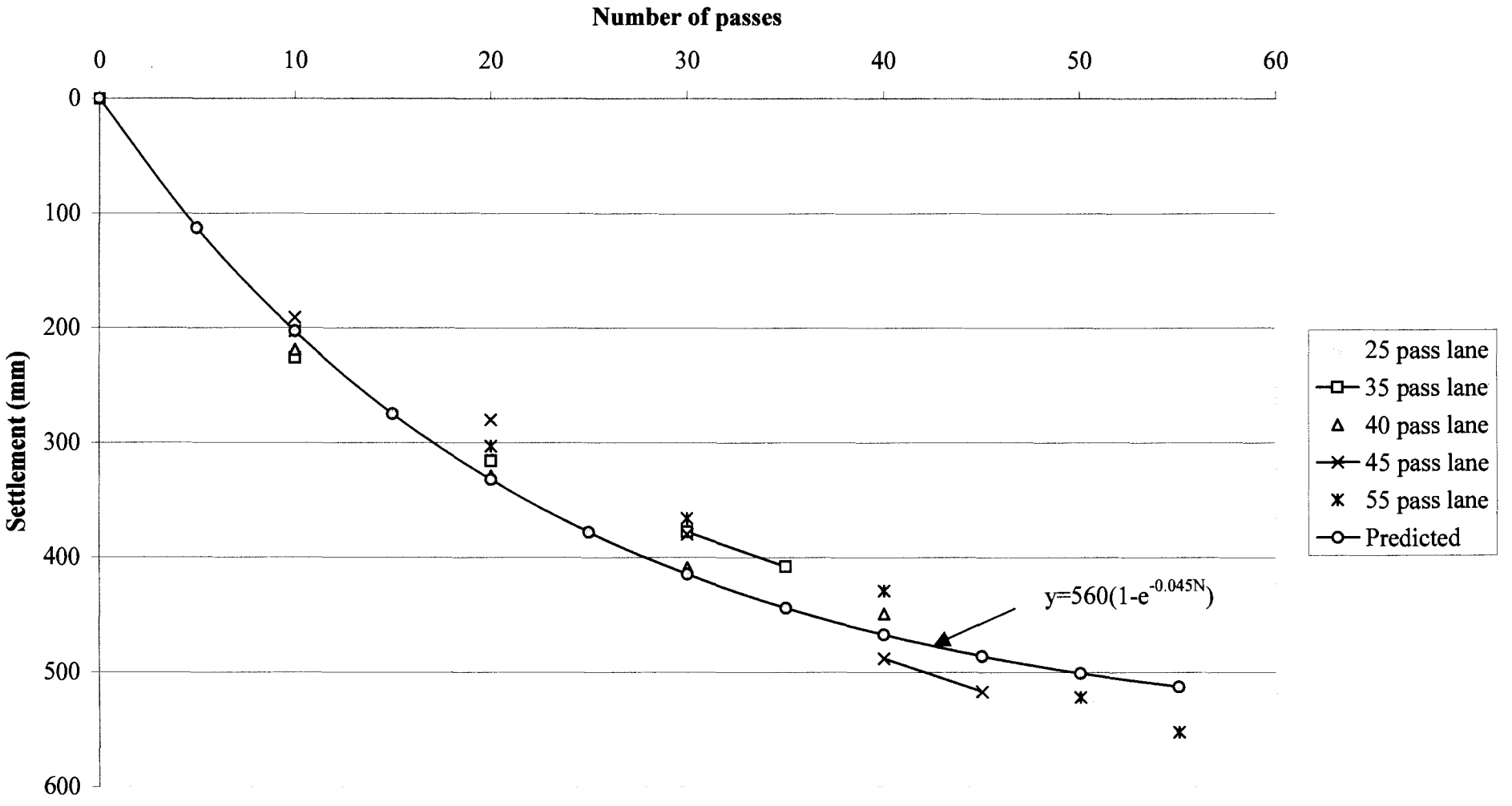

Regression analysis for exponential fit to settlement data

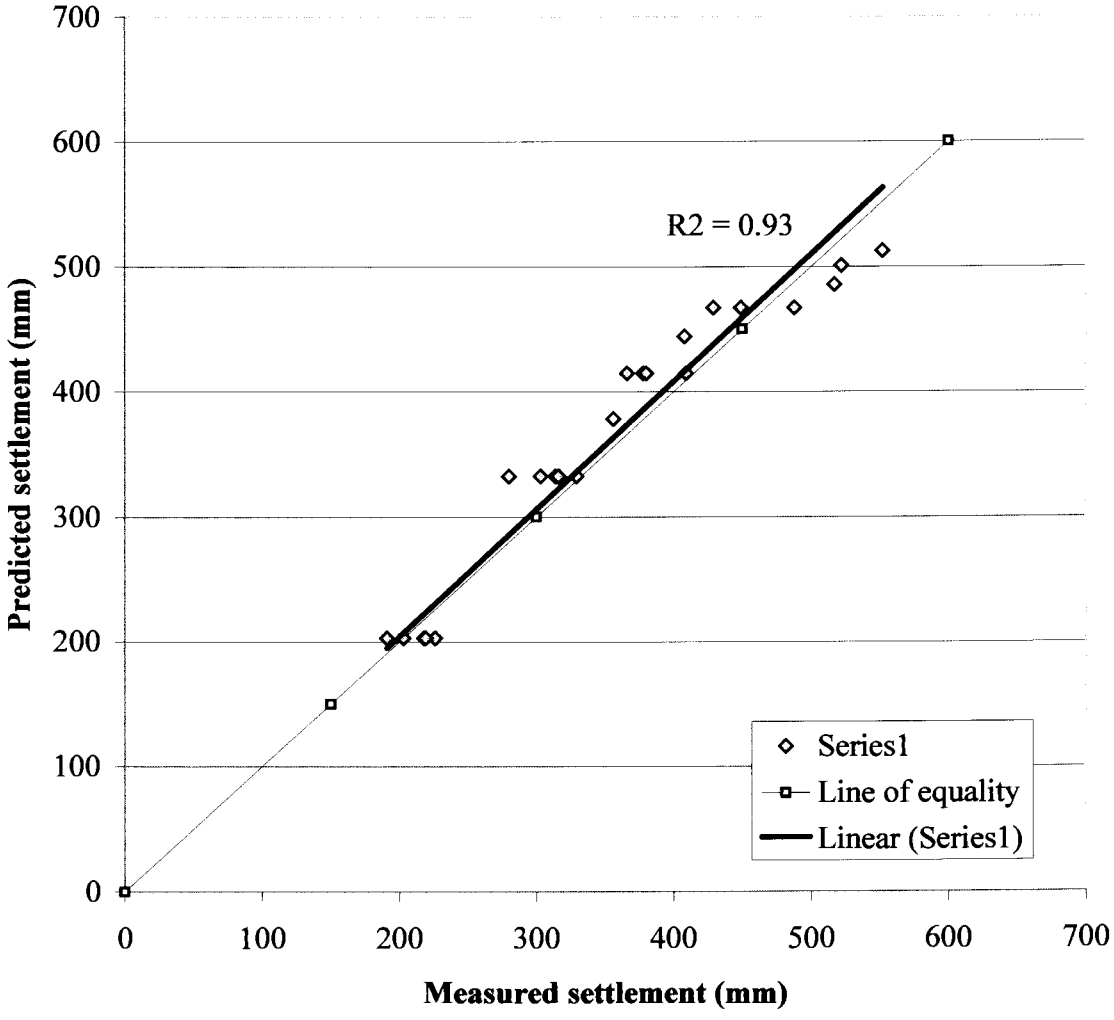

APPENDIX L

SOIL PROFILES AND PROPERTIES AT VARIOUS TEST SITES

Project summary:	Kriel trials			Date:	Sep-97		
Materials:	Aeolean			**Atterberg limits etc…**			
Sieve analysis	% passing [1]	% passing [2]	% passing [3]	Position:	TP1 [1]	TP2 [2]	TP6 [3]
37.500				LL	26	25	23
26.500				PI	14	15	12
19.000				LS	7	6.5	5.5
13.200				GM	0.56	0.55	0.65
4.750				AASHTO	A-6(5)	A-6(5)	A-6(3)
2.000				PI whole			
0.425				% Gravel			
0.250	100	100	100	% Sand	49	49	56
0.150	93	94	91	% Silt	51	51	44
0.075	51	51	44	% Clay			
0.050				Collapse%			
0.005				CBR@90%			
0.002				MOD AASHTO		1958@11.1%	
Depth:	TP1	TP1	TP6	Depth:	0-2m	0-2m	0-2m

Machine used:	Passes:		PREP
25kJ	60	LANDPAC	001

Settlement results:

Passes:	0	10	20	30	40	50	60
Level (m)	0	0.241	0.351	0.429	0.484	0.532	0.560

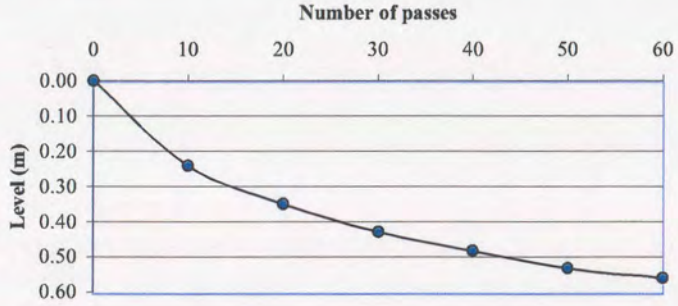

Measured improvement profile:

HDCP's

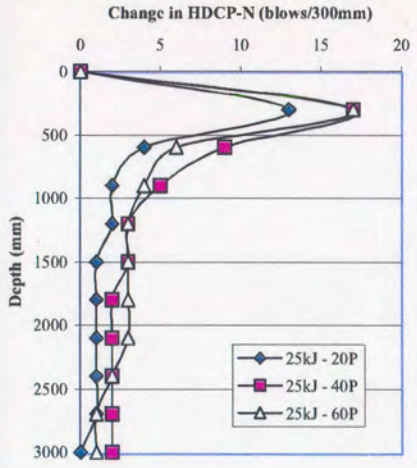

Other testing

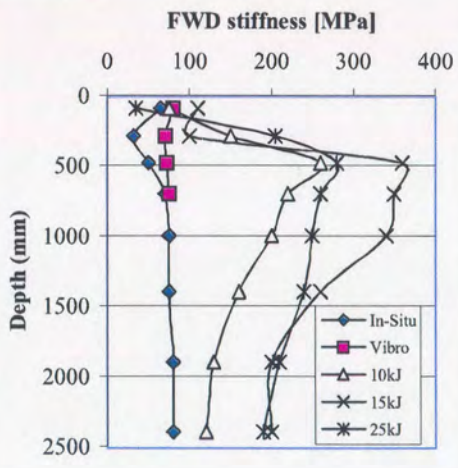

Soil & moisture profile:

z(m)	Description:	m.c
0	Redbrown clayey fine silty sand, soft to firm but stiff close to the surface	12.2
		14.2
>2.5	Bedrock varied from 2-6m but was in general >3m below the surface	15.1
	No water table	

Comments:

Depth of compaction: +/-2.5m
Plate load, oedometer, sand replacement, Falling weight deflectometer, Heavy DCP, and visual settlement strain indicator testing done by independent consultants, Africon Engineering International.

Conclusions:

All impact compactors very effective at compacting this type of material. Significant improvement in stiffness, void ratio and collapse potential

For detailed results see:
U:\alan\Kriel report\Kriel Verslag.doc
U:\rienk\Trial Reports Database\Kriel trials\
This document: U:\Project database\Kriel 1997

Project summary: Highveld steel | Date: 1969 | Machine used: 12t 5 sided | Passes: 20 | LAND PAC | PREP 004

Materials: Medium dense silty sand

Sieve analysis	% passing [1]	% passing [2]	% passing [3]
37.500			
26.500			
19.000			
13.200			
4.750			
2.000			
0.425			
0.250			
0.150			
0.075	22	45	
0.050			
0.005			
0.002			
Depth:	0-1.2m	1.2-2.7m	

Atterberg limits etc...

Position:	Test [1]	Test [2]	Test [3]
LL			
PI	SP	14	
LS			
GM			
AASHTO			
PI whole			
% Gravel			
% Sand			
% Silt	22	45	
% Clay			
Collapse%			
CBR@90%			
MOD AASHTO			
Depth:	0-1.2m	1.2-2.7m	

Settlement results:

Passes:	0	2	5	10	20	50	60
Level (m)	0	0.051	0.071	0.091	0.145		

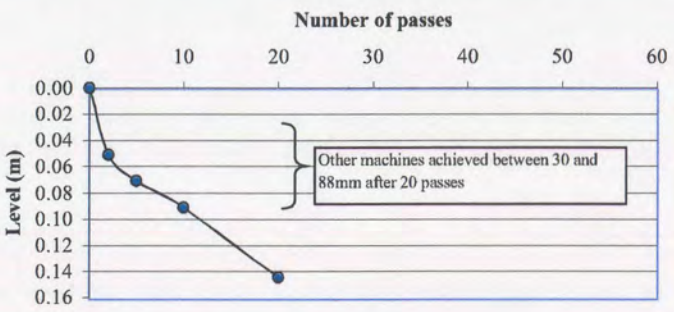

Measured improvement profile:

Density

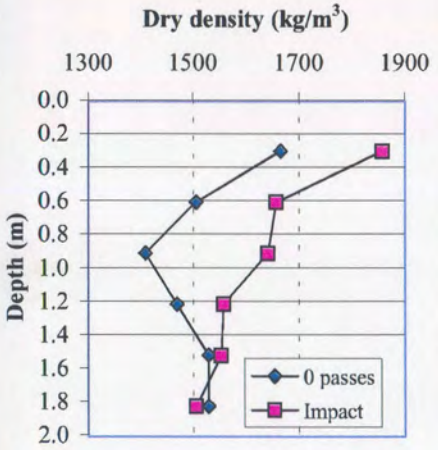

Other testing

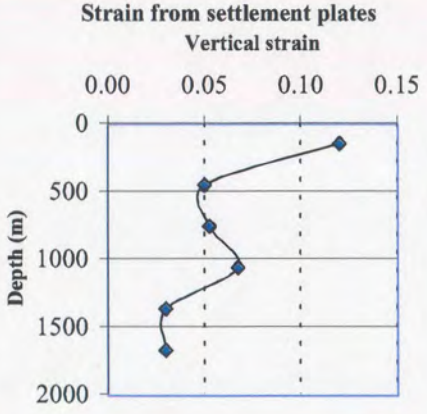

Soil & moisture profile:

z(m)	Description:	m.c
0	Medium dense	
	slightly cemented	7.5
0.9	sand, transported	
1,2	Silty sand	12
	Dark redish brown	
	soft medium dense	15
	unifrom silty sand	
	Scattered Fe	
	concretions	
2.5	(transported)	17
	No water table	

Comments:

Depth of compaction: +/-1.5m

From paper by Clegg et al, 1969
CSIR Report No RC/3/69

Conclusions:

Better than other plant utilised
Economical in terms of depth/unit cost
Settlements and DCP adequate to observe changes
Well worth further research
For detailed results see:
U:\Alan\My documents\Prediction model\Raleigh\
This document : U:\Project Database\

Project summary:	Middleberg Coal Mine			Date:	1984		
Materials:	Aeolean sand			**Atterberg limits etc…**			
Sieve analysis	% passing [1]	% passing [2]	% passing [3]	Position:			
37.500				LL			
26.500				PI			
19.000				LS			
13.200		100		GM			
4.750		92		AASHTO			
2.000	100	80		PI whole			
0.425	71	75		% Gravel			
0.250	65	55		% Sand			
0.150	48	38		% Silt			
0.075	36	28		% Clay			
0.050	32	23		Collapse%	10.4	12.6	12.8
0.005	18	16		Void ratio	0.89	1.05	0.96
0.002	0	0		MOD AASHTO	2080 @ 9%		
Depth:	Upper sand	Ferruginised		Depth:	0.5m	1.0m	1.5m

Machine used:	Passes:		PREP
18kJ 3 sided	Varied	LANDPAC	020

Settlement results:

Passes:	0	10	20	30	40	50	60
Level (m)	0	0.061	0.087	0.097	0.100	0.113	

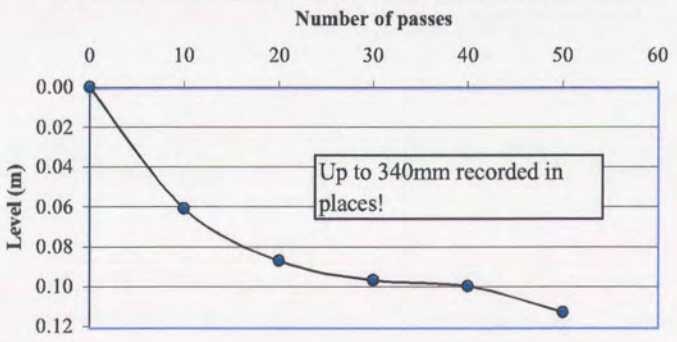

Measured improvement profile:

Density

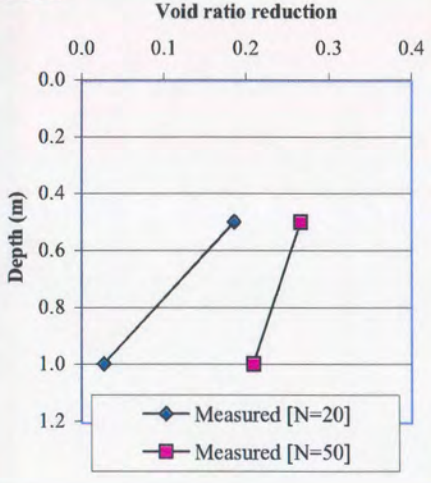

Other testing

Soil & moisture profile:

z(m)	Description:	m.c
0	Aeolean sand with fine ferricrete from 1.3 m down	
2.5		

Comments:

Aeolean sand from the surface to 2.5m-3m

Sands loose to very loose becoming medium dense from about 2m down the profile.

Trial was 230mx 10m wide

Conclusions:

Higher densities were achieved where the ferricrete was present

Reduction in collapse potential not enough in this trial but further rolling could improve the results.

Appreciable additional settlement was obtained after early summer rains.

The trial lead to SRK not using impact compaction for some time

Project summary:	**Serowe - Orapa**			Date: 1988			Machine used:	Passes:	LAND PAC	PREP
Materials:	Aeolean			**Atterberg limits etc…**			25kJ	10 - 60		028

Sieve analysis	% passing [1]	% passing [2]	% passing [3]	Position:			
37.500				LL			
26.500				PI	26.8	23.9	27.3
19.000				LS			
13.200				GM	0.9	0.9	0.9
4.750	96	97	96	FI (index)	429	359	410
2.000				PI whole			
0.425				% Gravel			
0.250				% Sand			
0.150				% Silt			
0.075	16	15	15	% Clay			
0.050				Collapse%			
0.005				CBR@90%			
0.002				MOD AASHTO			
Depth:	0.2 - 0.35	0.45 - 0.6	0.7 - 0.85	Depth:	0.2 - 0.35	0.45 - 0.6	0.7 - 0.85

Settlement results:

Passes:	0	10	20	30	40	50	60
Level (m)	0	0.080	0.110	0.125	0.138	0.160	0.175

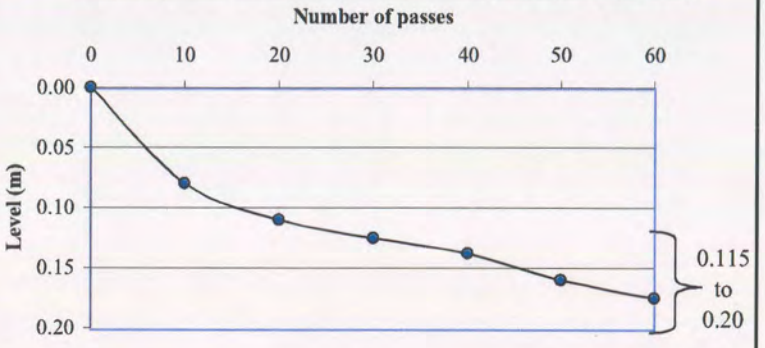

Measured improvement profile:

Void ratio reduction

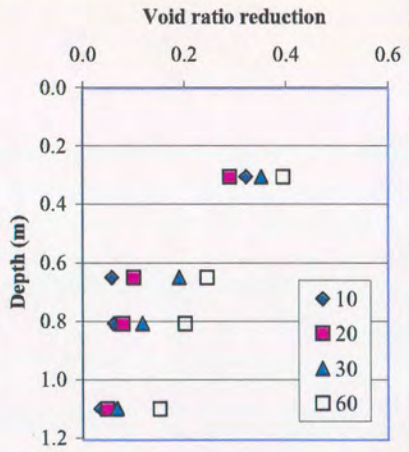

Other testing

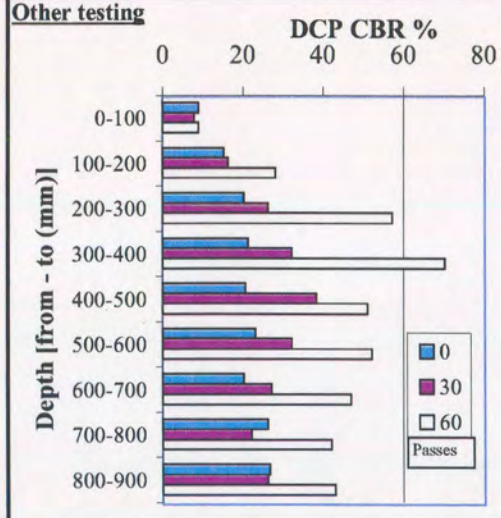

Soil & moisture profile:

z(m)	Description:	m.c
0	Kalahari sands	

Comments:

Initial material properties:

Dry density < 1600 kg/m^3 - average =1432 kg/m^3

Relative density < 85% MDD

Conclusions:

Economics:	Plant & labour	Water	Total
Impact	1.75	0.27	2.02
Conventional	2.22	0.67	2.89
1Pula=0.6 US$	Pula/m^3 (1987)	% diff	-30%

Well suited for arid regions-compaction dry of optimum

Stiffer, uniform subgrade for minimum thickness pavements

Use less water - cost savings

Little moisture control required

(after Pinard et al, ATC 1988)